Solubilities and ion exchange properties of solid solutions between the OH, Cl and CO_3 end members of the monocalcium aluminate hydrates

By

Monique Y. Hobbs

A thesis
presented to the University of Waterloo
in fulfillment of the
thesis requirement for the degree of
Doctor of Philosophy
in
Earth Sciences

Waterloo, Ontario, Canada, 2001

© Monique Y. Hobbs 2001

National Library of Canada
Acquisitions and Bibliographic Services
395 Wellington Street
Ottawa ON K1A 0N4
Canada

Bibliothèque nationale du Canada
Acquisitions et services bibliographiques
395, rue Wellington
Ottawa ON K1A 0N4
Canada

Your file Votre référence

Our file Notre référence

The author has granted a non-exclusive licence allowing the National Library of Canada to reproduce, loan, distribute or sell copies of this thesis in microform, paper or electronic formats.

The author retains ownership of the copyright in this thesis. Neither the thesis nor substantial extracts from it may be printed or otherwise reproduced without the author's permission.

L'auteur a accordé une licence non exclusive permettant à la Bibliothèque nationale du Canada de reproduire, prêter, distribuer ou vendre des copies de cette thèse sous la forme de microfiche/film, de reproduction sur papier ou sur format électronique.

L'auteur conserve la propriété du droit d'auteur qui protège cette thèse. Ni la thèse ni des extraits substantiels de celle-ci ne doivent être imprimés ou autrement reproduits sans son autorisation.

0-612-65246-7

Canada

The University of Waterloo requires the signatures of all persons using or photocopying this thesis. Please sign below, and give address and date.

Solubilities and ion exchange properties of solid solutions between the OH, Cl and CO_3 end members of the monocalcium aluminate hydrates

Abstract

Friedel's salt ($3CaO \cdot Al_2O_3 \cdot CaCl_2 \cdot 10H_2O$) is the chloride phase most often identified in hydrated cement pastes and concrete, and is likely the dominant mineralogical control on chloride concentrations in these materials. When exposed to radiation from nuclear reactors (e.g. reactor shielding walls), stable chlorine isotopes present in concrete structures can become activated to radioactive chlorine-36. Chlorine-36 is considered a critical nuclide in radioactive waste disposal, because it has a moderately long half-life ($3.01 \pm 0.04 \times 10^5$ years), and is highly mobile in terrestrial environments. Although detailed studies have been conducted on the crystal structure of Friedel's salt, and on solid solutions formed between the OH and Cl, Cl and CO_3, and OH and CO_3 end members, the solubility data published in the literature are limited primarily to the end members. The objectives of this thesis were 1) to measure the solubility of the solid solutions in these three series at thermodynamic equilibrium, 2) to confirm the miscibility gaps and regions of solid solution as determined by previous researchers, 3) to develop a description of the partitioning of chloride between the solid solution and the aqueous solution phases at thermodynamic equilibrium using solid-solution aqueous-solution (SSAS) theory, and 4) to investigate the rate and extent of exchange of anions from the interlayer of these phases.

The stability of solid phases between the Cl-OH, Cl-CO_3 and CO_3-OH end members was examined using solubility experiments conducted from both super- and undersaturated conditions. The solid and solution phases were examined for compositional variations, and the positions of miscibility gaps were determined based on the observed mineral phase assemblages and calculated mineral saturation indices in aqueous solution. The results of the solubility studies support the conclusion of previous researchers that the miscibility gap in the OH-Cl series begins at a Cl/(Cl+OH) ratio very close to 0.33, and confirms that the lower limit of the miscibility gap lies between ratios of 0.0 and 0.1. In agreement with previous research, a partial solid solution was observed in solids with carbonate ratios of up to 0.75 between the Cl and CO_3 end members. The upper limit of the miscibility gap is extended to a ratio of at least 0.91. From supersaturation, two miscibility gaps were observed in the OH-CO_3 series: one between the OH end member and hemicarboaluminate from carbonate ratios of 0.1 to 0.5, and a second between

hemicarboaluminate and the CO_3 end member at carbonate ratios of 0.6 to 0.8. After long reaction times from undersaturation, the OH end member and hemicarboaluminate were observed over a smaller range of carbonate ratios (0.0 to 0.25), whereas hemicarboaluminate and the CO_3 end member occurred together over a wider range carbonate ratios (0.4 and 0.7), and hydrogarnet was also observed in these solids. These results suggest that hemicarboaluminate may be a metastable phase that converts to monocarboaluminate and hydrogarnet with time.

A compilation and evaluation of solution composition data on the solubility of the Cl, OH and CO_3 end members from several published studies and from the current study yielded average solubility products of -27.57 ± 0.86, -31.23 ± 0.80, and -25.80 ± 0.62 for the Cl, CO_3 and OH end members, respectively (based on modeling using the geochemical equilibria model, SIMUL). The uncertainty given for these values is one standard deviation from the mean. Using these average K_{sp} values, Gibbs free energies of formation ($\Delta G^\circ_{f,\,298}$) for Friedel's salt, monocarboaluminate and the OH end member are -6822.51± 4.92, -7345.89 ± 1.09, and -8761.59 ± 3.54 kJ/mol, respectively. These free energy of formation values for the end members are consistent with those calculated based on the solubility products determined using PHREEQC (-6823.10± 4.69, -7347.86 ± 2.79, and -8761.13 ± 3.54 kJ/mol, respectively). The solubility products measured for solid solutions between the OH and Cl end members were two orders of magnitude lower than those measured in a previous study. These results suggest that thermodynamic equilibrium was more closely approached in the current study.

The solubilities of the solid solutions measured as a function of solid composition for the OH-Cl series were used to derive the excess free energy parameters that are required for modeling using SSAS theory. These values were fit to the two parameter Guggenheim's expansion series

$$G^E = x\,(1\text{-}x)\,RT\,[a_0 + a_1\,(x\,(1\text{-}x)) + a_2(x - (1\text{-}x)^2)]$$

where x is the mole fraction of the substituting ion (in this case, chloride). The derived parameters a_0 = -0.324 and a_1 = -7.95 were used to construct a Lippmann diagram that can be used to estimate the solubility of solid solutions between the OH and Cl end members. In order to solve the solutus equation, a modification to the definition of the aqueous mole fraction of the substituting ions was necessary because the stoichiometric ratio of the substituting ions is not equal to one. In the Cl-CO_3 series, excess free energy parameters (a_0 = -19.3, a_1 = 10.7) were derived from on the observed miscibility gaps in the system using the geochemical equilibria model, PHREEQC. These parameters are thought to be most representative of equilibrium

conditions. Excess free energy parameters based on solubility data were not determined in the OH-CO_3 series, primarily because of complications arising from the presence of two miscibility gaps.

Excess free energy parameters derived for the OH-Cl and Cl-CO_3 systems can be used to construct Lippmann diagrams for estimating the partitioning of Cl^- ions between the solid solution and aqueous solution phases. Validation of these parameters requires further solubility studies where either attainment of thermodynamic equilibrium or stoichiometric saturation can be verified. Determining the solubilities of the solid solutions in all three series was complicated by the long reaction times required to reach equilibrium, by the presence of two solid solution phases within the miscibility gaps, and by the presence of additional mineral phases. If single solid solution phases with compositions spanning the miscibility gaps can be precipitated, in future studies the solubility of these phases may be measured using an alternative approach, by dissolution to stoichiometric saturation. In the OH-Cl exchange experiments, single solid solution phases with compositions within the miscibility gap were generated, indicating that at least in the OH-Cl series, the stoichiometric saturation approach is potentially applicable. The partitioning of OH^- and Cl^- ions between the solid solution and aqueous solution phases in both the solubility and ion exchange experiments can be described using a Langmuir isotherm where K=7.65.

Exchange of ions from the interlayer of these minerals was investigated between the Cl and OH end members as a function of time, and as a function of Cl^- concentration. The solution composition was monitored to determine the extent of exchange, and selected solid samples were examined using X-ray diffraction analysis. The maximum fraction of Cl^- exchanged into the OH end member was ≈0.7 in the ion exchange experiments, whereas in the solubility experiments, the Cl(Cl+OH) ratio in the solid was above 0.9 for the same total Cl^- in the system. Comparison of the results from both the ion exchange and solubility experiments shows a well-defined relationship between the Cl/(Cl+OH) ratio in the solid and the ratio in the aqueous phase. Because the hydroxyl concentration is higher in the ion exchange experiments, the Cl/(Cl+OH) ratio in both the aqueous phase and solid solution phases is lower. Although CO_3^{2-} ions are reportedly preferred in the monocalcium aluminate hydrate structure, only 20% of the Cl^- ions in Friedel's salt were replaced by CO_3^{2-} ions after 2 months of reaction in the ion exchange experiments. This suggests that at least in the short term, the bulk of the Cl^- ions in Friedel's salt, which is the most probable mineralogical control on chloride in cement-based materials, will not be readily released to the environment through exchange processes with carbonate ions in groundwater or CO_2 in the atmosphere.

Acknowledgments

Many thanks to my supervisor, Dr. Eric Reardon, for his support and encouragement throughout my graduate studies. His interest in science and in particular, his enthusiasm for geochemistry continue to be a source of inspiration to me.

Sincere thanks to my committee members, Dr. Shaun Frape, Dr. Carolyn Hansson and Dr. Ron Nicholson for their insightful questions and comments while the thesis was in progress, and for their careful final reviews of the manuscript. I would like to extend a special thank-you to Dr. Frape for being a mentor to me during the course of my Ph.D. work. I would also like to thank my external examiners, Dr. Wayne Nesbitt from the University of Western Ontario, and Dr. Hartwig Peemoeller from the Department of Physics, University of Waterloo for reviewing this dissertation.

Thanks also to the many laboratory researchers and staff for providing assistance, and for performing experiments and analyses: Randy Fagan, Tracy Fowler, Marianne Vandergriendt, Krista Lau, Jessica Page, Sarah DellaValle, and the many students who worked with our group through the Ontario Work/Study Plan.

In particular, I would like to thank Dr. Min Zhang for the many hours of discussion and debate (both scientific and life-related) which have greatly enriched this journey. She also reviewed and corrected this manuscript during the preparation of the dissertation. She is my closest colleague and friend, and I hope that we will have many opportunities to work and perhaps even to travel together (Europe, China...and beyond) in the future.

I would like to express my deepest gratitude to my family, including my parents (Barbara J. Hobbs, and the late James T. Hobbs), my grandparents (Ruth M. Calvin, and the late Archibald A. Calvin), my godparents, (Barrie and Holly Down), and my friend, Ian Judd-Henrey. Without their unwavering encouragement, love, and support (both emotional and financial), I would have not attempted and surely would not have completed this doctorate degree. Finally, I would like to thank my partner, James Morgan for his support over this past year or so during the completion of my thesis. Now that my compass is set to "true North" and my doctorate is complete, we set out on the next journeys of our respective lives together.

Table of Contents

Abstract.....iv

Acknowledgments.....vii

List of Tables.....xv

List of Figures.....xviii

Chapter 1 Introduction

1.1 Mineralogical controls on chloride.....1

1.1.1 Chloroaluminates and oxychlorides.....2
1.1.2 Chloroferrite hydrates.....3
1.1.3 Calcium silicate hydrates.....4

1.2 Stability and solubility of the monocalcium aluminate hydrates.....5

1.2.1 Crystal structure.....5
1.2.2 Thermal stability.....5
1.2.3 Hydrotalcite-like phases.....6

1.3 Phase identification using X-ray diffraction analysis.....7

1.4 Solubility and ion exchange.....8

1.4.1 Solubility.....8
1.4.2 Ion exchange.....10

1.5 Objectives.....11

1.6 References.....13

Chapter 2 Solubility of solid solutions in the system $CaO-Al_2O_3-CaCl_2-H_2O$ from super- and undersaturation

2.1 Introduction 16

2.2 Experimental 19

2.2.1 Materials 19
2.2.2 Experimental procedure 19
2.2.3 Analytical methods 21

2.3 Results 23

2.3.1 Approach to equilibrium 23
2.3.2 Solution composition 26
2.3.3 Mineral saturation indices 30
2.3.4 Solids 33
2.3.5 Solid solution phase composition 36
2.3.6 Solubility of the Cl end member 40
2.3.7 Solubility products 42

2.4 Discussion 45

2.4.1 Evidence for the existence of a miscibility gap 45
2.4.2 Factors influencing solid solution stability 47
2.4.3 Solubilities of the solid solutions 49
2.4.4 Predicting chloride partitioning 51
2.4.4.1 Determining solid phase activity coefficients 51
2.4.4.2 Derivation of an expression for the solutus 54

2.5 Conclusions 60

2.6 Recommendations 62

2.7 References 63

Chapter 3 Solubility of solid solutions in the system CaO-Al_2O_3-$CaCl_2$-$CaCO_3$-H_2O from super- and undersaturation

3.1 Introduction.....67

3.2 Experimental.....68

3.3. Results.....69

3.3.1 Solutions.....69
3.3.2 Solids.....76
3.3.3 Solubility products.....80

3.4 Discussion.....84

3.4.1 Solid solution stability.....84
3.4.2 Attainment of equilibrium.....85
3.4.3 Equilibrium predictions.....87

3.4.3.1 Constructing a Lippmann diagram.....87
3.4.4.2 Calculation of the excess free energy parameters.....88

3.5 Conclusions.....92

3.6 Recommendations.....93

3.7 References.....94

Chapter 4 Solubility of solid solutions in the system CaO-Al_2O_3-CO_3-H_2O from super- and undersaturation

4.1 Introduction.....97

4.2 Results.....100

4.2.1 Reaction kinetics....100
4.2.2 Solution composition....100
4.2.3 Solids....107
4.2.4 Solubility products....112

4.3 Discussion....113

4.3.1 Mineral assemblages....113

4.3.1.1 OH end member....115
4.3.1.2 Miscibility gap: OH end member and hemicarboaluminate....115
4.3.1.3 Hemicarboaluminate....117
4.3.1.4 Miscibility gap: Hemicarboaluminate and monocarboaluminate....117
4.3.1.5 Monocarboaluminate....117

4.3.2 Attainment of equilibrium....118
4.3.3 Stability of the solid solutions....119
4.3.4 Solubility products....121
4.3.5 Predicting carbonate partitioning at equilibrium....123

4.4 Conclusions....124

4.5 Recommendations....126

4.6 References....127

Chapter 5 Re-evaluation of end member solubilities: Friedel's salt, monocarboaluminate and OH-hydrocalumite

5.1 Introduction....130

5.2 The chloride end member: Friedel's salt....130

5.3 The carbonate end member: Monocarboaluminate....132

5.4 The hydroxyl end member: OH-hydrocalumite 134

5.5 Calculation of solubility products (K_{sp}) 135

5.6 Discussion 143

5.6.1 Friedel's salt 143
5.6.2 Monocarboaluminate 144
5.6.3 OH-hydrocalumite 145
5.3.4 Effect of solution:solid ratio 146
5.6.5 Gibbs free energy 146

5.7 Conclusions 147

5.8 Recommendations 148

5.9 References 149

Chapter 6 Ion exchange reactions in the system CaO-Al_2O_3-$Ca(OH)_2$-$CaCl_2$-$CaCO_3$-H_2O

6.1 Introduction 152

6.2 Experimental 154

6.2.1 Materials 154
6.2.2 Experimental procedures 154

6.2.2.1 Formation of the OH and Cl end members 154
6.2.2.2 Exchange reactions as a function of time 155
6.2.2.3 Exchange reactions as a function of concentration 156

6.2.3 Analytical methods 158

6.3 Results.....159

6.3.1 Formation of the OH and Cl end members.....159
6.3.2 Exchange of OH by Cl.....162

6.3.2.1 Reaction time.....162
6.3.2.2 Concentration.....163

6.3.3 Exchange of Cl by CO_3.....170

6.4 Discussion.....175

6.4.1 Exchange of OH by Cl.....175
6.4.2 Exchange of Cl by CO_3.....181

6.5 Conclusions.....183

6.6 Recommendations.....184

6.7 References.....185

Chapter 7 Contributions

7.1 OH end member.....187

7.1.1 A re-evaluation of previous research.....187
7.1.2 OH end member solids as observed in the current study.....188

7.2 Preference for carbonate ions.....191

7.3 Solubility and stability.....191

7.3.1 Solubility.....191
7.3.2 Stability.....193

7.4 SSAS theory as applied to the monocalcium aluminate hydrates.....196

7.5 References.....198

Appendix A.....200

Appendix B.....201

List of Tables

Table 2.1 X-ray diffraction patterns used in the identification of solid phases....22
Table 2.2 Measured solution compositions for C-replicate samples of the Cl end member....25
Table 2.3 Solution compositions measured from supersaturation for samples between the Cl and OH end members....31
Table 2.4 Solution compositions measured from undersaturation for samples between the Cl and OH end members....31
Table 2.5 Solid phase compositions in the experiments from super- and undersaturation....40
Table 2.6 Solution data measured from supersaturation for the Cl end member in the extended solubility experiment....41
Table 2.7 Calculated log SI values of mineral phases for solution compositions from the extended solubility experiment....41
Table 2.8 Solid phase compositions for the Cl end member from the extended solubility experiment....42
Table 2.9 Solid phase observed as a function of the calculated Cl/(Cl+OH) ratio in the solid (combined results from several published studies)....46
Table 2.10 Comparison of solubility products for solids between the OH and Cl end members based on solution composition measurements from the current study and Birnin-Yauri and Glasser (1998)....51
Table 2.11 Predicted spinodal and miscibility gaps for the calculated excess free energy parameters....56

Table 3.1 Solution compositions measured for the A and B replicates between the Cl and CO_3 end members from supersaturation....72
Table 3.2 Solution compositions measured for the A and B replicates between the Cl and CO_3 end members from undersaturation....72
Table 3.3 Positions of possible spinodal and miscibility gaps predicted using the excess free energy parameters....89

Table 4.1 Solution data measured from supersaturation for samples with compositions between the CO_3 and OH end members....103

Table 4.2 Solution data measured from undersaturation for samples with compositions between the CO_3 and OH end members.....103
Table 4.3 Observed d-spacings for the primary peaks as a function of the calculated carbonate ratio in the solid from supersaturation.....109
Table 4.4 Observed d-spacings for the primary peaks as a function of the calculated carbonate ratio in the solid from undersaturation.....109

Table 4.5 Comparison of mineral phases observed between the CO_3 and OH end members as a function of the carbonate ratio from super- and undersaturation.....114
Table 4.6 Comparison of mineral phases observed between the CO_3 and OH end members as a function of the carbonate ratio compiled from other studies.....116

Table 5.1 Solution compositions measured for Friedel's salt from super- and undersaturation (compiled from other studies).....133
Table 5.2 Solution compositions measured for Friedel's salt measured from super- and undersaturation in the current study.....134
Table 5.3 Published compositions of solutions equilibrated with monocarbo-aluminate.....137
Table 5.4 Solution compositions after equilibration with monocarboaluminate in the current study.....137
Table 5.5 Published compositions of solutions equilibrated with OH-hydrocalumite.....138
Table 5.6 Solution compositions after equilibration with OH-hydrocalumite as measured in the current study.....139
Table 5.7 Calculated Gibbs free energies for the OH, Cl and CO_3 end members.....147

Table 6.1 Experimental parameters for the ion exchange experiments as a function of time.....155
Table 6.2 Experimental parameters for experiments examining the exchange of OH^- ions in the OH end member by increasing concentrations of Cl^-.....157

Table 7.1 Preparation methods, equilibration times, and primary d-spacings measured for the OH end member in the current study.....190

List of Figures

Figure 1.1 Solution chloride concentration versus pH with progressive carbonation of cementitious material....2

Figure 1.2 Schematic representation of hydrocalumite (layered double metal hydroxide structure)....6

Figure 2.1 Electrical conductance measurements versus reaction time for the experiments from super- and undersaturation....24

Figure 2.2 Solution concentrations of calcium as a function of Cl/(Cl+OH) ratio in the solid solution phases....27

Figure 2.3 Solution concentrations of aluminum as a function of Cl/(Cl+OH) ratio in the solid solution phases....28

Figure 2.4 Solution concentrations of chloride as a function of Cl/(Cl+OH) ratio in the solid solution phases....29

Figure 2.5 Calculated mineral saturation indices versus the Cl/(Cl+OH) ratio in the solid for the A and B replicates from super- and undersaturation....32

Figure 2.6 XRD patterns for the A-replicate solids from supersaturation....34

Figure 2.7 XRD patterns for the B-replicate solids from supersaturation....35

Figure 2.8 XRD patterns for solid samples (A-replicates) from undersaturation....37

Figure 2.9 Enlargement of the primary peak for the solid solution phase....38

Figure 2.10 Scanning electron micrographs of solids formed between the OH and Cl end members in the experiments from supersaturation....39

Figure 2.11 Log values of the solubility products (K_{sp}) for the solid solution as a function of Cl/(Cl+OH) ratio in the solid phase....44

Figure 2.12 ln K_{sp} values for the A replicates from undersaturation vs. the mole fraction of Cl^- in solution....58

Figure 2.13 Lippman phase diagram for the series between the Cl and OH end members at 25 °C....59

Figure 3.1 Electrical conductance measurements versus reaction time for the experiments from super- and undersaturation....70

Figure 3.2 Solution concentrations of calcium versus the calculated carbonate ratio in the solid measured from super- and undersaturation....73

Figure 3.3 Solution concentrations of chloride versus the calculated carbonate ratio in the solid measured from super- and undersaturation....74
Figure 3.4 Solution concentrations of aluminum versus the calculated carbonate ratio in the solid measured from super- and undersaturation....75
Figure 3.5 Calculated mineral saturation indices (SI) for the A and B replicates from super- and undersaturation....77

Figure 3.6 XRD patterns for A-replicate samples between the Cl and CO_3 end members from supersaturation....78
Figure 3.7 XRD patterns for A-replicate samples between the Cl and CO_3 end members from undersaturation....79
Figure 3.8 SEM photomicrographs of solids from the experiment from supersaturation....82
Figure 3.9 Log values of the solubility products (K_{sp}) for the solid solution phases versus the calculated carbonate ratio in the solid....83
Figure 3.10 Lippmann phase diagram for the series between the chloride and carbonate end members at 25 °C....91

Figure 4.1 Electrical conductance versus reaction time for experiments from super- and undersaturation....101
Figure 4.2 Solution concentrations of calcium as a function of the calculated carbonate ratio in the solid solution phases....104
Figure 4.3 Solution concentrations of aluminum as a function of the calculated carbonate ratio in the solid solution phases....105
Figure 4.4 Mineral saturation indices versus the calculated carbonate ratio in the solid for the A and B replicates from super- and undersaturation....106
Figure 4.5 XRD patterns for the A-replicate samples between the CO_3 and OH end members in the experiment from supersaturation....110
Figure 4.6 XRD patterns for the A-replicate samples between the CO_3 and OH end members in the experiment from undersaturation....111
Figure 4.7 Log values of the solubility product (K_{sp}) for solid solution phases as a function of the carbonate ratio in the solid measured from super- and undersaturation....122

Figure 5.1 Calculated log K_{sp} values for Friedel's salt versus measured solution concentrations of a) calcium, b) chloride and c) aluminum.....140
Figure 5.2 Calculated log K_{sp} values for monocarboaluminate versus measured solution concentrations of a) calcium b) aluminum and c) carbonate.....141
Figure 5.3 Calculated log K_{sp} values for OH-hydrocalumite versus measured solution concentrations of a) calcium and b)aluminum.....142

Figure 6.1 XRD patterns for solids during the formation of the OH end member.....160
Figure 6.2 XRD patterns for solids during the formation of the Cl end member.....161
Figure 6.3 Fraction of Cl^- exchanged into the OH end member as a function of time.....165
Figure 6.4 Mole fraction of Cl exchanged into the solid as a function of the mole fraction available for exchange.....166
Figure 6.5 XRD patterns for solids as a function of the amount of Cl^- added.....167
Figure 6.6 Fraction of Cl^- exchanged into the OH end member versus the Cl^- addition factor.....168
Figure 6.7 XRD patterns for solids as a function of the Cl^- addition factor.....169
Figure 6.8 Calculated saturation indices (SI) for portlandite, hydrogarnet, Ca-oxychloride and halite with increasing Cl^- addition factors.....171
Figure 6.9 Photographs of solids with a Cl- addition factor of 20 taken using an optical microscope.....172
Figure 6.10 Quantity of Cl^- released to solution from the solid as a function of reaction time.....173
Figure 6.11 Carbonate concentration in solution as a function of reaction time in the chloride-carbonate exchange experiment (using Na_2CO_3).....174
Figure 6.12 XRD patterns of solids from the chloride-carbonate exchange experiment 1 and 55 days after spiking with Na_2CO_3.....176
Figure 6.13 XRD patterns for solids from the chloride-carbonate exchange experiment 1, 7, and 21 days after spiking with $CaCO_3$.....177
Figure 6.14 Molar ratio of Cl/(Cl+OH) in the solid versus the ration in the aqueous solution (combined data from the solubility and ion exchange experiments.....180

Figure 7.1 Summary diagram of phase relations between the OH, Cl and CO_3 end members.....194

Chapter 1

Introduction

Portland cements contain trace amounts of chloride as an impurity, and chloride may constitute up to 0.6% of a concrete by weight if aggregates containing chloride are used to prepare the concrete. Alternatively, Cl^- ions may ingress into concrete structures if they are exposed to seawater or road salt. A literature review on the binding of chloride in cementitious systems was conducted in which monochloroaluminate hydrate (Friedel's salt) was identified as the dominant mineralogical control on chloride concentrations in cement-based materials. The results of this review are summarized in Section 1.1. The available data on the crystal structure and thermal stability of Friedel's salt are then reviewed, and the identification of Friedel's salt and related solid solutions using X-ray diffraction (XRD) analysis is discussed. In the final two sections of this chapter, an overview of the differences between the solubility and ion exchange approaches is given, and the objectives of the thesis are presented.

1.1 Mineralogical controls on chloride

Chloride can be incorporated into the hydrated products of tricalcium aluminate ($3CaO{\cdot}Al_2O_3$) and tetracalcium aluminoferrite ($4CaO{\cdot}Al_2O_3{\cdot}Fe_2O_3$); and to a lesser extent, tricalcium silicate ($3CaO{\cdot}SiO_2$). The importance that solubility controls have on chloride concentrations in cement/water systems can be observed by examining porewater compositional changes that occur when cementitious material is under chemical attack. For example, Reardon and Dewaele (1990) examined the effects of carbonation on the porewater composition in grout/water slurries with water/solid ratios of 4:1 and 8:1. Solution chloride concentrations with progressive carbonation are shown in Figure 1.1. Before carbonation, there is no difference in Cl^- concentration between the 4:1 and 8:1 samples, indicating a solubility control on its solution concentration. With progressive carbonation, the pH of the solution decreases. Below a pH of 11.5, the concentrations of Cl^- rise sharply and in the 4:1 samples become double those in the 8:1 samples, indicating a lack of solubility control.

1.1.1 Chloroaluminates and oxychlorides

Monochloroaluminate hydrate, more commonly referred to as monochloride or Friedel's salt, is the mineral most often identified in cement pastes containing chloride. Trichloroaluminate hydrate and calcium oxychlorides also have been suggested as possible chloride phases in cements (Birnin-Yauri, 1993; Pöllmann and Kuzel, 1998; Ramachandran, 1971).

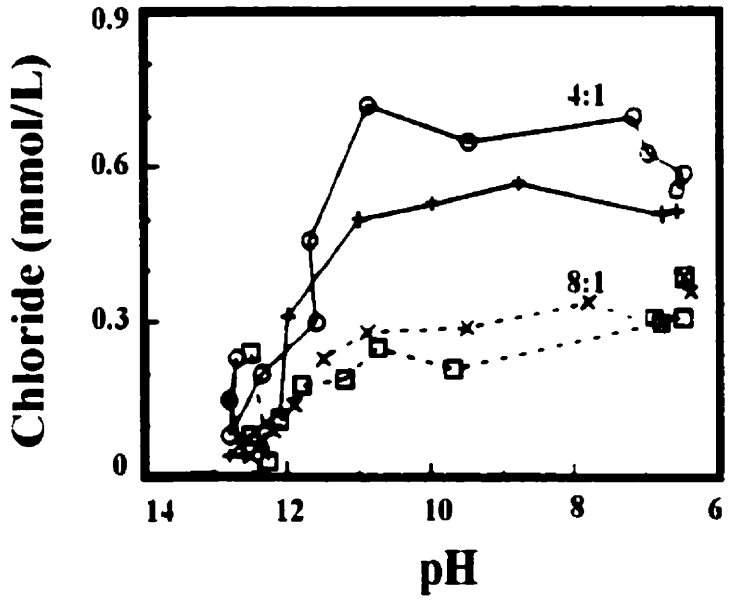


Figure 1.1: Chloride concentration in solution versus pH with progressive carbonation of cementitious material. The circles and plus symbols are replicates at a water:grout ratio of 4:1; Crosses and squares are replicate runs with a water:grout ratio of 8:1 (After Reardon and Dewaele, 1990).

Friedel's salt ($3CaO{\cdot}Al_2O_3{\cdot}CaCl_2{\cdot}10H_2O$ or $C_4ACl_2H_{10}$ in cement nomenclature) is the chloride phase most often identified in hydrated cement pastes and concrete. An extensive solid solution has been observed between Friedel's salt, tetracalcium aluminate hydrate ($3CaO{\cdot}Al_2O_3{\cdot}Ca(OH)_2{\cdot}18H_2O$), and monochloroferrite ($3CaO{\cdot}Fe_2O_3{\cdot}CaCl_2{\cdot}nH_2O$) (Benstead, 1977; Roberts, 1962). Monochloroaluminate is reported to be stable within the pH range 11 to 12.5 (Ben-Yair, 1971), which agrees well with the observations of Reardon and Dewaele (1990).

Trichloroaluminate has the formula $3CaO{\cdot}Al_2O_3{\cdot}3CaCl_2{\cdot}30H_2O$, and is similar in structure to ettringite. This mineral has been synthesized in the laboratory by Schwiete and Ludwig (1969), Ben-Yair (1971), and Bensted (1977). Schwiete and Ludwig (1969) found that trichloroaluminate formed when the calcium chloride concentration in solution was 18% or higher at reaction temperatures between 0 and -10 °C. Savvina (1966) (as discussed by Ben-Yair, 1971) reported the occurrence of trichloroaluminate at temperatures below freezing, and Bensted (1977) confirmed that this phase is not stable at ambient temperatures. Based on these findings, trichloroaluminate can be ruled out as an important control of chloride concentrations in cement/water systems.

Two oxychloride hydrates, tricalcium oxychloride ($3CaO{\cdot}CaCl_2{\cdot}15H_2O$) and monocalcium oxychloride ($CaO{\cdot}CaCl_2{\cdot}2H_2O$), exist in the system $CaO\text{-}CaCl_2\text{-}H_2O$ (Birnin-Yauri, 1993; Pöllmann and Kuzel, 1998; Ramachandran, 1971). Birnin-Yauri (1993) found that tricalcium oxychloride is stable when in contact with solutions containing 3.0-6.0 M Cl^- (10 to 21% by weight), and monocalcium oxychloride is stable in solutions containing 6.0 to 8.0 M Cl^- (21 to 28% by weight). These results agree well with those of Ramachandran (1971), where tricalcium oxychloride was found to be stable at $CaCl_2$ concentrations of 18% or more, and monocalcium oxychloride at concentrations of 34% or more. Tricalcium oxychloride has a solubility product of $10^{-15.25}$ when the Pitzer model is used to calculate activity coefficients (Reardon, personal communication), and is highly soluble compared to monochloroaluminate ($K_{sp} = 10^{-28}$). Therefore, in most cement pastes, as long as aluminum is present, chloride will be precipitated as monochloroaluminate. Even in cement pastes without aluminum, very high concentrations of chloride would be necessary to saturate the pore solution with respect to tricalcium oxychloride. Therefore, calcium oxychlorides can be ruled out as an important control on chloride concentrations in cement pastes.

1.1.2 Chloroferrite hydrates

Hydration of the ferrite phase ($4CaO{\cdot}Al_2O_3{\cdot}Fe_2O_3$) in Portland cements and admixtures results in hydration products that are similar to those formed during the hydration of tricalcium aluminate. The pure iron-rich end member of the solid solution series is monochloroferrite ($3CaO{\cdot}Fe_2O_3{\cdot}CaCl_2{\cdot}10H_2O$). During the early stages of hydration, ettringite and monochloroaluminate are formed from the hydration of the tricalcium aluminate phase, which is more reactive than the ferrite phase. However, at later stages of hydration, hydration of $4CaO{\cdot}Al_2O_3{\cdot}Fe_2O_3$ becomes more important (Bensted, 1977). It is important to note that

although the precipitation of monochloroferrite has been recognized as a possible sink for chloride in cementitious systems (Bensted, 1977, Roberts, 1962), this phase is rarely mentioned in the literature.

Trichloroferrite ($3CaO \cdot Fe_2O_3 \cdot 3CaCl_2 \cdot 30H_2O$) has a structure similar to ettringite, but is unstable at ambient temperatures (Benstead, 1977). Consequently, trichloroferrite would not contribute to the long-term chloride binding capacity of cement.

1.1.3 Calcium silicate hydrates

Results of several studies have suggested that chloride may exist in calcium silicate hydrate (C-S-H), as a chemisorbed complex, as an inter-layer ion, or bound in the lattice (e.g. Beaudoin et al., 1990; Ramachandran,1971). Beaudoin et al. (1990) studied the effect of CaO/SiO_2 and H_2O/SiO_2 ratios on the adsorption- desorption of chloride from C-S-H in a 3.8% calcium chloride solution. Free chloride in the pore solution was defined as the portion of the total chloride that could be removed by both ethanol and water, whereas chemisorbed Cl^- was defined as the portion that could not be removed with ethanol, but could be removed by water. Lattice-substituted Cl^- was defined as the proportion of chloride that could not be removed by ethanol or water leaching. The results of their experiment showed the quantity of chemisorbed Cl^- increased from approximately 0.6 to 1.5% of the total chloride as the CaO/SiO_2 ratio and the H_2O/SiO_2 ratios increased from 0.68 to 1.26 and 1.91 to 6.69, respectively. The quantity of lattice bound chloride varied between 0.01 and 0.25%. No correlation was found between the amount of lattice bound chloride and the H_2O/SiO_2 ratio, or the CaO/SiO_2 ratio. Based on their results, Beaudoin et al. (1990) concluded that chloride exists in both the interlayer positions and on the surface of C-S-H sheets, and that Cl^- may react with Ca^{2+} to form oxychloride complexes which are tightly bound. The sensitivity of the analytical procedures used in their study was not reported, and therefore percentages of 0.01 to 0.25% for lattice bound chloride may not be significant. The research efforts of Beaudoin et al. (1990) suggest that the maximum amount of the total chloride present in C-S-H is 1.5%. Therefore, C-S-H is probably not a major phase controlling the concentration of chloride in cement pastes.

1.2 Stability and solubility of the monocalcium aluminate hydrates

The results of the literature review show that Friedel's salt and its related solid solutions are likely the dominant mineralogical controls on chloride concentrations in cement-based materials. The crystal structure and thermal stability of these phases is examined in the following sections.

1.2.1 Crystal structure

Friedel's salt is the chloride-bearing end member of the hydrocalumite mineral group. The minerals of this group are anionic clay minerals, which have positively-charged main layers. Anions incorporated between the layers balance the charge on the main layers. Water molecules are also incorporated into the interlayers. The generalized structure of the hydrocalumite phases is shown in Figure 1.2. These phases crystallize as thin pseudo-hexagonal plates, composed of distorted portlandite-like octahedral layers, in which one third of the Ca^{2+} sites are occupied by Al^{3+}. The substitution of Al^{3+} for Ca^{2+} generates the net positive charge in the octahedral layers, and this substitution always occurs in a stoichometric 2:1 ratio. In addition to anions, the interlayer contains water molecules (Taylor, 1973), and its water content varies with the type of anion (Sacerdoti and Passaglia, 1988). The interlayer anion can be easily exchanged. Friedel's salt has been shown to form limited solid solutions with many other anions, including hydroxide, sulphate and carbonate.

1.2.2 Thermal stability

Tricalcium chloroaluminate hydrate ($3CaO{\cdot}Al_2O_3{\cdot}3CaCl_2{\cdot}30H_2O$) is reported to be stable below 0 °C (Ben-Yair,1971; Bensted, 1977; Savvina, 1966). Kuzel (1969) determined that the monoclinic form of Friedel's salt (α-$3CaO{\cdot}Al_2O_3{\cdot}CaCl_2{\cdot}10H_2O$) is stable from 0 to 28 °C, and at temperatures between 28 and 200 °C, the rhombohedral β-form is stable. Similarly, Renaudin et al (1999) determined that the phase transition from the monoclinic to rhombohedral structure occurs at 30 °C. Above 200 °C, Friedel's salt loses four waters of hydration to form a hexahydrate. This form is stable to 500 °C when an additional five waters of hydration are lost.

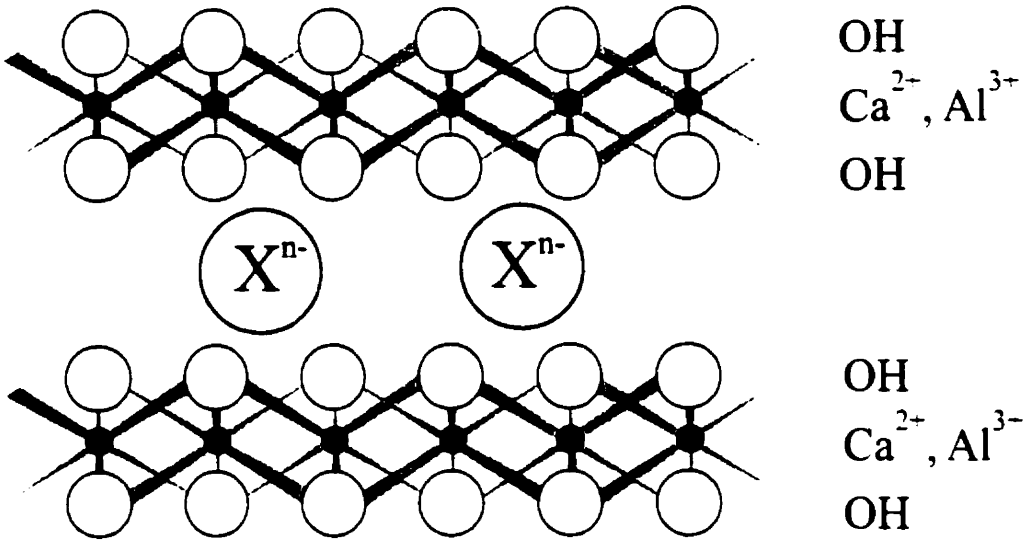


Figure 1.2: Schematic representation of hydrocalumite (layered double metal hydroxide structure) consisting of brucite-like layers intercalated by hydrated anions (from Zhang, 2000: with permission).

Pöllmann (1986) investigated the thermal stability of solids solutions between Friedel's salt and hemicarboaluminate ($3CaO\ Al_2O_3 \cdot 0.5Ca(OH)_2 \cdot 0.5CaCO_3 \cdot 11.5H_2O$). The thermal stability of the solid solutions was found to decrease with decreasing chloride content.

1.2.3 Hydrotalcite-like phases

Hydrotalcite ($Mg_6Al_2(OH)_{16}CO_3 \cdot 4H_2O$) and related layered double hydroxides (LDH) are the most extensively studied anionic clay minerals. Many of their most important applications as sorbents, catalysts, and as ion exchangers are due to their permanent anion-exchange and absorption capacity, and the mobility of their interlayer anions and water molecules (Wang, 2001). The main layers of hydrotalcite are similar to brucite, in which octahedra of Mg^{2+} in 6-fold co-ordinated to OH^- form sheets (Cavani et al., 1991). The substitution of Mg^{2+} by a trivalent ion of similar radius (e.g. Al^{3+}) generates a positive charge in the hydroxyl sheet, which is compensated by anions which lie in the interlayer regions between the brucite sheets. Unlike the hydrocalumite minerals, in which the Ca/Al ratio in the main layers is fixed, the Mg/Al ratio in the main layer of hydrotalcite can vary from 2 to 3.

As a result of the similar structures of the monocalcium aluminate hydrates (or hydrocalumite phases) and hydrotalcite, studies on hydrotalcite-like phases are useful resources for the current study. However, research on hydrotalcite and related phases is most often restricted to ion-exchange studies, because of the extensive use of these phases as sorbents and ion exchangers, or to investigations on their structures. Miscibility gaps (regions containing two solid solution phases with different compositions) have been observed (e.g. Le Bail et al., 1997), but their occurrence is not usually emphasized. Miyata (1983) discussed the appearance of two solid

solution phases at certain compositions, but does not relate this to the stability of these phases. Solubility determinations are rare for members of this mineral group.

1.3 Phase identification using X-ray diffraction analysis

The identification of two primary peaks in the XRD pattern of a solid solution indicates the presence of two different phases with different interlayer thicknesses. These two solid solutions may be

1. The same mineral, in two different hydration states (i.e. differ only in the amount of intercrystalline water).

2. Different minerals (e.g. polymorphs, or different compositions).

Identification of the chloride end member (Friedel's salt), is relatively straight forward. As discussed in Section 1.2.2, Friedel's salt can occur as two different polymorphs, a monoclinic form (α) with a d-spacing of 7.89Å, or a rhombohedral form (β) with a d-spacing of 7.77Å. The reported range of primary d-spacings measured for the carbonate end member, or monocarboaluminate ($3CaO{\cdot}Al_2O_3{\cdot}CaCO_3{\cdot}11H_2O$) is relatively small (7.56 to 7.62 Å). This phase is reported to contain either 10 or 11 waters. Hemicarboaluminate has a composition midway between the carbonate and hydroxyl end members ($3CaO{\cdot}Al_2O_3{\cdot}0.5CaCO_3{\cdot}0.5Ca(OH)_2{\cdot}10\text{-}12H_2O$). Roberts (1969) reported that a more highly hydrated form with 12 waters is stable between relative humidities of 53% and 81%. At relative humidities below 53%, this phase may occur together with a lower hydration product containing 10 water molecules, but below 33% R.H., the lower hydrate is the only phase observed.

Of the phases studied, the OH end member, or OH hydrocalumite ($3CaO{\cdot}Al_2O_3{\cdot}Ca(OH)_2{\cdot}nH_2O$), is the most difficult to identify conclusively. The two hydration states of OH-hydrocalumite most often identified are a lower hydration state with 12 waters, and a higher state with 18 waters. The primary d-spacings measured for the more highly-hydrated form fall in a relatively narrow range from 10.6 to 10.77 Å (Schwiete and Ludwig, 1969). This phase is the stable form in solution, and is reported to be stable in air at relative humidities above 88 % (Roberts, 1969). In contrast, the reported primary d-spacings for the less hydrated form with 12 waters range from 7.76 to 8.28 Å. Within this range, two different forms were originally identified: an α-form with a range of d-spacings from 8.18 to 8.28 Å, and a β-form with d-spacings ranging from 7.76-8.05 Å. Alégre (1962) determined that the two forms of this phase constituted different hydration states of the same phase. The alpha phase with a d-spacing of 8.18 Å contained 12 waters, and was converted to a solid with a d-spacing of 7.82 Å and 11 waters by drying it over lithium chloride. Roberts (1969) later reinterpreted the results of Alégre (1962), and based on the results of his own research, suggested that the phase with a d-spacing of 8.2 Å was hemicarboaluminate with 11 water molecules, and that this phase lost 2 water molecules to form a phase with a d-spacing of 7.7 Å when dried over LiCl (R.H. = 15%). Roberts (1969) further concluded that there was only one OH end member, which had a d-spacing of 7.9 Å and 12 water molecules in its interlayer.

1.4 Solubility and ion exchange

1.4.1 Solubility

The solubility of pure mineral phases is expressed by an equilibrium constant. For example, for pure calcite ($CaCO_3$) the dissolution reaction is

$$CaCO_{3(s)} \rightleftharpoons Ca^{2+} + CO_3^{2-} \qquad (1.1)$$

and the distribution of calcium and carbonate ions between the solid and aqueous phases at equilibrium can be described by the expression

$$\text{Log } K_{eq} = \frac{[Ca^{2+}][CO_3^{2-}]}{[CaCO_{3(s)}]} \qquad (1.2)$$

where K_{eq} is the solubility product of calcite at equilibrium, and the square brackets denote

activities. By definition, the activity of a pure solid phase is equal to 1. The aqueous concentrations of calcium and carbonate in solution can be measured at thermodynamic equilibrium, and the activity coefficients of these ions in solution can be calculated (e.g. using Debye-Huckel theory). The solubility product constant for calcite can then be calculated using equation 1.2.

When the mineral phase involved forms solid solutions, as is the case with Friedel's salt, the activity of the solid phase is not equal to 1. Instead, the solid phase activity depends on its composition, and therefore, the solubility product varies as a function of the solid solution composition. Unlike ionic species in solution, there is no generally accepted theory for calculating the activity coefficients for the substituting ions in the solid phase. However, the solubility of solid solutions at thermodynamic equilibrium can be described using solid solution aqueous solution theory (SSAS). The two basic conditions defining thermodynamic equilibrium in a binary solid-solution aqueous-solution (SSAS) system BA-CA-H_2O are (Glynn and Reardon, 1990):

$$[B^-][A^-] = K_{BA}\, a_{BA} = K_{BA}\, X_{BA}\, \gamma_{BA} \qquad (1.3)$$

$$[C^-][A^-] = K_{CA}\, a_{CA} = K_{CA}\, X_{CA}\, \gamma_{CA} \qquad (1.4)$$

where $[B^-]$, $[C^-]$ and $[A^-]$ are the aqueous activities of the ions; K_{BA} and K_{CA} are solubility products of pure BA and CA end members; a_{BA} and a_{CA} are the activities of the pure solids; X_{BA} and X_{CA} are the mole fractions of components BA and CA in the solid solution at equilibrium; and γ_{BA} and γ_{CA} are the solid-phase activity coefficients.

Lippmann (1977, 1980) derived an equilibrium variable by adding equations 1.3 and 1.4 together:

$$\Sigma\Pi = [A^-]([B^-] + [C^-]) = K_{BA}a_{BA} + K_{CA}a_{CA} \qquad (1.5)$$

This variable is referred to as the total solubility product ($\Sigma\Pi$), and can be used to describe the solubility of solid solutions between the solid and aqueous phases at thermodynamic equilibrium.

1.4.2 Ion exchange

In the anionic clays such as Friedel's salt, anions in the interlayers of the mineral structure are easily exchangeable for other anions. The exchange of OH^- ions in the OH end member of the monocalcium aluminate hydrates by Cl^- ions in solution can be formulated as

$$Cl^- + SOH \rightleftharpoons SCl + OH^- \qquad (1.6)$$

where S indicates positively charged sites in the main layer of the mineral. A selectivity coefficient (K_{ex}) for this exchange reaction is then defined by

$$K_{ex} = \frac{X_{SCl}[OH^-]}{X_{SOH}[Cl^-]} \qquad (1.7)$$

where the square brackets denote the activity of the anions in solution, and X represents the mole fraction of the counterion on the exchanger. Selectivity coefficients are not constants, because the activities of the anions within the interlayer are unknown, and vary with the composition of the ion-exchanger phase (Stumm and Morgan, 1981).

The relationship between the selectivity coefficient expression (equation 1.7) and the conditions which must hold at thermodynamic equilibrium for a solid solution can be obtained by dividing equations 1.3 and 1.4 by one another:

$$D = \frac{X_{CA}}{X_{BA}} \Big/ \frac{[C^-]}{[B^-]} \qquad (1.8)$$

In this expression, the terminology "distribution coefficient" (D) is used instead of selectivity coefficient. In the process of dividing the equations, information about the aqueous activity of the non-substituting ion (A^- in this case), and consequently, about the solubility of the solid solution is lost. Therefore, although distribution or selectivity coefficients derived from ion exchange experiments can be used as a measure of thermodynamic equilibrium in SSAS systems, they do not provide a measure of its solubility (Glynn and Reardon, 1990). Distribution coefficients are commonly used to describe experimentally observed partitioning of trace components between the solid and aqueous phases under specific conditions in a semi-empirical manner (Apello and Postma, 1994).

Although there are limitations to the usefulness of selectivity or distribution coefficients, ion exchange experiments can provide important information about the kinetics of the exchange process, if the exchange of one ion by another is monitored with time. This is information that can not be obtained from solubility measurements of solid solution phases at thermodynamic equilibrium.

1.5 Objectives

The study of Friedel's salt and related solid solutions has important applications to concrete engineering, because the concentration of chloride in concrete pore solutions has been identified as a key factor in the corrosion of reinforcing bar. An understanding of the stability of this phase is also required in disposal concepts for irradiated concrete, because radioactive ^{36}Cl (which is considered a critical radionuclide), has been identified in these materials. In the early stages of cement hydration, the interlayer of the monocalcium aluminate hydrates is dominated by OH^- and SO_4^{2-} ions, but with time, these may be exchanged by chloride or carbonate. For this reason, information on the stability of both the hydroxyl and carbonate end members, and the solid solutions formed between these phases and Friedel's salt is required to assess the stability range of Friedel's salt.

Detailed crystallographic studies have been conducted on the solid solution series between Friedel's salt (or the Cl end member) and the hydroxyl end member, between the Cl and CO_3 end members, and between the OH and CO_3 end members of the monocalcium aluminate hydrates. However, solubility data for these phases in the literature is limited primarily to the Cl, OH and CO_3 end members. The first objective of this thesis was to measure the solubility of the solid solutions in these three series at thermodynamic equilibrium, and to confirm the miscibility gaps and regions of solid solution as determined by previous researchers. To this end, solubility experiments were conducted from both supersaturation and undersaturation. The solid and solution phases were examined for compositional variations, and the positions of miscibility gaps were determined from the observed mineral phase assemblages, combined with the mineral saturation indices calculated from the solution compositions.

A second objective of this thesis was to develop a description of the partitioning of chloride between the solid solution phase and the aqueous solution phase at equilibrium, using SSAS theory. The solubilities of the solid solutions measured as a function of the composition of the solid solution phase were used for this purpose in both the OH-Cl and Cl-CO_3 systems.

Although solubility measurements at thermodynamic equilibrium are useful, cement-based systems are rarely at equilibrium. Hydration of the high temperature minerals used to prepare cement pastes can continue for years, and "foreign" ions, such as Cl^-, can ingress into cement materials by exposure to seawater or road salt. Alternatively, chloride ions in the interlayer of Friedel's salt may be exchanged by carbonate ions, releasing Cl^- to the pore solution. Consequently, the final objective of this study was to investigate the rate and extent of exchange of anions in the monocalcium aluminate hydrates. Exchange of anions from the interlayer of these minerals was investigated between the OH and Cl end members as a function of time, and as a function of Cl^- concentration. The exchange of Cl^- ions from Friedel's salt by carbonate ions was also investigated. The solution composition was monitored to determine the extent of exchange, and selected solid samples were examined using X-ray diffraction analysis.

The results of the solubility experiments and SSAS modeling in the OH-Cl, Cl-CO_3 and OH-CO_3 solid solutions series are discussed in Chapters 2, 3 and 4, respectively. In Chapter 5, solubility data for the hydroxyl, chloride, and carbonate end members from published research and from the current study are compiled and evaluated to generate average solubility products for these end members. These values were required in the SSAS modeling of the solid solution series. The results of the ion exchange experiments are discussed in Chapter 6, and in Chapter 7, the contributions of this thesis to the scientific continuum are reviewed.

1.6 References

Alégre (1962). Investigations on hexagonal C_4AH_x. *Rev. Mater. Constr.*, **566**, 301-314.

Apello C. A. J. and Postma D. (1994). Geochemistry, groundwater and pollution. A. A. Balkema Publishers, Brookfield, U.S.A.

Beaudoin J. J., Ramachandran V. S., and Feldman R. F. (1990). Interaction of chloride and C-S-H. *Cem. Concr. Res.*, **20**, 875-883.

Bensted J. (1977). Chloroaluminates and the role of calcium chloride in accelerated hardening of Portland cement. *World Cement Technology*, **September-October**, 171-175.

Ben-Yair M. (1971). Studies on the stability of calcium chloroaluminate. *Israel Journal of Chemistry*, **9**, 529-536.

Birnin-Yauri U. A. (1993). Chloride in cement: Study of the system $CaO-Al_2O_3-CaCl_2-H_2O$. Ph.D. Thesis, University of Aberdeen, Aberdeen, United Kingdom.

Cavani F., Trifir F., and Vaccari A. (1991). Hydrotalcite-type anionic clays: Preparation, properties and applications. *Catalysis Today*, **11**, 173-301.

Glynn P. D. and Reardon E. J. (1990). Solid-solution aqueous-solution equilibria: Thermodyanmic theory and representation. *Am. J. Science*, **290**, 164-201.

Kuzei H.J. (1969). X-ray investigations of some complex calcium aluminate hydrates and related compounds. *Proc. 5th Int. Symp. Chem. Cem.*, Tokyo, **II**, 92-97.

Le Bail C., Thomassin J. and Touray J. (1987). Hydrotalcite-like solid solutions with variable SO_4^{2-} and CO_3^{2-} contents at 50 °C. An X-ray Diffraction and Raman spectrometry study. *Phys. Chem. Minerals*, **14**, 377-382.

Lippmann F. (1977). The solubility product of complex minerals, mixed crystals and three layer clay minerals. *N. Jb. Miner. Abh.*, **130**, 243-263.

Lippmann F. (1980). Phase diagrams depicting aqueous solubility of binary mineral systems. *N. Jb. Miner. Abh.*, **139**, 1-25.

Miyata S. (1983). Anion-exchange properties of hydrotalcite-like compounds. *Clays and Clay Minerals*, **31**, 305-311.

Pöllmann H. (1986). Solid solution of complex calcium aluminate hydrates containing Cl^-, OH^- and CO_3^{2-} anions. *Proc. 8th Int. Symp. Chem. Cem.*, Rio de Janeiro, Supplementary paper, **Vol. III**, 300-306.

Pöllmann H. and Kuzel H. J. (1988). Synthesis and polymorphic transformations of solid solutions in the system $3CaO{\cdot}Al_2O_3{\cdot}CaCl_2{\cdot}nH_2O$- $3CaO{\cdot}Al_2O_3{\cdot}Ca(OH)_2{\cdot}nH_2O$-$H_2O$. *N. Jb. Miner. Mh.*, 193-202.

Ramachandran V. S. (1971). Possible states of chloride in the hydration of tricalcium silicate in the presence of calcium chloride. *Materials and Structures. Research and Testing*, **4**, 3-12.

Reardon E. J. and Dewaele P. (1990). Chemical model for the carbonation of a grout/water slurry. *J. Am. Ceram. Soc.*, **73**, 1681-1690.

Renaudin G., Kubel F., Rivera J.-P., and Francois F. (1999). Structural phase transition and high temperature phase structure of Friedels salt, $3CaO{\cdot}Al_2O_3{\cdot}CaCl_2{\cdot}10H_2O$. *Cem. Concr. Res.*, **29**, 1937-1942.

Roberts, M. H. (1962). Effect of calcium chloride on the durability of pre-tensioned wire in prestressed concrete. *Magazine of Concrete Research*, **14**, 143-154

Roberts M. H. (1969). Calcium aluminate hydrates and related basic salt solutions. Supplementary Paper II-29. *Proc. 5th Int. Symp. Chem. Cem.*, 104-117.

Sacerdoti M. and Passaglia E. (1988). Hydrocalumite from Latium, Italy: its crystal structure and relationship with synthetic phases. *N. Jb. Miner. Mh.*, **10**, 462-475.

Savvina Y.A. et al. (1966). *Stroit. Prom.*, **9**, 31

Schwiete H. E. and Ludwig U. (1969). Crystal structures and properties of cement hydration products (hydrated calcium aluminates and ferrites). *5th Int. Symp. Chem. Cem.*, Session **II-2**. Tokyo. 37-67.

Stumm W. and Morgan J. J. (1981). Aquatic Chemistry: An introduction emphasizing chemical equilibria in natural waters. 2nd Ed., John Wiley & Sons.

Taylor H.F.W. (1973). Crystal structures of some double hydroxide minerals. *Min. Mag.*, **39**, 377-389.

Wang J., Kalinichev A. G., Kirkpatrick R. J. and Hou X. (2001). Molecular modeling of the structure and energetics of hydrotalcite hydration. *Chem. Mater.*, **13**, 145-150.

Zhang M. (2000). Incorporation of oxyanions B, Cr, Mo, and Se into hydrocalumite and ettringite: application to cementitious systems. Ph.D. Thesis, University of Waterloo, Waterloo, Canada.

Chapter 2

Solubility of solid solutions in the system $CaO\text{-}Al_2O_3\text{-}CaCl_2\text{-}H_2O$

2.1 Introduction

The monocalcium aluminate hydrate phases ($4CaO{\cdot}Al_2O_3{\cdot}nH_2O$) play an important role in cement hydration reactions. These minerals crystallize as thin pseudohexagonal plates, and their crystal structure consists of distorted portlandite-like layers of $[Ca_2Al(OH)_6]^+$, separated by interlayer regions of anions and water molecules $[X \cdot nH_2O]^-$. The chloride-rich phase, Friedel's salt ($3CaO{\cdot}Al_2O_3{\cdot}CaCl_2{\cdot}10H_2O$), forms limited solid solutions with many other anions including hydroxide, sulphate and carbonate (Glasser et al., 1999). Friedel's salt is the chloride-bearing phase most often identified in hydrated cement pastes and concrete, and is likely the dominant mineralogical control on chloride concentrations in cement-based materials. Understanding the stability of this phase is particularly important in the disposal of irradiated concrete, because radioactive ^{36}Cl has been identified in this material (Kimura et al., 1994). Chlorine-36 is considered a critical radionuclide in disposal concepts, because of its long half-life (3.01×10^5 years), and its high mobility in terrestrial environments (Bentley et al., 1980). The study of Friedel's salt and related solid solutions also has important applications to concrete engineering, because the concentration of chloride in pore solutions has been identified as key factor in the corrosion of reinforcing bar.

Several studies have examined the solid solution phases that form between Friedel's salt, and the hydroxide end member ($3CaO{\cdot}Al_2O_3{\cdot}Ca(OH)_2{\cdot}nH_2O$) of this series (Turriziani and Schippa, 1955; Roberts, 1969; Pöllmann and Kuzel, 1988; Birnin-Yauri,1993; and Birnin-Yauri and Glasser, 1998). The largest discrepancy between the various studies is over the existence and/or the extent of a miscibility gap. The formation of a complete solid solution between the chloride and hydroxide end members was reported by Turriziani and Schippa (1955), and by Birnin-Yauri and Glasser (1998). In the study conducted by Turriziani and Schippa (1955), calcium chloride solutions were mixed with saturated calcium aluminate solutions at chloride molar ratios ranging from 1.0 to 0.1. The chloride molar ratio is defined as the ratio of chloride to total anions (Cl/(Cl + OH)) in the interlayer of the solid solution phase. XRD analysis of the moist

solids showed that the solid solutions consisted of a single phase. At a Cl/(Cl+OH) ratio of 1.0, the basal spacing was 7.95 Å, but increased to 8.10 Å as the chloride ratio in the solid decreased to 0.2.

Birnin-Yauri (1993) and Birnin-Yauri and Glasser (1998) report the occurrence of a complete solid solution between the chloride and hydroxide end members. However, this interpretation is inconsistent with their reported results. In their study, samples with Cl/(Cl+OH) ratios between 1.0 and 0.1 were prepared by the hydration of mixtures of tricalcium aluminate ($3CaO.Al_2O_3$), CaO, and $CaCl_2 \cdot 2H_2O$ in an excess of aqueous phase. The samples were maintained at 20 °C, and agitated intermittently for 17 months. The solids were analyzed using XRD analysis (equilibrated at 100% relative humidity) and scanning electron microscopy (SEM) with energy dispersive x-ray (EDXA) analysis. The XRD results indicated the presence of two solid solutions at a chloride ratio of 0.2. One solid solution was identified as the OH end member ($3CaO \cdot Al_2O_3 \cdot Ca(OH)_2 \cdot 18H_2O$) with a d-spacing of 10.7 Å. The composition of the other phase was determined as $3CaO \cdot Al_2O_3 \cdot 0.25CaCl_2 \cdot 0.75Ca(OH)_2 \cdot xH_2O$ using EDXA analysis. The co-existence of two solid solution phases with different compositions demonstrates the existence of a miscibility gap.

A miscibility gap between the chloride and hydroxide end members has been reported by Roberts (1969) and by Pöllmann and Kuzel (1988). In the study by Roberts (1969), suspensions of $3CaO \cdot Al_2O_3 \cdot Ca(OH)_2 \cdot 18H_2O$ were treated with increasing additions of $CaCl_2$. The solids from these experiments were equilibrated at 81% relative humidity before XRD analysis. The molar compositions of the solids were calculated using the total initial composition of the reaction mixture and the final measured solution compositions. Based on the XRD results, the solid solution was the dominant phase between chloride ratios of 1.0 and somewhere between 0.58 and 0.4. From 0.4 to 0.13, a miscibility gap was evidenced by the coexistence of two phases: the OH end member with a basal spacing of 10.7 Å, and a solid solution phase with a basal spacing between 7.9 and 8.0 Å. Roberts (1969) suggested that the solid with the smaller d-spacing was the chloride-bearing solid solution phase.

Pöllmann and Kuzel (1988) performed a detailed characterization of the solids formed between the chloride and hydroxide end members. Solid solutions were prepared by hydration of pastes prepared with monocalcium aluminate ($CaO \cdot Al_2O_3$), CaO, and $CaCl_2 \cdot 2H_2O$. The samples were shaken continuously at 25 °C for 6 months, before the precipitates were filtered in a N_2 - atmosphere. X-ray diffraction analysis of the solid phases was performed at relative humidities of 100% and 35%, using silica as an internal standard. The XRD results at 100% relative

humidity demonstrated the formation of a limited solid solution between Cl/(Cl+OH) ratios of 1.0 to 0.4. Below 0.4, two solid solution phases with distinctive d-spacings coexisted. The solid solution phase with a d-spacing of 10.6 Å was identified as the OH end member, and the other solid solution phase with a d-spacing of 7.9 Å was attributed to a phase with composition $3CaO{\cdot}0.33CaCl_2{\cdot}0.67\ Ca(OH)_2{\cdot}11.4\ H_2O$. This demonstrates the presence of a miscibility gap that begins slightly above a Cl/(Cl+OH) ratio of 0.3 and extends down to at least 0.1, whereas the results of Roberts (1969) suggest the miscibility gap begins slightly above 0.4 and extends down to at least 0.13. However, Roberts (1969) were not certain of the occurrence of a trace amount of $3CaO{\cdot}Al_2O_3{\cdot}Ca(OH)_2{\cdot}18H_2O$ in the solid with a chloride ratio of 0.4, and the next ratio examined was 0.17. This suggests that the upper limit of the miscibility gap is better defined by the data of Pöllmann and Kuzel (1988). The lowest Cl/(Cl+OH) ratio examined by Roberts (1969) was 0.13, which was still within the miscibility gap. The lowest chloride ratio where Pöllmann and Kuzel (1988) observed two solid solution phases present was 0.1. This suggests that the lower limit of the miscibility gap lies between chloride ratios of 0.1 and 0.0.

In a binary solid solution series, predictions of the final equilibrium partitioning between the solid solution and aqueous solution phases can be made using solid-solution aqueous-solution (SSAS) theory (Glynn and Reardon, 1990; Glynn et al. 1990), if the solid-phase activity coefficients are known. Thermodynamic equilibrium measurement of solid solution solubilities is the best method for obtaining solid solution excess-free energies, but stoichiometric saturation measurements may also be used in some cases. The excess-free energies are then used to calculate solid phase activities.

The current study was undertaken to determine the solubility of solid solutions with varying amounts of chloride, between the pure hydroxide and chloride end members of the calcium aluminate hydrates. Solubility experiments were conducted starting from supersaturated conditions, and were then repeated from undersaturation, to determine if equilibrium had been attained in the system. The solution compositions were measured, and the solid phases were identified using X-ray diffraction (XRD) analysis and scanning electron microscopy. Solubility data measured from undersaturation as a function of the chloride ratio in the solid phase was fitted to Guggenheim's (1937, 1952) expansion series for a binary, sub-regular solid solution using regression analysis. The derived parameters have been used in conjunction with the solubility products of the pure end members to create a Lippmann diagram (Lippmann, 1980) for this system. This diagram can be used to estimate equilibrium partitioning between the solid solution and aqueous solution.

2.2 Experimental

The materials, experimental procedures and analytical methods described in this section are the general procedures used for the solubility experiments performed between the chloride and hydroxide end members (Chapter 2), the chloride and carbonate end members (Chapter 3), and the carbonate and hydroxide end members (Chapter 4) of the calcium aluminate hydrate phases.

2.2.1 Materials

All chemicals used were reagent-grade quality. Calcium chloride dihydrate was used to prepare all $CaCl_2$ solutions. Doubly-deionized water with a conductance of <1.0 μS/cm was used to prepare solutions and standards. Dispensing of all water, solution and solid aliquots was done by mass and recorded to at least three significant figures.

Monocalcium aluminate ($CaO{\cdot}Al_2O_3$) was prepared by combusting an aluminum nitrate-calcium nitrate-urea mixture according to the procedure described by Kingsley and Patil (1988). A typical combustion run yields approximately 4 g of recoverable monocalcium aluminate. A total of ten batches of the material was prepared, and a sample from each batch was analyzed by X-ray diffraction (XRD). Two homogeneous materials for use in the solid-solution synthesis experiments were prepared by mixing five of the solids together by grinding with an agate mortar and pestle. Each mixed solid was then used to prepare a set of replicate samples for use in the solubility experiment from supersaturation.

Calcium oxide was prepared by calcination of $CaCO_3$ at 950°C in a muffle furnace. Calcium carbonate was weighed into a ceramic crucible and placed into the muffle furnace for approximately 24 hours. The crucible was transferred to a glass desiccator under vacuum and cooled to room temperature. The final mass of the crucible was measured and the mass loss due to calcination was calculated to be within 0.5% of the theoretical mass loss.

2.2.2 Experimental procedure

Experiments were performed from supersaturation by preparing particular composition solids in the solid solution series, according to the method of Pöllmann and Kuzel (1988). Weighed

amounts of $CaO{\cdot}Al_2O_3$ and CaO were added to 60 ml high density polyethylene bottles (HDPE). For solid solutions containing carbonate, a weighed amount of solid $CaCO_3$ was also added. The bottles were transferred into a glove box under a nitrogen atmosphere to minimize sample contamination by CO_2. For solids with compositions between the chloride and hydroxide end members, or between the chloride and carbonate end members, doubly-deionized water and varying amounts of 0.09 molal $CaCl_2$ solution were added to a final volume of 55 ml to produce a range of Cl/(Cl+OH) or CO_3 ($2Cl+CO_3$) ratios from 0 to 1. In the carbonate-hydroxide series, 55 ml of doubly-deionized water was added to the samples. The samples were prepared to have a final solution:solid ratio of 20:1. All samples were prepared in duplicate. Three additional samples (triplicates) were prepared for the end members in the solid solution series and for the solid having a composition mid-way between the end members. After preparation, the reaction bottles were transferred out of the glove box, placed on a vertically-rotating wheel, and submerged in a 25 °C constant temperature bath. The approach to equilibrium for the entire set of samples was monitored by regular conductance measurements on the triplicate samples.

After 170 days, the solubility experiment from supersaturation was terminated, and the samples were transferred into the glove box. The bottles were shaken, 1 ml of slurry removed using a glass Pasteur pipette, and placed onto a glass slide for X-ray diffraction (XRD) analysis. The remainder of the solution was filtered through a 0.45 μm cellulose nitrate filter paper using a Buchner funnel, a vacuum flask and an aspirator. The filtered solution was split for analysis for cations, anions, and pH measurements. For solid solution phase compositions containing carbonate, CO_2 analysis was conducted on a portion of the anion sample before it was diluted with doubly deionized water to a final sample:water ratio of 1:1. The cation samples were acidified using 1:1 nitric acid. The recovered solids were transferred into pre-weighed scintillation vials. The recovered solids from both super- and undersaturation, and the slurries on glass slides (for XRD analysis) were dried in a desiccator over a saturated $CaCl_2{\cdot}6H_2O$ solution (35% R.H.). The desiccator was stored in the glove box, to minimize contamination of the solids by atmospheric CO_2.

A second solubility experiment from undersaturation was conducted by adding 0.5 g of each solid recovered from the supersaturation experiment to 30 ml HDPE bottles. The reaction bottles were transferred to the glove box, and 10 g of doubly-deionized water was added, with a resultant solution:solid ratio of 20:1. The conditions for reaction, monitoring and sampling were the same as those used in the experiment from supersaturation, except that the reaction time was 515 days, and CO_2 analysis was not conducted.

The investigation of the solubility of the Cl end member was extended in an additional experiment, because the calculated ratio of Cl in the end member sample from supersaturation was calculated to be 0.91, instead of the predicted value of 1.0. The sample preparation and sampling methods were the same as those used in the experiment from supersaturation, except that the amount of calcium chloride added to the samples was increased by 25 or 50%. The experiment was sampled after 170 days of reaction.

2.2.3 Analytical methods

The pH of samples was measured using a Fisher Scientific Accumet® 50 pH meter with an Orion Ross® combination electrode calibrated against NBS pH buffer 7.01 and a 0.01 *m* boric acid solution with a pH of 9.18 at 25 °C. Solution conductance was measured using a Cole-Parmer ® conductivity meter. The conductivity probe was calibrated against a 0.01 *m* KCl solution (1408 μS at 25 °C), and the temperature of the solution was recorded using a thermometer. The conductance measurements were corrected for the cell constant and corrected to 25 °C from the temperature of the sample solution. All measurements were made in a glovebox to minimize CO_2 contamination.

Solutions were analyzed colorimetrically for aluminum using the catechol violet method adapted from Dougan and Wilson (1974). The lower and upper detection limits of this method were 0.03 and 0.3 ppm, respectively. Calcium was analyzed using atomic adsorption spectrophotometry (AAS). Chloride was analyzed colorimetrically using the mercuric thiocyanate method (automated) with a detection limit of 0.2 mg/L. The analytical uncertainty of all analyses was better than ±5%.

The dissolved inorganic carbon (DIC) of solutions was determined using a method adapted from Barker and Chatten (1982). In this method, the addition of acid to solutions converts dissolved CO_3^{2-} and HCO_3^- ions to $CO_{2\,(aq)}$, which partitions into the gas phase as described by Henry's law. The headspace is then analyzed for CO_2. All blanks, standards and samples were prepared 50 ml glass syringes, in a nitrogen atmosphere. The barrel of a syringe was withdrawn slightly to create 10 ml of headspace, a known mass of sample or standard was injected into the glass syringe, and then the tip of the syringe was sealed with a septum. The glass syringes were removed from the glove box, and 2 ml of 2.0 *m* HNO_3 was injected into each syringe. The glass syringes were lightly shaken, and allowed to equilibrate for approximately 2 hours before

analysis. Headspace concentrations of CO_2 were measured using a GOW-MAC gas chromatograph with a thermal conductivity detector. Standards with headspace concentrations between 0.1% and 7.0% CO_2 were prepared from a 0.1 *m* Na_2CO_3 stock solution. A calibration curve was constructed by plotting the measured peak areas for the gas standards against their known DIC concentrations. The reproducibility for this technique is ± 5%, and the detection limit is 0.061 mmol/L CO_2.

The solids from the undersaturation experiment were prepared on glass slides, and these were secured to aluminum planchettes before XRD analysis. Solids from the undersaturation experiment were packed directly into aluminum planchettes. XRD analyses were performed using a Siemens Kristalloflex diffractometer. All solids were irradiated with nickel-filtered Cu K alpha radiation (λ_1=1.5406 Å, λ_2=1.5444 Å) generated at 50 kV and 30 mA. Complete ranges were scanned from 5 to 55 degrees, using steps of 0.05, and 1 second per step. The recorded data were interpreted using powder diffraction files from the Joint Committee on Powder Diffraction Standards and the International Center for Diffraction Data (JCPDS-ICDD), and from XRD patterns reported in the literature (Table 2.1). Electron micrographs were taken using a JOEL JMS-840 scanning electron microscope (SEM).

Solid Phase	Pattern No.	Temp. (C)	R.H. (%)	Basal Spacing	Reference
α-Friedel's salt	19-202	150	35	7.89	JCPDS-ICDD
(monoclinic)		22	35	7.90	Fisher et al. (1980)
β-Friedel's salt	31-245	---	---	7.771	JCPDS-ICDD
(rhombohedral)		40	35	7.81	Fisher et al. (1980)
Monocarboaluminate		RT	33	7.565	Carlson and Berman (1960)
		22	36	7.570	Fisher and Kuzel (1982)
OH-end member					
$3CaO{\cdot}Al_2O_3{\cdot}Ca(OH)_2{\cdot}10H_2O$		25	11	7.4	Schwiete and Ludwig (1969)
$3CaO{\cdot}Al_2O_3{\cdot}Ca(OH)_2{\cdot}12H_2O$		5	11-88	7.92	Buttler et al. (1959)
$3CaO{\cdot}Al_2O_3{\cdot}Ca(OH)_2{\cdot}18H_2O$	14-631	25	>88	10.8	JCPDS-ICDD

Table 2.1: X-ray diffraction patterns used in the identification of the solid phases and references. RT = room temperature.

2.3 Results

In sections 2.3.1 through 2.3.5, the results of the experiments from super- and undersaturation are compared. The results of the extended solubility experiment are then presented separately, in section 2.3.6.

2.3.1 Approach to equilibrium

Figure 2.1 illustrates the conductance measurements with time for the three samples used to monitor the approach of the system to equilibrium in the experiments from supersaturation and undersaturation. In the experiment from supersaturation, the measured conductance for the hydroxide end member was essentially stable at 8400 μS/cm after only 3 days of reaction, and remained at this value for the duration of the experiment. This suggests that a thermodynamic or metastable equilibrium condition was quickly established. In the experiment from undersaturation, this sample immediately attained a similar conductance (7900 μS/cm), and remained relatively constant at this value for 170 days. With continued reaction time, however, the conductance values gradually decreased, reaching a value of 5400 μS/cm when the experiment was terminated after 472 days of reaction. This suggests that the constant conductance attained initially in the experiments from super- and undersaturation represent a metastable condition, and that the solids may be undergoing a phase transformation, indicated by the 30% decrease in conductance during the experiment from undersaturation.

In the experiment from supersaturation, the conductance values measured for the sample with a composition midway between the chloride and the OH end member were stable for the first 40 days of reaction, then decreased gradually, reaching a final value of 4000 μS/cm after 170 days of reaction. Throughout the experiment from undersaturation, the conductance of this sample was approximately stable at 3700 μS/cm, which is approximately 7% lower than the final value measured from supersaturation. The similarity in the conductance values measured from both directions suggests that both experiments closely approached a metastable or thermodynamic equilibrium condition.

The measured conductance of the chloride end member was approximately 11500 μS/cm at the beginning of the experiment from supersaturation, but decreased gradually to a stable value of $\approx$ 3700 μS/cm after 100 days of reaction. In the experiment from undersaturation, the

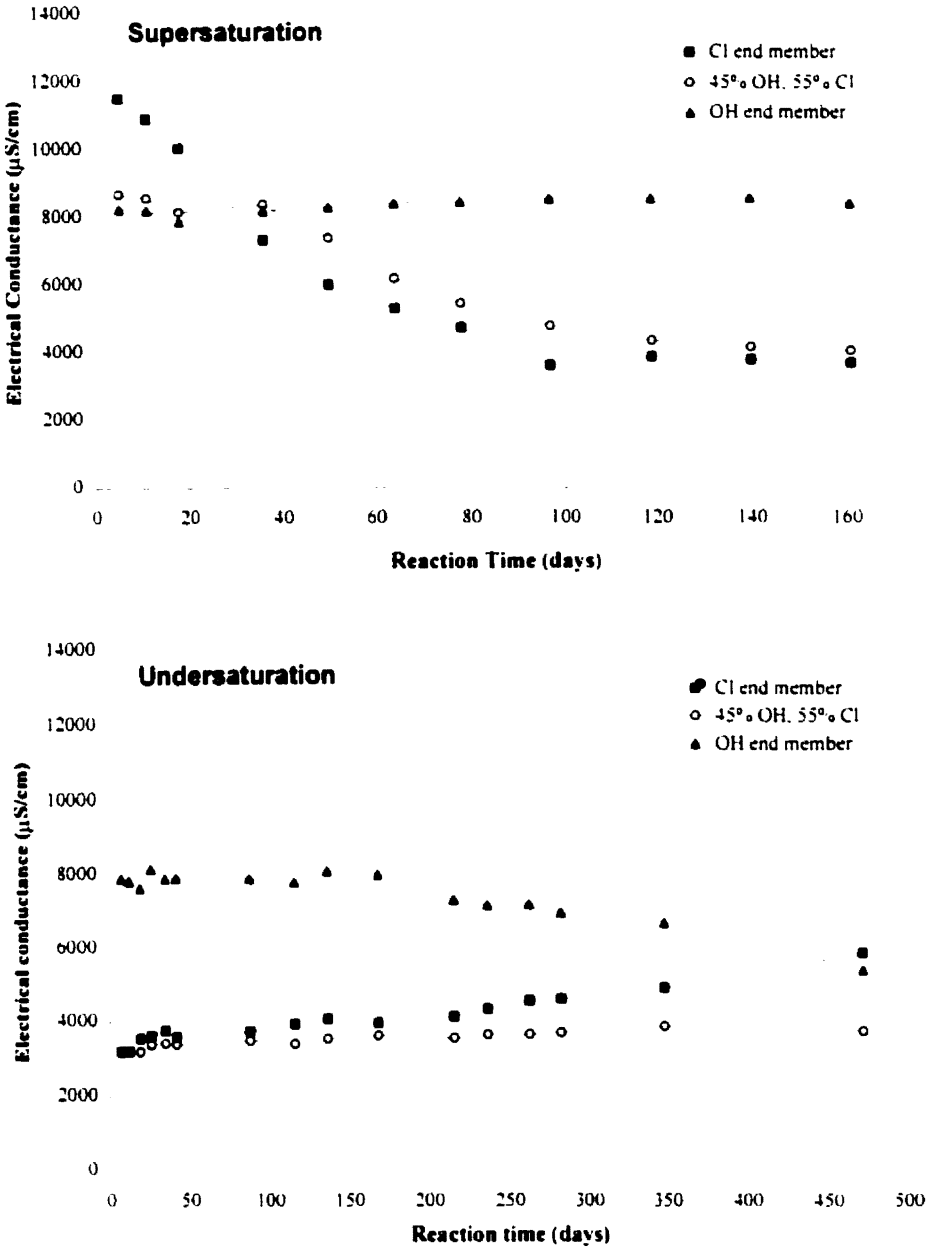


Figure 2.1: Electrical conductance measurements versus reaction time for the experiment from supersaturation and undersaturation. The Cl and OH end members, and a sample with a composition midway between the end members were used to monitor the approach to equilibrium in both experiments.

conductance initially increased to 3500 μS/cm after 20 days of reaction, and remained approximately stable at this value for 70 days. The conductance then gradually increased, reaching a value of 5400 μS/cm after 472 days. This final conductance value is approximately 50% higher than the stable conductance value reached after 100 days from supersaturation. The final solution compositions measured from super- and undersaturation for the chloride end member samples used for conductance measurements (the C-replicates) are provided in Table 2.2. The calcium concentration measured from undersaturation is twice that measured from supersaturation, whereas the aluminum concentration is approximately half, and the chloride concentration is approximately 20% lower. The pH value measured from undersaturation is within 2% of the value from supersaturation.

Experiment	pH	Calcium (mmol/kg)	Aluminum (mmol/kg)	Chloride (mmol/kg)
Supersaturation	11.76	13.21	1.683	15.21
Undersaturation	11.59	28.70	0.8842	12.46

Table 2.2: Solution compositions measured for the C-replicate samples of the chloride end member. The electrical conductance of these samples was measured to monitor the approach to equilibrium of the chloride end member (Figure 2.1).

If the conductance sample from undersaturation had become contaminated by atmospheric CO_2 over time, carbonate in solution would be exchanged for Cl^- in the solid, releasing Cl^- into solution, which was not observed. Alternatively, the changes in the solution composition, and consequently, in the measured conductance may be caused by a decrease in the solution:solid ratio over time, as a result of repetitive measurements of a small quantity of sample ($\approx$10 ml). As the solution:solid ratio changes, the composition of the solid solution phase may also change, and the composition of the aqueous solution in contact with this solid phase will also be different. In general, if there is more solid for a given water volume (i.e. the lower the solution:solid ratio), the greater its solubility will be (Glynn et al., 1990). A lowering solution:solid ratio during the conductance measurements was observed. However, the fact that the other samples used for conductance measurements were apparently not effected by this process, suggests that this was not the cause of the increase in conductance of the Cl end member. To date, no other reasonable explanation has been found.

2.3.2 Solution composition

The solution compositions for samples from super- and undersaturation experiments are presented in Tables 2.3 and 2.4. In Figures 2.2, 2.3, and 2.4 the concentrations of Ca, Al and Cl measured in both experiments are plotted versus the calculated chloride (Cl/(Cl+OH)) ratio in the solid. The ratio of Cl to Cl+OH in the solid solution phase was calculated based on the quantities of reagents used. Within a given solubility experiment, the reproducibility of the measured Ca and Cl concentrations are good between the replicates, and the trends in these elements as a function of the chloride ratio are very similar. In contrast, there are marked differences in the measured Al concentrations between the A and B replicates from both solubility experiments, and in the trends in these concentrations as a function of the chloride ratio.

The pH values of the samples in the experiment from supersaturation increase progressively from approximately 11.8 for the chloride end member (Cl/Cl+OH = 1.0) to 12.5 for the hydroxide end member (Cl/Cl+OH = 0.0). A similar trend was seen in the pH values measured for samples from undersaturation, and these values were the same as those measured from supersaturation, within the analytical uncertainty of ± 0.2 pH units.

The concentration of calcium in solution is high in the Cl end member, but decreases as the chloride ratio in the solid decreases from 1.0 to 0.85. The calcium concentration remains relatively constant as the chloride ratio decreases to approximately 0.4, but then increases by a factor of two, reaching a value of 21 mmol/L in the hydroxide end member (Cl/(Cl+OH) = 0.0).The trend observed for the aluminum concentrations as a function of the chloride ratio in the solid is the inverse of that seen for the calcium concentrations. As the chloride ratio decreases from 1.0 to 0.7, the Al concentrations increase slightly, but then decrease abruptly by two orders of magnitude as the chloride ratio decreases to 0.40 and 0.25 in the A and B replicates, respectively. The Al concentration remains low in both sets of replicates as the Cl/(Cl+OH) ratio in the solid drops to zero. The chloride concentration decreases by approximately 2.5 times between samples with chloride ratios of 1.0 and 0.85, and decreases gradually to below detection as the Cl/(Cl+OH) ratio in the solid approaches zero. An examination of the ion concentrations in Table 2.4 reveals that the dissolution of the solid phase from undersaturation conditions was incongruent. If the solids had dissolved congruently, the ratio of the ions in aqueous solution should be approximately equal to those in the solid (e.g. Ca:Al = 2:1).

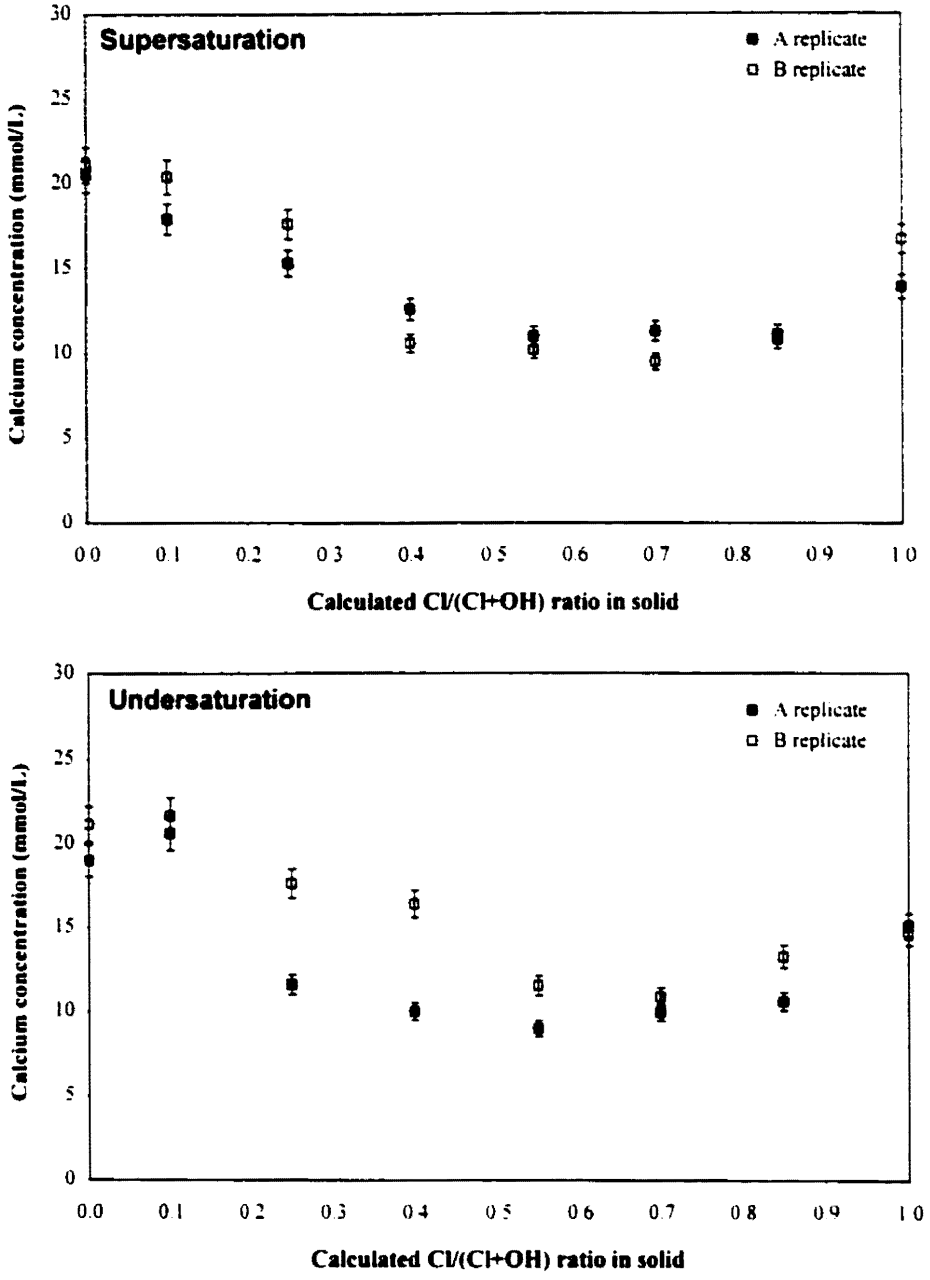


Figure 2.2: Solution concentrations of calcium as a function of the calculated Cl/(Cl+OH) ratio in the solid solution phases for the experiments from supersaturation and undersaturation. The error bars show the analytical uncertainty (± 5 %) in the measured concentrations.

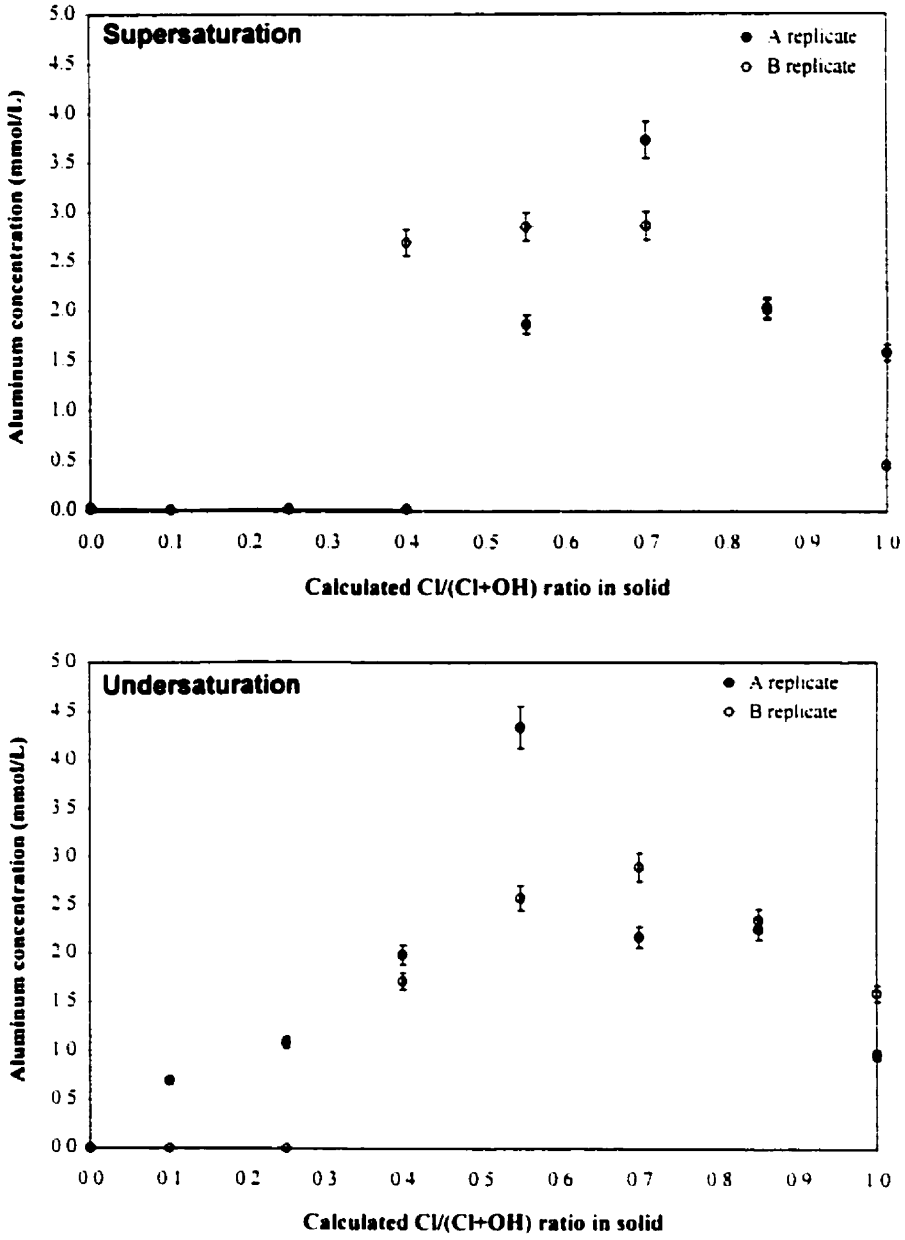


Figure 2.3: Solution concentrations of aluminum as a function of the calculated Cl/(Cl+OH) ratio in the solid solution phases for the experiments from supersaturation and undersaturation. The error bars show the analytical uncertainty (± 5 %) in the measured concentrations.

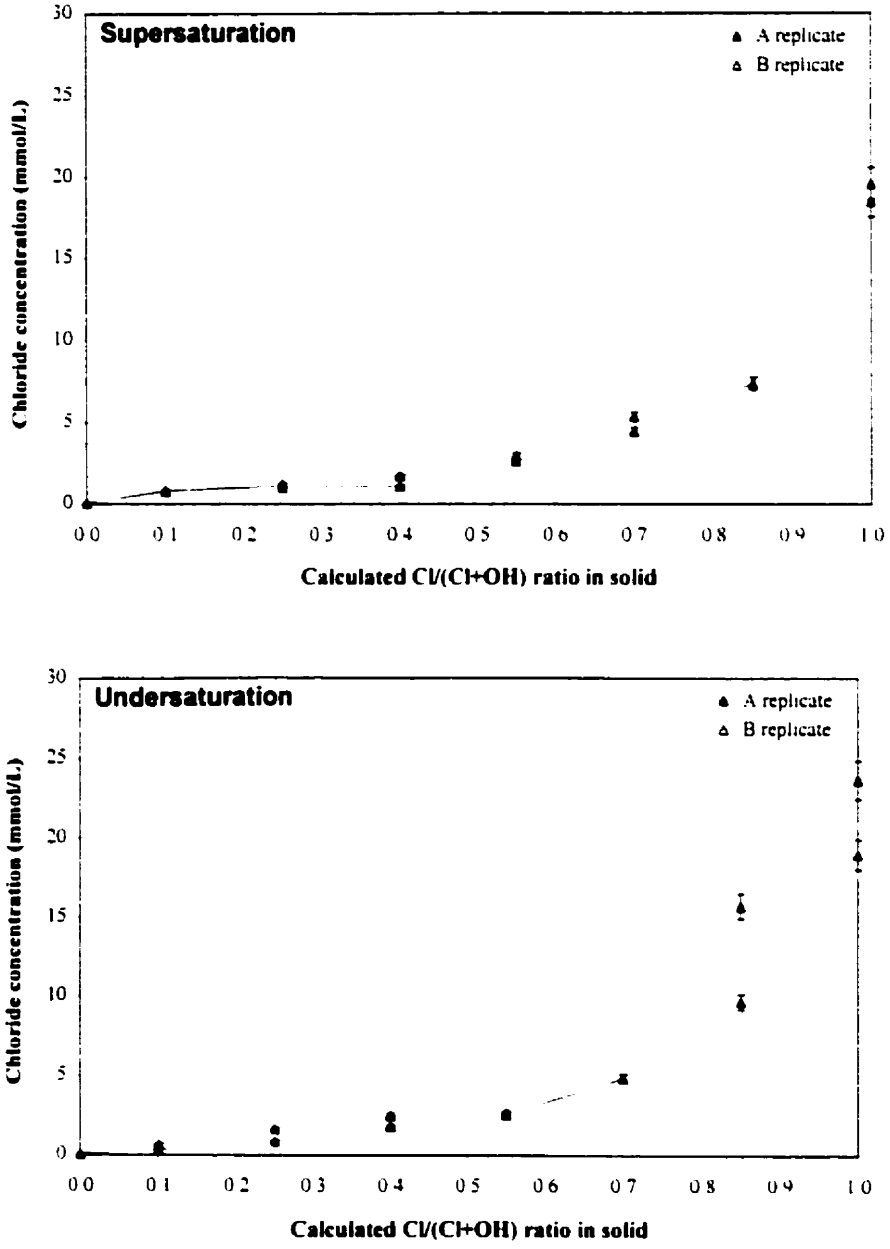


Figure 2.4: Solution concentrations of chloride as a function of the calculated Cl/(Cl+OH) ratio in the solid solution phases for the experiments from supersaturation and undersaturation. The error bars show the analytical uncertainty (± 5 %) in the measured concentrations.

2.3.3 Mineral saturation indices

The solution compositions for both the A and B replicates reported in Tables 2.3 and 2.4 were entered into the geochemical equilibria model SIMUL (Reardon, 1990) to calculate mineral saturation indices. This model was chosen because it is specifically designed for simulations of chemical reactions in cementitious material at 25 °C. A mineral saturation index or SI is usually represented as the log ratio of the ion activity product (IAP) for the mineral dissolution reaction and the mineral's solubility product (K_{sp}). Positive values indicate supersaturated conditions, and negative values, undersaturated conditions.

The calculated SI values for solutions from super- and undersaturation are plotted in Figure 2.5 versus the calculated Cl/(Cl+OH) ratio in the solid. The changes in the SI values for various minerals with decreasing chloride ratio in the solid are similar for both sets of replicates in the experiment from supersaturation, and are similar to those seen in the B replicates from undersaturation. These solutions are calculated to be supersaturated with respect to hydrogarnet between chloride ratios of 1.0 and 0.55 or 0.4. The saturation index then decreases sharply to just above saturation, and remains near saturation as the chloride ratio decreases to zero. In contrast, the A replicates in the experiment from undersaturation are calculated to be supersaturated with respect to hydrogarnet over the entire range of chloride ratios, with the degree of supersaturation increasing by a factor of 2 as the chloride ratio decreases from 1.0 in the Cl end member, to 0.0 in the OH end member.

Solutions from both experiments are calculated to be slightly undersaturated with respect to portlandite at the Cl end member (Cl/(Cl+OH) ratio = 1.0), but increase to saturation as the chloride ratio in the solid decreases. Gibbsite is calculated to be at saturation in samples with chloride ratios between 1.0 and 0.40, but becomes undersaturated as the ratio decreases below 0.4.

Calculated Cl/(Cl+OH)	pH		Calcium (mmol/kg)		Aluminum (mmol/kg)		Chloride (mmol/kg)	
	A	B	A	B	A	B	A	B
1.00	11.70	11.91	13.94	16.56	1.583	0.4625	18.47	19.58
0.85	11.96	11.96	11.15	10.78	2.013	2.023	7.375	7.394
0.70	12.06	11.93	11.26	9.488	3.728	2.860	5.379	4.467
0.55	12.12	12.09	11.00	10.17	1.859	2.848	2.973	2.640
0.40	12.24	12.14	12.56	10.60	0.0220	2.692	1.705	1.091
0.25	12.44	12.43	15.30	17.59	0.0165	0.0254	1.212	1.035
0.10	12.47	12.50	17.94	20.44	0.0123	0.0123	0.7889	0.8293
0.0	12.48	12.51	20.51	21.14	0.0325	0.0156	<0.006	<0.006

Table 2.3: Solution compositions measured from supersaturation for samples between the Cl end member (Cl/(Cl+OH) = 1.0) and the OH end member (Cl/(Cl+OH) = 0.0) after 170 days of reaction. A and B are replicate samples. The chloride ratio given for the solid phase is calculated based on the reagents added.

Calculated Cl/(Cl+OH)	pH		Calcium (mmol/kg)		Aluminum (mmol/kg)		Chloride (mmol/kg)	
	A	B	A	B	A	B	A	B
1.00	11.52	11.69	15.04	14.65	0.9682	1.598	23.64	18.95
0.85	11.82	11.60	10.60	13.24	2.257	2.348	9.664	15.70
0.70	12.06	11.90	9.940	10.85	2.173	2.896	4.891	4.859
0.55	11.94	12.14	8.989	11.52	4.336	2.574	2.551	2.654
0.40	12.17	12.09	9.991	16.35	1.987	1.715	1.827	2.502
0.25	12.28	12.21	11.57	17.57	1.090	0.0161	0.8788	1.655
0.10	12.46	12.30	20.61	21.66	0.6972	0.0267	0.3220	0.6755
0.0	12.47	12.33	19.00	21.16	0.5363	<0.0011	0.0322	0.0638

Table 2.4: Solution compositions measured from undersaturation for the samples between the Cl end member (Cl/(Cl+OH) = 1.0) and the OH end member (Cl/(Cl+OH) = 0.0) after 515 days of reaction. A and B are replicate samples. The chloride ratio given for the solid solution phase is calculated based on the reagents added.

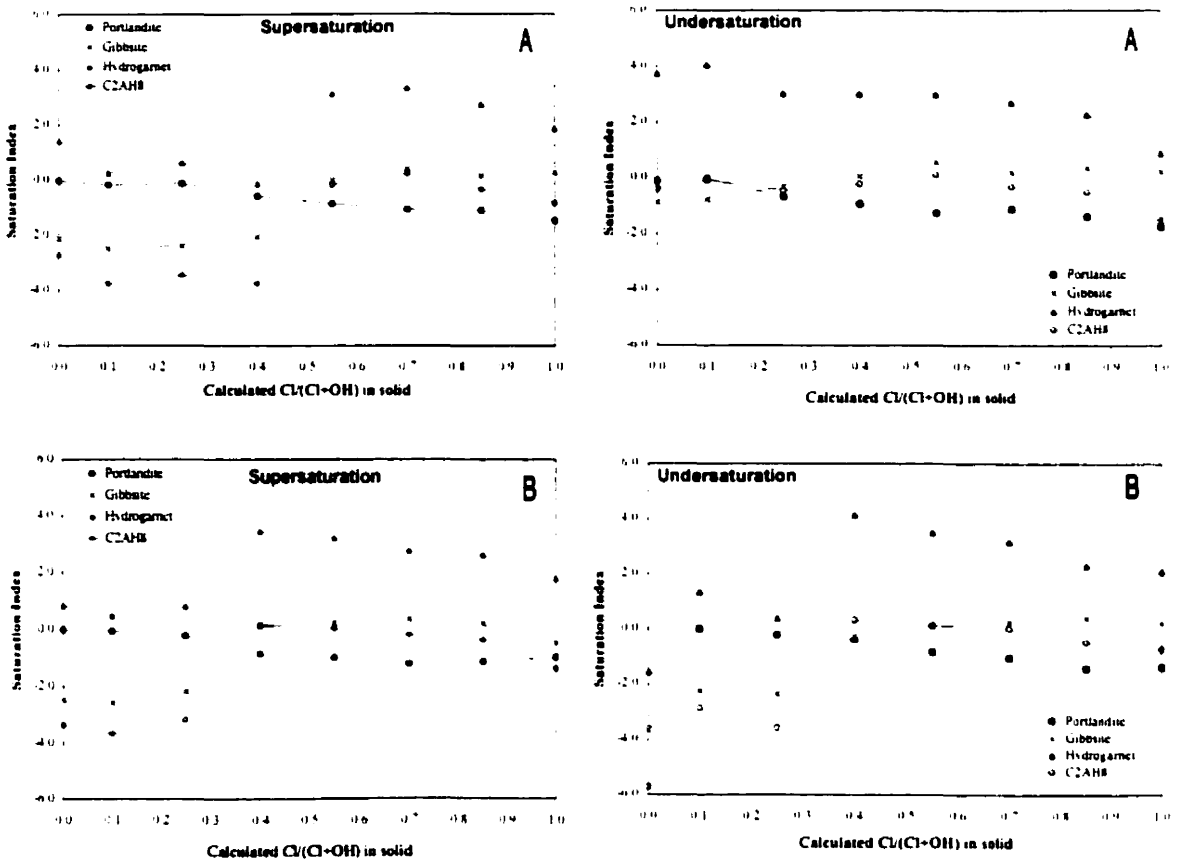


Figure 2.5: Calculated mineral saturation indices (SI) are plotted versus the calculated Cl/(Cl+OH ratio) in the solid for the A and B replicates from supersaturation (left) and undersaturation (right). The saturation indices were calculated using the geochemical equilibria model, SIMUL (Reardon, 1990).

2.3.4 Solids

The XRD patterns for the solid phases in the A and B replicate series from supersaturation are plotted in Figures 2.6 and 2.7, respectively. In the experiment from undersaturation, the A-replicate samples were examined using XRD analysis, and the results are plotted in Figure 2.8. In both experiments, a single solid solution phase with a basal spacing of 7.77 Å ($2\theta = 11.4°$) is observed in the Cl end member (Cl/(Cl+OH) = 1.0) and is identified as β-Friedel's salt. A small peak at a d-spacing of 4.85 Å ($2\theta = 18.3°$) in the A replicate solids with chloride ratios of 1.0 from saturation, and 1.0 and 0.85 from undersaturation is identified as gibbsite. The mineral saturation index calculations suggested that these samples were at saturation with respect to gibbsite, supporting the identification of this phase in the XRD patterns.

A single solid solution phase similar to β-Friedel's salt is the only solid phase observed as the chloride ratio in the solids decreases to 0.55. At a chloride ratio of 0.40, small splits are observed in the main peak of the solid solution phase (i.e. the {002} peak at $2\theta = 11.4$) in the A replicate from supersaturation. The peak-splitting is more pronounced in the secondary peak (the 004 peak at $2\theta = 22.5$). Split peaks are also observed in both the A and B replicates at a chloride ratio of 0.25, and in the B replicates with ratios of 0.1. A section of the XRD pattern for the A replicate sample with a chloride ratio of 0.25 has been expanded in Figure 2.9. The splitting of the main peaks indicates that there are two solid solution phases, one with a basal spacing similar to β-Friedel's salt (7.77 Å), and another with a basal spacing of 7.86 Å, which may be either the OH end member, or α-Friedel's salt. No splitting of the major or secondary peaks was observed in solids from undersaturation. The chloride end member was identified as α-Friedel's salt with a d-spacing of 7.9 Å, and the d-spacing of the solid solution increased to 8.0 Å as the chloride ratio in the solid decreased from 1.0 to 0.1.

In addition to the solid solution phase(s), hydrogarnet was observed in A replicate solids with chloride ratios of below 0.4. Both hydrogarnet and portlandite are present in replicates with ratios of 0.25 to 0.0, with the exception of the A replicates solid with a chloride ratio of 0.25 from supersaturation, where portlandite was absent. At a chloride ratio of 0.10, an additional phase with a peak at 10.7 Å ($2\theta = 8.3°$) is seen in both replicates from supersaturation. This peak is identified as the highly hydrated form of the OH end member ($3CaO{\cdot}Al_2O_3{\cdot}Ca(OH)_2{\cdot}18H_2O$). The A replicate of the OH end member solid (Cl/(Cl+OH) = 0.0) from supersaturation consists predominantly of hydrogarnet, and only a small peak is observed for the solid solution phase. In contrast, the B replicate and the triplicate C sample (not shown) consist mainly of the

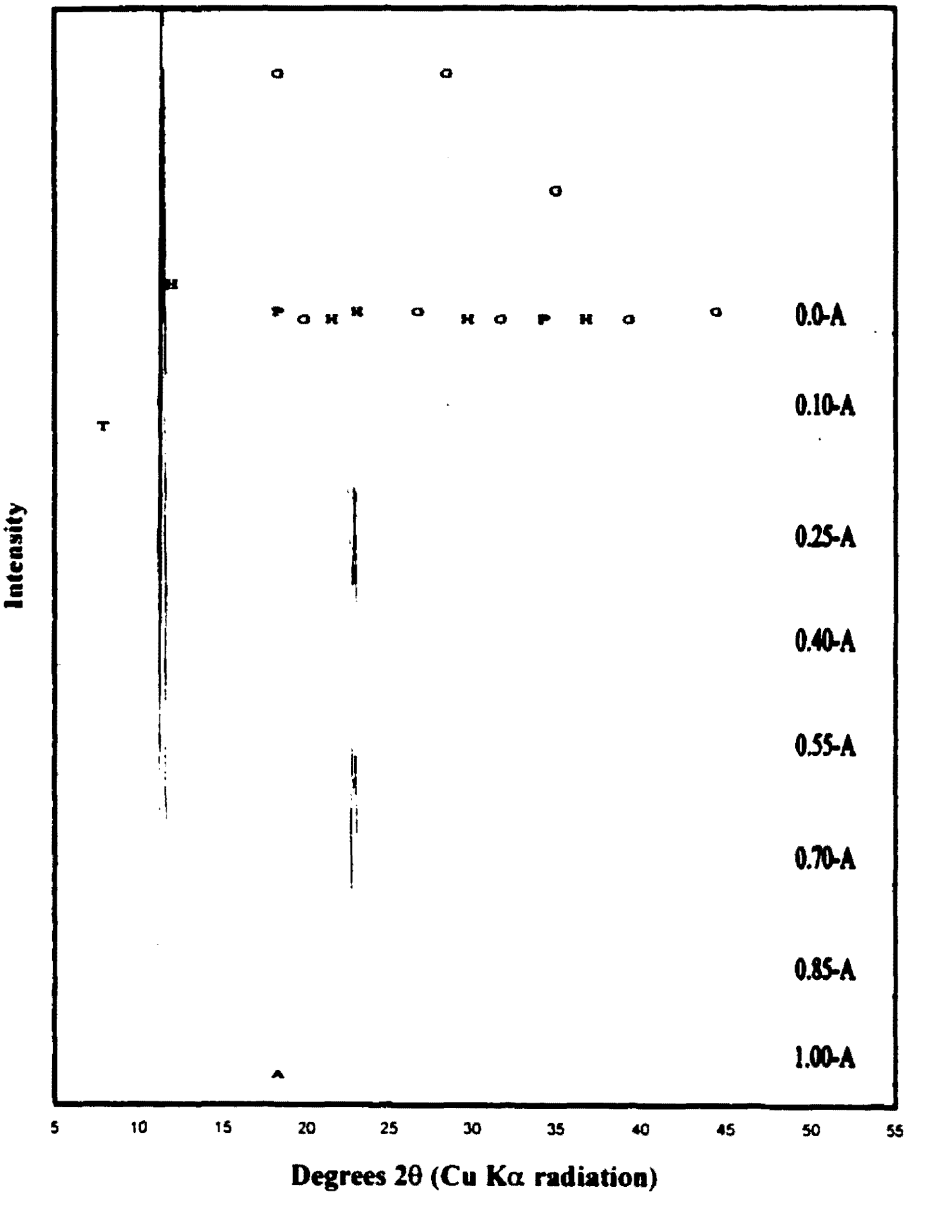


Figure 2.6: XRD patterns for the A-replicate solids from supersaturation. The label indicates the calculated Cl/(Cl+OH) ratio in the solid, from the Cl end member (1.0-A), to the OH end member (0.0-A). Peaks are labeled: H = solid solution phase; G = hydrogarnet ($3CaO{\cdot}Al_2O_3{\cdot}6H_2O$); P = portlandite ($Ca(OH)_2$); T = hydrated OH end member ($3CaO{\cdot}Al_2O_3{\cdot}Ca(OH)_2{\cdot}18H_2O$); A= gibbsite ($Al(OH)_3$).

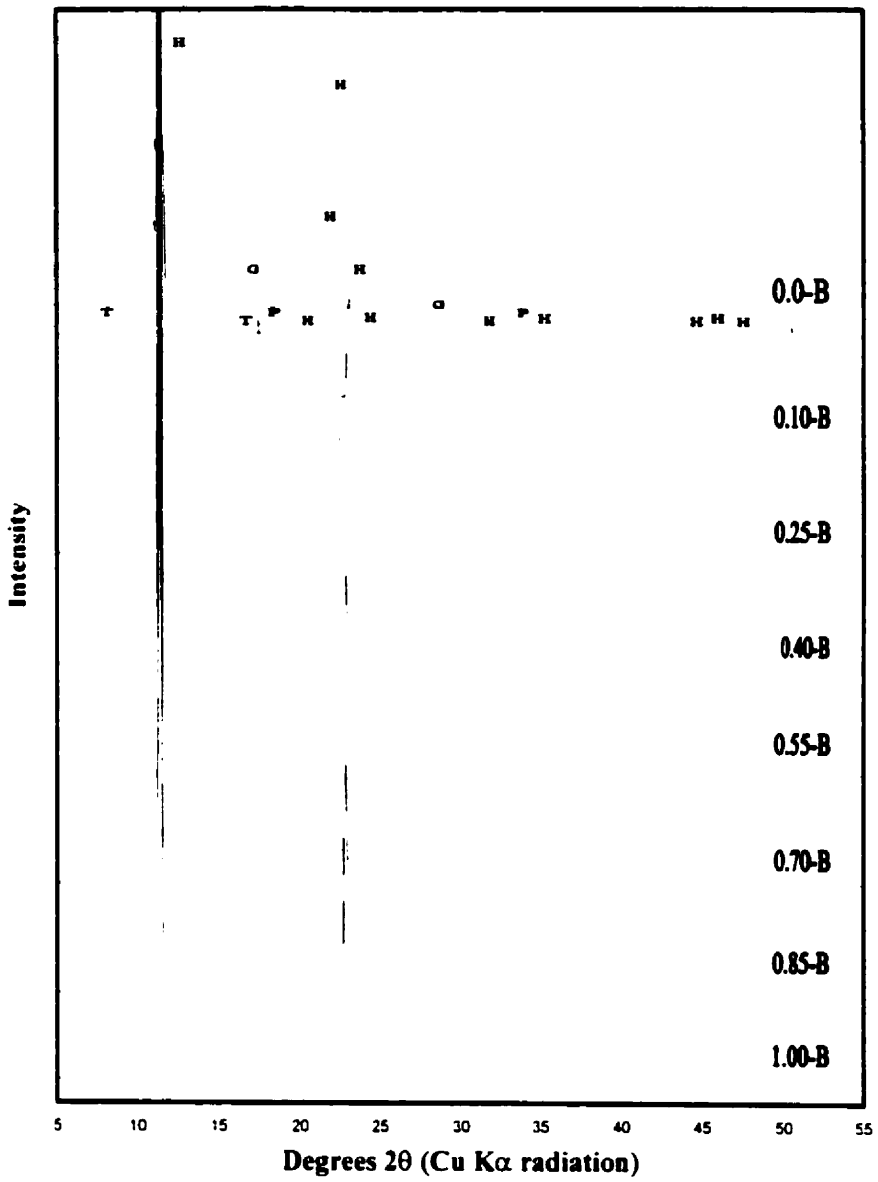


Figure 2.7: XRD patterns for B-replicate solids from supersaturation. The label indicates the calculated Cl/(Cl+OH) ratio in the solid, from the Cl end member (1.0-B) to the OH end member (0.0-B). Peaks are labeled: H = solid solution phase; G = hydrogarnet ($3CaO{\cdot}Al_2O_3{\cdot}6H_2O$); P = portlandite ($Ca(OH)_2$); T = hydrated OH end member ($3CaO{\cdot}Al_2O_3{\cdot}Ca(OH)_2{\cdot}18H_2O$).

dehydrated OH-end member solid solution phase with a d-spacing of 7.9 Å ($3CaO{\cdot}Al_2O_3{\cdot}Ca(OH)_2{\cdot}12H_2O$), and a trace peak with a d-spacing of 7.5 Å (which may belong to $3CaO{\cdot}Al_2O_3{\cdot}Ca(OH)_2{\cdot}10H_2O$). In both the B and C replicates, two additional peaks are observed for the solid solution phase. A small peak with a d-spacing of 8.0-8.2 Å could belong to hemicarboaluminate, if the sample has been contaminated by atmospheric CO_2. In the OH end member solid from undersaturation, the dominant peak for the solid solution occurs at 8.19 Å. Peaks with this d-spacing are usually identified as hemicarboaluminate (Roberts, 1969), and its presence would suggest that the solid has undergone significant carbonation. Small peaks at 7.8 Å and 7.5 Å are identified as different hydration states of the OH end member ($3CaO{\cdot}Al_2O_3{\cdot}Ca(OH)_2{\cdot}12H_2O$ and $3CaO{\cdot}Al_2O_3{\cdot}Ca(OH)_2{\cdot}10H_2O$, respectively).

Photoelectron micrographs of selected solid samples taken from the supersaturation experiment are shown in Figure 2.10. The Cl-rich phase (Cl/Cl+OH = 1.0) is composed of predominantly euhedral platy hexagonal crystals between 10 and 15 μm in width (a). The crystals in the solid with a chloride ratio of 0.4 are subhedral, with an average size between 2 and 5 μm (b). Many crystals are hexagonal in appearance, but most have rounded edges, suggesting that these crystals may have undergone some dissolution. No hydrogarnet crystals were observed in this sample. A solid with a calculated Cl/Cl+OH ratio of 0.1 (c) consists of clusters of platy, subhedral to euhedral hexagonal crystals. Dodecahedral crystals of hydrogarnet are also observed. The OH-end member (Cl/Cl+OH = 0.0) shown in (d) consists of similar platy crystals, with a higher proportion of hydrogarnet crystals than observed in the solid with a Cl/Cl+OH ratio of 0.1. These results are consistent with the XRD pattern for this sample, in which hydrogarnet was the dominant phase. A close-up photograph of a hydrogarnet crystal observed in the OH end member solid is shown in Figure 2.10 (e).

2.3.5 Solid solution phase composition

The composition of the solid solution phase can be calculated using mass balance relations, based on the quantities of reagents used, and corrected for the elemental concentrations in the aqueous phase. This approach is applicable if there is only one mineral phase present (the solid solution phase, in this case) as demonstrated by XRD analysis. The compositions of the solid solution phases in the samples which met this criteria in the experiments are given in Table 2.5.

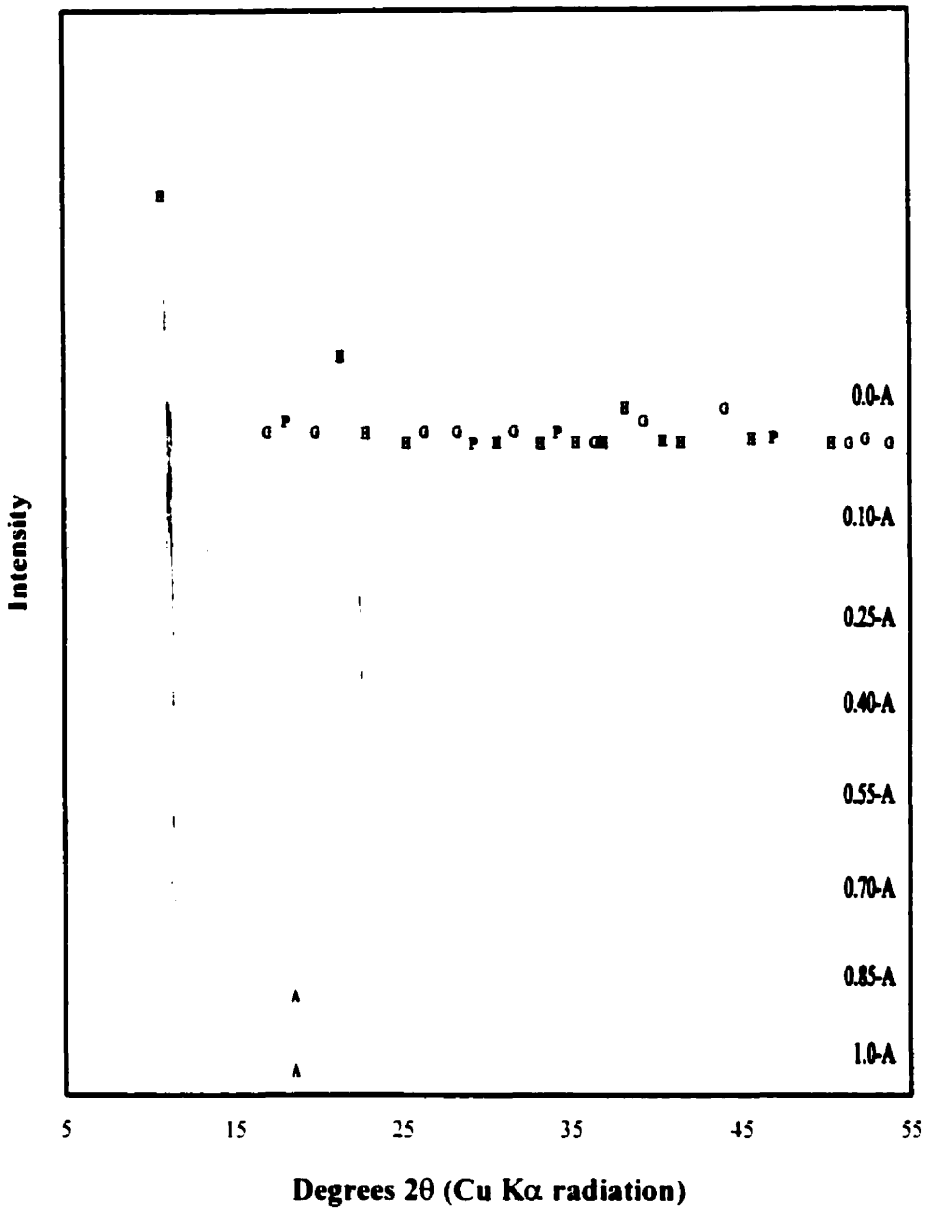


Figure 2.8: XRD patterns for solid samples (A replicates) from undersaturation. The label indicates the Cl/(Cl+OH) ratio calculated in the solid, from the Cl end member (1.0-A) to the OH end member (0.0-A). Peaks are labeled: H = solid solution phase; G = hydrogarnet ($3CaO{\cdot}Al_2O_3{\cdot}6H_2O$); P = portlandite ($Ca(OH)_2$); A= gibbsite ($Al(OH)_3$).

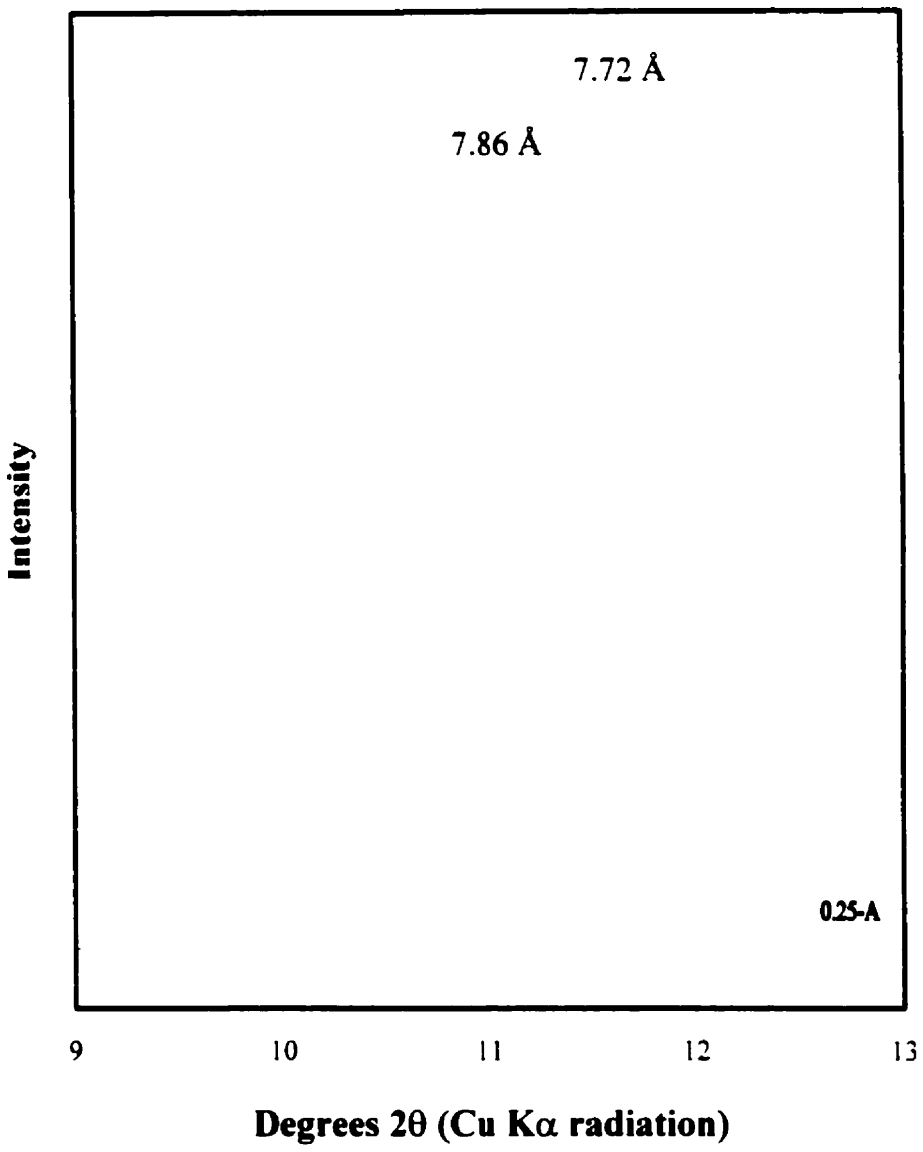


Figure 2.9: Enlargement of the primary peak for the solid solution phase, in the XRD pattern of the A replicate solid (supersaturation) with a Cl/(Cl+OH) ratio of 0.25. The splitting of this peak indicates the presence of two solid solution phases.

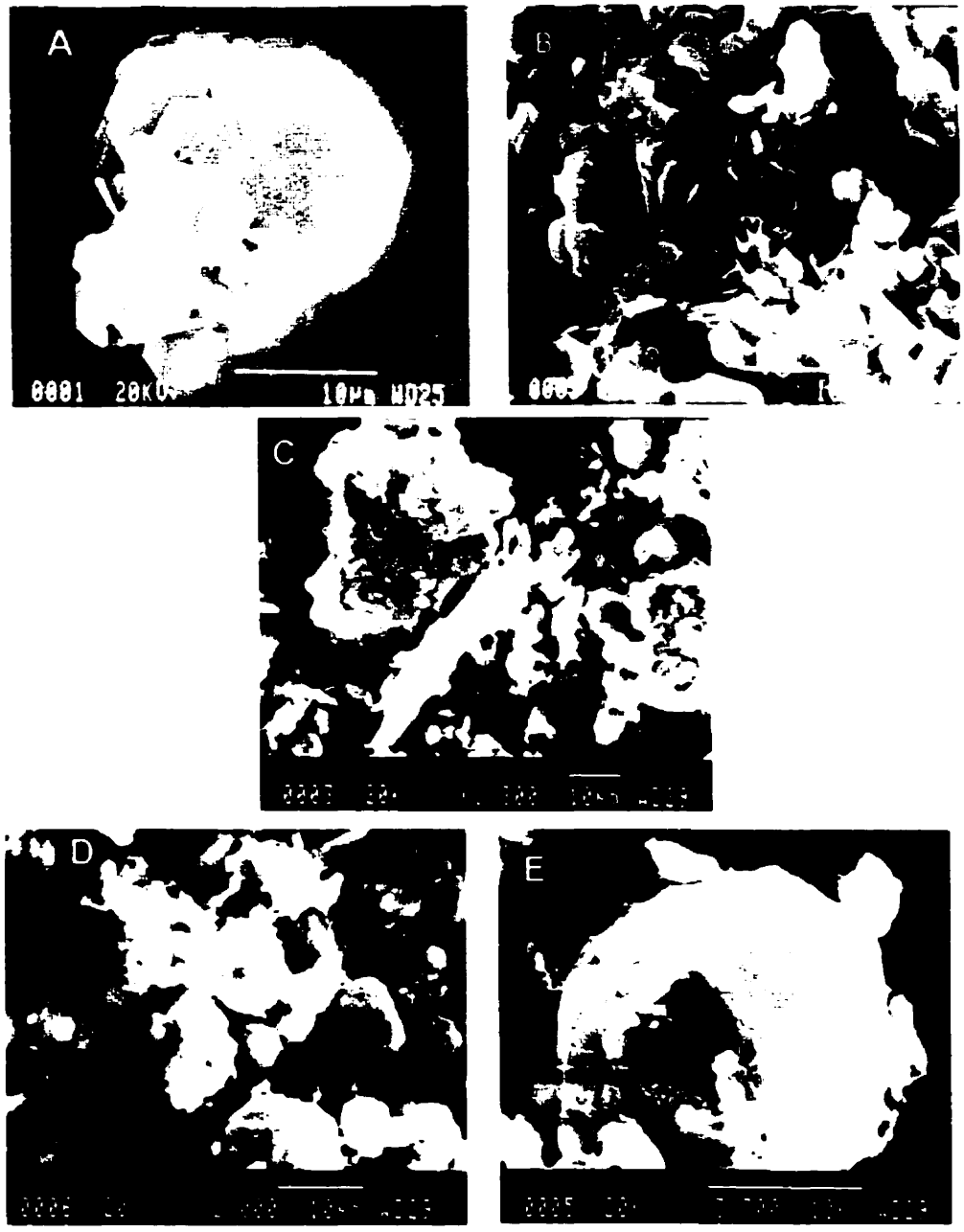


Figure 2.10: Scanning electron micrographs of a) euhedral, platy hexagonal crystals of the Cl-rich solid solution phase (Cl/(Cl+OH) ratio = 0.90) b) subhedral, rounded crystals of the solid solution phase with a Cl/Cl+OH ratio of 0.4. c) Solid with a Cl/(Cl+OH) ratio of 0.1 showing both platy, hexagonal crystals of the solid solution phase, and dodecahedral hydrogarnet crystals. d) OH end member (Cl/Cl+OH = 0.0) consists of platy, hexagonal solid solution phase, and a higher proportion of hydrogarnet crystals than observed in c). e) close-up of a hydrogarnet crystal observed in the OH end member solid.

2.3.6 Solubility of the Cl end member

The solution compositions measured for the chloride end member in the extended solubility experiment are presented in Table 2.6.

The pH values measured for solids with 25% more calcium chloride added are slightly lower (0.2 pH units) than those measured for the sample with a Cl/(Cl+OH) ratio of 1.0 in the experiment from supersaturation. The calcium and chloride concentrations are 2 and 3 times the concentrations measured for the Cl end member, respectively. The aluminum concentrations are similar to the values measured for the B replicate from supersaturation. In the replicates with 50% more calcium chloride, the pH values are essentially the same as those measured for the Cl end member in the experiment from supersaturation. Apart from the increase in the solution concentrations of calcium and chloride, the most marked difference is in the Al concentrations, which are an order of magnitude lower than those measured for the Cl end member from supersaturation.

Calculated Cl/(Cl+OH)	Supersaturation		Undersaturation	
	A replicate	B replicate	A replicate	B replicate
	Actual Cl/(Cl+OH)	Actual Cl/(Cl+OH)	Actual Cl/(Cl+OH)	Actual Cl/(Cl+OH)
1.00*	0.91	0.89	0.78	0.79
0.85	0.82	0.82	0.78	0.74
0.70	0.68	0.69	0.66	0.67
0.55	0.54	0.54	0.54	0.54

Table 2.5: Solid phase compositions in the experiments from super- and undersaturation. The actual chloride ratio (Cl/(Cl+OH) was determined based on the quantity of reagents used, and corrected for the elemental concentrations in the aqueous phase. The compositions of the solid phases from the experiment from supersaturation were used as the initial compositions for solids in the experiment from undersaturation. A star indicate that a trace amount of gibbsite was identified in the precipitates.

Calculated Cl/(Cl+OH)	Actual Cl/(Cl+OH)		pH		Calcium (mmol/kg)		Aluminum (mmol/kg)		Chloride (mmol/kg)	
	A	B	A	B	A	B	A	B	A	B
1.0 + 0.25	0.94	0.92	11.50	11.58	30.19	30.69	0.474	0.526	56.42	58.38
1.0 + 0.50	0.95	0.93	11.76	11.97	52.15	55.89	0.048	0.048	99.67	103

Table 2.6: Solution data measured from supersaturation for the samples of the Cl end member (Cl/(Cl+OH) = 1.0) in the extended solubility experiment after 170 days of reaction. A and B are replicate samples. The calculated Cl/(Cl+OH) ratio for the solid solution phase is based on the reagents added, whereas the actual ratio was calculated by mass balance.

The saturation indices for the samples in the extended solubility experiment are given in Table 2.7. All samples are predicted to be undersaturated with respect to portlandite. Samples with 25% extra $CaCl_2$ are predicted to be slightly saturated with respect to gibbsite, and just at saturation with respect to hydrogarnet, whereas the 50% samples were undersaturated with respect to both these phases.

Calculated Cl/(Cl+OH)	A replicate (Log SI)			B replicate (Log SI)		
	Portlandite	Gibbsite	Hydrogarnet	Portlandite	Gibbsite	Hydrogarnet
1.0-50%	-1.73	-1.45	-2.35	-1.20	-1.71	-1.26
1.0-25%	-2.04	0.13	-0.08	-2.33	0.33	-0.58

Table 2.7: Calculated log SI values of mineral phases for solution compositions from the extended solubility experiment.

The A replicates were examined using XRD analysis, and were identified as α-Friedel's salt. In the solid with 50% more chloride added, a small peak for portlandite was observed, although the solution phase was predicted to be undersaturated with respect to this phase. Assuming the quantity of portlandite was negligible, the chloride ratios in the solid were determined by mass balance of the reagents added and the final measured solution concentrations (Table 2.8).

Calculated Cl/ (Cl+OH)	Supersaturation			
	A replicate		B replicate	
	Cl	OH	Cl	OH
1.0 +50%*	0.95	0.05	0.93	0.07
1.0 +25%	0.94	0.06	0.92	0.08

Table 2.8: Solid phase compositions for the Cl end member from the extended solubility experiment. The chloride ratio in the solid was determined based on the quantity of reagents used, and corrected for the elemental concentrations in the aqueous phase. A star indicates that a trace amount of portlandite was identified in the precipitates.

2.3.7 Solubility Products

The solubility products (K_{sp}) of the solid-solution phases from all solubility experiments have been calculated, assuming that equilibrium between the solid and aqueous phases had been attained, and that the activity of the solid phase equals 1. These K_{sp} values were calculated with the measured solution compositions (Tables 2.3 and 2.4), the activity coefficients predicted using the geochemical equilibria model SIMUL (Reardon, 1990), and the calculated (Tables 2.5 and 2.7) or estimated solid phase compositions. To incorporate the solubility data into a different geochemical equilibria model, the solubility products must be re-calculated using the activities of the aqueous species generated by that model for the measured solution compositions. In Chapter 5, the solubility products and free energy data for the pure end members are presented for both SIMUL and PHREEQC (Parkhurst and Appello, 1999).

The general dissolution reaction for the solid solution series is given in equation 2.1, and the K_{sp} value for this reaction is formulated according to equation 2.2.

$$3CaO{\cdot}Al_2O_3{\cdot}xCaCl_2{\cdot}(1-x){\cdot}Ca(OH)_2{\cdot}(10-10x)H_2O \rightleftharpoons 4Ca^{2+} + 2Al(OH)_4^- + 2xCl^- + (6-2x)OH^- + (5-x)H_2O \quad (2.1)$$

$$K_{sp} = [m_{Ca^{2+}}\gamma_{Ca^{2+}}]^4\,[m_{Al(OH)_4^-}\gamma_{Al(OH)_4^-}]^2\,[m_{Cl^-}\gamma_{Cl^-}]^{2x}\,[m_{OH^-}\gamma_{OH^-}]^{(6-2x)}\,[a_{H_2O}]^{(5-x)} \quad (2.2)$$

where m is the concentration of the ion in mol/L of solution, γ is the activity coefficient, and aH_2O is the activity of water. The upper and lower uncertainty limits of the calculated K_{sp} values were determined by adding or subtracting the analytical uncertainty of 5% to the measured solution composition values for Ca, Al and Cl. The solutions were then re-modeled using these adjusted solution compositions, and the log K_{sp} values re-calculated. The calculated log K_{sp} values and the analytical uncertainty in these values are plotted in Figure 2.11.

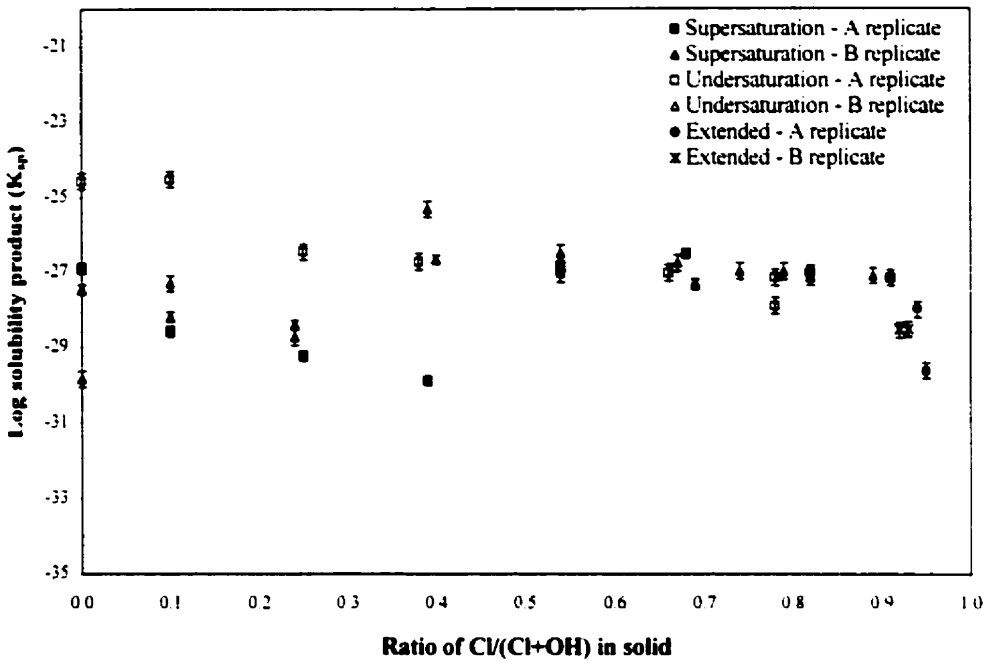


Figure 2.11: Log values of the solubility products (K_{sp}) for the solid solution phase as a function of the Cl/(Cl+OH) ratio in the solid phase. Solubility products were calculated using solubility data collected from both super- and undersaturation. Error bars show the estimated uncertainty in the log K_{sp} values.

2.4 Discussion

2.4.1 Evidence for the existence of a miscibility gap

The existence of a miscibility gap where two solid solution phases coexist has been clearly demonstrated in X-ray diffraction studies done on moist solids (Roberts, 1969; Pöllmann and Kuzel, 1988; Birnin-Yauri, 1993). The XRD results from these three studies, and from the current study are summarized in Table 2.9. The highly hydrated form of the OH end member which has a basal spacing of 10.7 Å, and an additional solid solution phase with a d-spacing of 7.9 Å were detected in samples with Cl/(Cl+OH) ratios of 0.25 to 0.1 in the studies by Roberts (1969), Pöllmann and Kuzel (1988) and Birnin-Yauri (1993). In the current study, two solid solution phases (the chloride end member, and the highly hydrated OH end member) were also identified in solids with chloride ratios of 0.25 and 0.1 in the experiment from supersaturation. Therefore, on the basis of the occurrence of two solid solution phases, the upper limit of the miscibility gap lies between chloride ratios of 0.3 and 0.25, and the lower limit between chloride ratios of 0.1 and 0.0.

Some evidence suggests that the miscibility gap may extend to higher chloride ratios. Roberts (1969) suggested the possible presence of a trace amount of the hydrated OH end member in solids with a chloride ratio of 0.4, although the identification of this phase was uncertain. Pöllmann and Kuzel (1988) determined the composition of the solid phase based on its chloride content, and reported that within the miscibility gap, a solid solution phase with the composition $3CaO{\bullet}0.33CaCl_2{\bullet}0.67Ca(OH)_2{\bullet}11.4H_2O$ occurs together with the OH end member.

In the current study, hydrogarnet and/or portlandite were identified in solids with chloride ratios of 0.4 or lower. The presence of portlandite is reflected in the high calcium concentrations (approx. 20 mmol/L) measured in solutions when chloride ratio of the solid was 0.25 to 0.0. These solutions were also predicted to be just at saturation with respect to portlandite. In solids with chloride ratios of 0.4 or less, most samples contain hydrogarnet, and had Al concentrations that were below detection (0.0011< mmol/L). The solutions are predicted to be close to saturation with respect to hydrogarnet. The only exceptions were the A replicates from undersaturation, which had between 0.5 and 1 mmol/L of Al, and were calculated to be supersaturated with respect to hydrogarnet over the same range of compositions. The OH end member is metastable, and converts to a mixture of hydrogarnet ($3CaO{\cdot}Al_2O_3{\cdot}6H_2O$), and portlandite ($Ca(OH)_2$) with time. Consequently, the occurrence of the solid solution phase with

Reference	Reaction Time	Cl/Cl+OH in solid	Solids Observed
Roberts (1969)	≈7 days	0.96-0.88	β-F
		0.72-0.58	SS
		0.40	SS, T (?)
		0.17 and 0.13	SS, T
Pöllmann & Kuzel (1988)	6 months	1.0 and 0.85	α-F
		0.83	β-SS
		0.70-0.3	α-SS
		0.22 and 0.1	α-SS, T
		0.0	T
Birnin-Yauri (1993)	17 months	1.0 and 0.98	α-F
		0.71-0.43	α-SS
		0.39	α-SS, P
		0.25	α-SS, T, P
		0.1 and 0.0	T, P, G
This study: Supersaturation	6 months	0.90	β-F, A*
		0.82, 0.69 and 0.54	SS
		0.40	SS, G*
		0.25	SS, G, P*
		0.10	SS, G, P, T
		0.0	H, G, P, T*
This study: Undersaturation (4 replicates)	17 months	0.90	β-F, A
		0.82	SS, A
		0.69 and 0.54	SS
		0.40	SS, G*
		0.25 and 0.10	SS, G, P
		0.0	H, G, P

Table 2.9: Solid phases observed as a function of calculated Cl/(Cl+OH) ratio in the solid. F = Friedel's salt ($3CaO{\cdot}Al_2O_3{\cdot}CaCl_2{\cdot}10H_2O$); SS = solid solution; H = OH-end member ($3CaO{\cdot}Al_2O_3{\cdot}Ca(OH)_2{\cdot}12H_2O$); T = highly hydrated OH-end member ($3CaO{\cdot}Al_2O_3{\cdot}Ca(OH)_2{\cdot}18H_2O$); P = portlandite ($Ca(OH)_2$); A = gibbsite ($Al(OH)_3$). A star (*) indicates that the phase was seen in only one replicate.

hydrogarnet and portlandite may be indicative of the presence of the OH end member at earlier reaction times, and therefore, indicative of the position of the miscibility gap. The splitting of the main peaks observed in solids with chloride ratios of 0.4 to 0.1 in the experiment from supersaturation indicates the presence of two solid solution phases. One phase is identified as β-Friedel's salt, and although the second solid solution can not be positively identified as the OH end member, this peak splitting is only observed within the range of the miscibility gap as observed by Pöllmann and Kuzel (1998), Birnin-Yauri (1993) and Roberts (1969).

The XRD results from both Birnin-Yauri (1993) and the current study support the conclusion of Pöllmann and Kuzel (1998) that the miscibility gap begins at a Cl/(Cl+OH) ratio of 0.33, rather than at a Cl/(Cl+OH) ratio above 0.4, as suggested by Roberts (1969). The lower limit for the miscibility gap lies between chloride ratios of 0.10 and 0.0, based on the XRD results of Birnin-Yauri (1993), Pöllmann and Kuzel (1988), Roberts (1969) and the current study.

2.4.2 Factors affecting solid solution stability

When the structure of two minerals is the same or very similar, complete solid solutions typically form if the substituting ions have the same charge, and similar ionic radii (Brownlow, 1979). In the hydrated calcium aluminate phases, the thickness of the interlayer varies as different anions are incorporated (Taylor, 1997). Consequently, the difference in ionic size between two substituting ions is probably not a key factor controlling the extent of solid solution, except perhaps when the difference between two substituting ions is very large (e.g. between OH^- and MoO_4^{2-} (Zhang, 2000)). The OH^- and Cl^- ions would be expected to form either a complete or extensive solid solution rather than the observed limited solid solution, because these ions have the same charge and similar ionic radii. Cl ions have an effective radius of 1.81 Å, and the smaller OH^- ion has a radius similar to oxygen (1.40 Å).

Other properties of the interlayer anions which may control the behavior of the solid solution are charge, geometry, and bonding characteristics. Sacerdoti and Passaglia (1988) have suggested that the continuity of the hydrogen bond network formed within the interlayer may also be an important factor in the stability of these phases. Chloride is a monovalent ion, and can be considered as spherical. Due to the small size of the H^+ atom, OH^- may also be considered as approximately spherical. Therefore, it is unlikely that there are any significant geometric barriers to fitting these two anions in the interlayer. However, unlike Cl^-, OH^- is

highly polar (Kotz and Purcell, 1991) and this may lead to significant differences in their bonding characteristics.

The structural unit formula for hydrocalumites and related synthetic compounds is $Ca_2Al(OH)_6[X \cdot nH_2O] \cdot 2H_2O$, where X are anions or anion groups (Sacerdoti and Passaglia, 1988). The "$2H_2O$" water molecules in this formula are attached to Ca atoms in the main layer by hydrogen bonds, and provide cohesion between the main layers and the interlayer regions. The "nH_2O " are additional water molecules which are present when necessary to ensure the continuity of the hydrogen net within the interlayer region. Sacerdoti and Passaglia (1988) observed that, as a general rule, in compounds containing monovalent anions (X= I, Br, or Cl), there are no additional water molecules in the structure (i.e. n = 0). In compounds with divalent anion groups (X= $\frac{1}{2}SO_4$), the number of "additional" water molecules is double with respect to the anion group (or n= 2X). OH^- is a monovalent anion, and according to the general rule should have n = 0, as for Cl. However, in solution, the OH-end member occurs in the highly hydrated form ($3CaO \cdot Al_2O_3\ Ca(OH)_2 \cdot 18H_2O$). This corresponds to n = 4 in the unit formula, and appears to contrast with the general rule (Sacerdoti and Passaglia, 1988). Alternatively, consider that OH^- is actually a monovalent anion group, consisting of an O and H atom. Applying the above rule for anion groups, the number of water molecules would be 2*X = 2 *(2OH) = 4, consistent with the observed stable hydration state of the OH end member in solution.

Particularly important is the observation that there is a large difference in the number of "additional "interlayer water molecules in the interlayer of the Cl and OH end members (n = 0 for Cl and n= 4 for OH^-). In the current study, the d-spacing of the solid solution was observed to increase slightly from 7.7 to 8.0 Å as the chloride ratio in the solid decreased from 1.0 to 0.1 (from undersaturation). Birnin-Yauri (1993) also observed this trend, and attributed it to an increase in the amount of interlayer water. Passaglia and Sacerdoti (1988) postulated that upon the substitution of $2OH^-$ for $2Cl^-$ in the structure of Friedel's salt, additional water molecules are required in the interlayer so that a sufficient number of hydrogen bonds are maintained between the upper and lower layers. It appears that, with a continued decrease in the chloride ratio in the solid to approximately 0.25, either differences in the bonding characteristics between the Cl^- ion and the polar OH^- ion group and/or the number of water molecules required to maintain the hydrogen-bond network are large enough that a single solid solution phase is not stable. Instead, two solid solution phases form: one more similar to Friedel's salt with fewer water molecules in the interlayer, and the other to the OH^- end member, with n=4 water molecules.

Experimentally probing the interlayer and even determining the detailed structure of the calcium aluminate hydrates and related hydrotalcite phases is difficult. However, recent research (e.g. Wang et al., 2001) suggests that molecular modeling of these phases may provide an alternative method to gain important insights into the behavior of the interlayer anions and water molecules.

2.4.3 Solubilities of the solid solutions

The log K_{sp} values calculated for the solid solution phases in the experiments from super- and undersaturation, and the estimated uncertainties in these values are plotted in Figure 2.11 versus the chloride ratio in the solid phase. The calculated log K_{sp} values for the Cl end member measured in the extended experiment are also plotted. The calculated log K_{sp} values for solids with chloride ratios of 0.55 or higher are representative of the solubility products of the solid solution phase. However, log K_{sp} values for solids with chloride ratios below 0.4 are estimates, because the composition of the solid solution phase was calculated assuming that the presence of additional phases such as hydrogarnet and portlandite are negligible.

The reproducibility of the log K_{sp} values calculated for replicates in the solubility experiments from both super- and undersaturation is excellent in solids with chloride ratios between 0.91 and 0.55. Over this range of chloride ratios, the log K_{sp} values are approximately constant at -27. As the chloride ratio in the solid is increased above 0.92 in the extended solubility experiment, there is a decrease in the calculated solubility product. For the samples with the highest Cl ratios (0.94 and 0.95), the decrease in the solubility products can be explained by the Al concentrations, which were an order of magnitude lower than those measured in solutions at chloride ratios of 0.92 and 0.93. The solutions are predicted to be just at saturation with respect to gibbsite, suggesting that gibbsite may be the mineralogical control on aluminum concentrations.

The solubility products calculated for solid solutions with chloride ratios between 0.4 and 0.1 in the A and B replicates from supersaturation, and the B replicates from undersaturation are approximately two orders of magnitude lower than those calculated for the A replicate samples from undersaturation. Comparison of the solution compositions at these ratios (Tables 2.3 and 2.4) reveals that there is a correlation between the low solubility products, and Al concentrations that are below detection. These solutions were calculated to be slightly saturated or just at

saturation with respect to hydrogarnet, and this phase was identified in the XRD patterns of the solids. This suggests that the solution concentrations of aluminum are controlled by hydrogarnet. In the experiment from undersaturation, the decrease in the conductance of the OH end member with long reaction times also suggests that the solutions may be approaching equilibrium with respect to hydrogarnet. For solid solutions with chloride ratios between 0.4 and 0.1, the log K_{sp} values calculated for the A-replicates from undersaturation are on the order of -25 to -26. Although hydrogarnet was observed in solids with Cl ratios of 0.4 or lower, the solutions are predicted to be supersaturated with respect to hydrogarnet over the entire range of compositions. This suggests that these solution compositions may be more representative of the solubilities of the solid solution phases.

Birnin-Yauri and Glasser (1998) also published solubility data for solid solution phases with chloride ratios between 1.0 and 0.40. In order to be able to compare the solubility products from their study to those from this study, the activities of the ions must be calculated using the same method. The geochemical equilibria model SIMUL (Reardon, 1990) was used to calculate ion activity coefficients for the solutions compositions using the Ca, Al and Cl values from both studies (measured from supersaturation). Solubility products were then calculated for the solid phases based on their calculated solid compositions. The compositions of the solids in the study by Birnin-Yauri and Glasser (1998) were measured using SEM (EDAX) analysis. The formations used to calculate the solubility products are included in Table 2.10.

The solubility products calculated for the solid solution phases in this study are approximately two orders of magnitude lower than those calculated for solids with similar chloride ratios from the data of Birnin-Yauri and Glasser (1998). This is due to the large differences in the calcium and chloride concentrations measured in solution by Birnin-Yauri and Glasser (1998), which are more than twice those measured in the current study. The log value of the solubility product for the Cl end member (Friedel's salt) measured from supersaturation by Birnin-Yauri and Glasser (1998) of -24.79 is anomalously high compared to those from other studies. A compilation and evaluation of data for the Cl end member (Chapter 5) shows that the average log K_{sp} for this phase is -27.57. Despite the similar reaction times (approximately 6 months) used in the current study and that of Birnin-Yauri and Glasser (1998), samples in the current study appear to have more closely approached equilibrium. The shorter time required to reach equilibrium in the current study may in part be a result of the larger water:solid ratio (20:1) of the samples, compared to a ratio of approximately 2:1 used by Birnin-Yauri and Glasser (1998) (as described in Birnin-Yauri, 1993). In addition, samples in the current study were mixed

continuously during the six months of reaction. which would facilitate the attainment of equilibrium between the solids and aqueous solution. In the experiments performed by Birnin-Yauri and Glasser (1998). sample mixing was intermittent.

This study (Values are average for two replicates)			Birnin-Yauri and Glasser (1998) (Values are average for three replicates)		
Cl/Cl +OH	K_{sp} Formulation	Log K_{sp}	Cl/Cl +OH	K_{sp} Formulation	Log K_{sp}
0.90	$[Ca^{2+}]^4[Al(OH)_4^-]^2[Cl^-]^2[H_2O]^4$	-27.13	1.00	$[Ca^{2+}]^4[Al(OH)_4^-]^2[Cl^-]^2[OH^-]^4$	-24.79
			0.98	$[Ca^{2+}]^4[Al(OH)_4^-]^2[Cl^-]^{1.96}[OH^-]^{2.04}[H_2O]^{4.04}$	-24.92
0.82	$[Ca^{2+}]^4[Al(OH)_4^-]^2[Cl^-]^{1.64}[OH^-]^{2.36}[H_2O]^{4.36}$	-27.07			
0.69	$[Ca^{2+}]^4[Al(OH)_4^-]^2[Cl^-]^{1.38}[OH^-]^{2.62}[H_2O]^{4.62}$	-26.90	0.71	$[Ca^{2+}]^4[Al(OH)_4^-]^2[Cl^-]^{1.42}[OH^-]^{2.58}[H_2O]^{4.58}$	-24.92
			0.61	$[Ca^{2+}]^4[Al(OH)_4^-]^2[Cl^-]^{1.22}[OH^-]^{2.78}[H_2O]^{4.78}$	-25.01
0.54	$[Ca^{2+}]^4[Al(OH)_4^-]^2[Cl^-]^{1.08}[OH^-]^{2.92}[H_2O]^{4.92}$	-26.85	0.52	$[Ca^{2+}]^4[Al(OH)_4^-]^2[Cl^-]^{1.04}[OH^-]^{2.96}[H_2O]^{4.96}$	-25.05

Table 2.10: Comparision of the log values of the solubility products for solids between the Cl and OH end members calculated from the solution compositions measured from supersaturation in the current study, and in the study by Birnin-Yauri and Glasser (1998).

2.4.4. Predicting chloride partitioning

2.4.4.1 Determining solid phase activity coefficients

Equilibrium partitioning between the solid-solution and aqueous-solution phases in a binary system at thermodynamic equilibrium can be determined if the activity coefficients of the solid phase can be calculated. Parameters which describe the variation in the solid-phase activity coefficients as a function of solid phase composition can be derived from either equilibrium or stoichiometric saturation measurements of solid solution solubilities. In low temperature environments. solid-solution aqueous-solution systems rarely achieve thermodynamic equilibrium. Thorstenson and Plummer (1977) developed the concept of stoichiometric

saturation, which refers to a metastable state between an aqueous solution and a solid solution "in situations where, owing to kinetic restrictions, the composition of the solid phase remains invariant, even though the solid phase may be part of a continuous compositional series". The stoichiometric saturation concept is not applicable to solid solution precipitation processes (Glynn and Reardon, 1990). However, this concept may be applied to solid solution dissolution processes when the initial dissolving solid has a homogeneous composition, and when the composition of the solid solution phase remains invariant during dissolution. In order to meet this second condition, the rate of precipitation of any secondary phases must be slow compared to the rate of dissolution of the solid solution phase. (Glynn and Reardon, 1990).

The only dissolution data currently available for the chloride-hydroxide system was measured from undersaturation in the current study. Of the two sample sets, the solution compositions measured for B replicate solids with chloride ratios of 0.4 or lower are thought be controlled in part by hydrogarnet. Although these samples are likely closer to thermodynamic equilibrium, the continued persistence of the solid solution phase in the solids indicates that equilibrium had not been reached. More importantly, solubility data for the stable phases (hydrogarnet and portlandite) could be collected at thermodynamic equilibrium, but not for the OH-end member, because this phase is unstable and would no longer be present. Therefore, in order to obtain solubility measurements for the OH end member, a metastable equilibrium condition with respect to this phase must have been achieved. The solution compositions measured for the A replicates from undersaturation are likely more representative of the solubility of the solid solutions. Although it can not be demonstrated that these samples are at stoichiometric saturation, this data will be used as a first approximation for estimating the partitioning of chloride between the solid and aqueous phases, because it is the best data currently available. In future studies to determine the dependence of solubility on the solid solution phase composition between the OH-end member and other phases, experiments to measure the solubility of these phases at stoichiometric saturation may be more appropriate.

The behavior of non ideal or real solutions can be evaluated with respect to the degree to which they deviate from ideality (Nordstrom and Munoz, 1986). In applying this comparison to free energy, the excess free energy of a solution is defined as the free energy of the real solution minus the free energy of the ideal solution ($G^E = G^{real} - G^{ideal}$). Guggenheim's (1937, 1952) expansion series is commonly used to represent the excess free energy (G^E) of the binary solid solution $B_{1-x}C_xA$ as a function of composition

$$G^E = x\,(1\text{-}x)\,RT\,[a_0 + a_1\,(x\,(1\text{-}x)) + a_2(x - (1\text{-}x)^2 \ldots) \qquad (2.3)$$

where x is the mole fraction of the substituting ion (in this case, chloride). The a_0 and a_1 terms are often sufficient to accurately represent the dependence of the solid-phase activity coefficients on the composition (Glynn et al., 1990). The solid solution is referred to as regular if the a_0 term alone is required to describe the dependence of the activity coefficients on the solid solution composition, and sub-regular if both the a_0 and a_1 parameters are required. The excess free energy of the solid solution can be calculated from the solubilities of the pure phases, and the solubilities of the solid solutions at stoichiometric saturation (K_{ss}) according to the expression

$$G^E = RT[\ln K_{SS} - x(\ln K_{CA} + \ln x) - (1\text{-}x)(\ln K_{BA} + \ln(1\text{-}x)] \qquad (2.4)$$

where K_{CA} and K_{BA} are the solubility constants of the pure end members. Equations (2.3) and (2.4) can be combined and re-arranged in terms of $\ln K_{ss}$. Writing this expression for a sub-regular solid solution (i.e. using a_0 and a_1 parameters)

$$\ln K_{ss} = a_0\,x\,(1\text{-}x) + a_1\,x(1\text{-}x)(x\,(1\text{-}x)) + x(\ln K_{CA} + \ln x) + (1\text{-}x)(\ln K_{BA} + \ln(1\text{-}x)) \qquad (2.5)$$

$\ln K_{SS}$ values measured as a function of the solid solution composition can be fit to equation 2.5, using regression analysis to solve for the a_0 and a_1 parameters. The solid phase activity coefficients (γ_{BA} and γ_{CA}) can then be calculated according to equations 2.6.

$$\ln \gamma_{BA} = X^2_{CA}[a_0 - a_1(3X_{BA} - X_{CA}) + \ldots.]$$
$$\ln \gamma_{CA} = X^2_{BA}[a_0 + a_1(3X_{CA} - X_{BA}) + \ldots.] \qquad (2.6)$$

The variables X_{CA} and X_{BA} are the mole fractions of the pure end members in the solid solution phase. In constructing a Lippmann diagram, the solidus curve is first determined according to equation 2.7. The total solubility product values ($\Sigma\ \Pi$) calculated for given solid-phase compositions are then substituted into the solutus equation (equation 2.8) to solve for the aqueous activity-fractions at thermodynamic equilibrium. The Lippmann diagram is constructed by plotting $\Sigma\ \Pi$ values on the ordinate, against two super-imposed scales on the abscissa; the chloride mole fraction in the solid, and the chloride mole fraction in solution.

$$\Sigma \Pi_{eq} = X_{BA}\,\gamma_{BA}K_{BA} + X_{CA}\,\gamma_{CA}\,K_{CA} \qquad (2.7)$$

$$\Sigma \Pi_{eq} = 1/\left(\frac{X_{B,aq}}{K_{BA}\,\gamma_{BA}} + \frac{X_{C,aq}}{K_{CA}\,\gamma_{CA}}\right) \qquad (2.8)$$

2.4.4.2 Derivation of an expression for the solutus

Glynn and Reardon (1990) derive the solutus equation (2.8) for the general case of a non-ideal solid solution phase $B_{1-x}C_xA$. by expressing the activities of the solid phase components in terms of activity coefficients and mole fractions. In this derivation, the activity fractions of the substituting cations are defined as

$$X_{B.aq} = \frac{[B^-]}{[B^-] + [C^-]} \qquad (2.9)$$

and

$$X_{C.aq} = \frac{[C^-]}{[B^-] + [C^-]}$$

where $[B^-]$ and $[C^-]$ are the activities of the substituting ions, and $X_{B.aq}$ and $X_{C.aq}$ are the mole fractions of ions B^- and C^- in solution. In most of the systems where SSAS theory has been applied to date (e.g. strontium carbonates (Plummer and Busenberg, 1987); magnesium carbonates (Busenberg and Plummer, 1989)), the substituting ions have been cations, they have occurred in a 1:1 ratio in the solid, and their stoichiometric coefficients in the solubility product expressions have also been equal to 1. However, in the monocalcium aluminate hydrates, the substituting ions are anions, and associated water molecules. For example, in the hydroxide-chloride system, two chloride ions substitute for two hydroxide ions plus eight associated water molecules in the interlayer of the OH end member. The dissolution reactions for the two end members are

$$3CaO{\cdot}Al_2O_3{\cdot}Ca(OH)_2{\cdot}18H_2O_{(s)} \rightleftharpoons 4Ca^{2+} + 2Al(OH)_4^- + 6OH^- + 12H_2O$$

$$3CaO{\cdot}Al_2O_3{\cdot}CaCl_2{\cdot}10H_2O_{(s)} \rightleftharpoons 4Ca^{2+} + 2Al(OH)_4^- + 2Cl^- + 4OH^- + 4H_2O \qquad (2.10)$$

and the corresponding solubility product expressions:

$$K_{sp\ OH} = [Ca^{2+}]^4[Al(OH)_4^-]^2[OH^-]^6[H_2O]^{12} \quad (2.11)$$

$$K_{sp\ Cl} = [Ca^{2+}]^4[Al(OH)_4^-]^2[Cl^-]^2[OH^-]^4[H_2O]^4 \quad (2.12)$$

Adding equations 2.11 And 2.12 together and collecting like terms gives the expression for the total solubility product:

$$\Sigma\,\Pi = [Ca^{2+}]^4[Al(OH)_4^-]^2\,[OH^-]^4[H_2O]^4\,\{[Cl^-]^2 + [OH^-]^2[H_2O]^8\} \quad (2.13)$$

In order to solve for the solutus, the mole fraction of the solid phase components ($X_{Cl}$and X_{OH}) must be expressed in terms of the pure end member solubilities (K_{OH} and K_{Cl}), the solid phase activity coefficients, and the aqueous mole fractions Cl^- and OH^-.

Kersten (1996) used SSAS theory to model the calcium silicate hydrate (C-S-H)-portlandite system. In the dissolution expression for the C-S-H phase, both calcium and silicate have stoichiometric coefficients of 2. Kersten's approach to this problem was to re-define the K_{sp} of the C-S-H phase as equal to K_{sp}^2, and then take the square root of both sides of the dissolution equation. The solutus expression can then be solved according to the method outlined by Glynn and Reardon (1990). A different approach has been used in the current study, in which the activity fractions in solution were redefined as:

$$X_{OH,\,aq} = \frac{[OH^-]^2[H_2O]^8}{[Cl^-]^2 + [OH^-]^2[H_2O]^8} \quad (2.14)$$

$$X_{Cl,\,aq} = \frac{[Cl^-]^2}{[Cl^-]^2 + [OH^-]^2[H_2O]^8} \quad (2.15)$$

This is equivalent to redefining the activity of the substituting ions in equations 2.8 as $[B^-] = [Cl^-]^2$ and $[C^-] = [OH^-]^2[H_2O]^8$. Conceptually, this represents the difference between the mineral phases after substitution occurs (i.e. two hydroxide ions in the mineral structure are replaced by two chloride ions and 8 water molecules).

Average ln K_{sp} values were calculated for the A replicate samples from undersaturation, and fit to equation 2.5. In this case, x in equation 2.5 is the measured mole fraction of chloride in the solid solution, determined by mass balance for solid compositions outside of the observed

miscibility gap. For solids within the miscibility gap, the calculated bulk mole fraction based on the reagents added were used. K_{BA} is the solubility of the hydroxide end-member (log K_{sp} = -25.80) and K_{CA} is the solubility of the chloride end member (log K_{sp}= -27.57). The values for the end member solubility products were derived by compiling and evaluating solubility data from the current study with that previous published in the literature (Chapter 5). The best fit gave a_0 = -0.324 and a_1 = -7.95 (n=8, df=7, r^2=0.75). The original data points and the regression line are plotted in Figure 2.12.

The excess free energy parameters (a_0, a_1) were input into the geochemical equilibria model PHREEQC (Parkhurst and Apello, 1999). This program was used to determine the position of possible spinodal gaps and miscibility gaps in the series. The results of this modeling are summarized in Table 2.11.

Original data	Parameters		Spinodal gap		Miscibility gap	
	a_0	a_1	Lower Cl ratio	Upper Cl ratio	Lower Cl ratio	Upper Cl ratio
A rep. from undersaturation	-0.324	-7.95	0.023	0.45	7.0E-05	0.66

Table 2.11: The excess free energy parameters (a_0, a_1) derived by fitting the measured solubility data were input into the geochemical equilibria model, PHREEQC (Parkhurst and Appello, 1999) to calculate the positions of the miscibility and spinodal gaps in the system.

Solid solutions with compositions within a spinodal gap are intrinsically unstable, and two solid solution phases will exist in this region. Within the miscibility gap, a single solid solution phase may form initially, but is metastable and will exsolve into two phases when thermodynamic equilibrium is attained (Prigogine and Defay, 1954). The predicted spinodal gap occurs between carbonate ratios of 0.023 to 0.45, and is wider than the observed miscibility gap which has a lower limit of 0.0 to 0.1 and an upper limit of 0.33 (Section 2.4.1). The predicted miscibility gap extends from 0.0 to 0.66, and is also wider than the observed occurrence of two phases in this system. These results demonstrate that the excess free energy parameters calculated based on the results from undersaturation over-predict the width of the miscibility gap in this system.

A Lippmann diagram has been constructed using the calculated excess free energy parameters as a first approximation of equilibrium in the hydroxide-chloride series. Total solubility products ($\Sigma \Pi$) have been calculated based on the aqueous compositions measured for the A replicates from undersaturation, and are plotted on Figure 2.13. The aqueous solution and solid solution compositions do not fall directly on the solutus and solidus, respectively, despite the fact that the solubility data from these samples was used to derive the excess free energy parameters used in the construction of the Lippmann diagram. For comparison, the solubility results were also plotted on a Lippmann diagram constructed by redefining the end member solubility products as K_{sp}^2, as done by Kersten (1996). Apart from difference in the absolute values of the end member solubility products, the Lippmann diagrams were very similar in appearance, and the fit to the A replicate data from undersaturation was approximately the same in both diagrams. Based on this comparison, the fact that the data used to derive the excess free energy parameters do not correlate well to the Lippmann diagram is due to the poor fit ($r^2 = 0.75$) of the regressed equation to the original solubility data, and not due to the simplifications made to solve the solutus expression. Most importantly, these results indicate that the usefulness of this model for predictions in the OH-Cl system is limited.

In the fitting procedure used to obtain the excess free energy parameters, the bulk compositions of samples with chloride ratios of 0.1 and 0.25 (within the miscibility gap) were included in the regression analysis. Although removal of these points significantly increased the fit of regressed equation to $r^2 = 0.87$, the excess free energy parameters derived failed to predict the presence of a miscibility gap when input into PHREEQC (Parkhurst and Apello, 1999). This highlights the fact that the number of solubility measurements in the system that were not in the miscibility gap (n=6) was not sufficient to clearly define the change in solubility as a function of the chloride ratio. This is an important consideration which must be taken into account in future solubility studies if excess free energy parameters are to be derived.

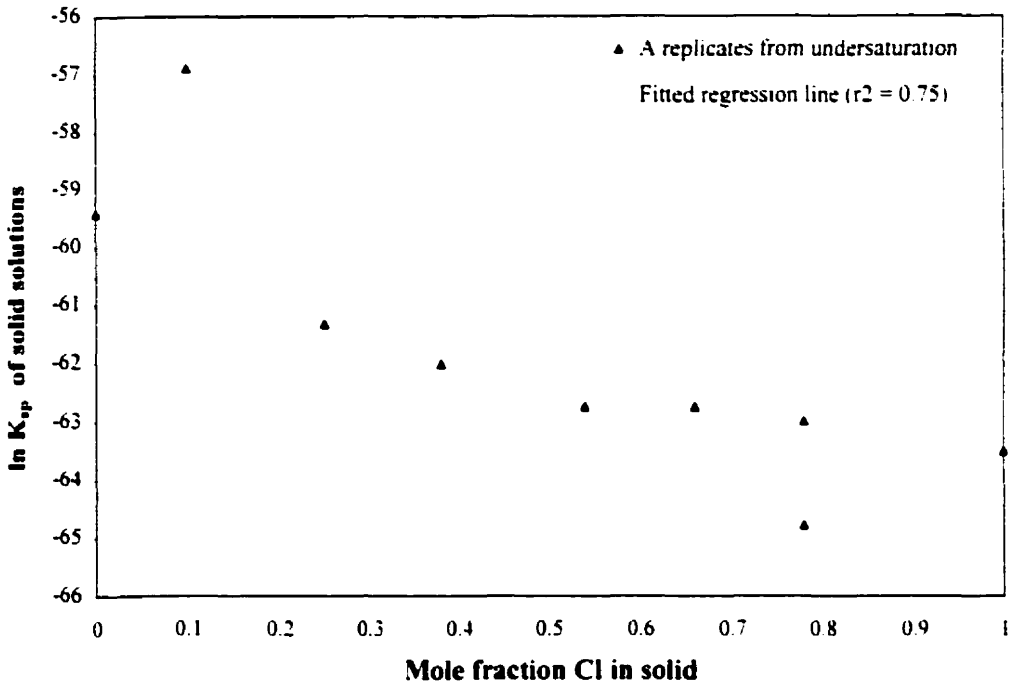


Figure 2.12: Natural log of the average K_{sp} values calculated for the A replicates from undersaturation plotted versus the mole fraction of chloride in the solid. The solid line is the fitted sub-regular solid solution model for this system, with excess free energy parameters of a_0= -0.624 and a_1 = -7.95.

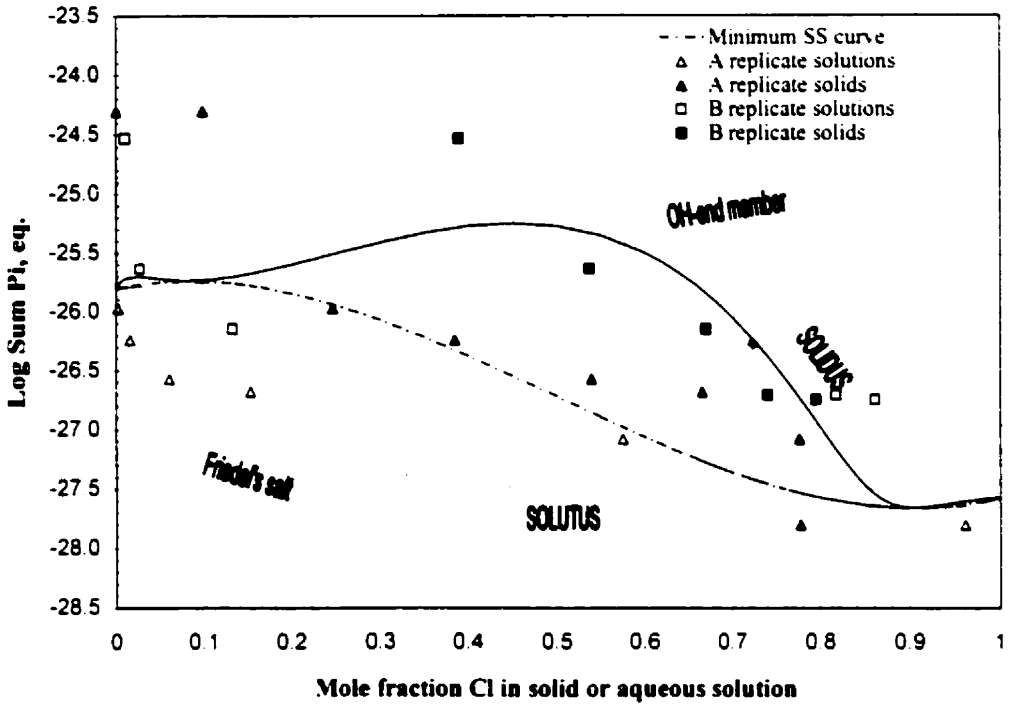


Figure 2.13: Lippmann phase diagram for the series between the chloride and hydroxide end member at 25 °C, constructed using excess free energy parameters $a_0 = -0.324$, $a_1 = -7.95$. The total solubility product ($\Sigma\Pi$) was calculated based on the solution compositions measured from undersaturation, and are plotted versus the mole fraction of Cl in the solid or aqueous solution (filled and open symbols, respectively). Saturation curves for the pure chloride (Friedel's Salt) and hydroxide end-members are drawn as short-dashed lines. The minimum stoichiometric saturation (SS) curve is also shown. The vertical, long-dashed lines define the limits of the observed miscibility gap.

2.5 Conclusions

The X-ray diffraction results from the current study support the conclusion of Pöllmann and Kuzel (1988) that the miscibility gap begins at a Cl/(Cl+OH) ratio of 0.33, rather than above a ratio of 0.4 as suggested by Roberts (1969). The lower limit of the miscibility gap lies between ratios of 0.0 and 0.1, based on the XRD results of Birnin-Yauri (1993), Pöllmann and Kuzel (1988), Roberts (1969) and the current study. The occurrence of a miscibility gap in this system may be caused by differences in the bonding characteristics between the Cl^- and OH^- ions and/or the number of water molecules required in the interlayer to maintain the hydrogen bond network, which is thought to provide cohesion between the main and interlayers of the structure.

The general rule developed by Sacerdoti and Passaglia (1988) for the number of extra water molecules present in the interlayer region of calcium aluminate hydrates can be applied to the hydroxide end member by considering hydroxide as a anion group consisting of an oxygen and a hydrogen atom. The number of extra water molecules is then predicted to be $2X = 2 (2OH^-) = 4$, consistent with the observed stable hydration state of the OH end member in solution.

The solubility products calculated for the solid solution phases between the chloride and hydroxide end member (measured from supersaturation) in the current study are approximately two orders of magnitude lower than those calculated for solids with similar chloride ratios from the data of Birnin-Yauri and Glasser (1998). The log value of the solubility product for the Cl end member (Friedel's salt) measured from supersaturation by Birnin-Yauri and Glasser (1998) is anomalously high compared to those from other studies. Despite the similar reaction times (approximately 6 months) used in the current study and that of Birnin-Yauri and Glasser (1998), samples in the current study appear to be much closer to equilibrium. This may be in part due to the higher water to solid ratio of 20:1 used in the current study, compared to the ratio of approximately 2:1 used by Birnin-Yauri and Glasser (1998). In addition, continuous mixing of the samples in the current study likely facilitated a quicker approach to equilibrium, compared to the intermittent mixing of samples in the experiments of Birnin-Yauri and Glasser (1998).

In the current study, the A replicate samples from undersaturation are thought to be the most representative of the solubilities of the solid solution phases. However, excess free energy parameters derived from this data set predict a wider miscibility gap than is actually observed. In addition, the aqueous and solid phase compositions from which the excess free energy parameters were derived are not well-reproduced by the solutus and solidus, respectively, on

the Lippmann diagram. This is likely a result of the poor fit of the regression equation to the solubility data ($r^2 = 0.75$). Therefore, the usefulness of the excess free energy parameters, and the Lippmann diagram constructed from them is limited. More measurements of solid solution phase solubilities outside of the miscibility gap (between chloride ratios of 0.33 and 1.0) are required in order to better define the variation in solubility of the solid solution phases as a function of composition.

2.6 Recommendations

Further solubility studies on the solid solutions between the OH and Cl end members are required to better delineate the effect of solid solution composition on the measured solubility products. These types of studies are complicated by the persistence of the metastable OH end member, which may render measurement of the stable phase assemblage (hydrogarnet and portlandite) unfeasible. Therefore, the possibility of measuring the solubility of the OH end member at stoichiometric saturation should be investigated.

The amount of data collected in regions where a single solid solution phase exists has been identified as an important design criterion when SSAS theory is to be used to derive excess free energy parameters. I would recommend a minimum of twice the number of points measured in the current study (≈16 solubility measurements).

2.7 References

Barker J. and Chatten S. (1982). A technique for determining low concentrations of total carbonate in geologic materials. *Chem. Geol.* **36**, 317-323.

Bentley H. W., Phillips F. M., and Davis S. N. (1980). Chlorine-36 in the terrestrial environment. *In:* Handbook of Environmental Isotope Geochemistry, Eds. Fritz P., and Fontes J. Ch., **Vol 2**, 427-480.

Birnin-Yauri U. A. (1993). Chloride in cement: Study of the system $CaO-Al_2O_3-CaCl_2-H_2O$. Ph.D. Thesis, University of Aberdeen, Aberdeen, United Kingdom.

Birnin-Yauri U. A. and Glasser F. P. (1998). Friedel's salt, $Ca_2Al(OH)_6(Cl,OH)\cdot 2H_2O$: Its solid solutions and their role in chloride binding. *Cem. Concr. Res.*, **28**, 1713-1723.

Brownlow A. H. (1979). *Geochemistry*. Prentice-Hall Inc., New Jersey, 498 p.

Buttler F. G., Dent Glasser L. S., and Taylor H. F. W. (1959). Studies on $4CaO\cdot Al_2O_3\cdot 13H_2O$ and the related natural mineral hydrocalumite. *J. Amer. Ceram. Soc.*, **42**, 121-126.

Carlson E. T. and Berman H. A. (1960). Some observations on the calcium aluminate carbonate hydrates. *Journal of Research, of the National Bureau of Standards - A. Physics and Chemistry*, **64A**, pp. 333-341.

Dougan W. K. and Wilson A. L. (1974). The absorptiometric determination of aluminum in water. A comparison of some chromogenic reagents and the development of an improved method. *Analyst*, **99**, 413-430.

Fischer V. R., Kuzel H.-J., and Schellhorn H. (1980). Hydrocalumit: Mischkristalle von "Friedschem Salz" $3CaO\cdot CaCl_2\cdot Al_2O_3\cdot 10H_2O$ und Tetracalciumaluminat- hydrat $3CaO\cdot Ca(OH)_2\cdot Al_2O_3\cdot 13H_2O$?. *N. Jb. Miner. Mh.*, **7**, 322-334.

Fisher R. and Kuzel H. J. (1982). Reinvestigation of the system $C_4A\cdot nH_2O$ - $C_4ACO_2\cdot nH_2O$. *Cem. Concr. Res.*, **12**, 517-526.

Glasser F. P., Kindness A. and Stronach S.A. (1999). Stability and solubility relationships in AFm phases Part I. Chloride, sulfate and hydroxide. *Cem. Concr. Res.*, **29**, 861-866.

Glynn P. D. and Reardon E. J. (1990). Solid-solution aqueous-solution equilibria: Thermodyanmic theory and representation. *Am. Jour. Science*, **290**, 164-201.

Glynn P. D., Reardon E. J., Plummer L. N., and Busenberg E. (1990). Reaction paths and equilibrium end-points in solid-solution aqueous-solution systems. *Geochim. Cosmochim. Acta*, **54**, 267-282.

Guggenheim E. A. (1937). Theoretical basis of Raoult's law. *Transactions of the Faraday Society*, **33**, 151-159.

Guggenheim E. A. (1952). Mixtures. London, Oxford University Press, 270 p.

Kersten M. (1996). Aqueous solubility diagrams for cementitious waste stabilization systems. 1. The C-S-H solid solution system. *Environ. Sci. Tech.*, 30, 2286-2293.

Kimura K., Ishikawa T., Kinno M., and Nakamura T. (1994). Compilation of neutron activation cross sections and trace element contents of concrete for estimating the induced radioactivities. *Proc. Int. Conf. Radiat. Shielding, 8th*, **1**, 35-42.

Kingsley J. J. and Patil K.C. (1988). A novel combustion process for the synthesis of fine particle α-alumina and related oxide materials. *Materials Letters*, **6** No. 11,12, pp. 427-432.

Kotz J. C. and Purcell K. F. (1991). *Chemistry & Chemical Reactivity*, 2nd edition, Saunders College Publishing.

Lea F. M. (1970). The chemistry of cement and concrete. Edward Arnold (Publishers) Ltd. 698 p.

Nordstrom D. K. and Munoz J. L. (1986). Geochemical Thermodynamics. Blackwell Scientific Publications, 477 p.

Parkhurst D. L. and Apello C. A. J. (1999). User's guide to PHREEQC (Version 2)-- A computer program for speciation, batch-reaction, one-dimensional transport, and inverse geochemical calculations. U.S. Department of the Interior, U.S. Geological Survey, Water-Resources Investigations Report 99-4259.

Passaglia E. and Sacerdoti M. (1988). Hydrocalumite from Montalto di Castro, Viterbo, Italy. *N. Jb. Miner. Mh.*, **10**, 454-461.

Pöllmann H. and Kuzel H. J. (1988). Synthesis and polymorphic transformations of solid solutions in the system $3CaO{\cdot}Al_2O_3{\cdot}CaCl_2{\cdot}nH_2O$- $3CaO{\cdot}Al_2O_3{\cdot}Ca(OH)_2{\cdot}nH_2O$-$H_2O$. *N. Jb. Miner. Mh.*, 193-202.

Reardon E. J. (1990). An ion interaction model for the determination of chemical equilibria in cement/water systems. *Cem. Concr. Res.*, **20**, 175-192.

Roberts M. H. (1969). Calcium aluminate hydrates and related basic salt solutions. Supplementary Paper II-29. *Proc. 5th Intl. Symp. on the Chemistry of Cements*, Tokyo, 104-117.

Sacerdoti M. and Passaglia E. (1988). Hydrocalumite from Latium, Italy: its crystal structure and relationship with synthetic phases. *N. Jb. Miner. Mh.*, **10**, 462-475.

Schwiete H. E. and Ludwig U. (1969). Crystal structures and properties of cement hydration products (hydrated calcium aluminates and ferrites). *5th Intl. Symp. on the Chem. of Cem.*, Session **II-2**, Tokyo, 37-67.

Taylor H.F.W. (1997). Cement Chemistry (2nd edition). Academic Press 459p

Thorstenson D. C. and Plummer L. N. (1977). Equilibrium criteria for two-component solids reacting with fixed composition in an aqueous-phase; example: the magnesian calcites. *Amer. J. Sci.*, **277**, 1203-1223.

Turriziani R. and Schippa G. (1955). Contribution to the knowledge of hydrated calcium chloro-aluminates. *Ric. Scient.* **25**, 3102-3106.

Wang J., Kalinichev A. G., Kirkpatrick R. J. and Hou X. (2001). Molecular modeling of the structure and energetics of hydrotalcite hydration. *Chem. Mater.*, **13**, 145-150.

Zhang M. (2000). Incorporation of oxyanionic B, Cr, Mo, and Se into hydrocalumite and ettringite: application to cementitious systems. Ph.D. thesis, University of Waterloo, Waterloo, Canada.

Chapter 3

Solubility of solid solutions in the system $CaO-Al_2O_3-CaCl_2-CaCO_3-H_2O$ from super- and undersaturation

3.1 Introduction

Carbonate is an important anion in reactions with cement-based materials. The universal presence of CO_2 in the atmosphere ensures that most cements will be in contact with a potential source of carbonate (Damidot et al., 1994). Calcium carbonate has also been used as cement additive, to influence its early setting and hardening characteristics (Ramachandran and Zhang, 1986). Carbonate is of particular importance in studies of the calcium aluminate hydrates, because carbonate ions are reported to be highly preferred in these minerals (Glasser et al., 1999; Taylor, 1997). The carbonate end member of the calcium aluminate hydrates is monocarboaluminate ($3CaO{\cdot}Al_2O_3{\cdot}CaCO_3{\cdot}11H_2O$). Information on the stability of solid solutions formed between the chloride and carbonate end members is necessary for both waste disposal, and concrete engineering applications. The replacement of chloride ions by carbonate ions in irradiated concrete at disposal sites could result in the release of chlorine-36 to the environment. In concrete structures, the replacement of Cl^- in Friedel's salt by carbonate ions leads to increased chloride concentrations in pore solutions, and consequently, increased risk of corrosion to reinforcing bar.

Pöllmann (1986) conducted a crystallographic study of solid phases between the chloride and carbonate monocalcium aluminate hydrates. Solid solutions were prepared by mixing calcium salts ($CaCO_3$, $CaCl_2{\cdot}2H_2O$), calcined CaO, and monocalciumaluminate ($CaO{\cdot}Al_2O_3$) with distilled water, sealing the mixtures in polyethylene bottles, and shaking continuously for 12 months. This experiment showed that a complete solid solution exists between the chloride end member (carbonate ratio of zero), and solids with a carbonate ratio of 0.83, where the carbonate ratio is defined as the ratio of carbonate ions to the total ions in the interlayer of the solid solution phase (i.e. $CO_3/(CO_3+2Cl)$). At higher carbonate ratios, the carbonate end member (monocarboaluminate) coexists with a solid solution with the following composition:

$$3CaO{\cdot}Al_2O_3{\cdot}0.17CaCl_2{\cdot}0.83CaCO_3{\cdot}nH_2O$$

Pöllmann's study was restricted to examination of the solid phases. No information was provided on the solution compositions coexisting with these solid solutions.

In a binary solid solution series, predictions of the final equilibrium partitioning between the solid solution and aqueous solution phases can be made using solid-solution aqueous-solution (SSAS) theory (Glynn and Reardon, 1990; Glynn et al. 1990), if the solid-phase activity coefficients are known. From measurements of solid solution solubilities at thermodynamic equilibrium, solid solution excess free energies can be obtained which can be used to calculate solid phase activity coefficients. The solubilities measured as a function of solid solution composition are first fitted to Guggenheim's (1937, 1952) expansion series for the excess free energy of mixing of a binary solid solution. Regression analysis is used to derive the excess free energy parameters (a_0, a_1...). These parameters are used in conjunction with the solubility products of the pure end members and SSAS theory to create Lippmann diagrams (Lippmann, 1980). These diagrams can be used to predict the solubility of any solid solution at thermodynamic equilibrium (Glynn and Reardon, 1990).

The current study was undertaken to determine the solubility of solid solutions with varying amounts of carbonate, between the pure chloride and carbonate end members of the monocalcium aluminate hydrates. Solubility experiments were conducted from supersaturated conditions, and were then repeated from undersaturation, to determine if equilibrium had been attained in the system. The solution compositions were measured, and the solid phases were identified using X-ray diffraction (XRD) analysis and scanning electron microscopy. Solubility data measured as a function of the carbonate ratio in the solid phase was fitted to Guggenheim's expansion series for a binary, sub-regular solid solution. A second set of excess free energy parameters was derived based on the observed miscibility gaps. The derived parameters have been used to construct a Lippmann diagram for this system, which can be used to estimate equilibrium partitioning between the solid solution and aqueous solution.

3.2 Experimental

The experimental procedures and analytical techniques are described in Chapter 2.

3.3 Results

3.3.1 Solutions

Conductance measurements with time for the three samples used to monitor the approach to equilibrium from supersaturation and undersaturation are plotted in Figure 3.1. The conductance measurements of the chloride end member are described in Chapter 2, Section 2.3.1. In the experiment from supersaturation, the conductance of carbonate end member sample increased slightly between 0 and 14 days, after which time the conductance stabilized at ≈1600 μS/cm. The conductance values measured from undersaturation reached steady-state value of ≈1400 μS/cm after 14 days of reaction, which is approximately 12% lower than the final value measured from supersaturation. In the experiment from supersaturation, the sample with a composition between the chloride and carbonate end members had a high conductance initially (≈ 9000 μm/cm), which gradually decreased to a stable value of approximately 3300 μm/cm after 50 days of reaction. A conductance value of 3400 μS/cm was measured for this composition at the end of the experiment from undersaturation, within 3% of the value from supersaturation.

The solution compositions measured for the solid solutions in the experiments from supersaturation and undersaturation are presented in Tables 3.1 and 3.2, respectively. The concentrations of calcium, chloride and aluminum for these samples are plotted versus the calculated carbonate ratio in the solid in Figures 3.2, 3.3 and 3.4, respectively. The ratio of CO_3 to (CO_3 + 2Cl) in the solid solution phase is calculated based on the quantities of reagents used initially. The dissolved inorganic carbon contents of the solutions were measured in the experiment from supersaturation, but were below detection (<0.061 mmol/L) for all samples. Consequently, the DIC contents of the solutions were not measured in the experiments from undersaturation.

The measured pH values for the solutions in the experiment from supersaturation are approximately constant at an average value of 11.75 between the chloride end member (carbonate ratio = 0.0) and the carbonate end member (carbonate ratio = 1.0). The pH values measured from undersaturation are within 5% of those measured from supersaturation.

In the experiment from supersaturation, Ca^{2+} and Cl^- concentrations measured in the replicate samples are similar, except at a carbonate ratio of 0.6, where the Ca^{2+} concentration in the A replicate is 35% higher than in the B replicate. The concentrations of both Ca^{2+} and Cl^- are

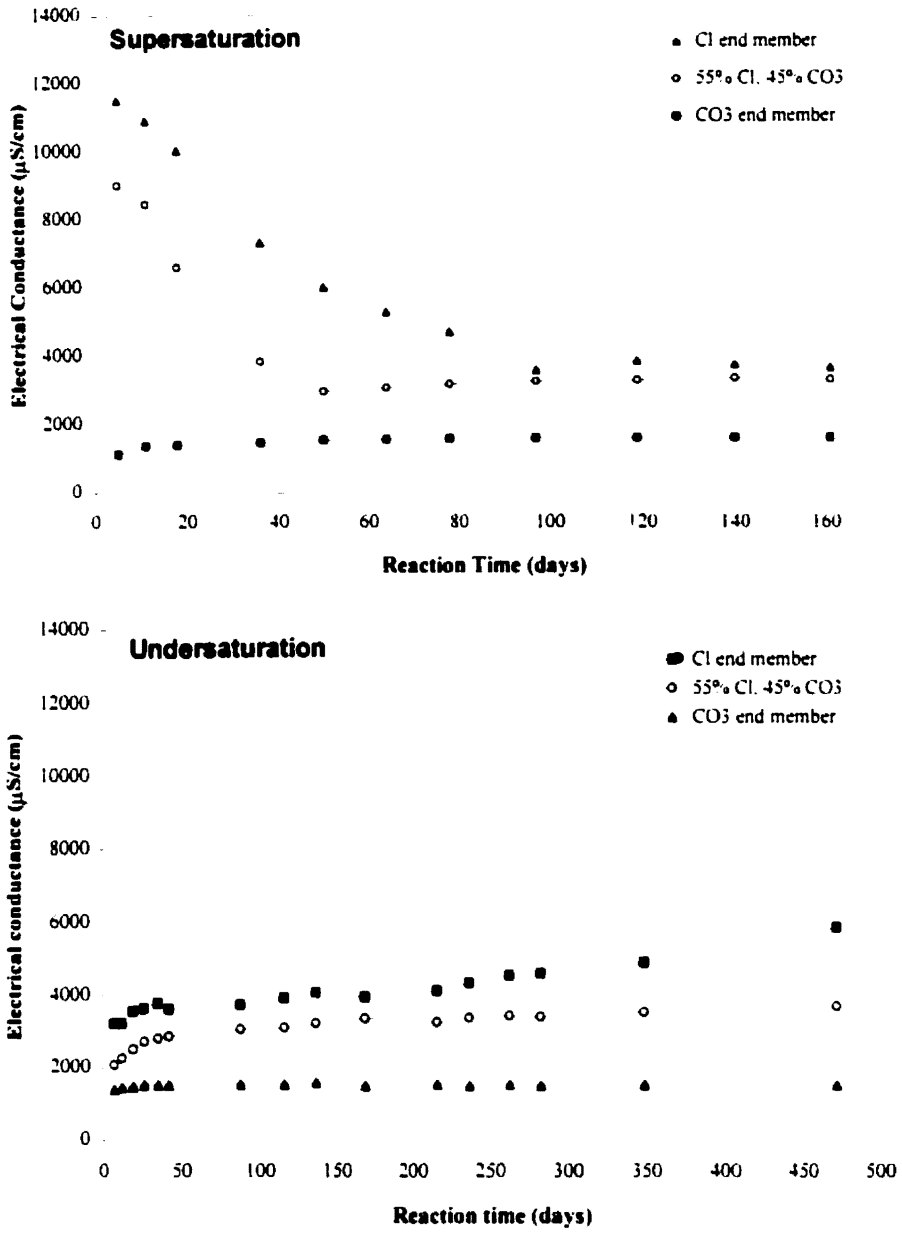


Figure 3.1: Electrical conductance measurements versus reaction time for the experiments from supersaturation and undersaturation. The conductance of both the Cl and CO_3 end members, and a sample with a composition midway between the end members were measured to monitor the approach of the system to equilibrium.

essentially stable between carbonate ratios of 0.0 to 0.30, and then decrease gradually as the carbonate ratio in the solid increases. In the experiment from undersaturation, the measured concentrations of Ca^{2+} and Cl^- are similar in the A and B replicates, except in the samples with carbonate ratios of 0.15, 0.30, and 0.45. In these samples, the Ca^{2+} concentrations are 22% higher in the A replicates than in the B replicates, and the Cl^- concentrations are also up to 55% higher in these samples. This suggests that the excess calcium in the A replicate is balanced by chloride. Overall, the Ca^{2+} and Cl^- solution concentrations measured in the experiment from undersaturation agree well with those from supersaturation, with the exception of the three A replicate samples from undersaturation which have elevated Ca^{2+} and Cl^- concentrations. An examination of the ratios of the ion concentrations (e.g. Ca:Al) in Table 3.2 shows that the dissolution of solid phases from undersaturation is incongruent, as observed for solids in the OH-Cl system (Chapter 2).

The trends in the aluminum concentrations as a function of carbonate ratio in the solid are not as well-reproduced between replicates as the trends observed in the Ca^{2+} and Cl^- concentrations. In general, the aluminum concentrations in solution are approximately 1.5 mmol/L at low carbonate ratios, but decrease between carbonate ratios of 0.45 and 0.60 to 1.0 mmol/L, and then gradually increase again with increasing carbonate in the solid. This general trend is seen in both the experiments from super- and undersaturation.

Mineral saturation indices were calculated using the geochemical equilibria model SIMUL (Reardon, 1990). The solution compositions of the A and B replicates in both solubility experiments (Tables 3.1 and 3.2) were modeled. In these simulations, the carbonate concentrations in solution were estimated by equilibrating the solutions with calcite. The calculated SI values are plotted in Figure 3.5 versus the calculated carbonate ratio in the solid. In the experiment from supersaturation, the calculated SI values for the minerals are similar in both sets of replicates. Near the Cl end member, the samples are supersaturated with respect to hydrogarnet, but then decrease to close to saturation as the carbonate ratio increases above 0.5. The solutions are at or slightly supersaturated with respect to gibbsite over the entire range of carbonate ratios studied, and all solutions are calculated to be undersaturated with respect to portlandite.

CO_3/ (CO_3+2Cl)	pH		Calcium (mmol/kg)		Aluminum (mmol/kg)		Chloride (mmol/kg)	
	A	B	A	B	A	B	A	B
0.0	11.70	11.91	13.94	16.56	1.583	0.4625	18.47	19.58
0.15	11.75	11.75	14.15	13.40	1.394	1.392	18.01	17.24
0.30	11.74	11.77	13.34	13.34	1.667	1.281	16.98	17.30
0.45	11.72	11.78	10.09	11.60	1.156	1.887	11.97	12.98
0.60	12.10	11.62	13.53	8.562	0.0400	0.7490	9.320	9.149
0.75	11.66	11.63	6.254	5.987	0.7394	0.9355	4.869	4.755
0.91	11.74	11.72	5.022	4.758	1.033	1.152	1.485	1.521
1.00	11.72	11.73	4.141	4.050	1.233	1.378	0.0175	0.000

Table 3.1: Solution data measured in the experiment from supersaturation for the samples between the Cl end member (CO_3/(CO_3+2Cl) = 0.0) and the carbonate end member (CO_3/(CO_3+2Cl) = 1.0). A and B are replicate samples. The carbonate ratio given for the solid solution phase is predicted, based on the reagents added.

CO_3/ (CO_3+2Cl)	pH		Calcium (mmol/kg)		Aluminum (mmol/kg)		Chloride (mmol/kg)	
	A	B	A	B	A	B	A	B
0.0	11.52	11.69	15.04	14.65	0.9682	1.598	23.64	18.95
0.15	11.14	11.93	17.07	13.15	1.012	1.230	34.67	16.19
0.30	11.22	11.62	15.58	12.25	0.6141	1.431	32.76	15.03
0.45	11.33	11.48	15.36	12.22	0.5832	0.6805	27.35	20.54
0.60	11.70	11.72	8.399	7.579	0.6158	0.6617	11.91	10.64
0.75	11.60	11.73	5.853	5.498	0.8099	0.9023	6.160	4.932
0.91	11.79	11.75	4.459	4.135	0.9889	1.309	2.449	1.416
1.00	11.78	11.77	3.385	3.570	1.333	1.151	0.02915	0.03043

Table 3.2: Solution compositions measured in the experiment from undersaturation for solids between the Cl end member (CO_3/(CO_3+2Cl) = 0.0) and the carbonate end member (CO_3/(CO_3+2Cl) = 1.0) after 515 days of reaction. A and B are replicate samples. The carbonate ratio given for the solid solution phase is calculated based on the reagents added initially in the experiment from supersaturation.

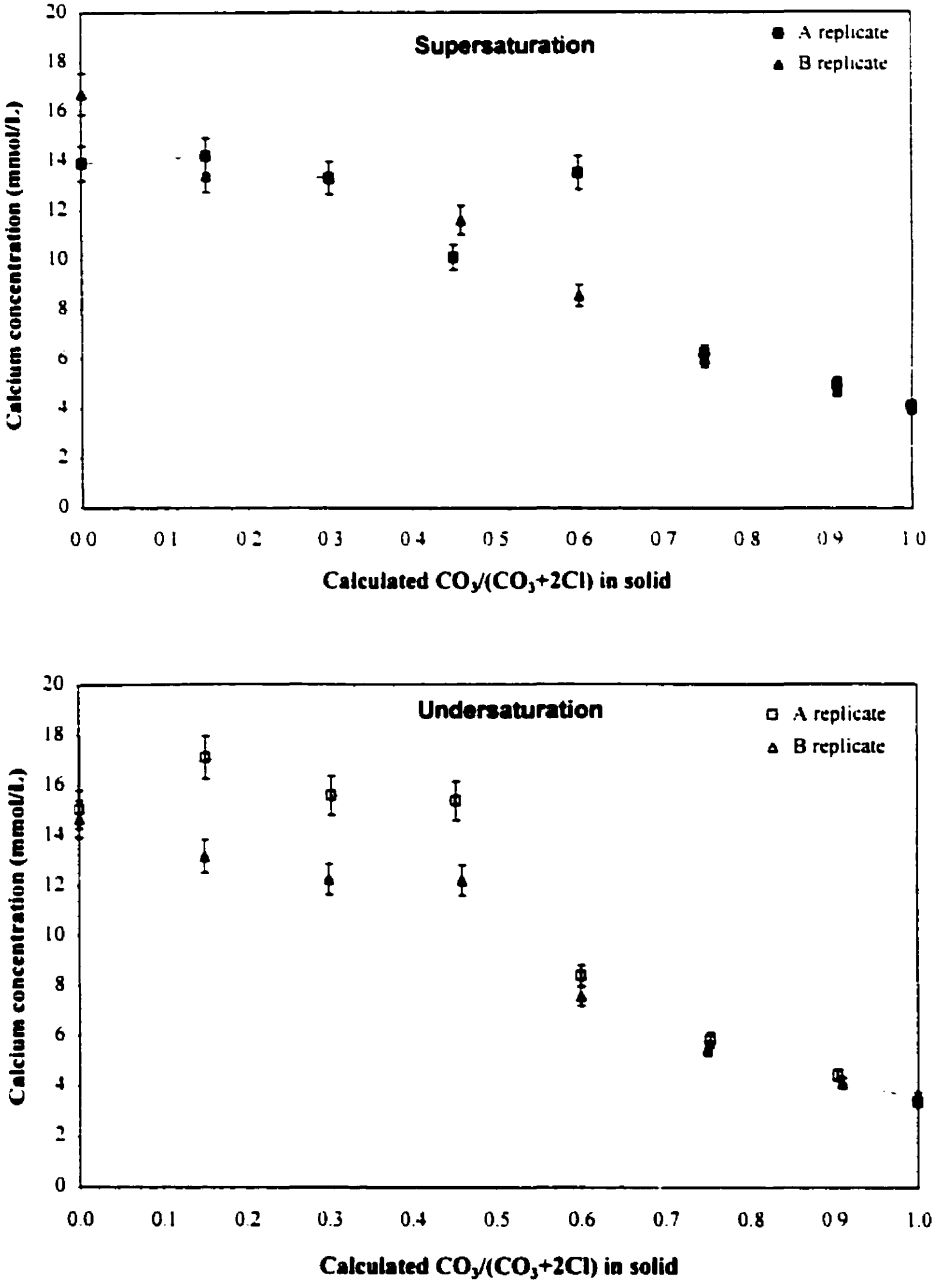


Figure 3.2: Solution concentrations of calcium verus the calculated carbonate ratio in the solid solution phase for the experiment from supersaturation and undersaturation. Error bars indicate the analytical uncertainties in the measured concentrations.

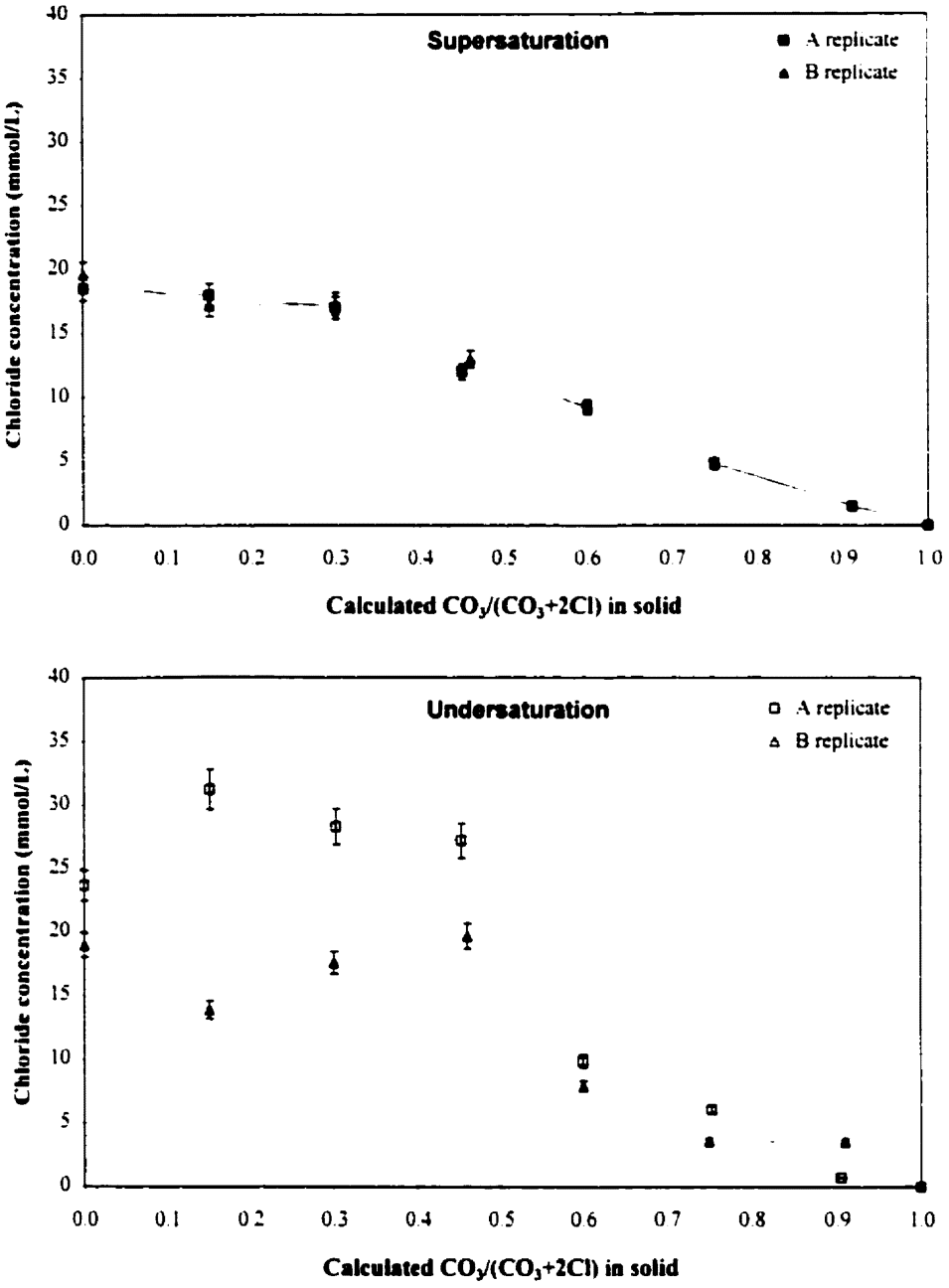
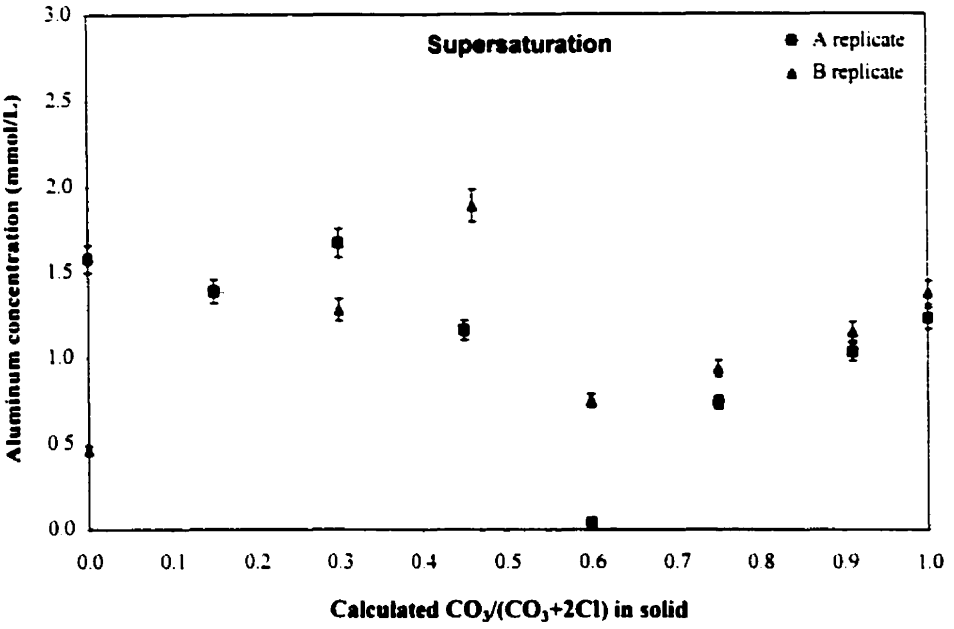


Figure 3.3: Solution concentrations of chloride verus the calculated carbonate ratio in the solid solution phase for the experiment from supersaturation and under-saturation. Error bars indicate the analytical uncertainties in the measured concentrations.



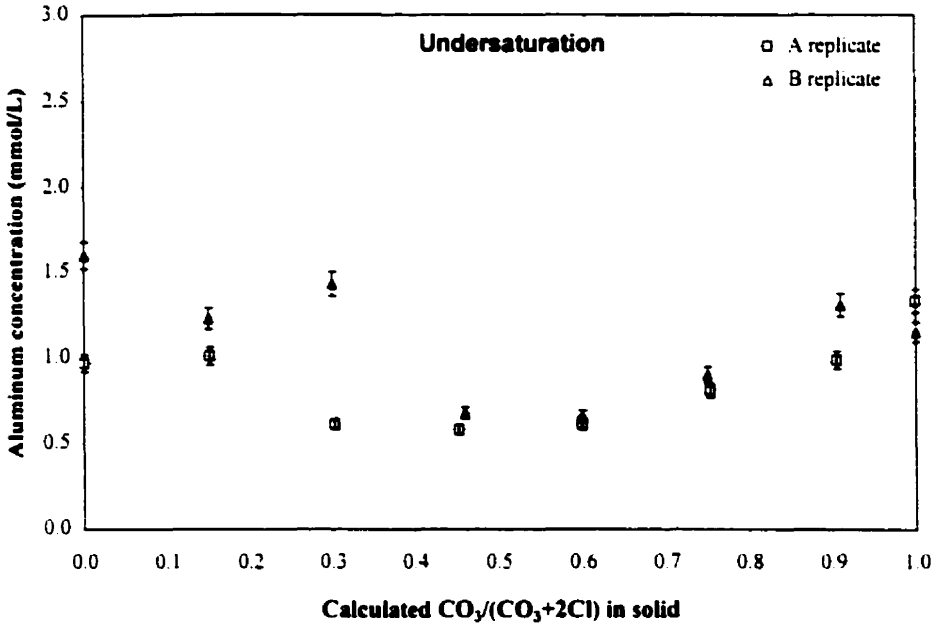


Figure 3.4: Solution concentrations of aluminum verus the calculated carbonate ratio in the solid solution phase for the experiment from supersaturation and under-saturation. Error bars indicate the analytical uncertainties in the measured concentrations.

The calculated mineral saturation indices for the solutions from undersaturation are similar to the results from supersaturation. The solutions from undersaturation are at saturation with respect to hydrogarnet between carbonate ratios of 0.6 and 1.0, in agreement with the results from supersaturation. However, in samples with carbonate ratios of 0.45 or less, hydrogarnet is supersaturated in both replicates from supersaturation and in the B replicate from undersaturation, but undersaturated in the A replicates over the same range. All samples are at or near saturation with respect to gibbsite, and undersaturated with respect to portlandite throughout the series.

3.3.2 Solids

The XRD patterns for solids in the experiment from supersaturation (A-replicates) between the carbonate end member ($CO_3/(CO_3+2Cl) = 1.0$) and the chloride end member (0.0) are plotted in Figure 3.6. The interlayer spacing measured for Friedel's salt is 7.8 Å. As carbonate is added to the system, the interlayer spacing of the solid-solution decreases slightly to 7.7 Å, and then remains constant as the ratio of carbonate in the solid is increased to 0.75. The XRD patterns of the single solid solution phase present between carbonate ratios of 0.15 and 0.75 are very similar to the standard pattern for β-Friedel's salt (JCPDS card 31.245), except for the slight shift to smaller d-spacings. When the carbonate ratio increases to 0.91, the main peaks for the solid solution at $2\theta = 11.45°$ and $22.90°$ are split into two peaks, indicating that there are two solid solution phases present at this composition. The solid solution phase with a main peak at $2\theta = 11.45$ (7.7 Å) is identified as a Cl-rich solid solution phase, similar to β-Friedel's salt, while the other with a main peak at $2\theta = 11.90$ (7.43 Å) is identified as monocarboaluminate, the carbonate end member. At a carbonate ratio of 1.0, a single solid solution phase is present, and is identified as monocarboaluminate by comparison with the published powder XRD diffraction patterns for this phase (Fisher and Kuzel, 1982; Carlson and Berman, 1960).

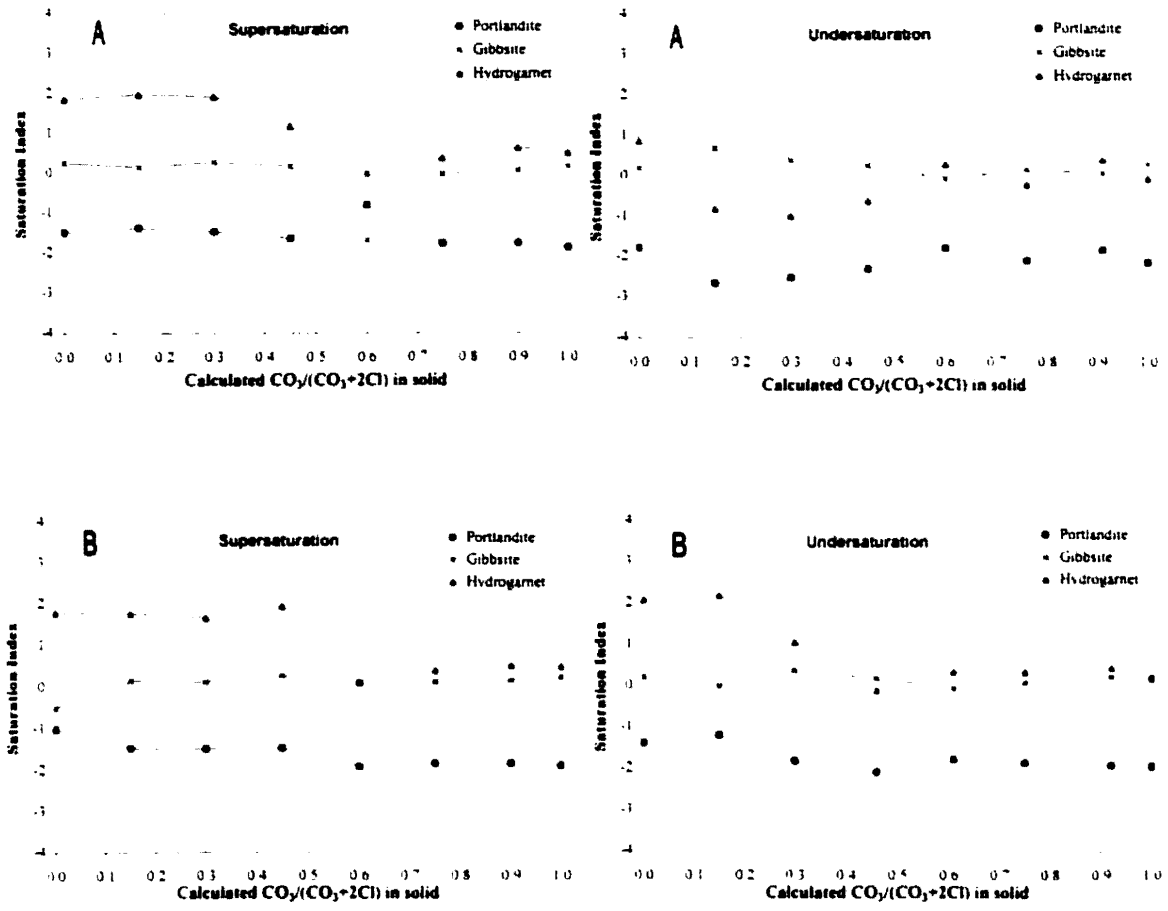


Figure 3.5: Calculated mineral saturation indices (SI) for the A and B replicates from supersaturation (left-hand diagrams) and undersaturation (right-hand diagrams). The SI values are plotted versus the calculated carbonate ratio in the solid. The saturation indices were calculated using SIMUL (Reardon, 1990).

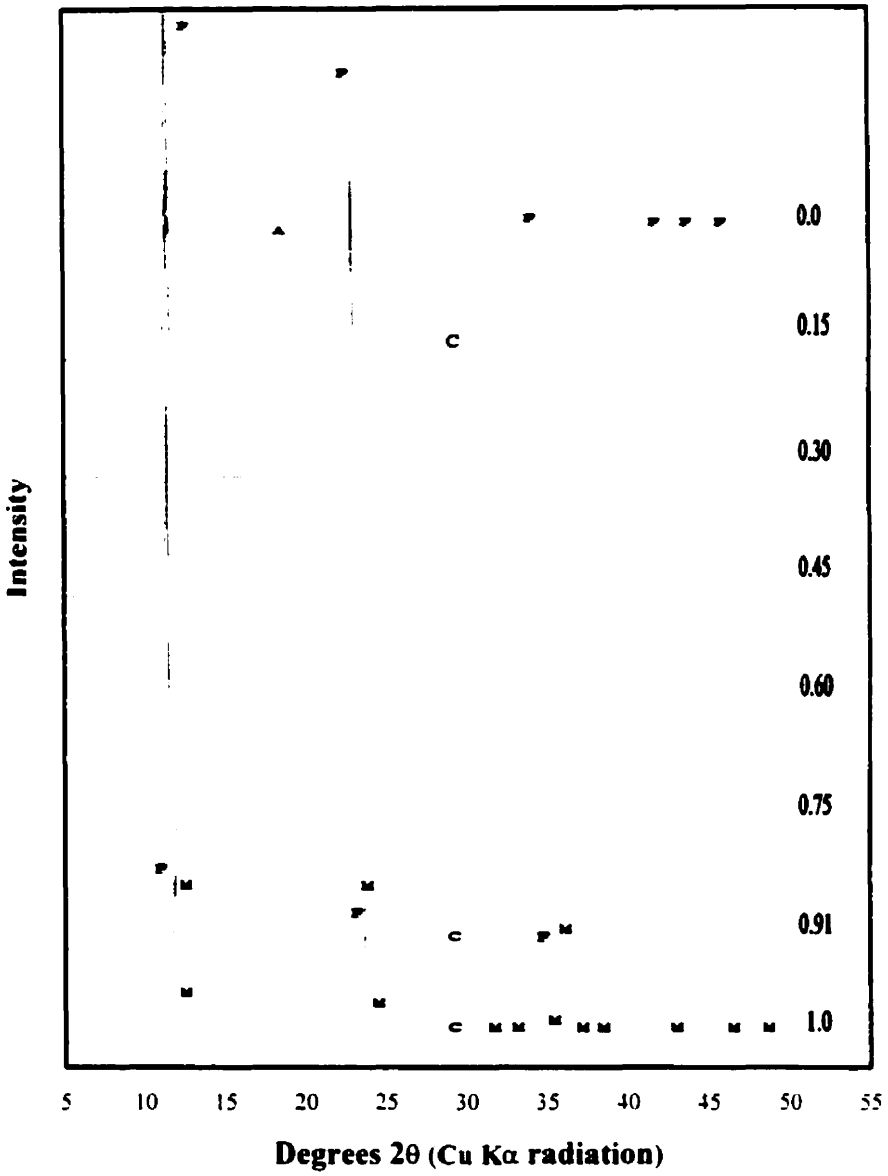


Figure 3.6: XRD patterns from the supersaturation experiment for A-replicate samples between the Cl (0.0) and CO_3 (1.0) end members. where the sample label indicates the calculated carbonate ratio in the solid. The occurrence of split peaks at $2\theta = 11°$ and $2\theta = 23°$ in sample 0.91 indicates the presence of two solid-solution phases. F = Cl end member ($3CaO{\cdot}Al_2O_3{\cdot}CaCl_2{\cdot}10H_2O$); M= CO_3 end member ($3CaO{\cdot}Al_2O_3{\cdot}CaCO_3{\cdot}11H_2O$); C = calcite ($CaCO_3$); A = gibbsite ($Al(OH)_3$).

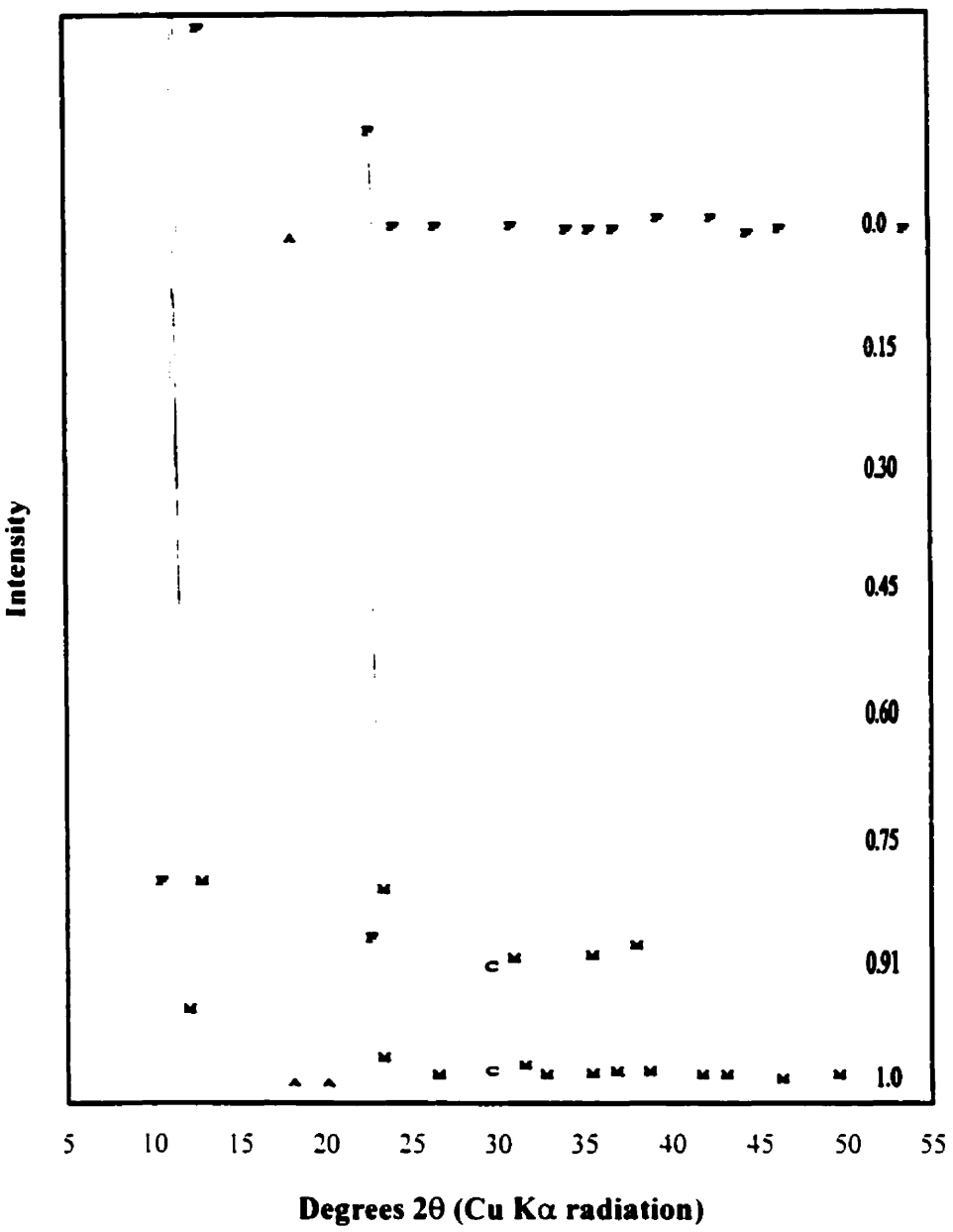


Figure 3.7: XRD patterns from the undersaturation experiment for A-replicate samples between the Cl (0.0) and CO_3 (1.0) end members, where sample label indicates the predicted carbonate ratio in the solid. The occurrence of split peaks at $2\theta = 11°$ and $2\theta = 23°$ in sample 0.91 indicates the presence of two solid-solution phases. F = Cl end member ($3CaO{\cdot}Al_2O_3{\cdot}CaCl_2{\cdot}10H_2O$); M = CO_3 end member ($3CaO{\cdot}Al_2O_3{\cdot}CaCO_3{\cdot}11H_2O$); C = calcite ($CaCO_3$); A = gibbsite ($Al(OH)_3$).

A small peak identified as calcite is present in all solids where carbonate was added (carbonate ratios of 0.15 to 1.0). In the solids with carbonate ratios of 0.0, 0.91 and 1.0, the peak at 2θ = 18.5 is identified as gibbsite. The patterns for the B replicates from supersaturation are similar (Appendix B). The major difference between the XRD patterns from these two sets of replicates is in the occurrence of gibbsite and calcite. Gibbsite is observed in solids with carbonate ratios of 0.6, 0.91, and 1.0 in the B-replicate solids, and calcite is only observed in solids with carbonate ratios of 0.75 or above.

In Figure 3.7, XRD patterns are plotted for the A-replicate solids in the experiment from undersaturation. A single solid solution phase was identified in all samples except for the sample with a carbonate ratio of 0.91, in agreement with the results from supersaturation. The small secondary peak at $2\theta = 23.6^{\circ}$ in solids with carbonate ratios between 0.0 and 0.75 is identified as the (112) peak of Friedel's salt. Although this peak has a d-spacing that is similar to the secondary peak of monocarboaluminate, two lines of evidence suggest that this peak belongs to a solid solution of Friedel's salt: 1) the primary peak for monocarboaluminate is not observed in these solids 2) the small (112) peak is observed in patterns of Friedel's salt or its solid solutions, even when carbonate is not present in the system (i.e. Figures 2.8). Additional phases were also observed in the solids. Between carbonate ratios of 0.3 and 1.0, the solids contain calcite, however, this phase was not observed in the solid with a carbonate ratio of 0.15. Gibbsite was identified in all solids from undersaturation, whereas in the solids from supersaturation, gibbsite was only observed in solids near the carbonate end member.

Scanning electron micrographs of solids from the experiment from supersaturation with carbonate ratios of 0.0, 0.91, and 1.0 are shown in Figure 3.8. The solid solution phase occurs as hexagonal plates. Photograph A shows a large, euhedral plate of the chloride end member, with smaller euhedral to subhedral plates on its surface. Approximately 40% of the solid with a carbonate ratio of 0.91 (A replicate) consists of large hexagonal (diamond or rhombohedral) crystals between 50-100 μm in length (photograph B). The other 60% consists of clusters of crystals that are approximately 10 μm or less in size. The carbonate end member ($CO_3/(CO_3+2Cl) = 1.0$) occurs as euhedral hexagonal plates (C). Photograph D is a close-up of an aggregate of hexagonal crystals of the solid solution phase ($CO_3/(CO_3+2Cl) = 0.15$) with rounded edges, taken from the undersaturation experiment.

3.3.3 Solubility Products

Assuming that equilibrium had been attained between the solid and aqueous phases, K_{sp} values

were calculated as a function of the solid phase composition between the chloride and carbonate end members. Activity coefficients for the aqueous species were calculated using the geochemical equilibria model SIMUL (Reardon, 1990), and the measured solution compositions (Tables 3.1 and 3.2). Because the measured solution concentrations of carbonate were below detection, these values were estimated by equilibrating the solutions with calcite in the modeling runs. This is likely a reasonable approach, because calcite was identified in many of the solids. In addition, it was necessary to use solid phase compositions calculated based on the reagents added, because the presence of additional mineral phases (e.g. calcite, gibbsite) precludes calculation of the actual final solid phase composition by mass balance. This may over-estimate the actual carbonate ratio of the solids. For solids with a carbonate ratio of 0.91, there were two solid solution phases observed in this sample. The log K_{ss} value is calculated for a solid with a bulk carbonate ratio of 0.91.

The general dissolution reaction for the chloride-carbonate solid solution series is given in equation 3.1.

$$3CaO{\cdot}Al_2O_3{\cdot}xCaCO_3{\cdot}(1-x)CaCl_2{\cdot}(10-x)H_2O = 4Ca^{2+} + 2Al(OH)_4^- + xCO_3^{2-} + 2(1-x)Cl^- + 4OH^- + (4+x)H_2O \qquad (3.1)$$

The solubility product K_{sp} expression for this reaction can be calculated according to equation 3.2:

$$K_{sp} = [m_{Ca^{2+}}\gamma_{Ca^{2+}}]^4\,[m_{Al(OH)_4^-}\gamma_{Al(OH)_4^-}]^2\,[m_{CO_3^{2-}}\gamma_{CO_3^{2-}}]^x\,[m_{Cl^-}\gamma_{Cl^-}]^{2(1-x)}\,[m_{OH^-}\gamma_{OH^-}]^4\,[a_{H_2O}]^{(4-x)} \qquad (3.2)$$

where m is the concentration of the ion in mol/kg H_2O; γ is the activity coefficient of the aqueous species; x is the mole fraction of carbonate in the solid, and aH_2O is the activity of water. The calculated log K_{sp} values are plotted in Figure 3.9 versus the calculated carbonate ratio in the solid. The log solubility product for the chloride end member is approximately -27. As the carbonate ratio in the solid is increased to 0.6, the solubility product value decreases gradually to -30, and then levels off at a value of approximately -31 as the carbonate ratio increases to 1.0. The solubility products calculated for the end members are compared to other published values in Chapter 5. Between carbonate ratios of 0.0 and 0.45, 3 out of 4 data sets give very similar log solubility products for the solids. However, the A replicates from undersaturation have much lower log K_{sp} values, consistent with the higher Ca^{2+} and Cl^- concentrations measured in these samples. In solids with carbonate ratios above 0.6, the reproducibility in the calculated log solubility products is excellent for all four replicates.

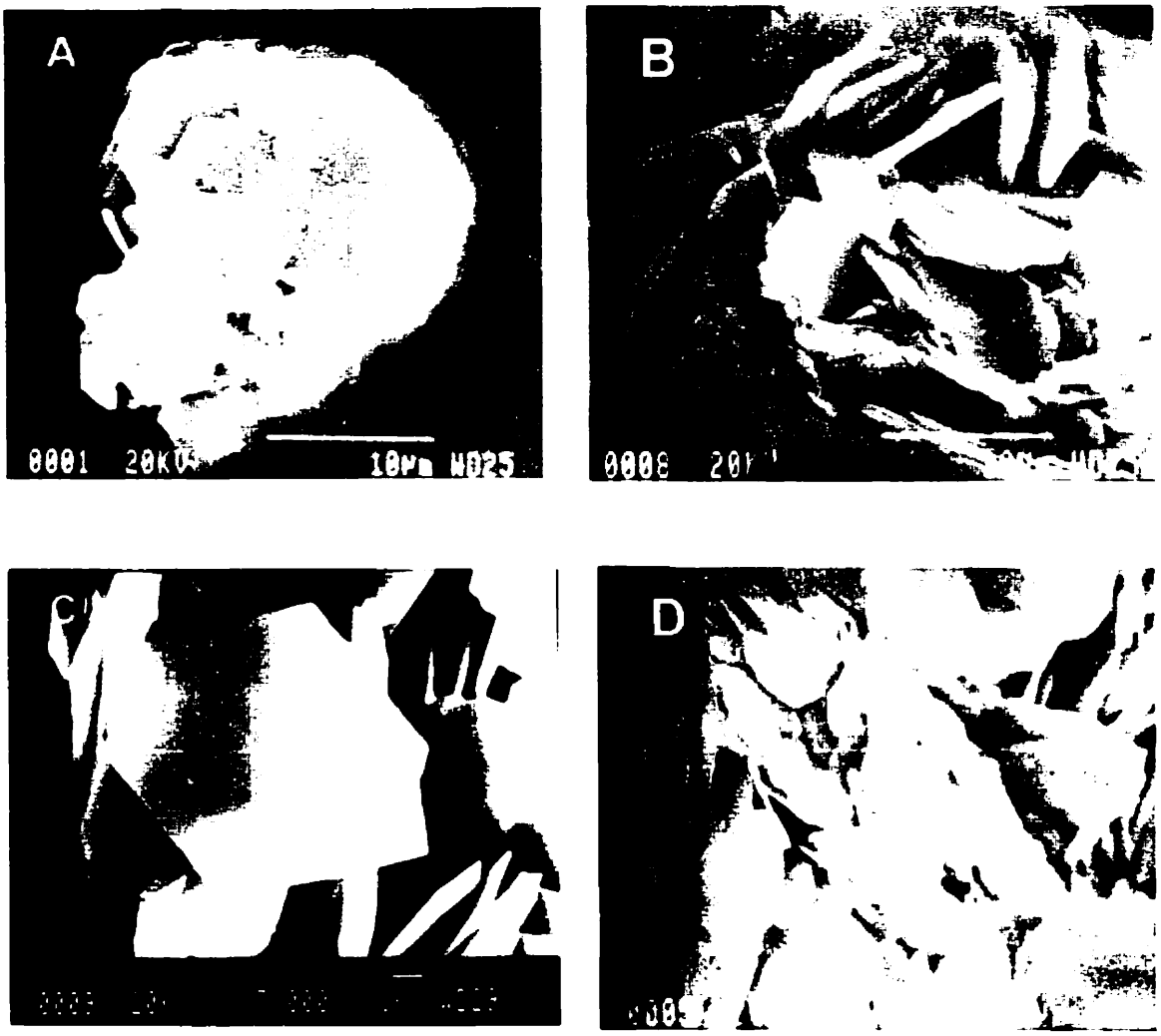


Figure 3.8: SEM photomicrographs of solids from the experiment from supersaturation: a) large, euhedral, hexagonal plate of the Cl end member ($CO_3/(CO_3+2Cl)= 0.0$), with smaller euhedral to subhedral plates; b) aggregate of hexagonal, platey crystals of the solid solution phase(s) with a carbonate ratio = 0.91. c) euhedral hexagonal plates of the carbonate end member ($CO_3/(CO_3+2Cl) = 1.0$); and from undersaturation: d) close up of an aggregate of hexagonal crystals ($CO_3/(CO_3+2Cl) = 0.15$). The crystals appear to have rounded edges, suggesting that they have undergone some dissolution.

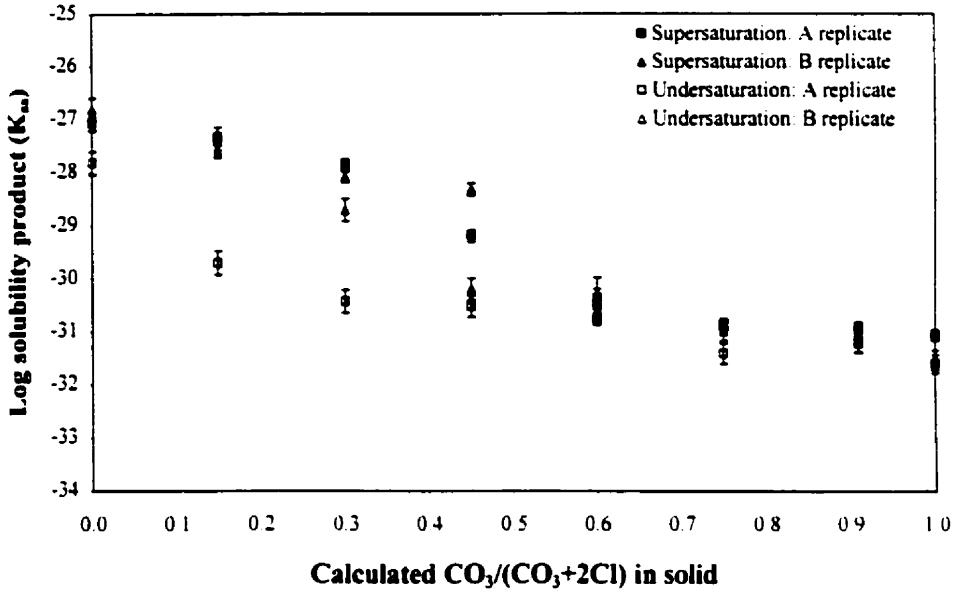


Figure 3.9: The log values of the solubility products (K_{ss}) for the solid solution phases are plotted versus the calculated carbonate ratio in the solid phase. These values are considered estimates, because the actual solid composition is unknown. The log K_{ss} value given for carbonate ratio of 0.91 is an estimate based on the bulk carbonate ratio of the solid. At this ratio, two solid solution phase coexist. Error bars show the calculated uncertainty in the K_{ss} values.

3.4 Discussion

A partial solid solution exists between the chloride end member and solids with a calculated carbonate ratio of 0.75. In this range, the XRD patterns for the solid solution are very similar to that of the chloride end member, but with a slightly smaller interlayer spacing. As the carbonate ratio in the solid increases to 0.91, a Friedel's salt-like solid solution and monocarboaluminate coexist. At a ratio of 1.0, monocarboaluminate is the only solid solution phase observed. Pöllmann (1986) also observed a limited solid solution between the chloride and carbonate end members. In Pöllmann's study, a solid-solution was observed between the chloride end member and solids with a carbonate ratio less than or equal to 0.83. At carbonate ratios above 0.83, two solid solution phases were identified. As the carbonate ratio was increased to 1.0, only monocarboaluminate was observed, consistent with the results from our study. The results of the study by Pöllmann (1986) constrain the lower limit of the miscibility gap to carbonate ratios above 0.83, and the current study shows that the upper limit of the miscibility gap must lie above a carbonate ratio of 0.91.

In addition to the solid solution phase(s), gibbsite and calcite were observed in the X-ray diffraction patterns of many of the solids in the current study. In contrast, no additional mineral phases were reported by Pöllmann (1986). In both the current study and that of Pöllmann (1986), calcite ($CaCO_3$) was added as a source of carbonate. It is possible that the calcite identified in the XRD patterns from the current study is unreacted starting material. Gibbsite was identified in the XRD patterns of several samples in the experiment from supersaturation, and in the patterns of all solids from undersaturation. All aqueous solutions in both experiments were calculated to be just at saturation with respect to gibbsite. It is possible that gibbsite is present in all samples, but was undetected by XRD analysis because the quantity of gibbsite in some solids is less than 5-10% (i.e. below the detection limit for XRD analysis), or because gibbsite was either poorly crystalline or amorphous.

3.4.1 Solid solution stability

Complete solid solutions are often formed between two minerals when their structures are the same or very similar, and when the substituting ions have similar ionic radii and the same charge (Brownlow, 1979). Other properties which may control the stability of the solid solution are the geometry and bonding characteristics of the substituting ions. Because the thickness of the interlayer in the calcium aluminate hydrates varies as different anions are incorporated

(Taylor, 1997), differences in ionic radii are not likely a key factor controlling the extent of solid solution.

There are differences in size, charge, and geometry between the Cl^- and CO_3^{2-} ions. The Cl^- ions are spherical, and have a radius of 1.81 Å (Douglas, 1994). The CO_3^{2-} ions are trigonal planar, with a carbon-oxygen bond length of 1.85 Å (Douglas et al., 1994), but perpendicular to the plane of the carbonate group, the thickness of the group is likely closer to the size of the oxygen ion, with a radius of 1.40 Å (Wedepohl, 1969). In addition, the substitution of $2Cl^-$ by CO_3^{2-} results in vacancies in the anion sites in the interlayer. These vacancies are filled by extra water molecules, which may be required to maintain the continuity of the hydrogen bond net between the inter- and main layers of the structure, and consequently, the stability of the structure (Sacerdoti and Passaglia, 1988).

With a continued increase in the carbonate ratio to 0.84, the differences in charge, geometry and/or the bonding characteristics between the chloride and carbonate ions are large enough that a single solid solution phase is not stable. Consequently, two solid solution phases form. The chloride-enriched phase has a slightly larger interlayer spacing (approximately 7.8 Å, similar to Friedel's salt), while the carbonate-rich phase has a slightly smaller interlayer spacing (7.6 Å). This immisciblity between the phases may occur because the carbonate, which has a charge of -2, creates a stronger bond between the main and interlayers than chloride. Experimental investigations of the interlayer and structure of the calcium aluminate hydrates are difficult. However, current and future efforts to model these phases (and the related hydrotalcite phases) at the molecular level are providing important insights into the behavior of the interlayer ions and water molecules (Wang et al., 2001).

3.4.2 Attainment of equilibrium

Similar final electrical conductance measurements for a given solid-solution from both super- and undersaturated conditions suggests that the solid phase may have reached either a metastable or thermodynamic equilibrium with respect to the aqueous phase. The sample with a carbonate ratio of 0.45 had a final conductance value from undersaturation that was within 3% of that measured from supersaturation, suggesting that this sample may have reached equilibrium. The final conductance value measured for the carbonate end member from undersaturation was approximately 12% lower than that measured from undersaturation, indicating that the same equilibrium state was not attained from both directions. The final

conductance value measured for the chloride end member in the experiment from undersaturation was 50% higher than the final value measured from supersaturation. As discussed in Chapter 2 (Section 2.3.1), this increase in conductance with reaction time is thought to be an artifact of the measurement process, rather than a reflection of changes in the phase assemblage.

Solids with carbonate ratios between 0.15 and 0.75 consist of three phases: the solid solution phase, gibbsite and calcite. At a carbonate ratio of 0.91, four phases coexist (two solid solution phases, calcite and gibbsite), and at a carbonate ratio of 1.0, calcite, gibbsite and monocarboaluminate are observed. In a system with four components, up to four phases can coexist at equilibrium, according to Gibb's phase rule. On this basis, the observed mineral phase assemblages could exist at equilibrium. However, given that calcite was added as a reagent, it is possible that this phase has still not completely reacted, even after over one and a half years of reaction (6 months from supersaturation, and 16 months from undersaturation). If the calcite still present in the solids is slowly dissolving, then the chloride-bearing calcium aluminate hydrate phase may be converting to a more carbonate-rich one with time. For example, the reaction of the pure Cl end member with x moles of calcite could be expressed as:

$$3CaO{\cdot}Al_2O_3{\cdot}CaCl_2{\cdot}10H_2O_{(s)} + xCaCO_{3(s)} + xH_2O_{(aq)} \rightleftharpoons$$

$$3CaO{\cdot}Al_2O_3{\cdot}xCaCO_3{\cdot}(1\text{-}x)CaCl_2{\cdot}(10+x)H_2O_{(s)} + 2xCl^- + xCa^{2+} \qquad (3.3)$$

As the carbonate ions from calcite are incorporated into the calcium aluminate phase, Cl^- ions are released to solution, and these must be balanced by Ca^{2+} ions in solution. This reaction may explain the observed changes in the solution composition between carbonate ratios of 0.15 and 0.45 in the A-replicates from undersaturation. In the solid with a carbonate ratio of 0.15, calcite was detected in the XRD pattern from supersaturation, but not in the pattern for the same solid from undersaturation. This suggests that the quantity of calcite present is lower in the experiment from undersaturation, consistent with the dissolution of this phase. Based on this interpretation, the A-replicate samples from undersaturation are actually closer to the final equilibrium state of the system than the other three replicates.

3.4.3 Equilibrium Predictions

3.4.3.1 Constructing a Lippmann diagram

In the chloride-carbonate series of the calcium aluminate hydrates. two chloride ions substitute for one carbonate ion and one associated water molecule. The dissolution reactions for the two end members are

$$3CaO{\cdot}Al_2O_3{\cdot}CaCl_2{\cdot}10H_2O_{(s)} \rightleftharpoons 4Ca^{2+} + 2Al(OH)_4^- + 2Cl^- + 4OH^- + 4H_2O$$

$$3CaO{\cdot}Al_2O_3{\cdot}CaCO_3{\cdot}11H_2O_{(s)} \rightleftharpoons 4Ca^{2+} + 2Al(OH)_4^- + CO_3^{2-} + 4OH^- + 5H_2O \quad (3.4)$$

and the corresponding solubility product expressions:

$$K_{sp\ Cl} = [Ca^{2+}]^4[Al(OH)_4^-]^2[Cl^-]^2[OH^-]^4[H_2O]^4 \quad (3.5)$$

$$K_{sp\ CO3} = [Ca^{2+}]^4[Al(OH)_4^-]^2[CO_3^{2-}][OH^-]^4[H_2O]^5 \quad (3.6)$$

Adding equations 3.5 and 3.6 together and collecting like terms gives the expression for the total solubility product variable:

$$\Sigma\,\Pi = [Ca^{2+}]^4[Al(OH)_4^-]^2\,[OH^-]^4[H_2O]^4\,\{[Cl^-]^2 + [CO_3^{2-}][H_2O]\} \quad (3.7)$$

Glynn and Reardon (1990) present an expression for the solutus in the general case of non-ideal solid solutions by expressing the activity of the solid phase components in terms of activity coefficients and mole fractions. When the stoichiometric coefficients of the substituting ions in the solid are not equal to 1. solving the expression for the solutus using the approach used by Glynn and Reardon (1990) requires a manipulation of the data. In this thesis. the approach taken is to redefine the activity fractions of the substituting ions in solution:

$$X_{Cl,\,aq} = \frac{[Cl^-]^2}{[Cl^-]^2 + [CO_3^{2-}][H_2O]} \quad (3.8)$$

$$X_{CO3,\,aq} = \frac{[CO_3^{2-}][H_2O]}{[Cl^-]^2 + [CO_3^{2-}][H_2O]} \quad (3.9)$$

This is equivalent to redefining the activity of the substituting ions in equations 2.9 (Chapter 2) as $[B^-] = [Cl^-]^2$ and $[C^-] = [CO_3^{2-}][H_2O]$. Conceptually, this represents the difference between the mineral phases when the substitution occurs (i.e. two chloride ions in the mineral structure are replaced by a carbonate ion and one water molecule).

3.4.3.2 Calculation of the excess free energy parameters

The method used to derive excess free energy parameters from solubility data is presented in Chapter 2, Section 2.4.4. In the current study, it is postulated that the A replicate samples from undersaturation are more representative of equilibrium conditions. Therefore, average ln K_{sp} values were calculated for these samples and plotted as a function of the mole fraction of carbonate and fit to equation 2.5 (Chapter 2). In this case, x in equation 2.5 is the mole fraction of carbonate in the solid solution, K_{BA} is the solubility of the chloride end-member (log K_{sp} = -27.57) and K_{CA} is the solubility of monocarboaluminate (log K_{sp}= -31.23). An evaluation of the solubility data for the end members is given in Chapter 5. The best fit gave a_0 = -10.48 and a_1 = 12.07 (n=8, df=7, r^2=0.92). It must be noted that in this fitting procedure, the bulk composition of the sample at a carbonate ratio of 0.91 was included in the regression analysis. Removal of this point significantly reduced the fit of regressed equation to r^2= 0.82, and changed the values of regressed parameters. This highlights the fact that the number of solubility measurements in the system that were not in the miscibility gap (n = 7) was not sufficient to clearly define the change in solubility as a function of the carbonate ratio.

Although there is evidence to suggest that the A replicates are closer to equilibrium, it is not possible to verify that equilibrium had been attained. A good check on the applicability of the fitted excess free energy parameters is to compare the miscibility gap calculated based on these parameters with the observed miscibility gaps in the system (Busenberg and Plummer, 1989). The excess free energy parameters (a_0, a_1) derived for the chloride-carbonate system were input into the geochemical equilibria model PHREEQC (Parkhurst and Apello, 1999). This program was used to determine the position of possible spinodal gaps and miscibility gaps in the series. The results of this modeling are summarized in Table 3.3.

Solid solutions with compositions within a spinodal gap are intrinsically unstable, and two solid solution phases will exist in this region. Within the miscibility gap, a single solid solution phase may form initially, but is metastable and will exsolve into two phases when thermodynamic equilibrium is attained (Prigogine and Defay, 1954). The predicted spinodal gap occurs between

carbonate ratios of 0.68 to 0.98. The observed occurrence of two phases in the study by Pöllmann (1986) and in the current study above 0.84 demonstrates that the predicted spinodal gap is too broad. The predicted miscibility gap extends from 0.53 to 0.99, and is also wider than the observed occurrence of two phases in this system. These results demonstrate that the excess free energy parameters calculated based on the results from undersaturation over-predict the range of the miscibility gap in this system.

Original data	Parameters		Spinodal gap		Miscibility gap	
	a_0	a_1	Lower CO_3 ratio	Upper CO_3 ratio	Lower CO_3 ratio	Upper CO_3 ratio
A rep. from undersaturation	-10.48	12.07	0.68	0.98	0.53	0.99

Table 3.3: The excess free energy parameters (a_0, a_1) derived by fitting the measured solubility data were input into the geochemical equilibria model, PHREEQC (Parkhurst and Appello, 1999) to calculate the positions of the miscibility and spinodal gaps in the system.

Using the observations from Pöllmann (1986) and the current study, the limits of the miscibility gap were set at 0.84 and 0.96. The geochemical equilibria model PHREEQC (Parkhurst and Appelo, 1999) was then used to predict a second set of excess free energy parameters. The excess free energy parameters derived using this method are a_0 = -19.294 and a_1 = 10.678.

Ideally, excess free energy parameters derived from solubility data collected under well-controlled laboratory conditions is thought to provide the best prediction of thermodynamic equilibrium - if attainment of thermodynamic equilibrium can be proven. However, in the current study, it is not possible to prove that thermodynamic equilibrium has been attained. Alternatively, when excess free energy parameters are derived based on the observed miscibility gaps in a system, the maximum mole-fraction observed in the solid solution may not correspond to the miscibility gap fraction. In this case the excess free energy of the system may be overestimated (Glynn, 1989). The excess free energy parameters derived based on the observed miscibility gap have been used to construct a Lippmann diagram (Figure 3.10). This set of parameters is thought to be more representative, because they were derived based on the consistent observations of the miscibility gap in the current study, and in the study by Pöllmann (1986). When using this diagram to make "equilibrium" predictions, the underlying assumption

that the observed mole fractions correspond to the miscibility gaps in the system at thermodynamic equilibrium must be taken into account.

Total solubility products ($\Sigma\ \Pi$) have been calculated based on the aqueous compositions measured for the A and B replicates from undersaturation, and are also plotted on Figure 3.10. If the samples have reached equilibrium, the measured aqueous and solid phases will plot on the solutus and solidus, respectively, in the Lippmann diagram. Although approximately half of the A and B replicate solutions plot on or close to the solutus, the corresponding solid phases do not plot on the solidus. These results suggest that although there is some evidence to suggest that the A replicates may be closer to saturation, neither set of replicates had reached thermodynamic equilibrium when they were sampled.

In future studies, solubilities should be measured for a greater number of different solid solution compositions. However, perhaps the greatest difficulty in working with the calcium aluminate hydrates is the long times required to reach equilibrium. Considering this, it may be more appropriate to attempt to reach stoichiometric saturation, rather than thermodynamic equilibrium. In order to be able to use this method, solid-solutions with varying ratios of the substituting ion (e.g. carbonate) must first be precipitated. The dissolution of these solid solutions must then be monitored to determine if dissolution is congruent, and if so, it must be verified that stoichiometric saturation can be reached. Measurements of the solubility made at stoichiometric saturation can then be used to derive the excess free energy parameters, and ultimately, to predict partitioning between the solid solution and aqueous solution phases at thermodynamic equilibrium. An explanation of the link between stoichometric saturation measurements and thermodynamic equilibrium is given by Glynn and Reardon, (1990).

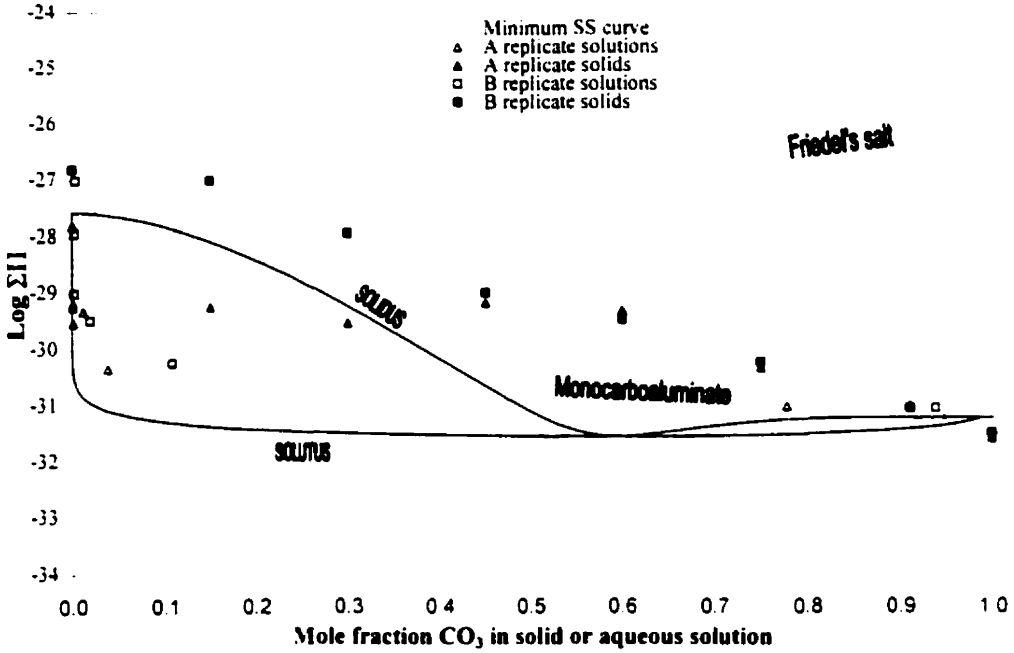


Figure 3.10: Lippmann phase diagram for the series between the chloride and carbonate end member at 25 °C, constructed using the excess free energy parameters a_0 = -19.29, a_1 =10.68. These fitting parameters were derived using the observed miscibility gap in the system. The vertical, long-dashed lines define the limits of the miscibility gap. Total solubility products calculated for the measured aqueous phase compositions from undersaturated conditions are also plotted.

3.5 Conclusions

A partial solid solution exists between the chloride end member and solids with a calculated carbonate ratio of 0.75. As the carbonate ratio in the solid increases to 0.91, a Friedel's salt-like solid solution and monocarboaluminate coexist. At ratio of 1.0, monocarboaluminate is the only solid solution phase observed. These results are consistent with those reported by Pöllmann (1986), who reported the occurrence of two solid solution phases above a carbonate ratio of 0.83. The current study demonstrates that two solid solution phases persist to a carbonate ratio of at least 0.91.

Gibbsite and calcite were observed in the X-ray diffraction patterns of many of the solids in the current study. All aqueous solutions in both experiments were calculated to be just at saturation with respect to gibbsite, suggesting that this phase may actually be present in all samples, but below detection by XRD (i.e. less than 5-10% or poorly crystalline). Calcite ($CaCO_3$) was added as a source of carbonate, and it is possible that the calcite identified in the XRD patterns is un-reacted starting material. If calcite is slowly dissolving, then the chloride-bearing calcium aluminate hydrate phase may be converting to a more carbonate-rich one with time. This conversion might be expressed by

$$3CaO{\cdot}Al_2O_3{\cdot}CaCl_2{\cdot}10H_2O_{(s)} + xCaCO_{3(s)} + xH_2O_{(aq)} =$$

$$3CaO{\cdot}Al_2O_3{\cdot}xCaCO_3{\cdot}(1\text{-}x)CaCl_2{\cdot}10H_2O_{(s)} + 2xCl^- + xCa^{2+}$$

With the incorporation of carbonate ions into the calcium aluminate phase, Cl- ions are released to solution, and these must be balanced by Ca^{2+} ions in solution. This reaction appears to explain the higher Ca^{2+} and Cl^- concentrations measured in the A replicates from undersaturation. The lower quantity of calcite observed in the XRD pattern for one of the samples also supports this interpretation.

Although thermodynamic equilibrium was not attained in this system, the A replicate samples from undersaturation are thought to have most closely approached equilibrium, based on the measured solution compositions and the XRD results for these samples. Excess free energy parameters where $a_0 = -10.48$ and $a_1 = 12.07$ were derived from this solubility data. The possible miscibility gap between carbonate ratios of 0.53 and 0.99 predicted using PHREEQC (Parkhurst and Apello, 1999), demonstrates that these excess free energy parameters over-predict the width of the miscibility gap, compared to laboratory observations.

In an alternate approach, the limits of the miscibility gap were estimated at 0.84 and 0.96 based on laboratory observations, and this data was then input into PHREEQC (Parkhurst and Apello, 1999) to derive a second set of excess free energy parameters. These parameters are thought to be more suitable for predications of equilibrium partitioning between the solid and aqueous phase than those derived from the solubility measurements, because they are based on consistent observations of the miscibility gap from two independent studies. Ideally, more solubility data is required to determine the excess free energy parameters for the chloride-carbonate series of the calcium chloroaluminates. However, because long times are required for these systems to reach equilibrium, an alternative approach would be to attempt to reach stoichiometric saturation, rather than thermodynamic equilibrium. The stoichiometric solubility measurements could then be used to derive the excess free energy parameters, which in turn can be used to make predictions at thermodynamic equilibrium.

3.6 Recommendations

The excess free energy parameters derived for the chloride-carbonate series based on the miscibility gap likely provide a reasonable estimate of the conditions at thermodynamic equilibrium. However, solubility measurements of the solid solution phases made when either thermodynamic equilibrium or stoichiometric saturation has been verified provide the best estimates of these parameters, and therefore, further solubility studies are recommended.

It is recommended that the prospect of measuring the solubility of these phases at stoichiometric saturation is investigated, because of the long reaction times required to attain thermodynamic equilibrium in this system (> 16 months).

3.7 References

Busenberg E. and Plummer N. L. (1989). Thermodynamics of magnesian calcite solid-solutions at 25° C and 1 atm total pressure. *Geochim. Cosmochim. Acta*, **53**, 1189-1208.

Brownlow A. H. (1979). Geochemistry. Prentice-Hall Inc., N.J., 498 p.

Carlson E. T. and Berman H. A. (1960). Some observations on the calcium aluminate carbonate hydrates. *Journal of Research, of the National Bureau of Standards - A. Physics and Chemistry*, **64A**, pp. 333-341.

Damidot D., Stronach S., Kindness A., Atkins M. and Glasser F.P. (1994). Thermodynamic investigation of the CaO-Al_2O_3-$CaCO_3$-H_2O closed system at 25 °C and the influence of Na_2O. Cem. Concr. Res., **24**, 563-572.

Douglas B., McDaniel D., and Alexander J. (1994). Concepts and models of inorganic chemistry. John Wiley & Sons, Inc., 928p.

Fischer R. and Kuzel H.-J. (1982). Reinvestigation of the system $C_4A{\cdot}nH_2O$-$C_4A{\cdot}CO_2{\cdot}nH_2O$. *Cem. Concr. Res.*, **12**, 517-526.

Glasser F.P., Kindness A., and Stronach S. A. (1999). Stability and solubility relationships in Afm phases Part I. Chloride, sulfate and hydroxide. *Cem. Concr. Res.*, **29**, 861-866.

Glynn P.D. (1989). Modeling solid-solution reactions in low-temperature aqueous solutions. *In*: Chemical modeling in aqueous systems II. (Eds. Melchior D.C. and Bassett R.L.). *Am. Chem. Soc. Symposium Series*, **416**, 74-86.

Glynn P. D. and Reardon E. J. (1990). Solid-solution aqueous-solution equilibria: Thermodynamic theory and representation. *Am. Jour. Sci.*, **290**, 164-201.

Glynn P. D., Reardon E. J., Plummer L. N., and Busenberg E. (1990). Reaction paths and equilibrium end-points in solid-solution aqueous-solution systems. *Geochim. Cosmochim. Acta*, **54**, 267-282.

Guggenheim E. A. (1937). Theoretical basis of Raoult's law. *Transactions of the Faraday Society*, **33**, 151-159.

Guggenheim E. A. (1952). Mixtures. London, Oxford University Press, 270 p.

Lippmann F. (1980). Phase diagrams depicting aqueous solubility of binary mineral systems. *N. Jb. Miner. Abh.*, **139**, 1-25.

Parkhurst D. L. and Apello C. A. J. (1999). User's guide to PHREEQC (Version 2)-- A computer program for speciation, batch-reaction, one-dimensional transport, and inverse geochemical calculations. U.S. Department of the Interior, U.S. Geological Survey, Water-Resources Investigations Report 99-4259.

Pöllmann H. (1986) Solid solution of complex calcium aluminate hydrates containing Cl^-, OH^- and CO_3^{2-} anions. *Proc. 8th Int. Symp. Chem. Cem.*, Rio de Janeiro, Supplementary paper, **Vol. III**, 300-306.

Plummer L. N. and Busenberg E. (1987). Thermodynamics of aragonite-strontianite solid solutions: Results from stoichiometric solubility at 25 and 76 ° C. *Geochim. Cosmochim. Acta*, **51**, 1393-1411.

Prigogine I. and Defay R. (1954). Chemical Thermodynamics. Longmans, Green & Co., Ltd.

Ramachandran V. S. and Zhang Chun-Mei (1986). Hydration kinetics and microstructural development in the $3CaO{\cdot}Al_2O_3$-$CaSO_4{\cdot}2H_2O$-CaCO3-H2O system. *Matériaux et Constructions*, **19**, 437-444.

Reardon E.J. (1990). An ion interaction model for the determination of chemical equilibria in cement/water systems. *Cem. Concr. Res.*, **20**, 175-192.

Sacerdoti M. and Passaglia E. (1988). Hydrocalumite from Latium, Italy: its crystal structure and relationship with synthetic phases. *N. Jb. Miner. Mh.*, **10**, 462-475.

Taylor H.F.W. (1997). Cement Chemistry (2nd edition). Academic Press 459p.

Wang J., Kalinichev A. G., Kirkpatrick R. J. and Hou X. (2001). Molecular modeling of the structure and energetics of hydrotalcite hydration. *Chem. Mater.*, **13**, 145-150.

Wedepohl K. H. (ed.) (1969). *Handbook of Geochemistry*. Springer-Verlag, Berlin.

Chapter 4

Solubility of solid solutions in the system $CaO-Al_2O_3-CO_3-H_20$ from super- and undersaturation

4.1 Introduction

In the early stages of Portland cement hydration, the interlayer of the calcium aluminate hydrates contains predominantly OH^- and SO_4^{2-} ions. With time, these anions may be exchanged for carbonate, chloride or sulphate ions (Glasser et al., 1999). Of the ions which can replace hydroxide in the interlayer, carbonate is of particular interest because divalent ions are usually preferred over monovalent ions (Mascolo and Marroccoli, 1986), and because the almost universal presence of CO_2 in the atmosphere and in water ensures that most cements will be in contact with a potential source of carbonate (Damidot et al., 1994). Other potential sources for carbonate ions in cement-based materials include calcium carbonate additives to influence the early setting and hardening characteristics of cement (Ramachandran and Zhang, 1986), or calcareous aggregates (Barret et al., 1983).

In aqueous solution, or at a relative humidity of 100%, the hydroxide end member occurs in a highly hydrated form, $3CaO{\cdot}Al_2O_3{\cdot}Ca(OH)_2{\cdot}18H_2O$ (Roberts, 1969; Fischer and Kuzel, 1982). This phase has a layer thickness of 10.7 Å. With a decrease in the relative humidity below 88%, this phase loses one layer of water from its structure, forming $3CaO{\cdot}Al_2O_3{\cdot}Ca(OH)_2{\cdot}12H_2O$, with a layer thickness of 7.9 Å. Hemicarboaluminate has a composition that is mid-way between the hydroxide and carbonate end members. Roberts (1969) determined that at relative humidities between 81 and 11%, hemicarboaluminate occurs in two different hydration states, $3CaO{\cdot}Al_2O_3{\cdot}0.5Ca(OH)_2{\cdot}0.5CO_3{\cdot}11H_2O$ with a layer thickness of 8.2 Å, or this phase can dehydrate losing one water molecule from the interlayer, forming $3CaO{\cdot}Al_2O_3{\cdot}0.5Ca(OH)_2{\cdot}0.5CaCO_3{\cdot}10H_2O$. The carbonate end member, monocarboaluminate ($3CaO{\cdot}Al_2O_3{\cdot}CaCO_3{\cdot}11H_2O$) has a water content very close to 11 H_2O, and has a layer thickness of only 7.56 Å (Fischer and Kuzel, 1982).

Detailed studies of the solid phases formed between the hydroxide and carbonate end members were performed by Roberts (1969), Fischer and Kuzel (1982), and Pöllmann (1986). In these

studies, the solid phase(s) were examined as a function of the carbonate ratio in the solid, where the carbonate ratio is defined as the ratio of carbonate ions to the total anions in the interlayer of the solid ($CO_3/(CO_3+2OH)$). Precautions were taken to minimize sample contamination by atmospheric carbon dioxide during sample preparation, sampling, and analysis.

Roberts (1969) prepared a series of reaction mixtures by treating suspensions of the hydroxide end member with increasing amounts of CO_2. The reaction mixtures were shaken continuously at 25 °C for at least 7 days. The samples were then filtered and dried to a constant weight at 81% relative humidity. The XRD results showed the presence of a miscibility gap with two solid solutions, hemicarboaluminate and the OH end member between carbonate ratios of 0.13 and 0.35. In samples with carbonate ratios of 0.48 to 0.53, hemicarboaluminate was the only phase observed. When the ratio increased to 0.67, a second miscibility gap was observed where hemicarboaluminate and monocarboaluminate were both present. With further increases in the carbonate ratio, the amount of monocarboaluminate increased. In addition to the solid solution phases, portlandite was observed in samples with carbonate ratios of 0.78, 0.98, and 1.62, and calcite was observed in samples with carbonate ratios 0.98 or higher. The d-spacing measured for hemicarboaluminate was 8.2Å, and did not change with the addition of increasing amounts of carbonate. This suggests the formation of a unique quaternary carbonate hydrate with a composition approximating $3CaO{\cdot}Al_2O_3{\cdot}0.5CaCO_3{\cdot}11H_2O$ (hemicarboaluminate), rather than the formation of a partial solid solution.

Fischer and Kuzel (1982) also investigated solids with compositions between the hydroxide and carbonate end members. Reaction mixtures were prepared from freshly ignited CaO, bayerite ($Al(OH)_3$), or from monocalcium or tricalcium aluminates. Carbonate compositions were obtained by the addition of $CaCO_3$. The reaction mixtures were placed in sealed polyethylene bottles and shaken continuously at 22 °C, for unspecified reaction times. The solids were then separated by filtration, equilibrated at 100% and 65% relative humidity, and analyzed using X-ray diffraction. The XRD results demonstrated that the carbonate-free compound in metastable equilibrium with solution at 22 °C is $4CaO{\cdot}Al_2O_3{\cdot}19H_2O$. The observed phase assemblages agree well with those reported by Roberts (1969), and further define the range of carbonate ratios for each assemblage. For example, hemicarboaluminate and the OH end member formed between carbonate ratios of approximately 0.05 and 0.4, extending the observed miscibility gap compared to the results of Roberts (1969). At ratios between 0.4 to 0.6, hemicarboaluminate was the only phase present. The second miscibility gap containing hemicarboaluminate and monocarboaluminate was observed between carbonate ratios of 0.6 and 0.8, and above 0.8, monocarboaluminate was the only phase present.

In the experiments performed by Pöllmann (1986), solid solutions between the carbonate and hydroxyl end members were synthesized by mixing $CaCO_3$, calcined CaO, and monocalcium aluminate with freshly distilled water. The reaction mixtures were sealed in polyethylene bottles, and shaken continuously. After 12 months of reaction, the crystalline phases were filtered and analyzed using X-ray diffraction analysis. The results of these experiments also demonstrate the existence of two miscibility gaps. The observed miscibility gap containing the OH end member and hemicarboaluminate occurred between carbonate ratios of 0.05 and 0.45, consistent with the results of both Roberts (1969) and Fischer and Kuzel (1982). At a carbonate ratio of 0.5, hemicarboaluminate was the only phase present. As the carbonate ratio increased to between 0.55 to 0.95, mono- and hemicarboaluminate occurred together in the second miscibility gap. These results extend the upper limit of the mono-hemicarboaluminate miscibility gap from a carbonate ratio 0.8 as reported by Fischer and Kuzel (1982), to a ratio of 0.95. Above 0.95, monocarboaluminate was the only phase identified.

Although the study by Roberts (1969) showed a constant d-spacing of 8.2 Å for hemicarboaluminate, Fischer and Kuzel (1982) observed decrease of approximately 0.03Å in the layer thickness of hemicarboaluminate as the ratio of carbonate in the solid increased from 0.25 to 0.6. Both studies suggest that hemicarboaluminate forms only a very limited solid solution with hydroxide. The overall composition of this solid solution is approximated by the composition of hemicarboaluminate.

The focus of previous research by Roberts (1969), Fischer and Kuzel (1982), and Pöllmann (1986) was on identifying the solid phases present as a function of the carbonate content of the solid. In these studies, attainment of equilibrium conditions can not be verified, because equilibrium was approached only from supersaturated conditions. In the current study, long equilibration times (between 6 and 16 months) were used in an effort to approach equilibrium conditions, and equilibrium was approached from both supersaturated and undersaturated conditions. Particular composition solids in the solid solution series between the hydroxide and carbonate end members were prepared. The main objectives of this study were to identify the solid solution phase(s) present at each composition, to determine the aqueous solution and solid solution phase compositions at equilibrium, and to use these measurements to calculate the solubilities of the solid solutions. The materials, experimental procedure, and analytical methods used are outlined in Chapter 2 (Section 2.2).

4.2 Results

4.2.1 Reaction Kinetics

Conductance measurements with time for the three samples used to monitor the approach to equilibrium of the OH-CO_3 series are plotted in Figure 4.1. In the experiment from supersaturation, the measured conductance for the hydroxide end member had reached an essentially stable value of 8400 μS/cm after 3 days of reaction. From undersaturation, the conductance measured for the OH-end member was 7700 μS/cm initially, approximately 10% lower than that measured from supersaturation. The conductance remained stable at this value for 160 days, then gradually decreased to 5000 μS/cm after 472 days of reaction.

The sample with a composition midway between the hydroxide and carbonate end members had a measured conductance of approximately 7000 μS/cm at the beginning of the experiment from supersaturation. The conductance decreased to approximately 3900 uS/cm after 20 days of reaction, and remained stable at this value for the duration of the experiment. The opposite trend was observed in the experiment from undersaturation. The measured conductance was initially low (2700 μS/cm), but increased to 3000 μS/cm after 20 days. The conductance then remained stable at this value for the duration of the experiment. This final value is approximately 24% lower than the final conductance measurement taken from supersaturation.

The measured conductance for the carbonate end member was essentially stable after 3 days of reaction in both the experiments from super- and undersaturation, but the conductance measured from undersaturation was 15% lower than that measured from supersaturation.

4.2.2 Solution Composition

The solution compositions measured from supersaturation and undersaturation are presented in Tables 4.1 and 4.2, respectively. The concentrations of calcium and aluminum measured in solution are plotted versus the calculated ratio of carbonate in the solid solution phase in Figures 4.2 and 4.3. The ratio given is the calculated ratio of carbonate to total anions ($CO_3/(CO_3 + 2OH)$) in the interlayer of the solid solution phase, based on the quantities of reagents added, and assuming that the solid solution was the only mineral phase present. The dissolved inorganic carbon (DIC) contents of the samples were measured in the experiment from

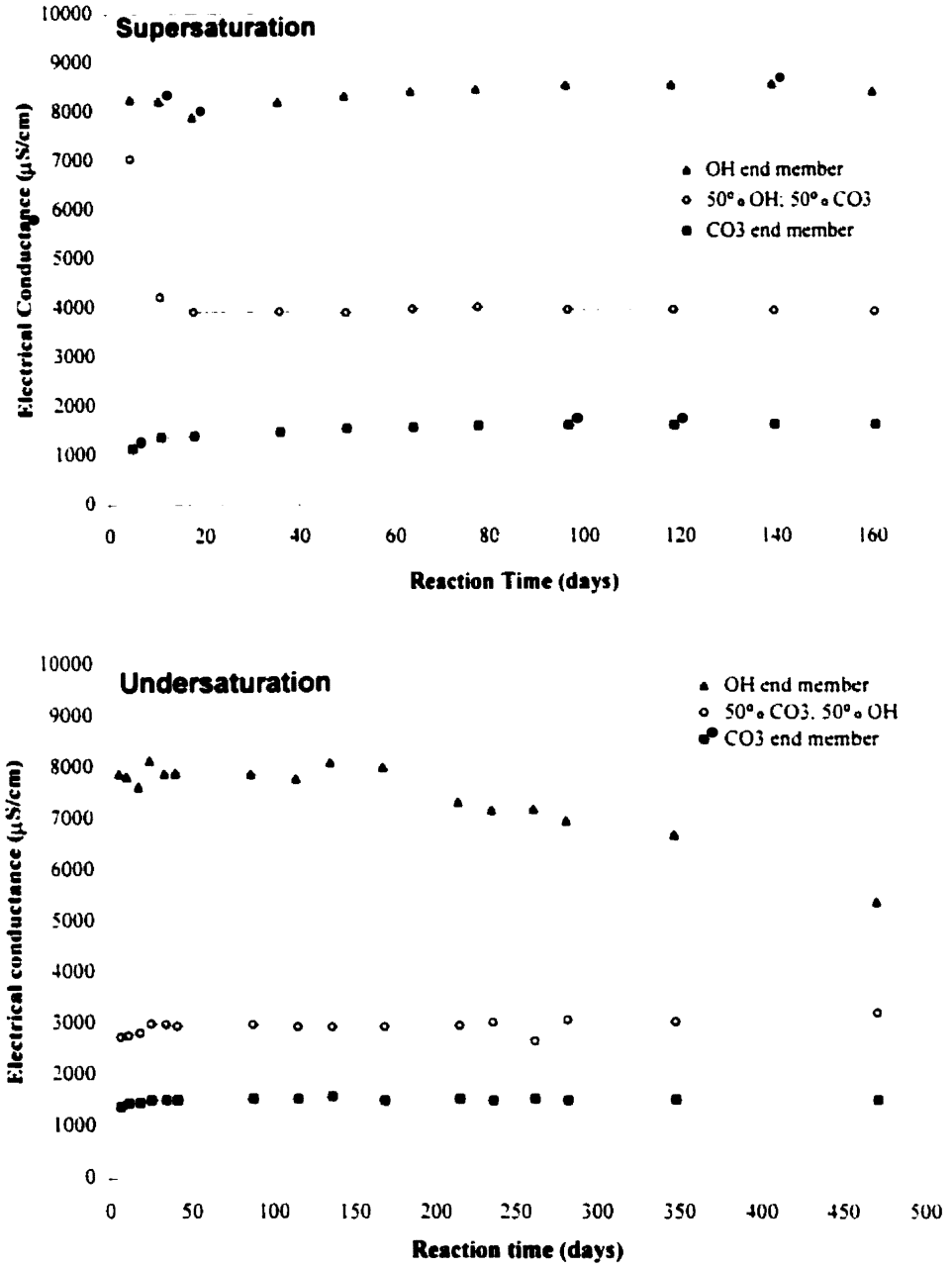


Figure 4.1: Electrical conductance versus reaction time for the experiments from supersaturation and undersaturation. Conductance measurements are shown for the OH- end member, the carbonate end member, and for a sample with a composition midway between the end members.

supersaturation. but were below detection (< 0.061 mmol/L) for all samples. Consequently. the DIC contents of the solutions were not measured in the experiment from undersaturation.

In both the experiments from super- and undersaturation. the measured pH values increase from approximately 11.8 to 12.5 between the carbonate and hydroxide end members. The pH values measured from undersaturation are a maximum of 0.5 units lower than those measured from supersaturation.

The calcium concentrations measured in the A and B replicates from supersaturation are the same. within the analytical uncertainty of 5%. Calcium concentrations are approximately 20 mmol/L for solid compositions with carbonate ratios between the hydroxide end member (0.0). and 0.25. As the ratio of carbonate in the solid increases to 0.4. the calcium concentration decreases to approximately 10 mmol/L. It then remains stable at this value with further increases in the carbonate ratio up to 0.85. but decreases in concentration to 5 mmol/L in the carbonate end member. In the experiment from undersaturation. the calcium concentrations measured in the two replicates are close or within the analytical uncertainty in samples with carbonate ratios between 0.25 and 0.70. but show greater variability close to the end members ($CO_3/(CO_3+2OH)$ ratios of 0.1 and 0.85). Overall. the trend in the calcium concentration as a function of the carbonate ratio is similar to that measured from supersaturation. except that the calcium concentrations are slightly lower in the experiment from undersaturation.

The difference in the aluminum concentrations between replicates was greater than the analytical uncertainty for the majority of samples in the experiments from both super- and undersaturation. However. the trends in the aluminum concentrations as a function of carbonate ratio are similar in both experiments. The aluminum concentrations measured in solution are below dectection ($<1.1 \times 10^{-3}$ mmol/L) in the hydroxide end member for the replicates from undersaturation. Aluminum remains below detection until the carbonate ratio increases above 0.1. In both experiments. the aluminum concentration in solution increases to a maximum value of approximately 2.9 mmol/L in samples with carbonate ratios between 0.5 and 0.85. and then decreases to 1.5 mmol/L in the carbonate end member.

Calculated $CO_3/(CO_3+2OH)$	pH		Calcium (mmol)		Aluminum (mmol)	
	A	B	A	B	A	B
1.00	11.72	11.73	4.141	4.050	1.233	1.378
0.85	12.09	12.11	8.892	9.138	2.267	1.298
0.70	12.10	12.08	8.713	8.715	2.062	2.257
0.50	12.16	12.10	9.481	9.110	0.0360	2.024
0.40	12.27	12.23	12.09	11.55	0.0192	0.7120
0.25	12.50	12.47	20.16	21.29	0.0486	0.0202
0.10	12.51	12.48	21.19	20.67	0.0105	0.0148
0.0	12.48	12.51	20.51	21.14	0.0325	0.0156

Table 4.1: Solution data measured in the experiment from supersaturation for samples with compositions between the carbonate end member ($CO_3/(CO_3+2OH) = 1.0$) and the hydroxide end member ($CO_3/(CO_3+2OH) = 0.0$) after 170 days of reaction. A and B are replicate samples.

Calculated $CO_3/(CO_3+2OH)$	pH		Calcium (mmol/L)		Aluminum (mmol/L)	
	A	B	A	B	A	B
1.00	11.78	11.77	3.385	3.570	1.333	1.151
0.85	11.73	11.96	3.291	7.438	1.465	2.510
0.70	11.96	11.99	8.657	7.624	2.587	2.860
0.50	12.17	11.98	8.902	8.491	2.552	2.738
0.40	12.08	12.13	9.049	9.891	2.117	1.482
0.25	12.06	12.33	10.84	10.87	1.296	1.037
0.10	12.22	12.47	12.94	20.99	0.7167	<0.0011
0.0	12.47	12.33	19.00	21.16	<0.0011	<0.0011

Table 4.2: Solution data measured in the experiment from undersaturation for samples with compositions between the carbonate end member ($CO_3/(CO_3+2OH) = 1.0$) and the hydroxide end member ($CO_3/(CO_3+2OH) = 0.0$) after 515 days of reaction. A and B are replicate samples.

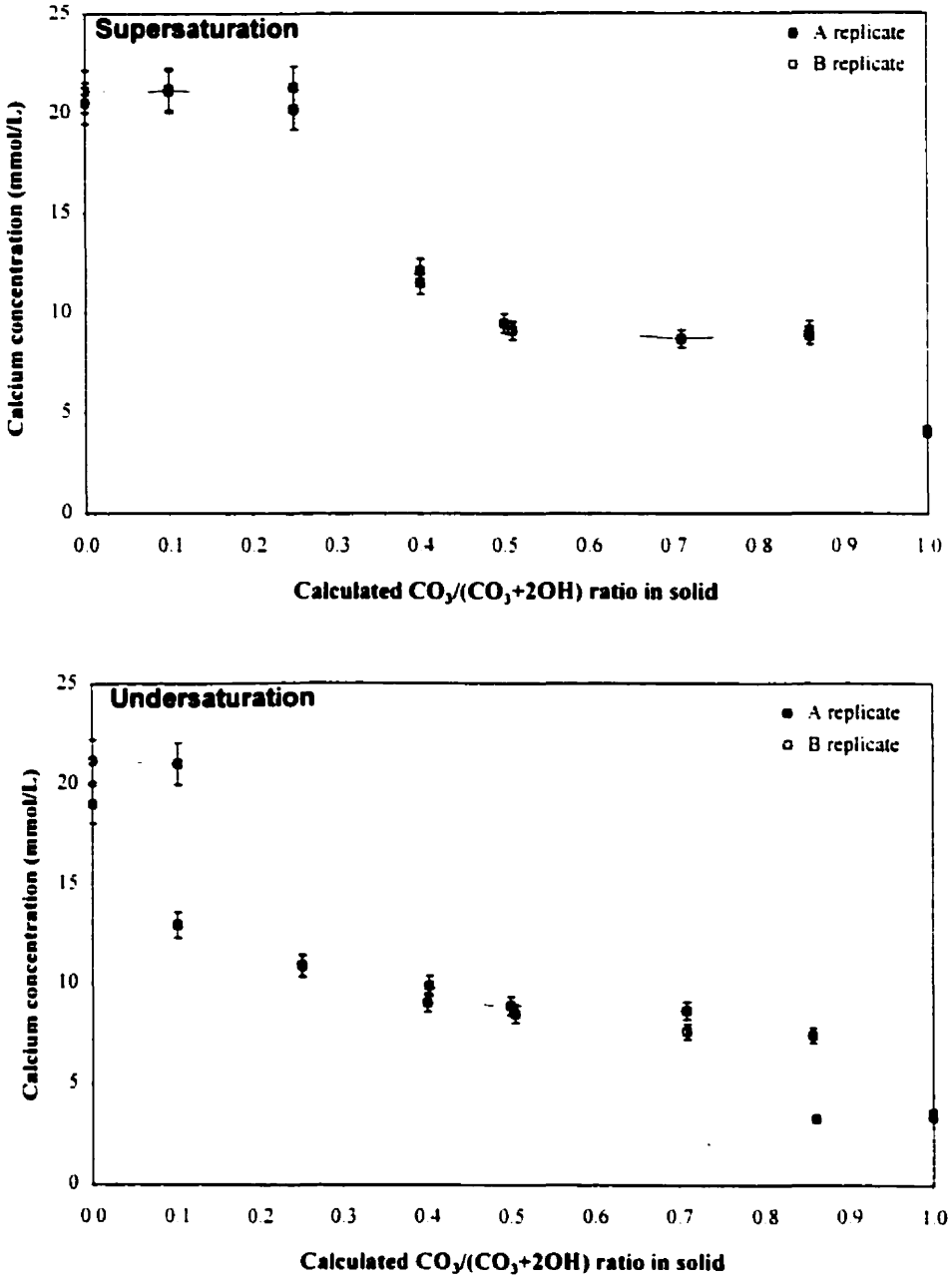
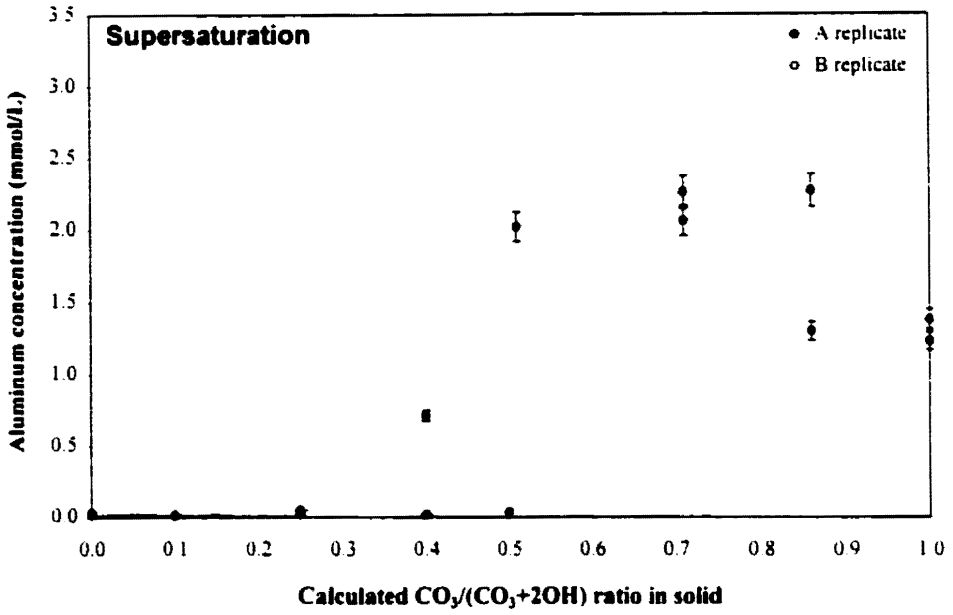


Figure 4.2: Solution concentrations of calcium as a function of the calculated carbonate ratio in the solid solution phases for the experiments from super- and undersaturation. The error bars show the analytical uncertainty of ± 5 %.



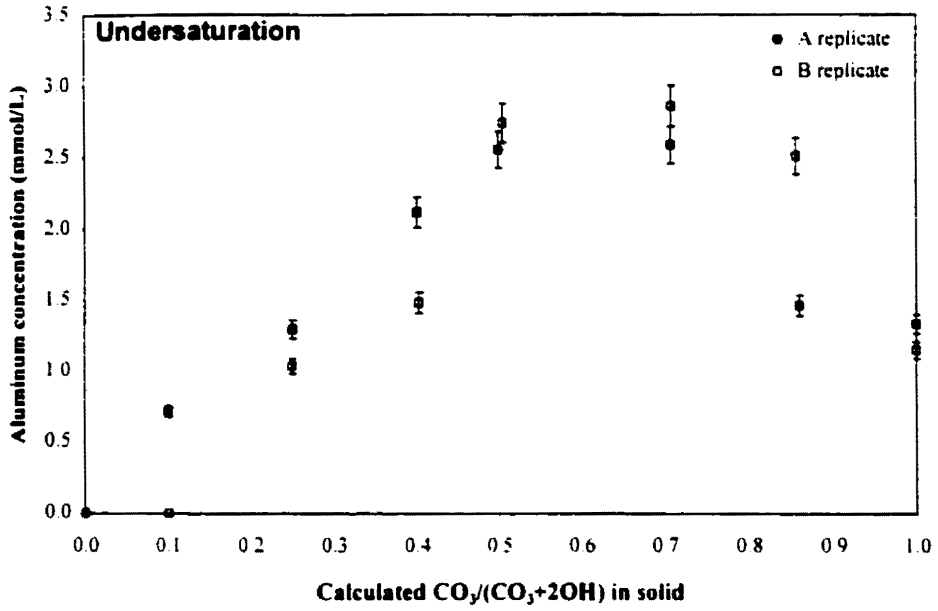


Figure 4.3: Solution concentrations of aluminum as a function of the calculated carbonate ratio in the solid solution phases for the experiment from super- and undersaturation. The error bars show the analytical uncertainty of ± 5 %.

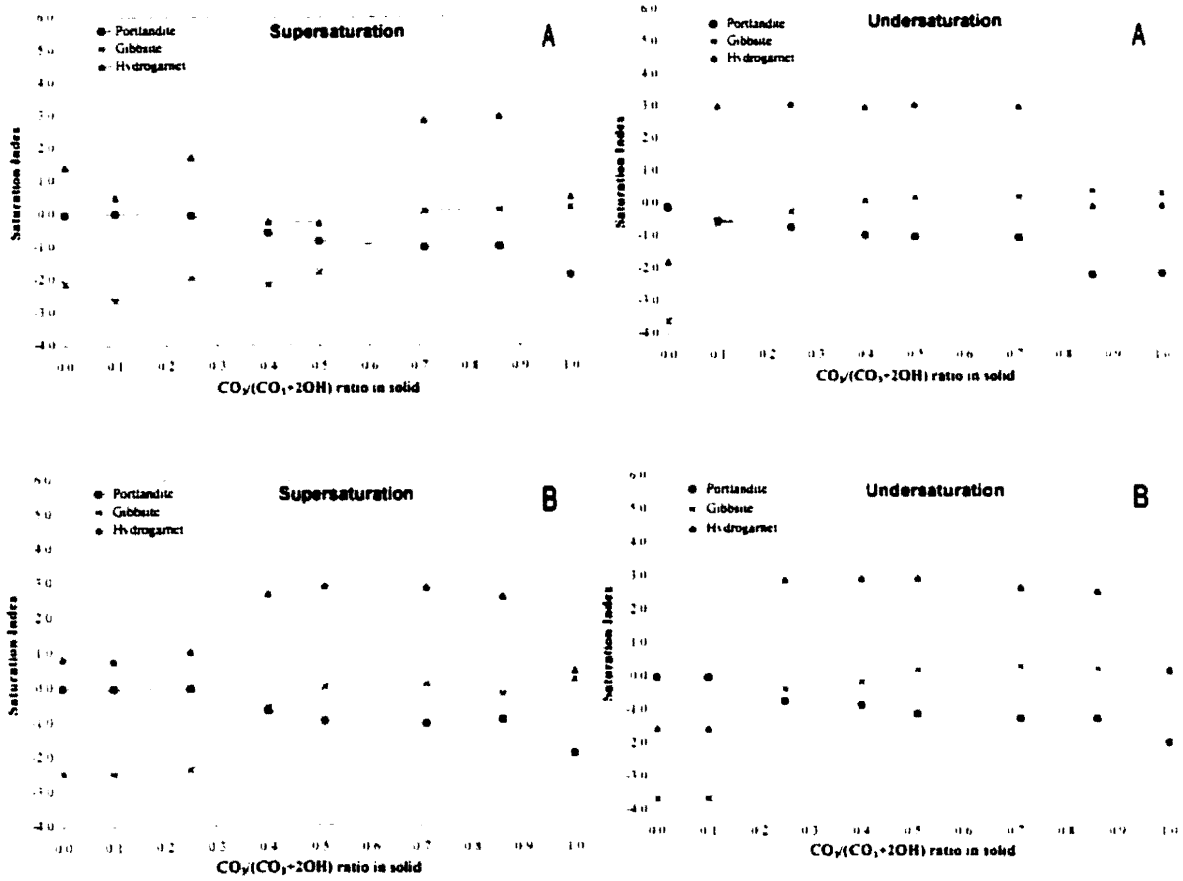


Figure 4.4: Mineral saturation indices versus the calculated carbonate ratio in the solid for the A and B replicates from supersaturation (left) and undersaturation (right). The saturation indices were calculated using the measured solution compositions, and the geochemical equilibria model SIMUL (Reardon, 1990).

Mineral saturation indices were calculated by inputting the solution compositions given in Tables 4.1 and 4.2 into the geochemical equilibria model SIMUL (Reardon, 1990). An estimate of the carbonate concentrations in these solutions was determined by assuming the solution compositions were in equilibrium with calcite in the simulations. This should have a limited effect on the calculated parameters, because the predicted carbonate concentrations are low (<0.061 mmol/L). The mineral saturation indices calculated for portlandite ($Ca(OH)_2$), gibbsite ($Al(OH)_3$), and hydrogarnet ($3CaO{\cdot}Al_2O_3{\cdot}6H_2O$) in the solutions as a function of the carbonate ratio are plotted in Figure 4.4.

The trends in the mineral saturation indices for portlandite and gibbsite are similar for the A and B replicates in both experiments. At low carbonate ratios (close to the hydroxide end member), the solutions are predicted to be just at saturation with respect to portlandite. As the carbonate ratio is increased, the solutions become increasingly undersaturated with respect to this phase. The saturation indices for gibbsite show the opposite trend. Close to the hydroxide end member, the solutions are undersaturated with respect to gibbsite, and as the carbonate ratio increases, the SI of gibbsite increases to approximately saturation. In the experiment from supersaturation, hydrogarnet is predicted to be above saturation at low carbonate ratios and increases to a maximum between carbonate ratios of 0.5 and 0.9. Hydrogarnet is just at saturation in the carbonate end member ($CO_3/(CO_3+2OH)=1.0$). In the experiment from undersaturation, the hydroxide end member solutions are predicted to be undersaturated with respect to hydrogarnet, but sharply increase to supersaturated conditions as the carbonate ratio is increased above 0.1. The saturation index remains high until the carbonate ratio in the solid increases above 0.7, and then decreases to approximately saturation with respect to hydrogarnet.

4.2.3 Solids

The XRD patterns for the A-replicates of the solid phases from super- and undersaturation are plotted in Figures 4.5 and 4.6, respectively. In some samples, the primary and secondary peaks for the solid solution were split into two or more peaks, indicating the presence of more than one solid solution phase. The d-spacings measured for the primary peak(s) are reported in Tables 4.3 and 4.4.

In solution or at relative humidities above 88%, the OH end member occurs in a highly hydrated form, $3CaO{\cdot}Al_2O_3{\cdot}Ca(OH)_2{\cdot}18H_2O$, with an interlayer spacing of 10.7Å. At lower relative humidities, this phase dehydrates forming $3CaO{\cdot}Al_2O_3{\cdot}Ca(OH)_2{\cdot}12H_2O$, with an interlayer

spacing of 7.9 Å. Hemicarboaluminate also occurs in two hydration states. The more highly hydrated form ($3CaO{\cdot}Al_2O_3{\cdot}0.5CaCO_3{\cdot}0.5Ca(OH)_2{\cdot}12H_2O$) has a primary d-spacing of 8.11 Å. and is stable between relative humidities of 53 to 81% (Roberts. 1969). Below relative humidities of 53%. this phase may occur together with a lower hydration product ($3CaO{\cdot}Al_2O_3{\cdot}0.5CaCO_3{\cdot}0.5Ca(OH)_2{\cdot}10H_2O$). which has an interlayer spacing of 7.7Å. Below relative humidities of 33%. the lower hydration state is the only phase observed. A d-spacing spacing of 7.56 has been reported for monocarboaluminate ($3CaO{\cdot}Al_2O_3{\cdot}CaCO_3{\cdot}10\text{-}11H_2O$) by Carlson and Berman (1960) and Fischer and Kuzel (1982). However. in the current study. a d-spacing of 7.45 Å was measured for this phase. Although an internal standard was not used in the current study. the dominant peaks for portlandite and hydrogarnet. where present. are approximately 0.04 to 0.08Å lower than the values given in the powder diffraction files from JCPDS-ICDD. This suggests that the lower d-spacing measured for monocarboaluminate (and the other solid phases) may be due to a calibration error in the goniometer of the X-ray diffractometer.

In the experiment from supersaturation. a single solid solution phase occurs at carbonate ratios of 1.0 and 0.85. and is identified as monocarboaluminate. As the carbonate ratio decreases to 0.71. both the primary and secondary peaks for the solid solution are split into two peaks. indicating that there are two solid solution phases present. The dominant phase is monocarboaluminate. with a primary peak at 2θ = 11.9 degrees (7.43 Å). The other peak at 2θ = 11.6 degrees (7.62 Å) is identified as the lower hydration form of hemicarboaluminate. At a carbonate ratio of 0.5. hemicarboaluminate is the only phase identified. and this phase persists as the carbonate ratio in the solid is decreased to 0.25. In the samples with a carbonate ratio of 0.1. a small peak at 2θ = 8.3 degrees (10.4 Å) has been identified as the highly hydrated form of the OH end member. $3CaO{\cdot}Al_2O_3{\cdot}Ca(OH)_2{\cdot}19H_2O$. The XRD pattern for the A replicate of the OH end member ($CO_3/(CO_3+2OH)=0.0$) is dominated by hydrogarnet. with small peaks indicating that the OH solid solution phase and portlandite are also present in limited quantities. In contrast. the B-replicate consists predominantly of the OH end member ($3CaO{\cdot}Al_2O_3{\cdot}Ca(OH)_2{\cdot}12H_2O$). with a primary peak at 7.8 Å. and a small peak at 8.05 Å also probably belongs to this phase. The small peak at 7.6 Å may belong to hemicarboaluminate.

Calculated $CO_3/(CO_3+2OH)$	Primary d-spacings -A replicates			Primary d-spacings - B replicates		
	Most intense	2nd most intense	3rd most intense	Most intense	2nd most intense	3rd most intense
1.00	7.43			7.43		
0.85	7.46			7.46		
0.70	7.46	7.66		7.46	7.62	
0.50	7.62			7.66		
0.40	7.62			7.62		
0.25	7.62			7.62		
0.10	7.82	8.11	7.66	7.66	8.11	
0.0	7.69			7.79	8.04	7.59

Table 4.3: Observed d-spacings for the primary peaks of the solid solution phases as a function of the calculated carbonate ratio ($CO_3/(CO_3+2OH)$) in the solid phase in the experiment from supersaturation.

Calculated $CO_3/(CO_3+2OH)$	Dominant basal d-spacing (Å)	2nd basal d-spacing (Å)	3rd basal d-spacing (Å)
1.00	7.46		
0.85	7.49		
0.70	7.53	8.11	
0.50	8.11	7.56	
0.40	8.11	7.69	7.49
0.25	8.15		
0.10	8.19		
0.0	8.15	7.82	7.49

Table 4.4: Observed d-spacings for the primary peak of the solid solution phases as a function of the calculated carbonate ratio ($CO_3/(CO_3+2OH)$) in the solid phase in the experiment from undersaturation (A replicate samples only).

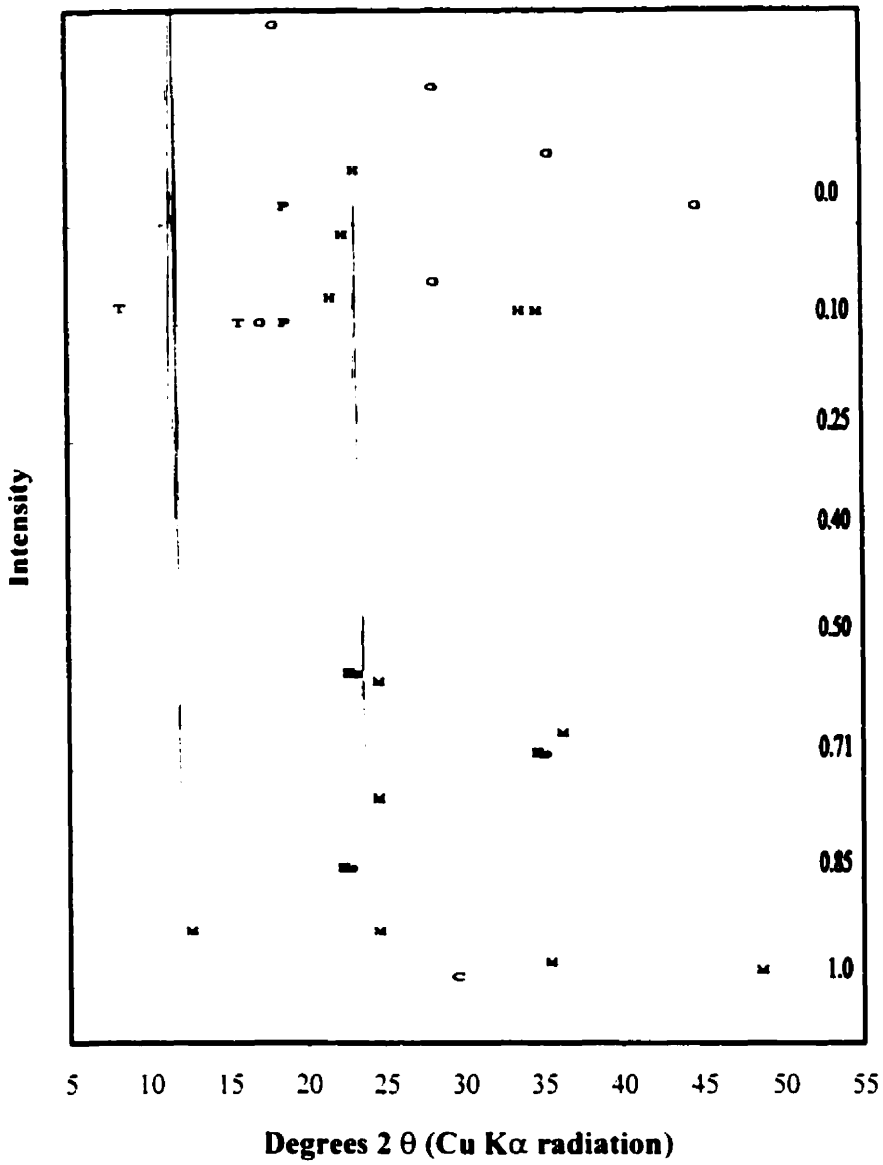


Figure 4.5: XRD patterns for A-replicate samples from the supersaturation experiment. The number indicates the calculated carbonate ratio in the solid. from the carbonate end member (1.0) to the OH end member (0.0). Peaks are labeled: H= OH end member ($3CaO{\cdot}Al_2O_3{\cdot}Ca(OH)_2{\cdot}12H_2O$); Hc = hemicarboaluminate ($3CaO{\cdot}Al_2O_3{\cdot}0.5Ca(OH)_2{\cdot}0.5CaCO_3{\cdot}10H_2O$); M= CO_3 end member: C= calcite ($CaCO_3$); G= hydrogarnet ($3CaO{\cdot}Al_2O_3{\cdot}6H_2O$); P= portlandite ($Ca(OH)_2$); T = hydrated OH end member ($3CaO{\cdot}Al_2O_3{\cdot}Ca(OH)_2{\cdot}18H_2O$).

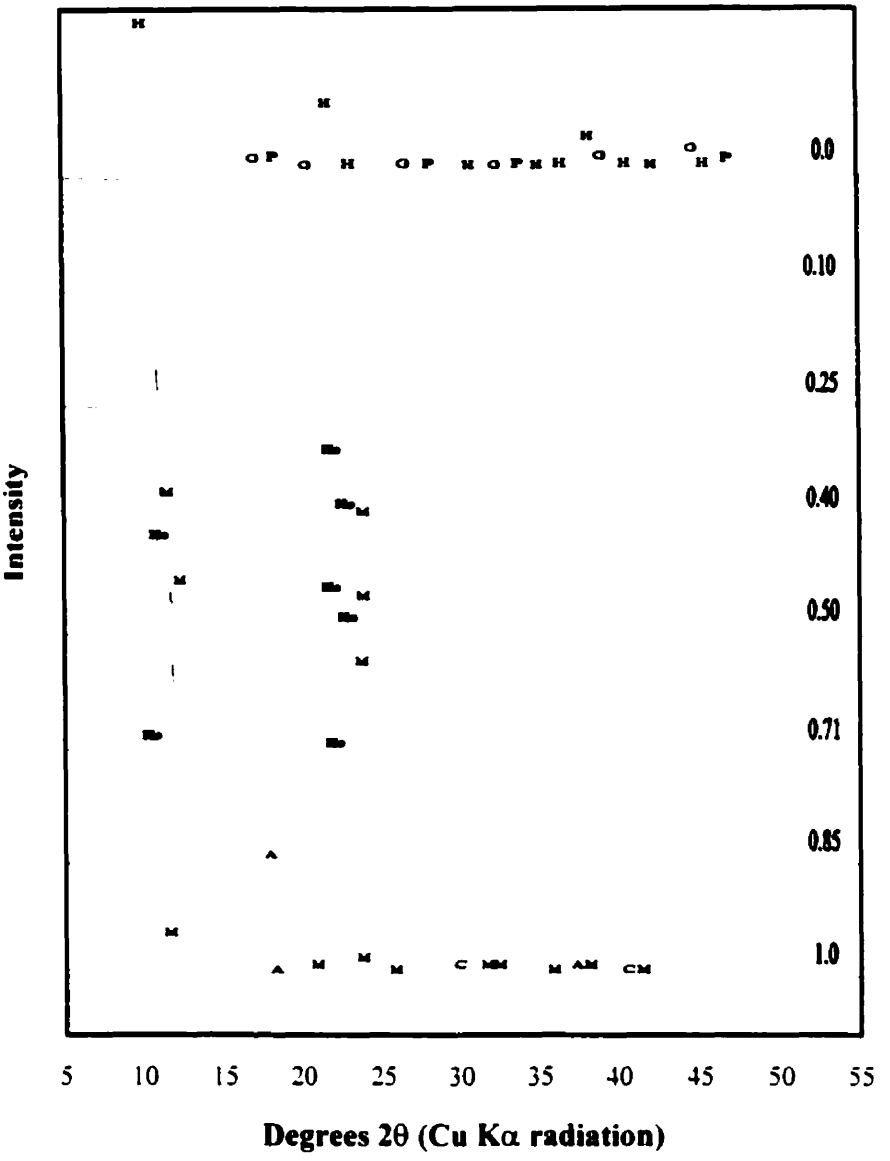


Figure 4.6: XRD patterns for A-replicate samples from the undersaturation experiment. The number indicates the calculated carbonate ratio in the solid, from the carbonate end member (1.0) to the OH end member (0.0). Peaks are labeled: H = OH end member ($3CaO{\cdot}Al_2O_3{\cdot}Ca(OH)_2{\cdot}12H_2O$); Hc = hemicarboaluminate $3CaO{\cdot}Al_2O_3{\cdot}0.5Ca(OH)_2{\cdot}0.5CaCO_3{\cdot}12H_2O$); M = CO_3 end member; G = hydrogarnet ($3CaO{\cdot}Al_2O_3{\cdot}6H_2O$); P = portlandite ($Ca(OH)_2$); C = calcite ($CaCO_3$); A = gibbsite ($Al(OH)_3$).

In addition to monocarboaluminate, calcite was observed in solids with a carbonate ratio of 1.0. The A replicate solids with carbonate ratios of 0.0 to 0.85 contained small amounts of hydrogarnet, and solids with ratios of 0.0 to 0.5 also contained portlandite. In the B replicate solids, hydrogarnet and portlandite both occur over smaller ranges, from carbonate ratios of 0.0 to 0.71 and 0.0 to 0.4, respectively.

The XRD patterns for the A-replicate solids from undersaturation are shown in Figure 4.6. In agreement with the results from supersaturation, monocarboaluminate is the only solid solution phase in solids with carbonate ratios of 1.0 and 0.85. Monocarboaluminate coexists with hemicarboaluminate at a carbonate ratio of 0.71 as seen in the experiment from supersaturation, although hemicarboaluminate is present in a higher hydration state ($3CaO{\cdot}Al_2O_3{\cdot}0.5CaCO_3{\cdot}0.5Ca(OH)_2{\cdot}12H_2O$), with a primary d-spacing of 8.11 Å. These two phases persist as the carbonate ratio in the solid is decreased to 0.4, with a decrease in the quantity of the monocarboaluminate phase (=7.5 Å) and an increase in the quantity of hemicarboaluminate. At carbonate ratios of 0.4 and 0.25, hemicarboaluminate is the only solid solution phase present, with a primary peak at 8.1Å. A small peak at 7.7 Å in solids with a carbonate ratio of 0.4 is attributed to the lower hydration state of this phase. In the OH end member sample, the dominant peak has a primary d-spacing of 8.15 Å, and based on this d-spacing, would be identified as hemicarboaluminate. This suggests that this solid has undergone extensive carbonation. However, a small peak at approximately 7.8 Å confirms that at least a small quantity of the OH-end member is present, in agreement with the results from supersaturation.

In addition to monocarboaluminate and calcite, which were identified in the experiment from supersaturation, a small peak at 2θ = 18.3 degrees (4.85 Å) is attributed to gibbsite ($Al(OH)_3$) in samples with carbonate ratios of 1.0. Gibbsite is also present in the solid with a carbonate ratio of 0.85. In agreement with the B replicate solids from supersaturation, hydrogarnet is present in solids with carbonate of 0.0 to 0.71. However, portlandite was only observed in the OH end member solid (carbonate ratio = 0.0).

4.2.4 Solubility Products

If the solid solution phase is the only phase present, its composition can be calculated by mass balance of the quantity of reagents added and the final solution composition. The only solids which meet this criteria are those with a carbonate ratio of 0.5 in the experiment from supersaturation. For the remainder of the samples, the carbonate ratios have been estimated by

assuming that the quantity of additional phases such as hydrogarnet, calcite or portlandite are negligible. For solids within either of the miscibility gaps, a bulk composition assuming a single solid solution phase was calculated.

The solubility products (K_{sp}) of the solid-solution phases have been calculated, assuming that equilibrium between the solid and aqueous phases had been attained, and that the activity of the solid phase equals 1. These K_{sp} values were calculated with the measured solution compositions (Tables 4.1 and 4.2), the activity coefficients and solution carbonate concentrations predicted using the geochemical equilibria model SIMUL (Reardon, 1990), and the calculated solid phase compositions.

The general dissolution reaction for the solid solution series is given in equation 1. The K_{sp} value for this reaction is formulated according to equation 2, where m is the concentration of the ion in mol/L of solution, γ is the activity coefficient, and aH_2O is the activity of water.

$$3CaO{\cdot}Al_2O_3{\cdot}xCaCO_3{\cdot}(1\text{-}x)Ca(OH)_2{\cdot}(12\text{-}x))H_2O = 4Ca^{2+} + 2Al(OH)_4^- + xCO_3^{2-} + (6\text{-}2x)OH^- + (6\text{-}x)H_2O \quad (4.1)$$

$$Ksp = [mCa^{2+}{\cdot}\gamma Ca^{2+}]^4\,[mAl(OH)_4^-{\cdot}\gamma Al(OH)_4^-]^2\,[mCO_3^{2-}{\cdot}\gamma CO_3^{2-}]^x\,[mOH^-{\cdot}\gamma OH^-]^{(6-2x)}\,[aH_2O]^{(6-x)} \quad (4.2)$$

The upper and lower uncertainty limits in the calculated K_{sp} values were determined by adding or subtracting the analytical uncertainty (5%) to the measured solution concentrations of Ca and Al. The solutions were then re-modeled with these revised concentrations, and the K_{sp} values re-calculated.

4.3 Discussion

4.3.1 Mineral assemblages

Five mineral assemblages can be distinguished based on the results from super- and undersaturation in the current study (Table 4.5), and include ranges in which the hydroxide end member, the carbonate end member, or hemicarboaluminate is the only solid solution phase

present. There are also two miscibility gaps in the system. These observed assemblages agree well with the XRD results presented by Roberts (1969), Fischer and Kuzel (1982), and Pöllmann (1986) (Table 4.6), although there are some differences in the carbonate ratios over which the miscibility gaps are observed to occur. The carbonate ratios for the changes in the observed phase assemblages reported by Pöllmann (1986) have been estimated from their published triangular diagram, because the actual carbonate ratios for the observed changes were not given. These assemblages are very similar to those described by Fischer and Kuzel (1982), and therefore the data from Pöllmann (1986) has not been included in the following discussions of each observed mineral assemblage.

Experiment	Reaction Time	CO_3 ratio in solid	Solids Observed
Supersaturation	6 months	0.0	A-replicate: mostly C_3AH_6 and P, minor C_4AH_{13}. B-replicate: C_4AH_{13} and Hemi (?), minor C_3AH_6 and P C-replicate:
		0.1-0.5	Hemi, minor C_3AH_6 and P
		0.71	Mono, Hemi
		0.85	Mono
		1.0	Mono, minor calcite
Undersaturation	16 months	0.0	Hemi (?), C_4AH_{13}, C_3AH_6, P
		0.25-0.1	Hemi, minor C_3AH_6
		0.4	Hemi, minor C_3AH_6, trace Mono
		0.5-0.71	Mono, Hemi, minor C_3AH_6
		0.85	Mono, Hemi, trace $Al(OH)_3$
		1.0	Mono, minor calcite, trace $Al(OH)_3$

Table 4.5: Comparison of the observed mineral phases in the current study between the carbonate and hydroxyl end members as a function of the carbonate ratio in the solid. Results from both super- and undersaturation are presented. C_4AH_{19} = OH end member ($3CaO{\cdot}Al_2O_3{\cdot}Ca(OH)_2{\cdot}18H_2O$); C_4AH_{13} = OH end member ($3CaO{\cdot}Al_2O_3{\cdot}Ca(OH)_2{\cdot}13H_2O$); C_3AH_6 = hydrogarnet ($3CaO{\cdot}Al_2O_3{\cdot}6H_2O$); P = portlandite $Ca(OH)_2$; Calcite = $CaCO_3$.

4.3.1.1 OH end member

In the experiment from supersaturation, the OH end member was the only solid solution phase observed at a carbonate ratio of 0.0. Hydrogarnet and portlandite were also observed, in varying amounts. In the studies by Roberts (1969) and Fischer and Kuzel (1982), the highly hydrated form of the OH-end member ($4CaO{\cdot}Al_2O_3{\cdot}Ca(OH)_2{\cdot}19H_2O$) was the only phase observed at a carbonate ratio of 0.0 and relative humidities of 88 and 100 %, respectively. At a relative humidities 65%, the less hydrated form ($4CaO{\cdot}Al_2O_3{\cdot}Ca(OH)_2{\cdot}12H_2O$) was the dominant phase (Fisher and Kuzel, 1982). The absence of hydrogarnet and portlandite in the study by Roberts (1969) is likely due to the short reaction time (≈ 7 days).

4.3.1.2 Miscibility gap: OH end member and hemicarboaluminate

After 6 months of reaction from supersaturation, solids with carbonate ratios between 0.1 and 0.5 consist of hemicarboaluminate, hydrogarnet, and portlandite. Calcium concentrations of 21 mmol/L and pH values of 12.5 were measured in samples with carbonate ratios of 0.0 to 0.25, consistent with the presence of portlandite. The solutions are also predicted to be just at saturation with respect to portlandite, based on saturation index calculations. As the carbonate ratio in the solid increases above 0.25, the calcium concentration and the solution pH decrease, and the solutions become undersaturated with respect to portlandite. This is consistent with a decrease in the intensity of the portlandite peaks with increasing carbonate ratio in the solid (Figure 4.5). In the experiment from undersaturation, hemicarboaluminate and hydrogarnet were observed in the XRD pattern of the A-replicate solids with carbonate ratios of 0.1 and 0.25. The absence of portlandite in this phase assemblage is consistent with the lower Ca and pH values measured in solution at these ratios, and with the saturation index calculations, which show that these solutions are undersaturated with respect to portlandite.

Roberts (1969) reported the occurrence of the OH-end member and hemicarboaluminate between carbonate ratios of 0.13 and 0.35, and the quantity of hemicarboaluminate relative to the OH-end member was observed to increase as the carbonate ratio in the solid increased. Fisher and Kuzel (1982) observed this same phase assemblage between carbonate ratios of 0.05 and 0.4.Based on these two studies, the OH-end member and hemicarboaluminate co-exist at carbonate ratios of 0.05 to 0.4. The presence of two solid solution phases demonstrates the existence of a miscibility gap over this range of compositions. In the current study, the results from supersaturation support the existence of this miscibility gap. Over the range 0.1 to 0.5,

hemicarboaluminate is observed, and the presence of the OH-end member is suggested by the presence of its stable reaction products, hydrogarnet and portlandite. However, this phase assemblage was observed over a much smaller range (0.0 to 0.25) in the experiment from undersaturation.

Reference	Reaction Time	CO_3 ratio in solid	Solids Observed
Roberts (1969)	≈7 days	0.13-0.35	C_4AH_{19}, Hemi
		0.48-0.53	Hemi
		0.67	Hemi, Mono
		0.78	Hemi, Mono, P
		0.95	Mono, trace Hemi
		0.98	Mono, calcite, trace P and Hemi
		1.12	Mono, calcite
		1.62	Mono, P, and some calcite
Fischer and Kuzel (1982)	Not given	0.0	C_4AH_{19}
		0.05-0.4	C_4AH_{19}, Hemi
		0.5	Hemi
		0.6-0.8	Hemi, Mono
		0.9-1.0	Mono
Pöllmann (1986)	12 months	0.0	C_4AH_{13}
		0.05-0.45	C_4AH_{13}, Hemi
		0.45-0.55	Hemi
		0.55-0.95	Hemi, Mono
		1.0	Mono

Table 4.6: Comparison of the mineral phases observed to form between the carbonate and hydroxyl end members as a function of the carbonate ratio in the solid. C_4AH_{19}= OH end member ($3CaO{\cdot}Al_2O_3{\cdot}Ca(OH)_2{\cdot}18H_2O$); C_4AH_{13}= OH end member ($3CaO{\cdot}Al_2O_3{\cdot}Ca(OH)_2{\cdot}13H_2O$); Hemi = hemicarboaluminate ($3CaO{\cdot}Al_2O_3{\cdot}0.5Ca(OH)_2{\cdot}0.5CaCO_3{\cdot}11H_2O$); Mono= monocarboaluminate ($3CaO{\cdot}Al_2O_3{\cdot}CaCO_3{\cdot}11H_2O$); C_3AH_6 = hydrogarnet ($3CaO{\cdot}Al_2O_3{\cdot}6H_2O$); P = portlandite $Ca(OH)_2$; calcite = $CaCO_3$.

4.3.1.3 Hemicarboaluminate

After 6 months of reaction from supersaturation, hemicarboaluminate was the dominant phase at a carbonate ratio of 0.5, in agreement with the results of Roberts (1969), and Fischer and Kuzel (1982). These authors observed that hemicarboaluminate alone was formed at ratios of 0.48-0.53, and 0.5, respectively. In solids from the current study, hydrogarnet and portlandite (A replicate solid only) were present as additional phases. These additional phases may not have been observed in the experiments of Roberts (1969), because the equilibration time was only 7 days. In contrast to these results, after 16 months of reaction from undersaturation in the current study, the solids were dominated by a mixture of hemicarboaluminate and monocarboaluminate, with a trace amount of hydrogarnet.

4.3.1.4 Miscibility gap: Hemicarboaluminate and monocarboaluminate

Hemicarboaluminate and monocarboaluminate occur together at a ratio of 0.71 in the experiment from supersaturation. These two solid solution phases were identified in solids with carbonate ratios between 0.67 and 0.98 in the study by Roberts (1969), however, the identification of trace amounts of hemicarboaluminate in solids with carbonate ratios above 0.78 was uncertain. In the study by Fischer and Kuzel (1982), hemi- and monocarbo-aluminate occurred together at carbonate ratios between 0.6 and 0.8. Based on the results of these two studies, this phase assemblage appears to be stable between a carbonate ratio of 0.6 and 0.8. The occurrence of these two phases demonstrates the existence of a second miscibility gap in the system. After 16 months of reaction from undersaturation in the current study, hemicarboaluminate and monocarboaluminate occur in solids with carbonate ratios between 0.4 and 0.7, and hydrogarnet is also present. These results suggest that at very long reaction times, this miscibility gap may expand to carbonate ratios as low as 0.4. This may indicate that the stable phase assemblage consists of a mixture of monocarboaluminate and hydrogarnet. This conversion is discussed in more detail in Section 4.3.2.

4.3.1.5 Monocarboaluminate

Based on the XRD results from the current study, monocarboaluminate is the only solid solution phase present at carbonate ratios of 0.85 or higher, in agreement with the results of Fischer and Kuzel (1982). These authors reported that monocarboaluminate was the only phase present

above a carbonate ratio of 0.8. Above carbonate ratios of 0.78, Roberts (1969) also reported that monocarboaluminate was the dominant solid solution phase. Although trace amounts of hemicarboaluminate was reported in solids with carbonate ratios of 0.95 and 0.98, the identification of the presence of this phase was uncertain (Roberts, 1969).

In addition to monocarboaluminate, calcite was observed in solids with a carbonate ratio of 1.0 from both super- and undersaturation in the current study. Roberts (1969) reported the presence of both calcite and portlandite at carbonate ratios of 0.98 or higher. In the current study, gibbsite was also observed in solids with carbonate ratios of 0.85 and 1.0. The calculated saturation indices show that solutions from both experiments are at saturation with respect to gibbsite, consistent with the identification of this phase in the XRD patterns.

4.3.2 Attainment of equilibrium

In the experiment from supersaturation, solids with a carbonate ratio of 0.0 consist of the OH-end member ($4CaO{\cdot}Al_2O_3{\cdot}Ca(OH)_2{\cdot}12H_2O$), hydrogarnet and portlandite, in varying amounts. In solution, the OH-end member has an extra layer of water molecules in the interlayer of its structure ($3CaO{\cdot}Al_2O_3{\cdot}Ca(OH)_2{\cdot}18H_2O$). The OH-end member is metastable with respect to hydrogarnet at room temperature (Wells et al., 1943; Roberts, 1957), and is reported to convert to hydrogarnet with time by Steinour (1951). This transformation can be described by the reaction:

$$3CaO{\cdot}Al_2O_3{\cdot}Ca(OH)_2{\cdot}18H_2O \rightarrow 3CaO{\cdot}Al_2O_3{\cdot}6H_2O + Ca(OH)_2 + 12H_2O \quad (4.3)$$

In the experiment from undersaturation, the decrease in conductance with long reaction times suggests that these solutions may be approaching equilibrium with respect to hydrogarnet. This conversion is also supported by the calculated mineral saturation indices. Solutions at a carbonate ratio of 0.0 are supersaturated with respect to hydrogarnet in the experiment from supersaturation, however, the B replicate sample from undersaturation is calculated to be slightly undersaturated with respect to hydrogarnet. The continued persistence of the OH-end member demonstrates that this system has not yet reached equilibrium, and indicates that the reaction kinetics are very slow for the conversion of this phase to hydrogarnet. The persistence of the OH-end member in solution after long reaction times has been observed by numerous researchers (e.g. Zhang, 2000; Pöllmann, 1986;Wells et al., 1943).

Hemicarboaluminate was the only solid solution phase observed at a carbonate ratio of 0.5 in the experiment from supersaturation. However, after 16 months of reaction from undersaturation, the solids were dominated by hemicarboaluminate and monocarboaluminate, with a trace amount of hydrogarnet. In the experiment from undersaturation, hemicarboaluminate may be converting to a mixture of monocarboaluminate and hydrogarnet with time according to a reaction similar to the following (equation 4.4):

$$Ca_4Al_2O_6(OH)\cdot 0.5CO_3\cdot 12H_2O = 0.5Ca_4Al_2O_6\cdot CO_3\cdot 11H_2O + 0.5Ca_3Al_2O_6\cdot 6H_2O + 0.5Ca^{2+} + OH^- + 3.5H_2O$$

The conductance measurements for solids with a carbonate ratio of 0.5 were stable after only 3 days of reaction from both super- and undersaturation, however, the final conductance measurement from undersaturation was 24% lower than that measured from supersaturation. The fact that the measured conductances are different, verifies that the two experiments did not reach the same end point, and the relatively large change in conductance also could be indicative of the phase change. All solutions at this carbonate ratio are predicted to be strongly supersaturated with respect to hydrogarnet, providing further support for the phase change from hemicarboaluminate to monocarboaluminate and hydrogarnet.

The conductance measurements for the carbonate end member were stable after three days of reaction in the experiments from both super- and undersaturation. However, the final conductance measurement in the experiment from undersaturation is approximately 15% lower than that made from supersaturation. This could represent either a metastable or an equilibrium state. According to the phase rule, up to three phases can co-exist at equilibrium. Therefore, it is possible that the phase assemblage monocarboaluminate, calcite, and gibbsite observed at a carbonate ratio of 1.0 in the experiment from undersaturation is an equilibrium assemblage. At the carbonate end member, the aqueous phase is calculated to be just at saturation with respect to hydrogarnet. This suggests that there is little or no thermodynamic driving force for the conversion of monocarboaluminate to hydrogarnet.

4.3.3 Stability of the solid solutions

The investigations performed by Roberts (1969), Fischer and Kuzel (1982), and the current research demonstrate the existence of two miscibility gaps between the carbonate and hydroxyl end members of the calcium aluminate hydrates. These miscibility gaps span almost the entire range of compositions between the two end members. Differences in ionic radii and charge

between substituting ions can lead to the formation of limited solid solutions (Brownlow, 1979). Other properties which may contribute to the stability of the solid solution are the geometry and bonding characteristics of the substituting ions.

The arrangement of atoms in the carbonate group is trigonal planar, whereas the OH^- ion is approximately spherical. The length of the carbon-oxygen bond in the CO_3^{2-} group is 1.85 Å (Douglas et al., 1994), but perpendicular to the plane of the carbonate group, the thickness of the group is likely closer to the effective size of oxygen (Wedepohl, 1969). The OH^- ion also has a radius similar to the oxygen atom, or approximately 1.4 Å. In the calcium aluminate hydrates, the size difference between the substituting ions is not usually considered to be a key factor in determining stability, because the interlayer spacing changes easily to accommodate larger ions or extra water molecules. However, the charge difference between OH^- and CO_3^{2-} ions is probably an important factor, because carbonate ions with a charge of -2 form relatively strong bonds with calcium ions in the main layers and with water molecules in the interlayer. This provides cohesion to the structure (Francois et al., 1998; Newman and Jones, 1999), and may stabilize the structure of hemicarboaluminate, relative to the OH end member.

In solution, or in a controlled environment at 100% relative humidity, the OH-end member occurs in the highly hydrated form ($3CaO{\cdot}Al_2O_3\ Ca(OH)_2{\cdot}18H_2O$), with layer thickness of 10.7 Å. Upon drying to a relative humidity below 81%, this phase loses a layer of water from within the interlayer, forming $3CaO{\cdot}Al_2O_3Ca(OH)_2{\cdot}12H_2O$ with a layer thickness of 7.9 Å (Roberts, 1969). The "extra" layer of water molecules is postulated to lie between the principal layers and interlayer regions (Passaglia and Sacerdoti,1988). Hemicarboaluminate is more similar to the dehydrated form of OH-end member, in that it does not contain the additional layer of water molecules. This difference in the number of water molecules in the interlayer region may also contribute to the instability of solid solutions with compositions intermediate between the OH end member and hemicarboaluminate.

The layer thickness of hemicarboaluminate is 8.2 Å, and is significantly larger than that of both the OH end member (7.9 Å) and monocarboaluminate (7.6 Å). Based on the observed formation of a miscibility gap between mono- and hemicarbo-aluminate as the carbonate ratio in the solid decreases below 0.8, the structure of monocarboaluminate can not incorporate more hydroxyl ions. Instead, hemicarboaluminate precipitates, incorporating the additional hydroxyl ions. From refinements of single-crystal XRD patterns, Renaudin et al. (1999) determined that the carbonate anions in the interlayer of monocarboaluminate are tilted at an angle of between 20.5 and 21.8° from the plane of the main layers. Based on the observed layer thickness of

hemicarboaluminate. Taylor (1997) has suggested that the carbonate groups are actually oriented perpendicular to the main layers in this phase. To maintain charge balance, two OH^- ions are substituted for each CO_3^{2-} ion in the structure of monocarboaluminate. This results in an increase in the number of anions in the interlayer, and consequently, an increase in steric repulsion between the anions. As the ratio of carbonate ions in the interlayer decreases below 0.8, the increase in repulsion between anions may require that the planar carbonate groups tilt further away from the plane of the main layers (i.e. to an angle greater than 21.5°) to accommodate the extra hydroxyl ions. The most stable arrangement in this case may be with the carbonate group perpendicular to the main layers, as postulated for hemicarboaluminate.

4.3.4 Solubility products

Calculations of the solubility products for the solid solution phases are dependent on knowledge of their compositions. In the current study, the actual composition of the solid solution phase can only be calculated for solids with a carbonate ratio of 0.5 in the experiment from supersaturation. In all other solids from both experiments, there were small quantities of additional phases present such as hydrogarnet, portlandite or gibbsite, or within the miscibility gaps, two solid solution phases were identified. However, because no previous solubility data is available for solids with compositions between the hydroxide and carbonate end members, an approximation of the solubility of these phases may be useful. Therefore, in the miscibility gaps, a bulk composition for the solid solution phase has been calculated by mass balance between the reagents initially added and the final measured solution composition. The solubility products calculated for the carbonate and hydroxide end members are compared with previously published values in Chapter 5.

The calculated log K_{sp} values for the solid solution phases and the minimum estimated uncertainties in these values (error bars) versus the carbonate ratio in the solid from super- and undersaturation are plotted separately in Figure 4.7. The limits of the two miscibility gaps between the OH end member and hemicarboaluminate, and between hemi- and monocarboaluminate observed in each experiment are also plotted. In the experiment from supersaturation, the calculated log solubility products are between -27 and -28 over most of the series (i.e. between carbonate ratios of 0.0 and 0.85), but decrease sharply in the carbonate end member to values of -29 to -31. The two A replicate samples at carbonate ratios of 0.4 and 0.5 are notable exceptions to this general trend, having solubility products closer to -31. An examination of the solution composition data (Table 4.1) reveals that these two samples have

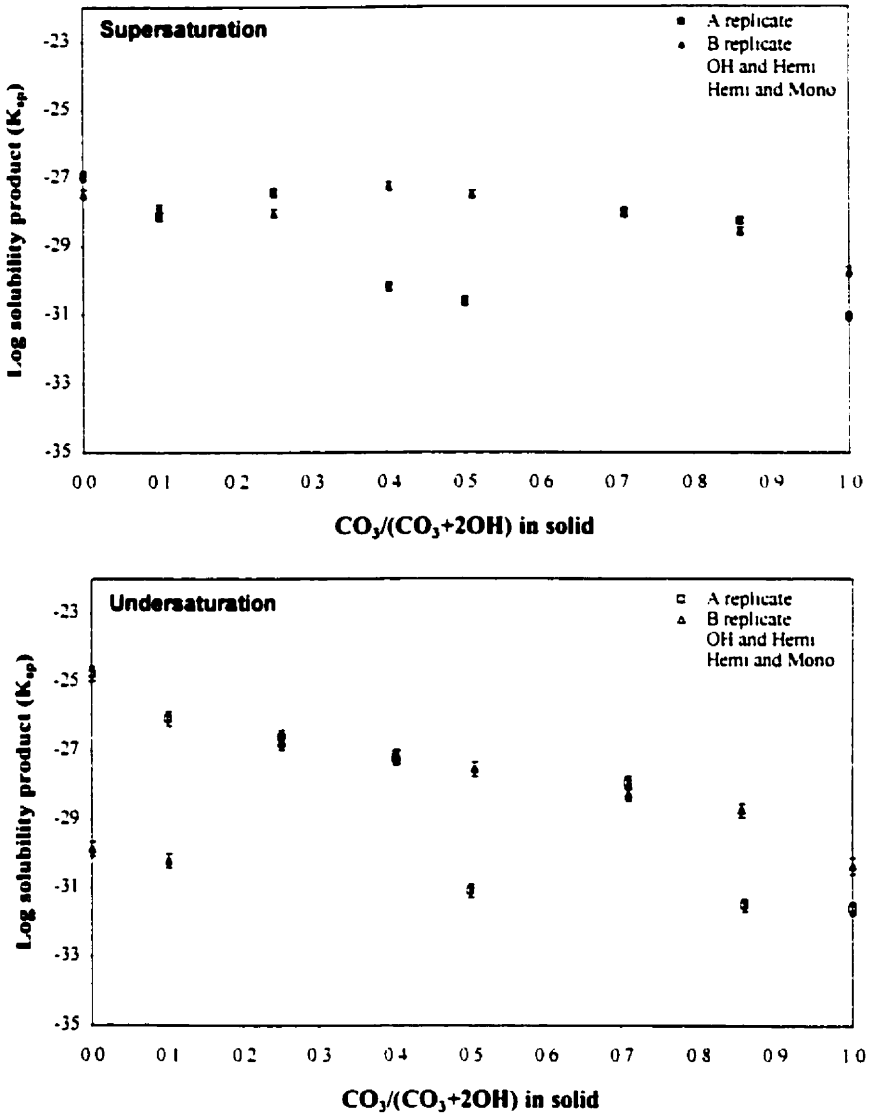


Figure 4.7: Log values of the solubility product (K_{sp}) for the solid solution phases as a function of the carbonate ratio in the solid, from the experiments from super- and undersaturation. Error bars show the minimum estimated uncertainty in the log K_{sp} values, based on the analytical uncertainty in the solution composition. The short-dashed lines indicate the limits of the miscibility gap for the OH end member (OH) and hemicarboaluminate (Hemi), and the long-dashed lines represent the observed limits of the miscibility gap between hemi- and monocarboaluminate (Mono), as observed in the current study.

very low aluminum concentrations. Both samples are predicted to be right at saturation with respect to hydrogarnet, whereas all other samples are supersaturated with respect to this phase. This suggests that the A-replicate samples with carbonate ratios of 0.4 and 0.5 more closely represent final solution composition equilibrated with respect the stable phase assemblage - hemicarboaluminate, hydrogarnet, and possibly portlandite. In turn, the B replicate samples at these same ratios likely represent the solution composition of the solution in metastable equilibrium with the solid solution phase(s). Within the miscibility gap, where two solid solution phases were observed, the estimated log K_{sp} value is probably representative of the more soluble of the two phases (hemicarboaluminate).

In the experiment from undersaturation, there is relatively smooth trend in the calculated log Ksp values to lower values with increasing carbonate ratio in the solid, with five notable exceptions. The A-replicate samples with carbonate ratios of 0.0 and 0.1, and B-replicate samples with carbonate ratios of 0.5, 0.85 and 1.0 have calculated log Ksp values between -30 and -31. All five samples have low solution concentrations of Al (Table 4.3), and are calculated to be at or below saturation with respect to hydrogarnet. This suggests that these five samples may be closer to the final equilibrium condition for this series, while the higher log K_{sp} result measured in the bulk of the samples are representative of a metastable equilibrium condition.

4.3.5 Predicting carbonate partitioning at equilibrium

Predictions of the partitioning of ions between a solid solution phase and the aqueous phase can be calculated at thermodynamic equilibrium, if the activities of the solid solution phases are known. In Chapters 2 (Section 2.4.4.1) and 3 (Section 3.4.3.1), equations were presented that enable solid phase activity coefficients to be derived based on changes in the solubility products of the solid solution phases as a function of composition. However, modeling the hydroxide-carbonate series poses some even larger challenges than those encountered in the hydroxide-chloride and chloride-carbonate series, in part because there are two miscibility gaps in this system.

When there are two miscibility gaps in a system, and a stable intermediate phase, it may be possible to divide the system into two parts, and model each half independently. In the hydroxide-carbonate series, the OH end member and hemicarboaluminate could be chosen as end members for the first half, and hemicarboaluminate and monocarboaluminate could be chosen as end members for the second half of the system. In this approach, hemicarboaluminate

is treated as a pure phase, with a constant solubility product. The assumption of a constant composition for hemicarboaluminate appears to be reasonable, because Roberts (1969) and Fischer and Kuzel (1982) have shown that hemicarboaluminate forms only very limited solid solutions. This approach is similar to that used by Busenberg and Plummer (1989) for the magnesian calcite solid solutions, where the stable phase (dolomite or disorder dolomite) with a composition intermediate to that of calcite and magnesite was treated as a pure phase, and used as one end member for equilibrium predictions. Although this is a reasonable approach, it has not been attempted here for several reasons:

1. Either two solid solution phases or one solid solution phase plus additional mineral phases were identified at most carbonate ratios studied. As a result, the solid phase compositions used to calculate the solubility products are only rough estimates. This influences the calculated solubility products, and subsequently, derivation of the excess free energy parameters and solid phase activity coefficients.

2. The number of data points between either end member (hydroxide or carbonate) and hemicarboaluminate is insufficient to delineate a curve (4 to 5 solubility measurements).

Detailed solubility studies, focusing on the range between the OH and CO_3 end members and hemicarboaluminate need to be conducted. As a result of the long times required for this system to approach equilibrium, and the probable metastability of hemicarboaluminate, measurement of solid solution solubilities at stoichiometric saturation should be investigated.

4.4. Conclusions

Five phase assemblages were observed in the hydroxide-carbonate series of the calcium aluminate hydrates: the OH end-member, hemicarboaluminate, monocarboaluminate and two miscibility gaps (OH end member with hemicarboaluminate; and hemicarboaluminate with monocarboaluminate). These are the same assemblages reported in previous studies (Roberts, 1969; Fischer and Kuzel, 1982; Pöllmann, 1986), but there are variations in the range of carbonate ratios over which the assemblages are observed to occur.

The miscibility gap between the OH end member and hemicarboaluminate was previously observed between carbonate ratios of 0.05 to 0.40. In the current study, the miscibility gap was observed between carbonate ratios of 0.1 and 0.5 in the experiment from supersaturation, but

over a much smaller range of 0.0 to 0.25 in the experiment from undersaturation. Hemicarboaluminate was the only solid solution phase observed at a ratio 0.5 in the experiment from supersaturation, with a small amount of hydrogarnet and portlandite as additional phases. However, after 16 months of reaction from undersaturation, the solids were dominated by hemicarboaluminate and monocarboaluminate, with a trace amount of hydrogarnet. In the experiment from undersaturation, hemicarboaluminate may be converting to a mixture of monocarboaluminate and hydrogarnet with time according to a reaction similar to the following:

$$Ca_4Al_2O_6(OH)\cdot 0.5CO_3\cdot 12H_2O = 0.5Ca_4Al_2O_6\cdot CO_3\cdot 11H_2O + 0.5Ca_3Al_2O_6(OH)\cdot 6H_2O + 0.5Ca^{2+} + OH^- + 2.5H_2O$$

The second miscibility gap was identified in previous studies between carbonate ratios of 0.6 and 0.8. The results from supersaturation in the current study were consistent with this range, but in the experiment from undersaturation, these two phases were observed over a wider range of compositions, from 0.4 to 0.7, and hydrogarnet was also present. This may indicate that the stable phase assemblage is a mixture of monocarboaluminate and hydrogarnet.

Monocarboaluminate, calcite and gibbsite were observed at a carbonate ratio of 1.0 in the experiment from undersaturation. The measured solution compositions were calculated to be just at saturation with respect to hydrogarnet. This suggests that there is no thermodynamic driving force for the conversion of monocarboaluminate to hydrogarnet, supporting the possibility that the observed phases are the equilibrium assemblage.

The occurrence of a miscibility gap between the OH end member and hemicarboaluminate is likely due to the difference in charge between the OH^- and CO_3^{2-} ions. The carbonate ions form strong bonds between the main and interlayers, which may increase the stability of this phase relative to the OH end member. The additional layer of water molecules present in the structure of the OH end member, but absent in hemicarboaluminate may also contribute to the formation of the miscibility gap. In the second miscibility gap between hemicarboaluminate and monocarboaluminate, the substitution of $2OH^-$ ions for each carbonate ions in the structure of monocarboaluminate increases the number of anions in the interlayer. Steric replusion between these ions may favor alignment of the carbonate groups perpendicular to the plane of the main layers (as in hemicarboaluminate), rather than tilted slightly from the plane ($\approx 20°$), as determined in the structure of monocarboaluminate (Renaudin et al., 1999).

The solution compositions and estimated solid phase compositions were used to calculate solubility products for the solids solution phases. Despite the uncertainties associated with these

calculations, these are useful as a first approximation, because no other solubility data is currently available for the solid solution phases as a function of composition. In the experiments from super- and undersaturation, several samples had log K_{sp} values that were two orders of magnitude lower than the remainder of the samples. These low values can be correlated to low solution concentrations of aluminum, which are likely controlled by hydrogarnet. These samples are likely closer to the final thermodynamic equilibrium condition for these series, whereas the higher log K_{sp} values measured in the majority of the samples are representative of metastable equilibrium with respect to the solid solution phase.

In the future, it may be possible to use solid-solution aqueous solution theory to make equilibrium predictions in the hydroxide-carbonate system by treating the system in two separate sections between 1) the OH end member and hemicarboaluminate and 2) hemicarboaluminate and monocarboaluminate. This approach was not attempted with the current data set, because of the uncertainties in the calculated solid phase compositions, and the paucity of solubility measurements. In the meantime, because the regions of solid solution are relatively restricted, it may be possible to adequately model this system by considering the OH-CO_3-calcium aluminate hydrate series as simple mixtures of one or two phases of the OH end member, hemicarboaluminate, and monocarboaluminate. In this case, the OH-end member and monocarboaluminate is considered an incompatible phase assemblage.

4.5 Recommendations

It may be possible to predict equilibrium partitioning of hydroxide and carbonate between the solid solution and aqueous solution phases in this system by treating it as two separate systems - one between the OH end member and hemicarboaluminate, and the other between hemicarboaluminate and monocarboaluminate. This would require the collection of sufficient solubility data for solid solutions with compositions between these three phases.

As observed for both the OH-Cl and Cl-CO_3 series of the monocalcium aluminate hydrates, long reaction times are required to approach thermodynamic equilibrium in this system. Therefore, an attempt to measure the solubility of the solid solution phases at stoichiometric saturation could be worthwhile.

4.6 References

Barret P., Bertrandie D. and Beau D. (1983). Calcium hydrocarboaluminate, carbonate, alumina gel and hydrated aluminates solubility diagram calculated in equilibrium with CO_{2g} and with Na^{+}_{aq} ions. *Cem. Concr. Res.*, **13**, 789-800.

Brownlow A. H. (1979). Geochemistry. Prentice-Hall Inc., N.J., 498 p.

Busenberg E. and Plummer L. N. (1989). Thermodynamics of magnesian calcite solid solutions at 25 °C and 1 atm total pressure. *Geochim. Cosmochim. Acta.*, 53, 1189-1208.

Carlson E. T. and Berman H. A. (1960). Some observations on the calcium aluminate carbonate hydrates. *J. Res. Nat. Bur. Std. - A. Phys. Chem.*, **64A**, pp. 333-341.

Damidot D., Stronach S., Kindness A., Atkins M. and Glasser F. P. (1994). Thermodynamic investigation of the $CaO-Al_2O_3-CaCO_3-H_2O$ closed system at 25 °C and the influence of Na_2O. *Cem. Concr. Res.*, **24**, 563-572.

Douglas B., McDaniel D., and Alexander J. (1994). Concepts and models of inorganic chemistry. John Wiley & Sons, Inc., 928p.

Fischer R. and Kuzel H. -J. (1982). Reinvestigation of the system $C_4A{\cdot}nH_2O-C_4A{\cdot}CO_2{\cdot}nH_2O$. *Cem. Concr. Res.*, **12**, 517-526.

Francois M., Renaudin G. and Evrard O. (1998). A cementitious compound with composition $3CaO{\cdot}Al_2O_3{\cdot}CaCO_3{\cdot}11H_2O$. *Acta Cryst.*, **C54**, 1214-1217.

Glasser F. P., Kindness A., and Stronach S. A. (1999). Stability and solubility relationships in Afm phases Part I. Chloride, sulphate and hydroxide. *Cem. Concr. Res.* **29**, 861-866.

Kuzel H.J. (1969). X-ray investigations of some complex calcium aluminate hydrates and related compounds. *Proc. 7th Int. Symp. Chem. Cem.*, Paris, France. 19-28.

Mascolo G. and Marroccoli M. (1986). A study on the reactivity of $C_4A.nH_2O$ with aqueous solutions. *Cem. Concr. Res.*, **16**, 679-684.

Newman S. P. and Jones W. (1999). Computer simulations of layered double hydroxides. *In* Advances in ion exchange for Industry and Research. (ed. Williams P. A. and Dyer A.). Special Publication. no. 239. Royal Society of Chemistry (Great Britain).

Passaglia E. and Sacerdoti M. (1988). Hydrocalumite from Montalto di Castro. Virterbo. Italy. *N. Jb. Miner. Mh.*, **10**. 454-461.

Pöllmann H. (1986) Solid solution of complex calcium aluminate hydrates containing Cl^-, OH^- and CO_3^{2-} anions. *Proc. 8th Int. Symp. Chem. Cem.*, Rio de Janeiro. Supplementary paper. **Vol. III**. 300-306.

Ramachandran V. S. and Zhang Chun-Mei (1986). Hydration kinetics and microstructural development in the $3CaO{\cdot}Al_2O_3$-$CaSO_4{\cdot}2H_2O$-$CaCO_3$-H_2O system. *Matériaux et Constructions*. **19**. 437-444.

Reardon E.J. (1990). An ion interaction model for the determination of chemical equilibria in cement/water systems. *Cem. Concr. Res.*, **20**. 175-192.

Renaudin G., Francois M., Evrard O. (1999). Order and disorder in the lamellar hydrated tetracalcium monocarboaluminate compound. *Cem. Concr. Res.*, **29**. 63-69

Roberts M. H. (1957). New calcium aluminate hydrates. *J. Appl. Chem.*, **7**. 543-546.

Roberts M. H. (1969). Supplementary paper II-29. Calcium aluminate hydrates and related basic salt solid solutions. *Proc. 5th Int. Symp. Chem. Cem.*, Toyko. **Vol. II**. 104-117.

Steinour H. H. (1951). Aqueous cementitious systems containing lime and alumina. *PCA Bull.*, **34**. 1-100.

Taylor H.F.W. (1997). Cement Chemistry (2nd edition). Academic Press 459p.

Wedepohl K. H. (ed.) (1969). *Handbook of Geochemistry*. Springer-Verlag. Berlin.

Wells L. S., Clarke W. F., and McMurdie H. F. (1943). Study of the system CaO-Al_2O_3-H_2O at temperatures of 21 ° and 90 °C. *J. Res. Nat. Bur. Std.*, **30**. 367-409.

Zhang M. (2000). Incorporation of oxyanionic B, Cr, Mo, and Se into hydrocalumite and ettringite: application to cementitious systems. Ph.D. thesis. University of Waterloo. Waterloo. Canada.

Chapter 5

Re-evaluation of End Member Solubilities: Friedel's Salt, Monocarboaluminate and OH-Hydrocalumite

5.1 Introduction

Values for the solubilities of the end members are required for modeling using solid-solution aqueous solution (SSAS) theory. The purpose of this study was to compile and evaluate the available solubility data in the literature for the chloride, carbonate and hydroxyl end members, and to compare these to the values measured in the current study (Chapters 2, 3 and 4), in order to establish an average solubility product for each end member.

Published solubility products (K_{sp}) from different studies can not be compared directly, because different methods are used to calculate the ion activity coefficients for the solution species. If solubility products from different studies are to be compared, the activity coefficients for the ions in solution must be calculated using a consistent method. The approach taken in the current study was to compile the solution composition data measured in the various studies. The calcium, aluminum (and where appropriate, chloride) concentrations were then input into the geochemical equilibrium models SIMUL (Reardon, 1990) and PHREEQC (Parkhurst and Apello, 1999), to solve for the ion activity coefficients for each reported solution composition. Using the solution concentrations of the ions and their calculated activity coefficients, solubility products are calculated and compared. An average solubility product is calculated for each end member based on the compiled data, and reported with the standard deviation. These average solubility products and associated uncertainties were then used to calculate the Gibbs free energy of formation for each end member.

5.2 The chloride end member: Friedel's salt

The solubility of Fridel's salt has been determined from supersaturation by Nacken and Mosebach, (1936) and Abate and Scheetz (1995), and from undersaturation by Goto et al. (1979), Zhang et al.(1981) and Birnin-Yauri and Glasser (1998). In the study conducted by

Nacken and Mosebach (1936), varying proportions of tricalcium aluminate ($3CaO\,Al_2O_3$) and $CaCl_2$ were added to water, and the solution composition and solid phase were examined after reaction times of between 18 and 35 days. The solid phases were identified using microscopic analysis. Abate and Scheetz (1995) determined the solubility of Friedel's salt at four invariant points in the system CaO-Al_2O_3-$CaCl_2$-H_2O: 1) Friedel's salt, gibbsite and $CaCl_2{\cdot}6H_2O$, 2) Friedel's salt, $CaO{\cdot}CaCl_2{\cdot}2H_2O$ and $CaCl_2{\cdot}6H_2O$, 3) Friedel's salt, hydrogarnet and portlandite, and 4) Friedel's salt, hydrogarnet and gibbsite. In the solubility experiments, portions of each solid were added to 25 ml of aqueous phase, in a quantity at least 10% in excess of each mineral's known solubility. The samples were continuously agitated at 22-25 °C for 10 days before filtration and subsequent solution analysis. Solid phase identification was performed using XRD analysis.

Zhang et al. (1981) determined the solubility of Friedel's salt from undersaturation, using Friedel's salt prepared from solutions of $Ca(OH)_2$ and $AlCl_3{\bullet}6H_2O$. To determine its solubility, Friedel's salt was added to water, and after an equilibration time of 3 days, the solution composition was determined and the solid phase was identified using XRD analysis. In the experiment performed by Birnin-Yauri and Glasser (1998), the solubility of Friedel's salt was determined by dispersing Friedel's salt in water at a water/solid ratio of 10. The slurries were reacted at 20 °C for one month before filtration. A small portion of the solid was analyzed using XRD analysis, while the remaining solid was re-dispersed in water and reacted for another month. Five successive dispersions were performed. Goto et al. (1979) prepared Friedel's salt by reacting $3CaO{\cdot}Al_2O_3{\cdot}6H_2O$ with a $CaCl_2$ solution at 80°C for 24 hours. The solubility of Friedel's salt was then measured from undersaturation by adding 0.5 g of Friedel's salt to 250 of water, and stirring in a reaction vessel controlled at 30 or 90°C. After 20 hours of reaction, the solution was sampled in an N_2 gas atmosphere, to prevent carbonation. The concentration of calcium in solution was measured, and assuming congruent dissolution, the $Al(OH)_4^-$ and Cl^- concentrations in solution were calculated. No solid phase identification was reported in this study.

The solution composition data from the solubility studies of Friedel's salt are recorded in Table 5.1. Experiment No. 1 from the study by Nacken and Mosebach (1936) was excluded because the final solid phase was identified as hydrogarnet, not Friedel's salt. The data for two of the invariant points from Abate and Scheetz (1995) have been included in this compilation (Friedel's salt-hydrogarnet-$Ca(OH)_2$ and Friedel's salt-hydrogarnet-$Al(OH)_3$), while the data for the other two invariant points were excluded, because ionic strengths of the solutions were two orders of magnitude higher than those in other solubility studies. The solution composition data

from Birnin-Yauri and Glasser (1998) are for five sequential dispersions of Friedel's salt in water. The solution compositions measured in the current study from supersaturation, undersaturation, and from the extended experiment are presented in Table 5.2.

5.3 The carbonate end member: Monocarboaluminate

Previous research on the solubility of monocarboaluminate has included measurements made from supersaturated conditions (Carlson and Berman, 1960), and from undersaturated conditions (Damidot et al., 1994; Zhang et al., 1981). The measured solution compositions from these studies are compiled in Table 5.3. The solution compositions measured from both super- and undersaturated conditions in the current study are compiled in Table 5.4.

Carlson and Berman (1960) prepared samples of monocarboaluminate by mixing solutions of calcium aluminate, calcium hydroxide, and sodium carbonate. The mixtures were allowed to stand for two months at temperatures between 25 and 30°C, before the precipitates were filtered, and the solution analyzed. The solids were dried over a saturated magnesium chloride solution (33% R. H.), and then examined using X-ray diffraction analysis.

Zhang et al. (1981) prepared monocarboaluminate by adding monocalcium aluminate and calcite to a portlandite-saturated solution. The solids were filtered, and X-ray diffraction analysis of the precipitates showed that the monocarboaluminate contained some $CaCO_3$. The solubility of the precipitate in aqueous solution at 25°C was then determined from undersaturation after 11 days of reaction.

Damidot et al. (1994) prepared monocarboaluminate using the method of Carlson and Berman (1960). The solubility of the solid from undersaturation was measured by re-dispersing the precipitate in water or sodium hydroxide solutions (0.5 mol/kg). After 180 days of equilibration at 25°C, the solutions were analyzed for pH, calcium, carbonate and aluminum. Using XRD analysis, the solid was identified as monocarboaluminate, with a small amount of calcite.

Authors	Expt.	Temp. (°C)	Ca (mmol/L)	Al (mmol/L)	Cl (mmol/L)	Time (days)	Phases Identified
Nacken & Mosebach (1936)	2	30	9.176	4.561	4.788	18	F, G
	3	30	9.068	4.563	4.640	18	F, G
	4	30	9.249	5.284	4.752	18	F, G
	5	30	9.478	4.225	7.224	18	F
	6	30	13.63	2.558	1.971	21	G, F
	7	30	13.04	2.574	1.770	21	F, G
	8	30	15.16	2.825	2.307	21	F, G
	9	30	17.02	1.954	2.8689	21	F
	10	30	17.76	2.166	2.861	21	F
	11	30	24.86	1.467	45.391	21	F
	12	30	31.11	1.193	58.279	21	F
	13	30	45.55	0.8160	87.49	35	F
	14	30	42.77	0.6120	83.71	35	F
	15	30	59.64	0.5178	114.3	18	F
	16	30	9.479	4.637	6.423	18	F
	17	30	9.644	4.708	7.259	18	F
Zhang et al. (1981)		25	3.870	1.20	1.33	3	F
Goto et al. (1979)		30	8.75			1	
		90	10.0			1	
Abate & Scheetz (1995)		22-25	19.1	0.15	0.84	10	P, F, G
		22-25	7.5	4.4	0.36	10	A, F, G
Birnin-Yauri and Glasser (1998)	1	20	9.17	4.40	6.03	180	F
	2	20	9.48	5.04	4.80	180	F
	3	20	9.11	4.89	4.89	180	F
	4	20	8.67	4.97	4.40	180	F
	5	20	8.73	5.07	4.49	180	F

Table 5.1: Solubility of Friedel's salt determined in experiments from supersaturation (Nacken and Mosebach, 1936; Abate and Scheetz, 1995) and from undersaturation (Goto et al., 1979; Zhang et al., 1981; Birnin-Yauri and Glasser, 1998). F = Friedel's salt ($3CaO{\cdot}Al_2O_3{\cdot}CaCl_2{\cdot}10H_2O$); G = hydrogarnet ($3CaO{\cdot}Al_2O_3{\cdot}6H_2O$), P = portlandite ($Ca(OH)_2$), A = $Al(OH)_3.xH_2O$.

Experiment	Replicate	Ca (mmol L)	Al (mmol L)	Cl (mmol L)	pH	Reaction Time (days)	Phases Identified
Supersaturation	A	13.94	1.58	18.47	11.70	170	F, A
	B	16.66	0.463	19.58	11.91	170	F
	C	13.21	1.68	15.21	11.76	170	F
Undersaturation	A	15.04	0.968	23.64	11.52	515	F
	B	14.65	1.60	18.95	11.69	515	---
	C	28.70	0.884	13.44	11.59	515	---
Extended	-25% A	30.19	0.474	56.42	11.50	172	F, P
	-25% B	30.69	0.526	58.38	11.58	172	---
	-50% A	52.15	0.048	99.67	11.76	172	F, P
	-50% B	55.89	0.048	103	11.97	172	---

Table 5.2 Solution compositions measured for Friedel's salt in the current study. The solid phases observed in the samples are labeled: F = Friedel's salt; P = portlandite ($Ca(OH)_2$). A solution:solid ratio of 20:1 was used in all samples.

5.4 The hydroxyl end member: OH-Hydrocalumite

The solubility data compiled from the literature for OH-hydrocalumite is presented in Table 5.5. Nikushchenko et al. (1973) was used as the reference for the solubility data from D'Ans and Eick (1953) and Jones and Roberts (1959). The solution compositions measured from both super- and undersaturated conditions in the current study are given in Table 5.6.

In the solubility experiments performed by Wells et al. (1943), equilibrium was approached from both super- and undersaturated conditions. In the experiments from supersaturation, OH-hydrocalumite was prepared by mixing a metastable monocalcium aluminate solution (containing up to 2.4 g/L Al_2O_3 and 1.4 g/L CaO) in various proportions with $Ca(OH)_2$ solutions of known concentration. The mixtures were sealed in flasks maintained at 21 ± 1 °C, and the mixtures were shaken periodically to facilitate an approach to equilibrium. In the experiments

from undersaturation, the solid phases were dispersed in $Ca(OH)_2$ solutions of different concentrations, and the changes in both the aqueous and solid phases were followed. The solids were identified based on their optical properties whenever possible, but many of the products could only be identified based on their X-ray diffraction patterns. Only solution compositions for precipitates where the molar ratio of CaO/Al_2O_3 in the initial solution was close to 4 (3.85 or above) have been included in the data compilation.

Lea (1956) report an apparent metastable invariant point for the di- and tetracalcium aluminate hydrates at 0.53 g/L CaO and 0.11 g/L Al_2O_3. This data is based on the point of intersection of the two metastable solubility curves for di- and tetracalcium aluminate on a stability diagram for the system $CaO-Al_2O_3-H_2O$ at 21-25 °C.

In the experiments performed by Zhang (2000), equilibrium was approached from supersaturated conditions. Monocalcium aluminate (2.0×10^{-3} mole) and freshly calcined CaO were added to doubly-deionized water, to give a final solution:solid ratio of 50:1. The samples were maintained at 25 ± 0.1 °C.

5.5 Calculation of solubility products (K_{sp})

Solubility products for the three end members are calculated according to the following dissolution reactions:

(1) Friedel's salt $3CaO \cdot Al_2O_3 \cdot CaCl_2 \cdot 10H_2O \rightarrow 4Ca^{2+} + 2Al(OH)_4^- + 2Cl^- + 4OH^- + 4H_2O$

(2) Monocarboaluminate $3CaO \cdot Al_2O_3 \cdot CaCO_3 \cdot 11H_2O \rightarrow 4Ca^{2+} + 2Al(OH)_4^- + CO_3^{2-} + 4OH^- + 5H_2O$

(3) OH-Hydrocalumite $3CaO \cdot Al_2O_3 \cdot Ca(OH)_2 \cdot 18H_2O \rightarrow 4Ca^{2+} + 2Al(OH)_4^- + 6OH^- + 12H_2O$

for which the solubility product expressions are given by:

(4) Friedel's salt $K_{sp} = [Ca^{2+}]^4[Al(OH)_4^-]^2[Cl^-]^2[OH^-]^4[H_2O]^4$

(5) Monocarboaluminate $K_{sp} = [Ca^{2+}]^4[Al(OH)_4^-]^2[CO_3^{2-}][OH^-]^4[H_2O]^5$

(6) OH-hydrocalumite $K_{sp} = [Ca^{2+}]^4[Al(OH)_4^-]^2[OH^-]^6[H_2O]^{12}$

where [ ] denotes activities. For each solution composition presented in Tables 5.1 through 5.6, ion activity coefficients were calculated using the geochemical equilibria models SIMUL (Reardon, 1990), and PHREEQC (Parkhurst and Apello, 1999). The measured ion solution concentrations and the calculated activity coefficients were then used to calculate solubility products for each of the end members, according to expressions 4, 5 and 6. The log K_{sp} values calculated based on the modeling results from SIMUL, for Friedel's salt, monocarboaluminate, and OH-hydrocalumite have been plotted versus the ion solution concentrations in Figures 5.1, 5.2, and 5.3, respectively.

Reference	Sample ID	Ca (mmol L)	Al (mmol L)	CO_3 (mmol L)	pH	Reaction Time (days)	Phases Identified
Carlson and Berman (1960)	1.1	6.90	0.137			60	M, G, C
	1.2	7.38	0.157			60	M, G, C
	1.3	5.19	0.137			60	M, C
	1.4	5.85	0.0981			60	M, C
Zhang et al. (1981)		2.11	1.27	0.674		11	M, C
Damidot et al. (1994)		2.72	1.39	0.90	11.30	180	M, C

Table 5.3: Published solution compositions measured for samples equilibrated with monocarboaluminate. The phases identified in the solids were M = monocarboaluminate ($3CaO{\cdot}Al_2O_3{\cdot}CaCO_3{\cdot}11H_2O$): G= hydrogarnet ($3CaO{\cdot}Al_2O_3{\cdot}6H_2O$): C = calcite ($CaCO_3$): A = gibbsite ($Al(OH)_3$).

Reference	Sample ID	Ca (mmol/L)	Al (mmol/L)	CO_3 (mmol/L)	pH	Reaction Time (days)	Phases Identified
Supersaturation	A	4.14	1.23	<0.061	11.72	170	M, C, A
	B	4.05	1.38	<0.061	11.73	170	M, C, A
	C	4.03	1.20	<0.061	11.72	170	M, C, A
Undersaturation	A	3.39	1.33	<0.061	11.78	515	M, C, A
	B	3.57	1.15	<0.061	11.77	515	---
	C	3.73	1.28	<0.061	11.76	515	---

Table 5.4: Measured compositions from the current study for solutions equilibrated with monocarboaluminate. The phases identified in the solids were M = monocarboaluminate ($3CaO{\cdot}Al_2O_3{\cdot}CaCO_3{\cdot}11H_2O$): C = calcite ($CaCO_3$): A = gibbsite ($Al(OH)_3$). A solution:solid ratio of 20:1 was used in both experiments.

Reference	Temp. (°C)	W/S ratio	Ca (mmol/L)	Al (mmol/L)	pH	Reaction Time (days)	Solid Phases
D'Ans and Eick (1953)*	20		11.8	1.28			T, A
	20		21.4	0.0651			T, P
	20		9.27	4.63			T
	20		10.9	1.86			T, D
Wells et al. (1943): Supersaturation	21		12.25	1.37		6	T, P
	21		13.05	0.824		6	
	21		14.50	0.549		8	
	21		15.51	0.490		8	
	21		16.30	0.373		8	
	21		18.40	0.235		8	
	21		18.67	0.235		39	
	21		20.19	0.118		8	
Undersaturation:	21	500:1	11.11	1.90		16	H
	21	500:1	12.55	0.824		16	H
	21	500:1	15.19	0.451		16	H
	21	500:1	18.15	0.294		16	H
	21	500:1	22.80	0.177		16	H
Lea (1956)	25		9.45	2.16			T, D
Jones and Roberts (1959)*	25		11.23	2.06			T, D
Zhang, (2000)	25	50:1	23.48	0.1207	12.16	383	G, P, H, T
	25	50:1	22.48	0.1444	12.64	479	G, P, H, T

Table 5.5: Published solution compositions equilibrated with OH-hydrocalumite (* from Nikushchenko et al.,1973). H = OH-hydrocalumite ($3CaO{\cdot}Al_2O_3{\cdot}Ca(OH)_2{\cdot}12H_2O$); T = highly hydrated OH-hydrocalumite ($3CaO{\cdot}Al_2O_3{\cdot}Ca(OH)_2{\cdot}18H_2O$); D = dicalcium aluminate ($2CaO{\cdot}Al_2O_3{\cdot}8H_2O$); G = hydrogarnet ($3CaO{\cdot}Al_2O_3{\cdot}6H_2O$), P = portlandite ($Ca(OH)_2$); A = $Al(OH)_3{\cdot}xH_2O$.

Experiment	Replicate	Ca (mmol L)	Al (mmol L)	pH	Reaction Time (days)	Phases Identified
Supersaturation	A	20.51	0.0325	12.48	170	G. P. H
	B	21.14	0.0156	12.51	170	H. G. P. T
	C	20.40	0.0180	12.47	170	H. P. G
Undersaturation	A	19.00	0.533	12.47	515	H. P. G
	B	21.16	<0.001	12.33	515	---
	C	13.27	<0.001	12.46	515	---

Table 5.6: Solution compositions for OH-hydrocalumite measured in the current study. A solution:solid ratio of 20:1 was used in both experiments. Solid phases are labelled: H = OH-hydrocalumite ($3CaO{\cdot}Al_2O_3{\cdot}Ca(OH)_2{\cdot}12H_2O$); G = hydrogarnet ($3CaO{\cdot}Al_2O_3{\cdot}6H_2O$). P = portlandite ($Ca(OH)_2$); A = gibbsite $Al(OH)_3.6H_2O$.

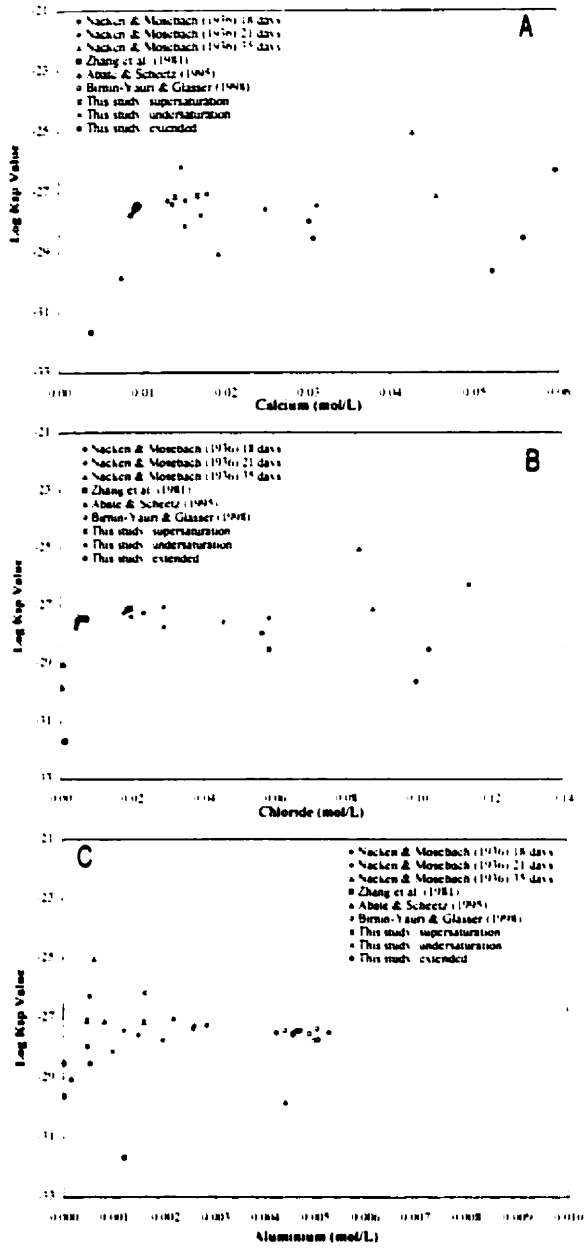


Figure 5.1: Calculated log K_{sp} values for Friedel's salt ($3CaO \cdot Al_2O_3 \cdot CaCl_2 \cdot 10H_2O$) versus the measured solution concentrations of a) calcium, b) chloride and c) aluminum. The dashed lines indicate one standard deviation from the mean in the average log K_{sp} calculated for the compiled data set. Log K_{sp} values were calculated based on modeling of solution compositions using SIMUL (Reardon, 1990).

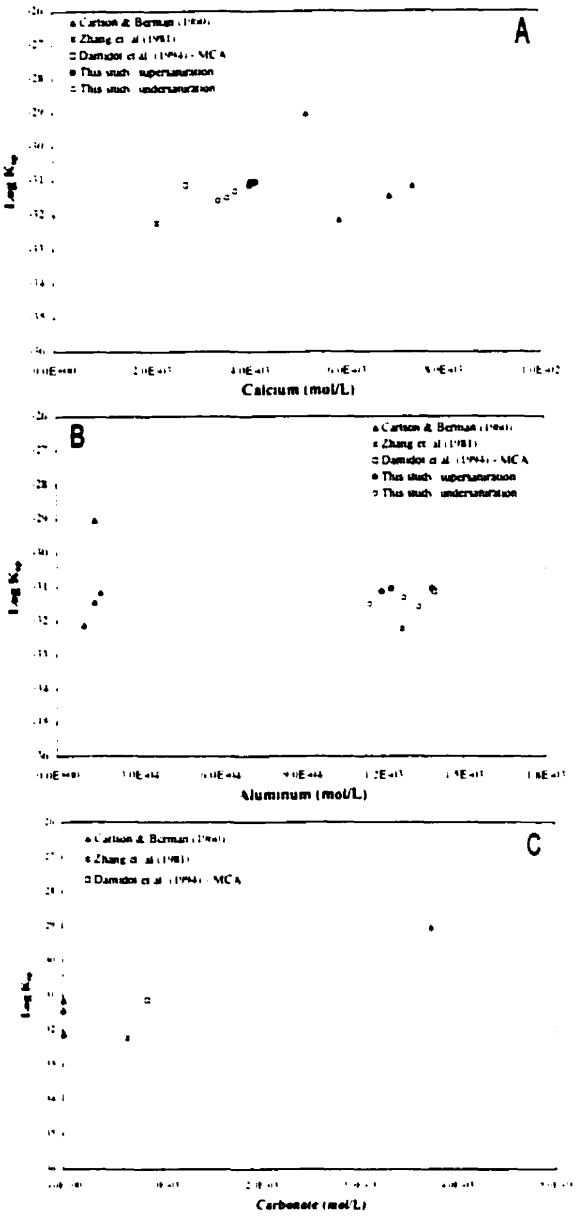


Figure 5.2: Calculated log K_{sp} for monocarboaluminate ($3CaO{\cdot}Al_2O_3{\cdot}CaCO_3{\cdot}11H_2O$) versus the measured solution concentrations of a) calcium, b) aluminum and c) carbonate. Dashed lines indicate one standard deviation from the mean for the average log K_{sp} of the compiled data set. The concentrations of carbonate for samples from the current study are not plotted, because they were below detection (<6.1 x 10^{-5} *m*). Log K_{sp} values were calculated based on modeling of solution compositions using SIMUL (Reardon, 1990).

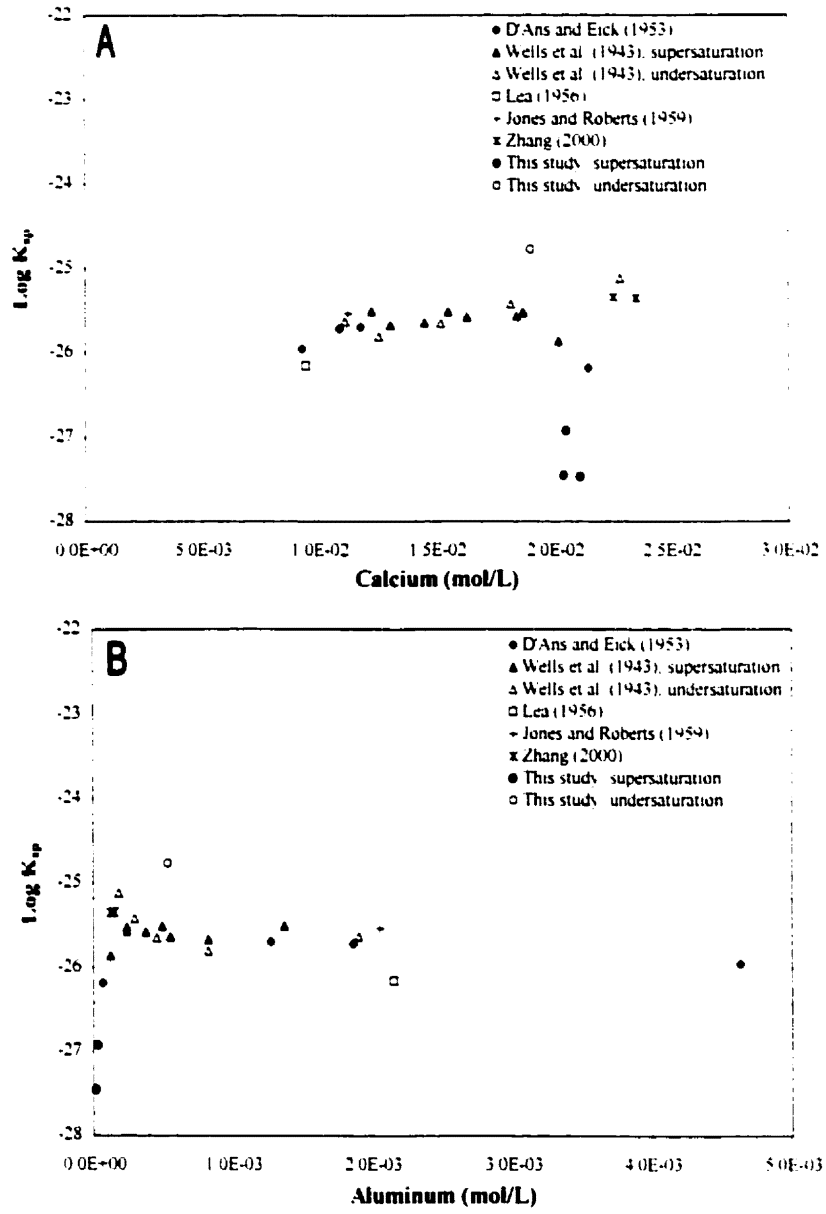


Figure 5.3: Calculated log K_{sp} for OH-hydrocalumite ($3CaO \cdot Al_2O_3 \cdot Ca(OH)_2 \cdot 12H_2O$) versus the measured solution concentrations of a) calcium, b) aluminum. The dashed lines indicate one standard deviation from the mean for the average log K_{sp} calculated for the compiled data set. Log K_{sp} values were calculated based on modeling of solution compositions using SIMUL (Reardon, 1990).

5.6 Discussion

5.6.1 Friedel's salt

Despite large differences in equilibration times used in the solubility studies (Tables 5.1 and 5.2), the calculated solubility products for Friedel's salt are similar. This suggests that equilibrium was closely reached in all experiments, even in the 18 day experiment of Nacken and Mosebach (1936).

In calculating the average log K_{sp} for the data sets, several data points were not included. The solubility data of Goto et al. (1979) was not included, because only the calcium concentrations in solution were actually measured in this study. The K_{sp} calculated using the data of Zhang et al. (1981) is almost four orders of magnitude lower than the solubility products calculated using data from the other studies. Zhang et al. (1981) reported that the precipitation of Friedel's salt was performed quickly, and that the precipitate was stored over a decarbonating agent to reduce contamination by atmospheric CO_2. However, it seems probable that some contamination of the precipitate occurred. On this basis, this data point has been excluded from the calculation of an average log K_{sp} for Friedel's salt.

The remaining solubility products calculated from the experimental data of Nacken and Mosebach (1936), Abate and Sheetz (1995), Birnin-Yauri and Glasser (1998), and from the current study (Table 5.2) give mean log K_{sp} values for Friedel's salt of -27.57 ± 0.86 (SIMUL) and -27.67 ± 0.82 (PHREEQC).The uncertainty given in these values is one standard deviation from the mean.

An examination of the log K_{sp} values versus the measured concentrations of calcium, aluminum, or chloride in solution plotted in Figure 5.1 reveals no obvious trends in the log K_{sp} values as a function of ion concentration. To test this conclusion, correlation coefficients (r) were calculated between each of the ion concentrations and the calculated log K_{sp} values, using the complete data set (Tables 5.1 and 5.2). Student *t*-tests were then performed to determine if the correlation between the calculated log K_{sp} values and the concentrations of calcium, aluminum or chloride are significantly different from zero. The results of the t-tests indicate that the correlation between the concentrations of calcium, aluminum or chloride and the log K_{sp} values is not significantly different from zero at the 97.5% confidence level (degrees of freedom (df) = 30).

5.6.2 Monocarboaluminate

Despite the large variation in the equilibration times used in the solubility experiments, there is excellent agreement between the calculated log K_{sp} values (Figure 5.2) for monocarbo-aluminate. This suggests that equilibrium was likely reached with respect to this phase in all the experiments, including the experiment of Zhang et al. (1981), which had the shortest equilibration time (11 days).

Using all the available data from previous research (Table 5.3) and from the current study (Table 5.4), average log solubility products for monocarboaluminate of -31.23 ± 0.80 (SIMUL) and -31.57 ± 0.49 (PHREEQC) are calculated. The uncertainty given for these values is one standard deviation from the mean.

The calculated log K_{sp} value for sample 1.3 from Carlson and Berman (1960) was -29.02, with a deviation from the mean that was almost 5 times higher than for the log K_{sp} values from the other experiments. If this value is omitted, an average log K_{sp} value of -31.35 ± 0.30 (SIMUL) is calculated, slightly lowering the average solubility product, and significantly reducing the standard deviation in the mean value. However, a careful review of the experimental procedures and results from Carlson and Berman (1960) revealed no experimental basis for omitting this point from the data set. Therefore, use of the average solubility product for the complete data set (31.23 ± 0.80) is recommended.

In Figure 5.2, no obvious trends in the K_{sp} values as a function of ion concentration are observed. Using the complete data set (Tables 5.3 and 5.4), correlation coefficients (r) were calculated between the concentrations of calcium or aluminum and the calculated log K_{sp} values. Student *t*-tests were then performed to determine if the correlation between the calculated log K_{sp} values and the ion concentrations are significantly different from zero. The results of the t-tests indicate that the correlation between the measured solution concentrations of calcium or aluminum and the log K_{sp} values is not significantly different from zero at the 97.5% confidence level (df =10). It was not possible to test for a correlation with solution concentrations of carbonate, because these were below detection in most of the reported solubility experiments.

5.6.3 OH-hydrocalumite

The solubility products calculated for OH-hydrocalumite from the solution compositions reported in the literature (Table 5.5) are in good agreement, despite the variation in the equilibration times used in these studies, from 6 days to 480 days. Of the data collected in the current study (Table 5.6), the log K_{sp} for the A-replicate sample (-24.78) from undersaturation is most similar to the log K_{sp} values calculated for the data compiled from the literature.

Using the solution compositions listed in Tables 5.5 And 5.6, average log K_{sp} values for OH-hydrocalumite of -25.80 ± 0.62 (SIMUL) and -25.72 ± 0.62 (PHREEQC) have been calculated. The uncertainty given is one standard deviation from the mean. In calculating this average solubility product, the B and C replicates measured from undersaturation in the current study (Table 5.6) have been omitted. These two samples do not have measured aluminum concentrations, because Al was below detection in these samples (Chapter 2, Section 2.4.1). Therefore, calculated log K_{sp} values are dependant on the estimate made for the Al concentrations.

There are no apparent trends in the calculated log solubility products as a function of calcium or aluminum concentrations for the overall data set (Figure 5.3). Correlation coefficients were calculated for calcium or aluminum and the log $_{Ksp}$ values. Student t-tests were then used to determine if the correlation was significantly different from zero. The results of these tests indicate that at the 97.5% confidence level, the correlation between the ion concentrations and the calculated log K_{sp} values is not significantly different from zero (df = 24).

The solubility products calculated for the A, B and C replicates from supersaturation, and the A and B replicates from undersaturation are approximately two orders magnitude lower than the average log K_{sp} value calculated for the overall data set. Comparison to the data of Zhang (2000) shows that the most significant difference between the solution compositions from the two studies is the Al concentration measured in solution. The lower aluminum concentrations in solution in the current study may reflect the progress of the reaction. OH-hydrocalumite is a metastable phase which converts to hydrogarnet with time (Wells et al., 1943; Roberts, 1957), according to the following reaction:

$$3CaO{\cdot}Al_2O_3{\cdot}Ca(OH)_2{\cdot}18H_2O_{(s)} = 3CaO{\cdot}Al_2O_3{\cdot}6H_2O_{(s)} + Ca(OH)_{2(s)} + 12H_2O_{(aq)}$$

Although OH-hydrocalumite is metastable, it has been observed to persist over long time periods (Wells et al., 1943; Jones, 1960; Taylor, 1961; Turriziani, 1964; Zhang 2000). This

implies that even after extended reaction periods (over a year and a half), the system has not reached equilibrium. An examination of the solution composition data for the samples with low aluminum concentrations in the current study showed that these samples are close to equilibrium with respect to hydrogarnet (Chapter 2, section 2.3.2), and suggests that the Al concentrations in these samples may be controlled by this phase. It seems probable that the measured solution compositions reported in the literature, and the A replicate from undersaturation in this study are representative of a metastable equilibrium with respect to OH-hydrocalumite, and therefore, reflect the solubility of this phase. In the other replicates measured in the current study, the aluminum concentrations may be controlled by hydrogarnet, and therefore, may be approaching the final equilibrium state for this system.

5.6.4 Effect of solution:solid ratio

In reactions of aqueous solutions with "pure" single-component solids, the resulting solution compositions are usually independent of the solution/solid ratio. This is not true for solid-solution phases, which often recrystallize to different compositions with changes in the solution/solid ratio (Glynn et al., 1990). In general, the solubility of solid-solution phases decreases as the solution:solid ratio increases (Glynn et al., 1990). Friedel's salt, monocarboaluminate, and OH-hydrocalumite all form solid solutions, and therefore, the solubilities measured for these phases may depend on the solution:solid ratio used. However, for the majority of the solubility studies compiled from the literature, the solution:solid ratio used in the experiments is not reported. As a result, it is currently not possible to evaluate the actual effect of the solution:solid ratio on the log K_{sp} values calculated for each of the end members. Further research would be required to investigate the effect of solution:solid ratio on the measured solubilities of the various calcium aluminate hydrate phases.

5.6.5 Gibbs free energy

The Gibbs free energy of formation ($\Delta G^\circ_{f,\,298}$) of the chloride, hydroxyl and carbonate end members were calculated using the average solubility products for each end member calculated using both SIMUL and PHREEQC, and the thermodynamic data base for the constituent ions assembled in SIMUL by Reardon (1990, 1992). The uncertainties in the free energies were determined from the uncertainties in the K_{sp} values. The results are given in Table 5.7.

End member	SIMUL		PHREEQC	
	Average log K_{sp} value	($\Delta G^\circ_{f,298}$) (kJ/mol)	Average log K_{sp} value	($\Delta G^\circ_{f,298}$) (kJ/mol)
Friedel's salt (Cl end member)	-27.57 ± 0.86	-6822.51 ± 4.92	-27.67 ± 0.82	-6823.10 ± 4.69
OH-hydrocalumite (OH end member)	-25.80 ± 0.62	-8761.59 ± 3.54	-25.72 ± 0.62	-8761.13 ± 3.54
Monocarboaluminate (CO_3 end member)	-31.23 ± 0.80	-7345.89 ± 1.09	-31.57 ± 0.49	-7347.86 ± 2.79

Table 5.7: Gibbs free energies calculated from the average solubility products for the OH, Cl and CO_3 end members. The uncertainty in these values was calculated using the uncertainity (1 standard deviation from the mean) given for the solubility products.

5.7 Conclusions

The average solubility products for Friedel's salt, monocarboaluminate, and OH-hydrocalumite are -27.57 ± 0.86, -31.23 ± 0.80, and -25.80 ± 0.62, respectively (based on modelling using SIMUL). The uncertainty given for these values is one standard deviation from the mean. Using these average K_{sp} values, Gibbs free energies of formation ($\Delta G^\circ_{f,298}$) for Friedel's salt, monocarboaluminate and OH-hydrocalumite are -6822.51± 4.92, -7345.89 ± 1.09, and -8761.59 ± 3.54 kJ/mol, respectively. These free energy of formation values for the end members are consistent with those calculated based on the solubility products determined using PHREEQC (-6823.10± 4.69, -7347.86 ± 2.79, and -8761.13 ± 3.54 kJ/mol for Friedel's salt, monocarboaluminate and OH-hydrocalumite, respectively).

There are no apparent trends in the calculated log K_{sp} values for Friedel's salt, monocarboaluminate, or OH-hydrocalumite when plotted versus the solution concentrations of calcium, aluminum, and chloride (for Friedel's salt). Student t-tests indicate that at the 97.5% confidence level, there is no significant correlation between the calculated log K_{sp} values and the measured solution concentrations of the ions for any of the end members in the compiled data sets.

The solubility products measured from super- and undersaturation in the current study for both Friedel's salt and monocarboaluminate are in good agreement with those reported in the

literature. The solubility product calculated for OH-hydrocalumite using the solution composition data measured in the A replicate from undersaturation in the current study is within the standard deviation of the average log K_{sp} calculated for OH-hydrocalumite. However, the log K_{sp} values calculated from the other replicates are two orders of magnitude smaller. The main difference in the measured solution compositions for these replicates is lower Al concentrations, which are likely controlled by hydrogarnet. It seems probable that the measured solution compositions reported in the literature, and the A replicate from undersaturation in this study are representative of a metastable equilibrium with respect to OH-hydrocalumite, and therefore, reflect the solubility of this phase. In the other three replicates measured in the current study, the aluminum concentrations may be controlled by hydrogarnet, and therefore, may be approaching the final equilibrium state for this system.

In the majority of the solubility studies compiled and discussed, no solution:solid ratio was given for the experiments. For this reason, it is not possible to evaluate the effect of the solution:solid ratio on the calculated log K_{sp} values. However, because all three of the end member phase examined form solid solutions, their solubilities may change depending on the solution:solid ratio. This may account for some of the deviation in the calculated log K_{sp} values for the samples.

5.8 Recommendations

All three of the end members examined in this study form solid solutions, and consequently, their solubilities may change depending on the solution:solid ratio used in these measurements. Therefore, experiments to evaluate the influence of solution:solid ratio on the solubilities of Friedel's salt, monocarboaluminate, and the OH end member (i.e. OH-hydrocalumite) are recommended.

5.9 References

Abate C. and Scheetz B.E. (1995). Aqueous phase equilibria in the system $CaO-Al_2O_3-CaCl_2-H_2O$: The significance and stability of Friedel's salt. *J. Am. Ceram. Soc.*, **78**, 939-944.

Birnin-Yauri U. A. and Glasser F. P. (1998). Friedel's salt, $Ca_2Al(OH)_6(Cl,OH)\cdot 2H_2O$: Its solid solutions and their role in chloride binding. *Cem. Concr. Res.*, **28**, 1713-1723.

Carlson E. T. and Berman H. A. (1960). Some observations on the calcium aluminate carbonate hydrates. *Journal of Research, of the National Bureau of Standards - A. Physics and Chemistry*, **64A**, pp. 333-341.

Damidot D., Stronach S., Kindness A., Atkins M. and Glasser F. P. (1994). Thermodynamic investigation of the system $CaO-Al_2O_3-CaCO_3$ closed system at 25 °C and the influence of Na_2O. *Cem. Concr. Res.*, **24**, pp. 563-572.

D'Ans J. and Eick H. (1953). Zement-Kalk-Gips, **6**, 197.

Glynn P. D., Reardon E. J., Plummer L. N. and Busenberg E. (1990). Reaction paths and equilibrium end-points in solid-solution aqueous-solution systems. *Geochim. Cosmochim. Acta.*, **54**, pp.267-282.

Goto S., Tsunetani M. and Kondo R. (1979). Free energy of formation of $3CaO\cdot Al_2O_3\cdot CaCl_2\cdot 12H_2O$ in connection with the durability of hardened cement immersed in sea water. *Ann. Chem. Fr.*, **4**, pp. 425-429.

Jones F. E. (1960). Hydration of calcium aluminates and ferrites. *Proc. 4th Int. Symp. Chem. Cem.*, **I**, Washington, pp. 205-246.

Jones F. E. and Roberts M. H. (1959). DSIR Building Research Station, No. E965, HMSO, London.

Lea F. M. (1956). The chemistry of cement and concrete. Edward Arnold (Publishers) Ltd., London, 637 p.

Nacken Von R. and Mosebach R. (1936). Untersuchungen an den vierstoffsystemen $CaO-Al_2O_3-CaCl_2-H_2O$ und $CaO-SiO_2-CaCl_2-H_2O$. *Z. anorg. und allg. Chem.*, **228**. 19-27.

Nikushchenko V. M., Khotimchenko V. S., Rumyantsev P. F. and Kalinin A. I. (1973). Determination of the standard free energies of formation of calcium hydroaluminates. *Cem. Concr. Res.*, **3**. pp. 625-632.

Parkhurst D. L. and Apello C. A. J. (1999). User's guide to PHREEQC (Version 2)-- A computer program for speciation, batch-reaction, one-dimensional transport, and inverse geochemical calculations. U.S. Department of the Interior, U.S. Geological Survey. Water-Resources Investigations Report 99-4259.

Reardon E.J. (1990). An ion interaction model for the determination of chemical equilibria in cement/water systems. *Cem. Concr. Res.*, **20**. 175-192.

Reardon E. J. (1992). Problems and approaches to the prediction of the chemical composition in cement/water systems. *Waste Management*, **12**. 221-239.

Roberts M. H. (1957). Calcium aluminate hydrates and related basic salt solid solutions. *Proc. 5th Int. Symp. Chem. Cem.*, **II**. Tokyo, pp. 104-117.

Taylor H. F. W. (1961). The chemistry of cement hydration. Progress in Ceramic Science, 1. pp.89-145.

Turriziniani R. (1964). The calcium aluminate hydrates and related compounds. *In:* The Chemistry of Cements, Vol. 1, Academic Press, London. pp. 233-286.

Wells L. S., Clarke W. F., and McMurdie H. F. (1943). Study of the system $CaO-Al_2O_3-H_2O$ at temperatures of 21° and 90 °C. *Journal of Research of the National Bureau of Standards*, **30**, pp. 367-409.

Zhang F., Zhou Z., and Lou Z. (1981). Solubility product and stability of ettringite. *Proc. 7th Int. Symp. Chem. Cem.*, Paris, **2**: 88-93.

Zhang M. (2000). Incorporation of oxyanions B, Cr, Mo, and Se into hydrocalumite and ettringite: application to cementitious systems. Ph.D. Thesis, University of Waterloo, Waterloo, Canada.

Chapter 6

Ion exchange reactions in the system $CaO-Al_2O_3-CaCl_2-Ca(OH)_2-CaCO_3-H_2O$

6.1 Introduction

During the early stages of Portland cement hydration, the interlayer of the calcium aluminate hydrate phases (AFm and AFt) are dominated by OH^- and SO_4^{2-} ions. However, with time, these ions may be exchanged for chloride, carbonate or additional sulphate ions (Glasser et al., 1999). Consequently, exchange reactions between the hydroxyl end member of the AFm phases ($3CaO{\cdot}Al_2O_3{\cdot}Ca(OH)_2{\cdot}18H_2O$) and other anions are of fundamental importance in concrete research. Exchange of OH^- ions by Cl^- to form Friedel's salt ($3CaO{\cdot}Al_2O_3{\cdot}CaCl_2{\cdot}10H_2O$) is of particular interest, because this is the chloride-bearing phase most often identified in hydrated cement pastes and concrete, and is likely the dominant mineralogical control on Cl^- concentrations in cement-based materials.

Carbonate ions are reported to be highly preferred in the calcium aluminate hydrates (Glasser et al., 1999; Taylor, 1997), and the presence of CO_2 in the atmosphere ensures that most cement materials will be in contact with a potential source of carbonate (Damidot et al., 1994). Preferential incorporation of carbonate ions into Friedel's salt could result in the release of Cl^- to the pore solutions in cement and ultimately, to the environment. This has important implications to the disposal of irradiated concrete containing radioactive ^{36}Cl, which is likely incorporated into Friedel's salt. The exchange of its Cl^- ions by carbonate ions due to interaction with groundwater, for example, could lead to the release of ^{36}Cl to the environment. Information on the extent of exchange between these two ions is therefore necessary to quantify potential releases. The exchange of Cl^- ions by carbonate also has important implications to concrete engineering. The concentration of Cl^- in pore solution has been identified as a key factor in the corrosion of reinforcing bar. As carbonate is exchanged into Friedel's salt, chloride is released into the pore solution, increasing its concentration.

The exchange of OH^- ions in the OH end member by chloride was investigated by Mascolo and Marroccoli (1986). In this study, the OH end member was prepared by reacting CaO, alumina

gel and water at 18-22°C for 10 days. The reaction product was filtered under CO_2-free conditions, dried by evacuation, and identified as $3CaO{\cdot}Al_2O_3{\cdot}Ca(OH)_2{\cdot}12H_2O$ with 8% $Ca(OH)_2$ using X-ray diffraction analysis. Exchange experiments were performed by placing the OH end member into a 1 *m* salt solution. After 1 day of reaction, the solids were filtered, dried over silica gel, and then characterized by powder XRD analysis. Reaction of the OH end member with NaCl resulted in the formation of the Cl-exchanged calcium aluminate (Friedel's salt) with a basal spacing of 7.85 Å, calcite and gibbsite. The presence of calcite indicates contamination by atmospheric CO_2 during the ion exchange reaction.

No previous studies examining the exchange of Cl^- ions in Friedel's salt by CO_3^{2-} ions were found. However, Mascolo and Marroccoli (1986) and Fischer and Kuzel (1982) investigated the exchange of hydroxyl ions in the OH end member by carbonate ions. Mascolo and Marroccoli (1986) found that when the OH end member was reacted in Na_2CO_3 solutions with concentrations between 0.05 and 1.0 *m*, the calcium aluminate phase was decomposed into a mixture of calcite ($CaCO_3$) and gibbsite ($Al(OH)_3$). In 0.01 *m* solutions, monocarbo-aluminate with a basal spacing of 7.70 Å was formed. These results suggest that different phases may be stable, depending on the solution carbonate concentration.

In the experiment by Fisher and Kuzel (1982), a suspension containing $3CaO{\cdot}Al_2O_3{\cdot}Ca(OH)_2{\cdot}18H_2O$ crystals was exposed to atmospheric CO_2. Examination of the crystals using optical microscopy showed that this exposure resulted in immediate carbonation of the rim zone of the crystals to hemicarboaluminate ($3CaO{\cdot}Al_2O_3{\cdot}0.5CaCO_3{\cdot}0.5Ca(OH)_2{\cdot}12H_2O$), while the bulk of the crystals remained unaffected. The XRD patterns of the crystals showed the presence of hemicarboaluminate and the OH end member simultaneously. The authors suggest that once the rim of carbonated material had formed, it created a barrier which severely retarded the penetration of carbonate ions into the crystals. Attempts to further carbonate the hydrocalumite by treating the crystals for 2 days in a CO_2 suspension, did not further the anion exchange. Instead, the hydrocalumite crystals were partly converted to calcite ($CaCO_3$) and gibbsite ($Al(OH)_3$), in agreement with the results of Mascolo and Marroccoli (1986).

Previous studies exploring exchange reactions between ions in the calcium aluminate hydrates (e.g. Mascolo and Marroccoli, 1986; Fischer and Kuzel, 1982), have focused on the resultant phase assemblages. The time required for exchange and the extent of exchange has not been previously quantified for these reactions. In the current study, the exchange of hydroxyl ions by Cl^- ions (as NaCl) has been investigated as a function of time and concentration. The partitioning of OH^- and Cl^- ions between the solid and aqueous phases measured in the OH-Cl

exchange experiment with concentration are compared to those measured in the solubility experiments conducted between the OH and Cl end members from both super- and undersaturation. This is the first time that data collected using these two different approaches has been compared. The reversibility of this reaction was also investigated by examining the exchange of Cl^- ions in Friedel's salt by hydroxyl ions as a function of time. Experiments were also performed to quantify the exchange of Cl^- ions in Friedel's salt by carbonate ions with time, and the results of experiments using Na_2CO_3 and $CaCO_3$ as sources of carbonate ions are compared.

6.2 Experimental

6.2.1 Materials

The materials are described in Chapter 2, section 2.2.1.

6.2.2 Experimental procedures

6.2.2.1 Formation of the OH and Cl end members

Batch experiments were used to study the formation of the OH and Cl end members as a function of time. The purpose of these experiments was to determine the length of time required for the end members to form. Equations 6.1 and 6.2 are the formation reactions used to prepare the OH and Cl end members, respectively.

$$CaO{\cdot}Al_2O_3 + 3CaO + 19H_2O \rightarrow 3CaO{\cdot}Al_2O_3{\cdot}Ca(OH)_2{\cdot}18H_2O \quad (6.1)$$

$$CaO{\cdot}Al_2O_3 + 2CaO + CaCl_2 + 10H_2O \rightarrow 3CaO{\cdot}Al_2O_3{\cdot}CaCl_2{\cdot}10H_2O \quad (6.2)$$

To prepare the solids, 4.95 mmol of monocalcium aluminate and stoichiometric quantities of CaO were weighed into a high density polyethylene bottle. The bottles were transferred into a CO_2 free glove box, and 55 ml of doubly-distilled water or 0.09 *m* $CaCl_2$ were added to the samples to prepare the hydroxyl and Cl end members, respectively. The final solution:solid ratio was approximately 20:1. Separate samples were prepared for each sampling time. The bottles were then sealed, removed from the glove box, and placed on a rotating wheel in a 25 °C

constant temperature bath. After a specified reaction time, the sample bottle was removed from the bath, and transferred into the glove box. The bottle was shaken, and 1 ml of slurry was removed using a glass Pasteur pipette and placed onto a glass slide for X-ray diffraction (XRD) analysis. The remainder was filtered through a 0.45 μm cellulose acetate filter paper using a Buchner funnel, a vacuum flask and an aspirator. The recovered solid was transferred into a scintillation vial, and the filtered solution was split for analysis for cations, anions and for pH measurements. The cation samples were acidified using 3 drops of 1:1 nitric acid. The glass slides prepared for XRD analysis and the recovered solids were stored in a desiccator over a saturated $CaCl_2 \cdot 6H_2O$ solution (relative humidity = 37%) for 7 days before XRD analysis was performed. The desiccator was stored in the glove box during this time to minimize CO_2 contamination.

6.2.2.2 Exchange reactions as a function of time

Five different ion exchange experiments were carried out in which ion exchange was monitored as a function of time. The experimental parameters used in these experiments are outlined in Table 6.1. The solution analyses performed, and the solids for which XRD patterns were measured are also indicated.

Expt. #	Starting solid (before exchange)	Formation time (days)	Spike	Range of sampling times (days)	Solution Analyses	XRD patterns
1	OH end member	9	NaCl	0.01 to 19	pH, Cl	None
2	OH end member	7	NaCl	0.13 to 27	pH, Cond., Cl, Ca, Al, Na	648h
3	Cl end member	7	10 mol/L NaOH	0.04 to 127	Cl, pH	12h, 3072h
4	Cl end member	> 34	Na_2CO_3	0.04 to 55	pH, Cl, CO_3	1, 55d
5	Cl end member	340	$CaCO_3$	0.13 to 21	pH, Cl, Al, Ca	1, 7, 21d

Table 6.1: Experimental parameters used in the ion exchange experiments performed as a function of time. After the time allotted for formation of the end member (second column), the samples were spiked, and then sampled after the specified reaction time.

Replicate samples of either the OH or the Cl end member were prepared as outlined in the previous section (6.2.2.1) for each sampling time. After a minimum formation time of 7 days, the sample bottles were transferred to the glovebox, and a weighed quantity of solid reagent grade NaCl, Na_2CO_3, or $CaCO_3$ was added. The only exception was the Cl-OH exchange experiment, in which samples were spiked with 1.1 ml of a 10 mol/L NaOH solution. The sample bottles were resealed, transferred out of the glove box, and placed on a rotating wheel in a 25 °C constant temperature bath. After the specified reaction times, sampling was performed according to the procedure outlined in section 6.2.2.1.

Based on the formula of the OH end member ($3CaO{\cdot}Al_2O_3{\cdot}Ca(OH)_2{\cdot}18H_2O$), the number of moles of OH in the interlayer of the solid (the amount theoretically available for exchange) is equivalent to the moles of aluminum. In experiments where the final Al concentration in solution was measured, the moles of Al in the final solid were determined by mass balance of the Al originally added. If Al concentrations were not measured, the Al in the final solid was estimated by assuming the quantity of Al in solution was negligible. This is a reasonable assumption, because measured solution concentrations of Al constituted a maximum of 0.2% of the total Al added to the samples.

The number of moles of chloride in the solid was determined by mass balance of the quantity remaining in solution after exchange and the total number of moles added in the NaCl spike. The fraction of chloride exchanged into the OH end member was calculated by dividing the number of moles of Cl in the solid by the total number of moles of OH available for exchange. In experiments 4 and 5, where the exchange of Cl^- ions in Friedel's salt by carbonate ions was investigated, the amount of Cl released into the solution from the solid was used as a measure of the degree of completion of the exchange reaction.

6.2.2.3 Exchange reactions as a function of concentration

Two experiments were performed investigating the exchange of hydroxyl ions in the OH end member by Cl^- ions. The procedure outlined in section 6.2.2.1 was used to prepare replicate samples of the OH end member. After reaction times of 6 or 8 days, the samples were spiked with a weighed quantity of NaCl, resealed, and placed in the constant temperature bath at 25 °C. After a reaction time of 9 or 10 days, sampling was performed according to the procedures outlined in section 6.2.2.1.

The experimental parameters for the two experiments performed as a function of concentration are presented in Table 6.2. In the first experiment, 11 samples were prepared with enough NaCl to exchange between 0 and 100 % of the OH^- ions originally present in the interlayer of the OH end member. In the second experiment, 8 samples were prepared. In this experiment, the quantities of NaCl added varied between 100% (1x) and 20 times (20x) the OH^- ions theoretically available for exchange in the interlayer.

Expt. #	Starting solid (before exchange)	Fraction Cl or Factor	Formation time (days)	Spike	Reaction time (days)	Solution Analyses	XRD
6	OH end member	0, 0.1, 0.2, 0.3, 0.4, 0.5, 0.6, 0.7, 0.8, 0.9, and 1.0	6	NaCl	10	pH, Cl, Ca, Al, Na	All
7	OH end member	1, 2, 4, 6, 8, 10, 15, and 20 times	8	NaCl	9	pH, Cl, Ca, Al and Na	1, 2, 8 and 20X

Table 6.2: Experimental parameters used in experiments examining the exchange of hydroxyl ions in the OH end member by Cl^- ions as a function of increasing chloride concentrations.

As described in section 6.2.2.2, the moles of OH in the interlayer of the solid before exchange is equivalent to the moles of Al in the solid. In these experiments, the moles of Al in the solid were estimated as the total number of moles of Al added as monocalcium aluminate, assuming that the moles of Al in solution is negligible. This is a reasonable assumption, because based on the maximum Al concentration measured in solution at the end of the exchange experiments, a maximum of 0.5% of the total aluminum added remained in solution.

The extent of the reaction was determined by measuring the chloride remaining in solution at the end of the experiment. The mole fraction of chloride in the solid was calculated by subtracting the moles of chloride measured in solution after exchange, from the moles of chloride originally added (as NaCl). The mole fraction of chloride available for exchange was calculated by dividing the moles of chloride added by the number of moles of OH originally in the solid.

6.2.3 Analytical methods

The pH of samples was measured using a Fisher Scientific Accumet® 50 pH meter with an Orion Ross® combination electrode calibrated against NBS pH buffer 7.01 and a 0.01 *m* boric acid solution with a pH of 9.18 at 25 °C. Solutions were analyzed for chloride colorimetrically using the mercuric thiocyanate method (automated) with a detection limit of 0.2 mg/L. Calcium, aluminum and sodium were analyzed using a Jarerell-Ash Inductively Coupled Plasma (ICP) spectrophotometer. The analytical uncertainty in the measured concentrations of all ions was better than ±5%.

The dissolved inorganic carbon (DIC) of the samples was determined using a method adapted from Barker and Chatten (1982). In this method, the addition of acid to solutions converts dissolved CO_3^{2-} and HCO_3^- ions to $CO_{2\,(aq)}$, which partitions into the gas phase as described by Henry's law. The headspace is then analyzed for CO_2. All blanks, standards and samples were prepared in 50 ml glass syringes, in a nitrogen atmosphere. The barrel of a syringe was withdrawn slightly to create 10 ml of headspace, a known mass of sample or standard was injected into the glass syringe, and then the tip of the syringe was sealed with a septum. The glass syringes were removed from the glove box, and 2 ml of 2.0 *m* HNO_3 were injected into each syringe. The glass syringes were lightly shaken, and allowed to equilibrate for approximately 2 hours before analysis. Headspace concentrations of CO_2 were measured using a GOW-MAC gas chromatograph with a thermal conductivity detector. Standards with headspace concentrations between 0.1% and 7.0% CO_2 were prepared from a 0.1 *m* Na_2CO_3 stock solution. A calibration curve was constructed by plotting the measured peak areas for the gas standards against their known DIC concentrations. The reproducibility for this technique is ± 5%, and the detection limit is 0.061 mmol/L CO_2.

In the formation experiments and in exchange experiment #1, samples for XRD analysis were prepared on glass slides. Solids from the other experiments were packed directly into aluminum planchettes. XRD analysis was performed using a Siemens Kristalloflex diffractometer. All solids were irradiated with nickel-filtered CuK alpha radiation (λ_1=1.5406 Å , λ_2=1.5444 Å) generated at 50 kV and 30 mA. Complete ranges were scanned from 5 to 55 degrees, using steps of 0.05, and 1 second per step. The recorded data were interpreted using powder diffraction files from the Joint Committee on Powder Diffraction Standards and the International Center for Diffraction Data (JCPDS-ICDD), and from XRD patterns reported in the literature (Chapter 2, Table 2.1).

6.3 Results

6.3.1 Formation of the end members

X-ray diffraction patterns for the formation of the OH end member with time are shown in Figure 6.1. After 8 hours of reaction, the solid consists predominantly of the OH end member and portlandite. In the solid taken after 1 day of reaction, the amount of portlandite present has decreased, and a small peak identified as hydrogarnet is present, in addition to the other phases. This phase assemblage (OH end member, portlandite and hydrogarnet) persists as the reaction time is increased to 7 days. In the samples taken after 1 and 7 days, the main peak of the OH end member is spilt into two peaks, one at $2\theta = 10.9°$, and the other at $2\theta = 11.3°$. These peaks correspond to d-spacings of 8.1 and 7.9 Å, respectively. The peak at 8.1 Å is usually identified as hemicarboaluminate ($3CaO{\cdot}Al_2O_3{\cdot}0.5CaCO_3{\cdot}0.5Ca(OH)_2{\cdot}10.5H_2O$), and the peak at 7.9 Å as $3CaO{\cdot}Al_2O_3{\cdot}Ca(OH)_2{\cdot}12H_2O$.

The formation of the Cl end member was monitored over a 91 day period, and the XRD patterns for the solid measured as a function of time are shown in Figure 6.2. In the pattern for the solid after one day of reaction, the main peak of the solid solution is split into two peaks, one at $2\theta = 10.9°$, and the other at $2\theta = 11.5°$. These peaks correspond to d-spacings of 8.1 and 7.7 Å, respectively. The peak at 8.1 Å is usually identified as hemicarboaluminate ($3CaO{\cdot}Al_2O_3{\cdot}0.5CaCO_3{\cdot}0.5Ca(OH)_2{\cdot}10.5H_2O$), and the peak at 7.7 Å corresponds to the standard XRD pattern for β-Friedel's salt. A small quantity of portlandite is also present. After 4 days of reaction, only the main peak for β-Friedel's salt is observed at $2\theta = 11.5°$. The XRD pattern taken after 7 days of reaction shows that the solid consists predominantly of the Cl end member (Friedel's salt), with a small quantity (<10%) of portlandite, and this phase assemblage is observed in the remainder of the solid samples, with reaction times up to 91 days.

The XRD patterns for both the OH and Cl end members show that these phases were dominant after 1 and 4 days, respectively. After 7 days of reaction, there is little to no change in the XRD patterns for both solids. Based on these results, a minimum formation time of 7 days was used for the end members, before initiation of the ion exchange reactions.

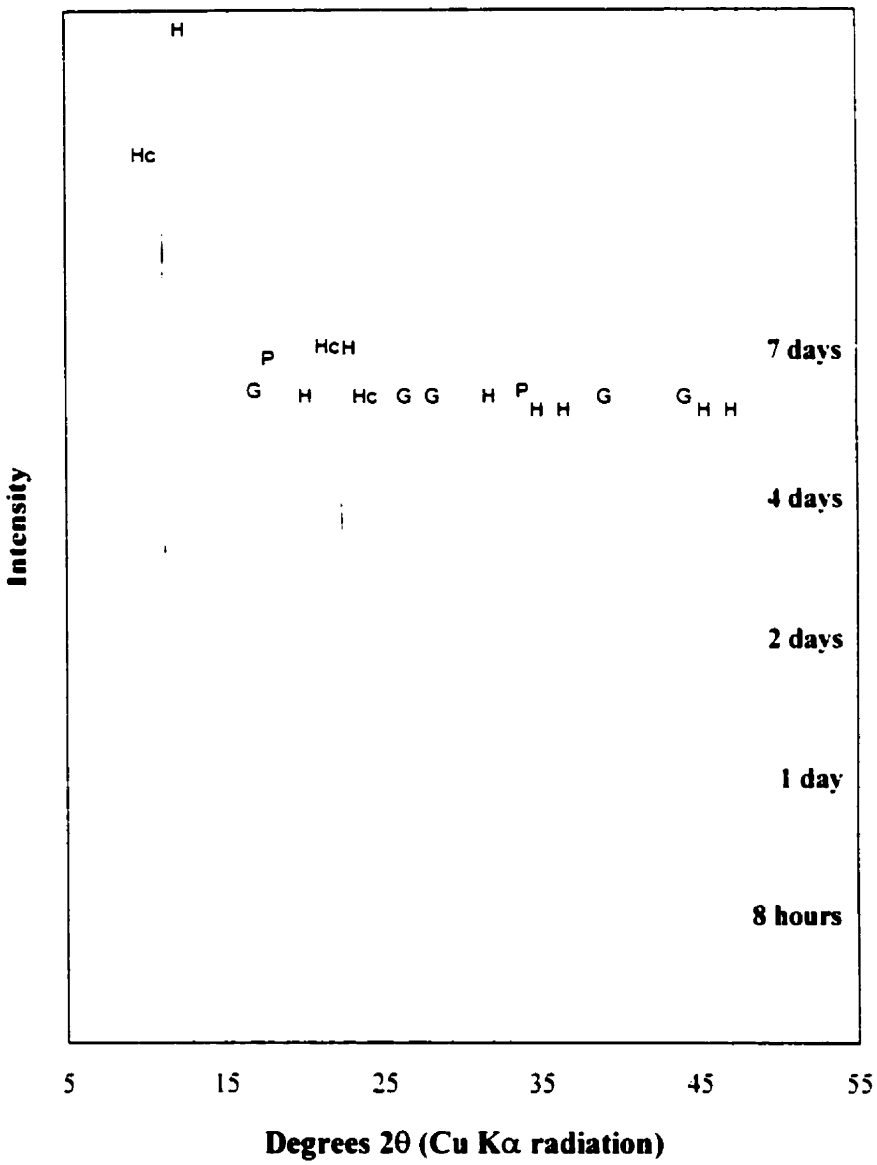


Figure 6.1: XRD patterns of the solid phases during the formation of the OH end member. The main peak of the OH end member is split into two in the 1 and 7 day samples. H = OH end member ($3CaO{\cdot}Al_2O_3{\cdot}Ca(OH)_2{\cdot}12H_2O$); Hc= hemicarboaluminate ($3CaO{\cdot}Al_2O_3{\cdot}CaCO_3{\cdot}Ca(OH)_2{\cdot}12H_2O$) P= portlandite ($Ca(OH)_2$); G= hydrogarnet ($3CaO{\cdot}Al_2O_3{\cdot}6H_2O$).

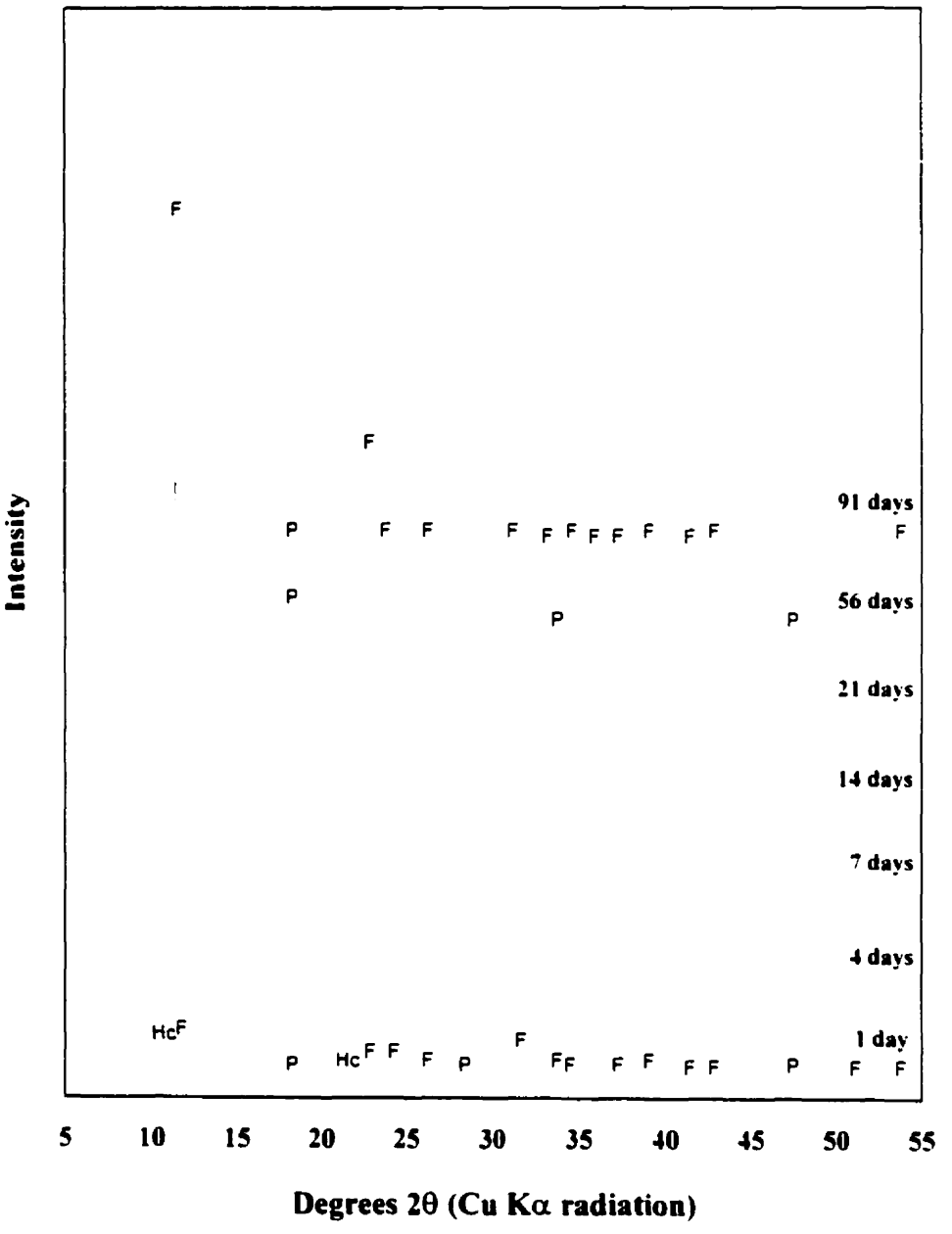


Figure 6.2: XRD patterns of solid phases during the formation of the chloride end member (Friedel's salt). F = β-Friedel's salt ($3CaO.Al_2O_3.CaCl_2.10H_2O$); P= portlandite ($Ca(OH)_2$).

6.3.2 Exchange of OH by Cl

6.3.2.1 Reaction time

The fraction of Cl exchanged into the OH end member as a function of reaction time for experiments 1 and 2 is shown in Figure 6.3. Apart from varying reaction times (9 vs. 7 days), the major difference between the samples in the two experiments is that in experiment 1 (depicted as open squares in Figure 6.3) no special precautions were taken to exclude atomospheric CO_2, while in experiment 2, filtration and sampling handling was performed in a CO_2-free environment. In both experiments, the maximum fraction of chloride exchanged into the solid was 0.65, and this maximum exchange was reached after 1 day of reaction. With continued reaction times of up to 27 days, the fraction of chloride in the solid remained at approximately 0.65. The XRD pattern of the 27 day sample from experiment 2 (CO_2-free) showed that the solid consists mainly of the Cl end member (Friedel's salt), with a small quantity (10%) of portlandite.

In experiment 3 (Table 6.1), the exchange of chloride ions in Friedel's salt by hydroxyl ions as a function of time was investigated. The Cl end member was first prepared, and after 7 days the samples were spiked with a NaOH solution. A separate sample was prepared for each time interval, and enough NaOH (plus an extra 10%) was added to exchange 100% of the Cl^- originally in the solid. The release of chloride into solution was monitored as a function of reaction time. The average of the chloride concentrations measured after 7 days of reaction in the timed experiments (1 and 2) was used as the initial Cl concentration in the current experiment. The percent change in the Cl^- solution concentration was calculated by subtracting the chloride solution concentration at each sampling time from the initial concentration. The measured concentrations of chloride in solution between 1 and 768 hours (32 days) fluctuate within ± 3.0% of the original concentration (within the analytical uncertainty). Based on these results, there is no measurable exchange of Cl by OH in this experiment. In fact, with further reaction (i.e. after 64 and 127 days), the concentration decreases by 5 to 6%, suggesting that Cl is being incorporated into the solid phase, rather than released. XRD patterns for solids collected after 12 hours and 127 days showed that the solid consists predominantly of the Cl end member (α-Friedel's salt), with a small quantity of portlandite.

6.3.2.2 Concentration

The exchange of hydroxyl ions in the OH end member by Cl^- ions was examined as a function of concentration in experiments 6 and 7 (Table 6.2). In experiment 6, the samples were spiked with chloride to exchange fractions of the OH^- ions in the interlayer solid between 0.0 and 1.0. In Figure 6.4, the mole fraction of Cl exchanged into the solid after 10 days of reaction is plotted versus the total mole fraction of chloride added. The maximum fraction of Cl exchanged was 0.7 in the sample where the mole fraction of Cl added was equal to 1.0.

The XRD patterns for the solids from this experiment are plotted in Figure 6.5. In the solid with no chloride added (0.0), the main peak of the OH end member is spilt into a peak at $2\theta = 10.9^\circ$ and one at 11.3°. These peaks correspond to d-spacings of 8.1 and 7.9 Å, respectively. The peak at 8.1 Å is identified as hemicarboaluminate, and the peak at 7.9 Å as the OH end member ($3CaO{\cdot}Al_2O_3{\cdot}Ca(OH)_2{\cdot}12H_2O$). Small amounts of both hydrogarnet and portlandite are also present in the solid. As the fraction of chloride added to the samples increases to 0.1, the main peak is split into two peaks at $2\theta = 11.2^\circ$ and 11.4°. These peaks correspond to d-spacings of 7.9 and 7.8 Å, respectively. The peak at 7.9 Å is identified as the OH end member, and the peak at 7.8 Å as β-Friedel's salt. With an increase in the fraction of Cl to 0.3, Friedel's salt is the only solid solution phase present. Small peaks for hydrogarnet and portlandite are present in the patterns of all solids where the Cl^- fraction added was between 0 and 0.7. In samples with chloride fractions of 0.8 or higher, the Cl end member is the only mineral phase identified.

The extended exchange experiment (#7) was conducted to determine if a mole fraction of Cl^- higher than 0.7 could be exchanged by increasing the amount of chloride added from a factor of 1 (i.e. enough to exchange 100% of the OH^- ions), up to a factor of 20. At a factor of 20, the measured solution concentration of Na^+ was 3.66 mol/L. In Figure 6.6, the mole fraction of chloride exchanged into the solid is plotted versus the quantity of chloride added (expressed as the factor by which chloride was increased). The fraction of Cl^- exchanged into the solid at a factor of 1 (or mole fraction of Cl^- added = 1.0) was 0.5. This is substantially lower than the fraction exchanged in the sample from experiment 6 with the same total quantity of Cl^- added (0.7), and from the two timed experiments (0.65). This apparent discrepancy can be resolved by examining the XRD patterns for several solids from this experiment (Figure 6.7). The pattern of the solid with a Cl factor of 1 is predominantly β-Friedel's salt, with some portlandite (≈15%), and hydrogarnet (≈10%). This phase assemblage persists as the factor of Cl added increases to 8. Hydrogarnet and portlandite are conversion products of the OH end member:

$$3CaO{\cdot}Al_2O_3{\cdot}Ca(OH)_2{\cdot}18H_2O_{(s)} \rightarrow 3CaO{\cdot}Al_2O_3{\cdot}6H_2O_{(s)} + Ca(OH)_{2(s)} + 12H_2O_{(aq)} \quad (6.1)$$

Although this conversion usually takes months to reach completion, small amounts of hydrogarnet and portlandite were observed in the XRD patterns during the formation of the OH end member (Figure 6.1). In the extended experiment, the precipitation of hydrogarnet and portlandite probably occurred before the NaCl was added. It is probable that the quantity of the OH end member was overestimated, resulting in a lower calculated total exchange. As the Cl addition factor increases from 1.0 to 6, the fraction of Cl in the solid increases to a maximum of 0.73, but then decreases to 0.44 as the Cl addition factor increased to 10. These variations may be due to variations in the quantity of additional mineral phases (portlandite, hydrogarnet) present in the samples. For example, the XRD results show that the amount of portlandite decreases between solids with Cl addition factors of 2 and 8. These results suggest that a key difficultly in conducting batch exchange experiments involving the OH end member may be preparing a pure solid containing only this phase.

In Figure 6.6, the fraction of Cl in the solid increases dramatically to 0.9 and to 4.0 at chloride addition factors of 15 and 20, respectively. The increase in the fraction of Cl^- in the solid to 4.0 (or 4 times the theoretical exchange capacity of the solid) suggests the presence of another Cl-bearing mineral phase. Mineral saturation indices were calculated using the measured solution compositions and the geochemical equilibria model, SIMUL (Reardon, 1990), and the results are plotted in Figure 6.8. The results show that the solutions are undersaturated with respect to calcium oxychloride ($3CaO{\cdot}CaCl_2{\cdot}15H_2O$). Halite is approaching saturation as the Cl addition factor increases to 20, but is still undersaturated with respect to this phase. The XRD pattern for the solid with Cl addition factor of 20 (Figure 6.7) shows that in addition to Friedel's salt, a large peak at $2\theta = 31.8^\circ$ (2.82 Å), and smaller peaks at $2\theta = 45.5^\circ$ and 27.4° (1.99 and 3.26 Å, respectively) are observed. These peaks are identified as halite (NaCl). Solids with a NaCl addition factor of 10 or higher were also examined using an optical microscope. At a factor of 20, large (up to approx. 20 μm) isometric crystals of halite with high relief were observed (Figure 6.9). The hydrocalumite crystals, in contrast, form hexagonal crystals with comparatively low relief.

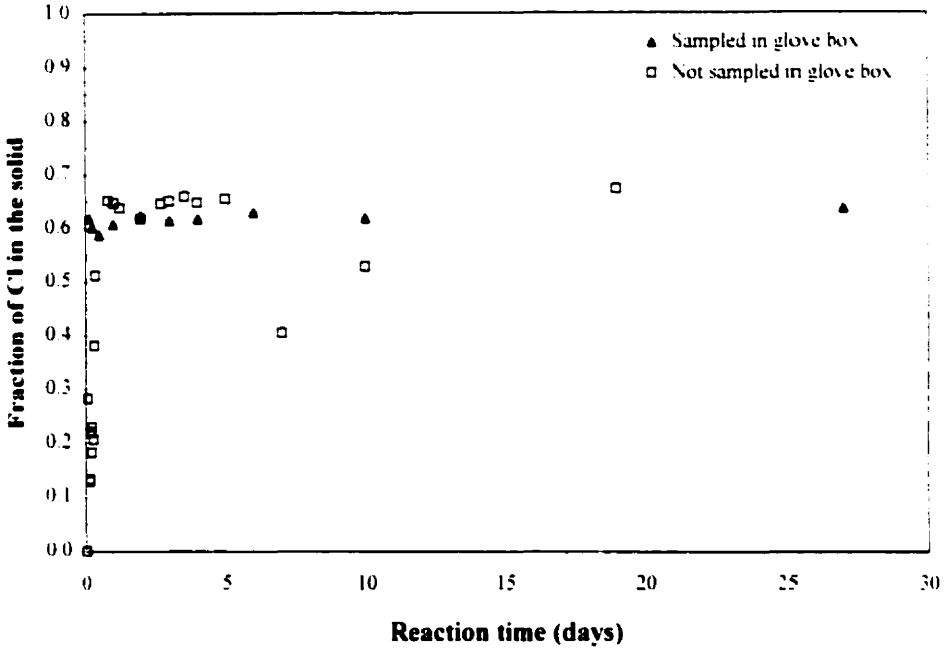


Figure 6.3: Fraction of Cl^- exchanged into the OH end member as a function of reaction time. In one experiment (open squares), no special precautions were taken to exclude atmospheric CO_2, whereas in the second experiment (filled triangles), the samples were handled exclusively in a CO_2-free atmosphere. In both cases, the fraction of chloride exchanged was calculated by dividing the number of moles of Cl^- in the solid after reaction by the total number of moles of OH^- available for exchange.

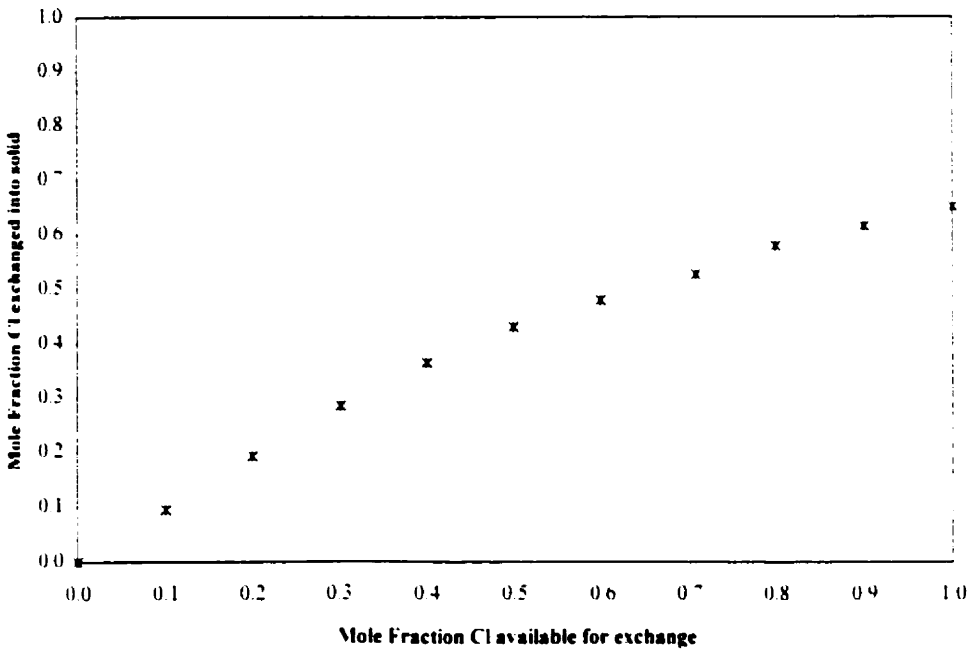


Figure 6.4: Results from the experiment investigating the exchange of OH^- by Cl^- as a function of chloride concentration. The mole fraction of chloride exchanged into the solid after 10 days of reaction is plotted versus the total mole fraction of Cl^- available for exchange. The mole fraction of chloride in the solid was calculated by subtracting the moles of chloride measured in solution after exchange from the moles of chloride added (as NaCl).

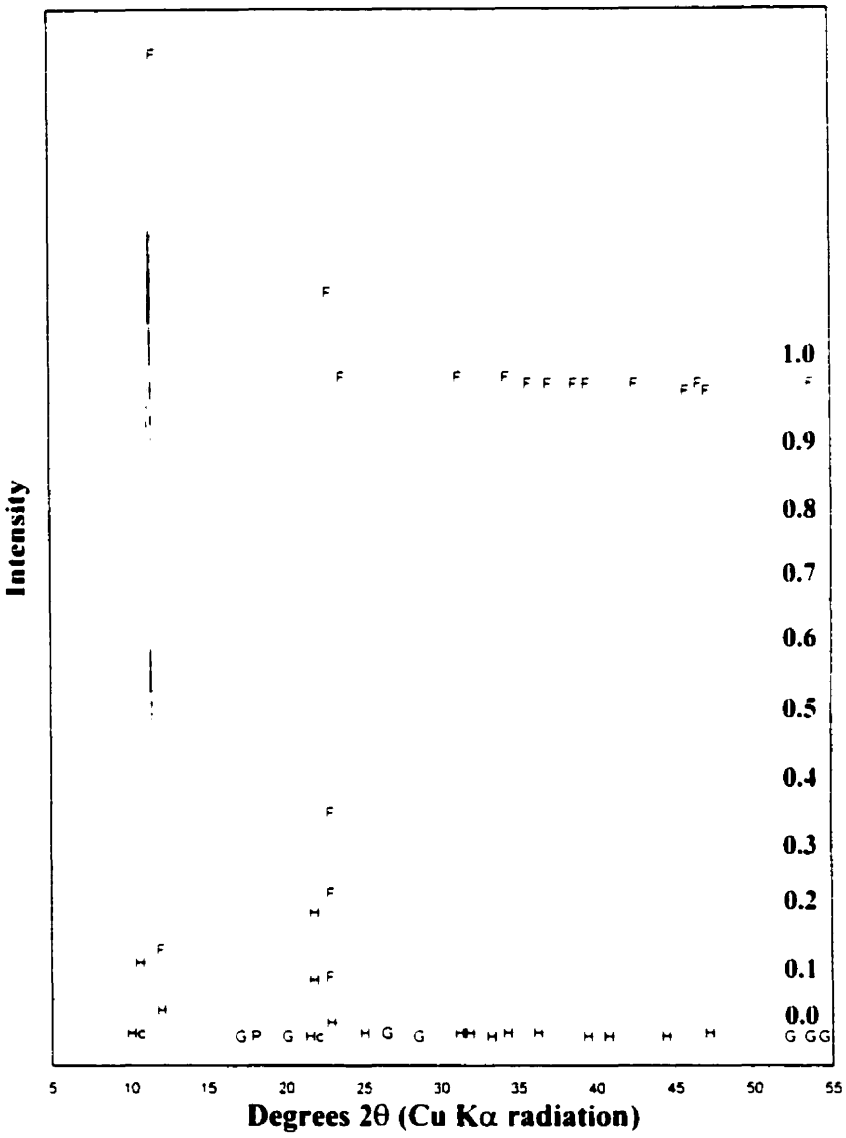


Figure 6.5: XRD patterns for solids after 10 days of reaction in the experiment which examined the exchange of OH^- by Cl^- as a function of concentration. The label indicates the fraction of Cl^- added to each solid. F = β-Friedel's salt ($3CaO{\cdot}Al_2O_3{\cdot}CaCl_2{\cdot}10H_2O$); H = OH-hydrocalumite ($3CaO{\cdot}Al_2O_3{\cdot}Ca(OH)_2{\cdot}12H_2O$; Hc = Hemicarboaluminate ($3CaO{\cdot}Al_2O_3{\cdot}0.5Ca(OH)_2{\cdot}0.5CaCO_3{\cdot}12H_2O$; G = hydrogarnet ($3CaO{\cdot}Al_2O_3{\cdot}6H_2O$); P = portlandite ($Ca(OH)_2$).

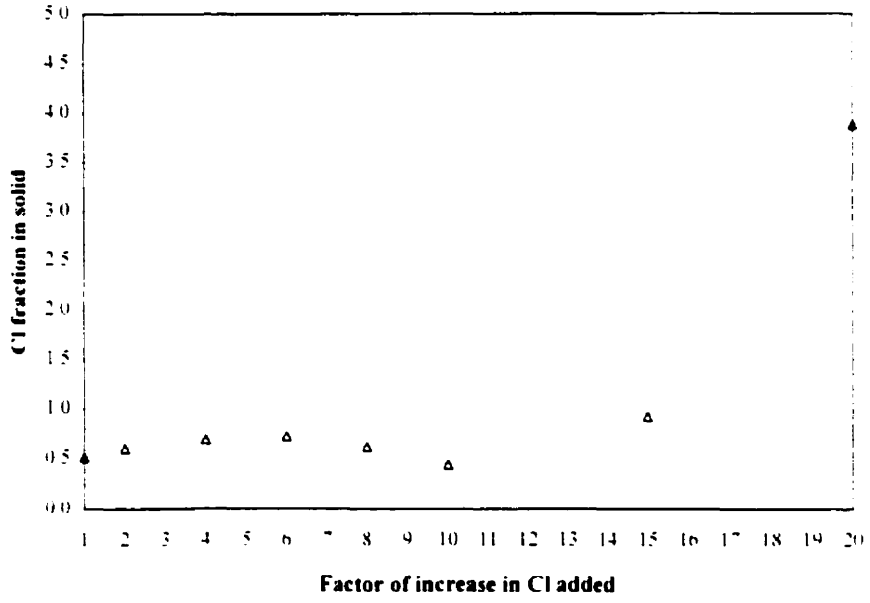


Figure 6.6: The fraction of Cl^- exchanged into the OH end member is plotted versus the factor by which the amount of Cl^- added was increased (a factor of 1 is the moles of Cl^- theoretically required to exchange 100% of the OH^- ions originally present in the interlayer of the solid).

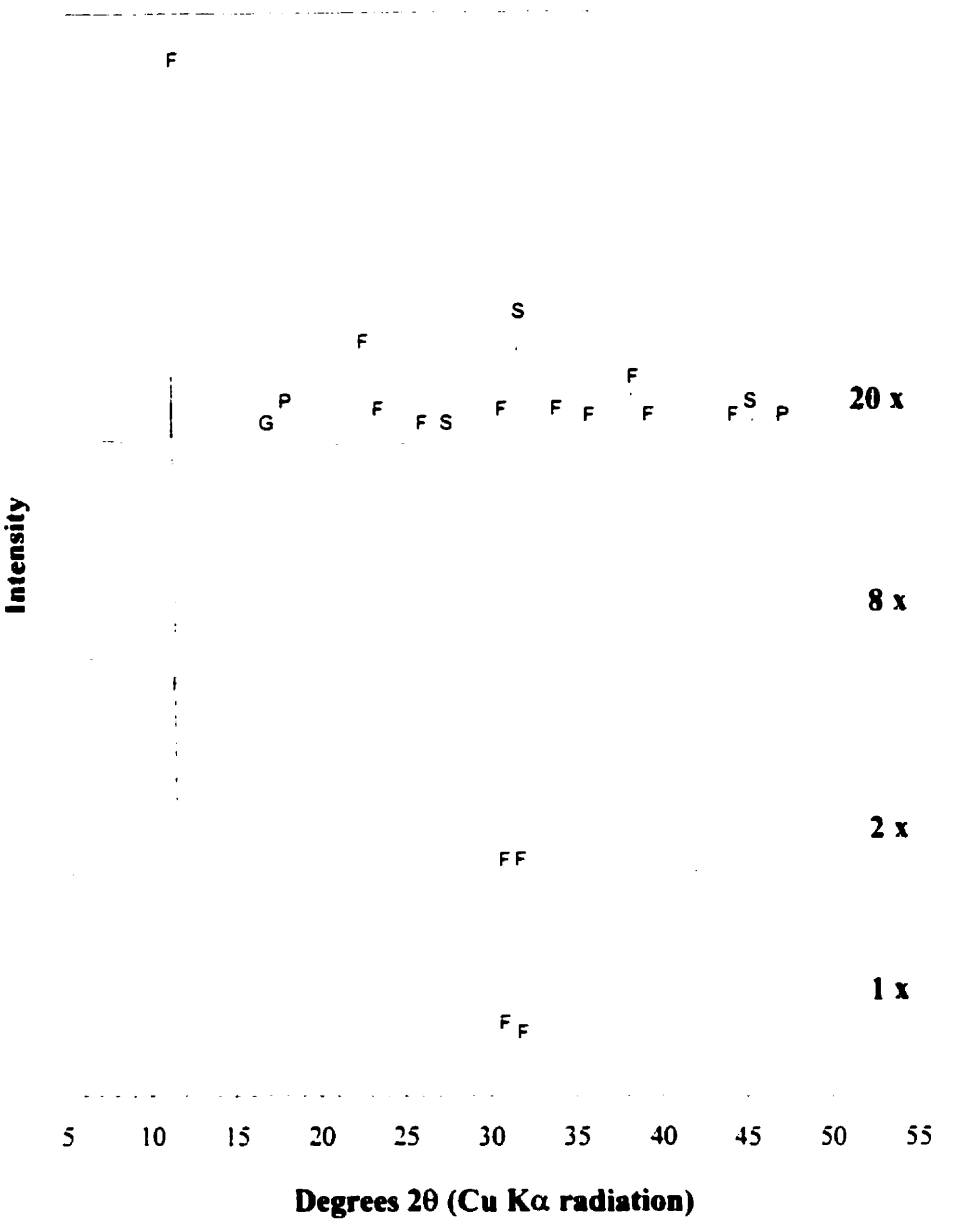


Figure 6.7: XRD patterns for solids after 10 days of reaction in the second experiment examining the exchange of OH^- by Cl^- as a function of concentration. The label indicates the factor by which the quantity of Cl^- added was increased (where 1 = the amount required to exchange 100 % of the OH^- ions originally present in the interlayer of the solid). F = β-Friedel's salt ($3CaO{\cdot}Al_2O_3{\cdot}CaCl_2{\cdot}10H_2O$); G = hydrogarnet ($3CaO{\cdot}Al_2O_3{\cdot}6H_2O$); P = portlandite ($Ca(OH)_2$); S = Halite (NaCl).

These results suggest that the "extra" Cl^- in the solid phase as calculated by mass balance for solids at Cl addition factors of 15 and 20 may be accounted for by the presence of halite. The persistence of halite in the solids after 10 days of reaction suggests that the rate of dissolution of halite is reduced when the Cl addition factor is high. This interpretation is consistent with the results of Alkattan et al. (1997). These authors determined that the rate of halite dissolution decreased linearly as the degree of saturation increased, decreasing by a factor of 5 as the saturation index for halite increased from -1.3 to -0.086.

6.3.3 Exchange of Cl by CO_3

The results of the two timed experiments (4 and 5 in Table 6.1) conducted to investigate the exchange of chloride ions in the Cl end member by carbonate ions are shown in Figure 6.10. In experiment 4, where sodium carbonate was added as a spike, the quantity of chloride released to solution increased to a maximum of 2.2 mmol after 20 days of reaction, and remained at this value as the reaction time was increased to 55 days. The quantity of chloride released to solution in experiment 5 (spiked with $CaCO_3$), increased gradually to 1.7 mmol after 21 days of reaction, which is 20% lower than the amount released in the experiment with Na_2CO_3 after the same reaction time.

Reaction progress in experiment 4 was also monitored by measuring the carbonate concentration in solution with time, and the results are plotted in Figure 6.11. The concentration of carbonate in solution reached a maximum concentration of 4.6 mmol/L after 6 hours of reaction, and then decreased rapidly, leveling off at a concentration of 0.7 mmol/L after 7 days of reaction. These results are consistent with the release of Cl^- to solution, which had also reached a maximum value after 7 days of reaction. However, the total increase in the quantity of Cl^- in solution was1.95 mmol after 7 days of reaction, whereas the quantity of CO_3^{2-} in solution decreased by 0.18 mmol. The lack of mass balance between the Cl^- released and carbonate incorporated into the solid is likely due to the precipitation of calcite. Therefore, the change in the carbonate concentrations with time are not a reliable measure of carbonate uptake by the solid solution.

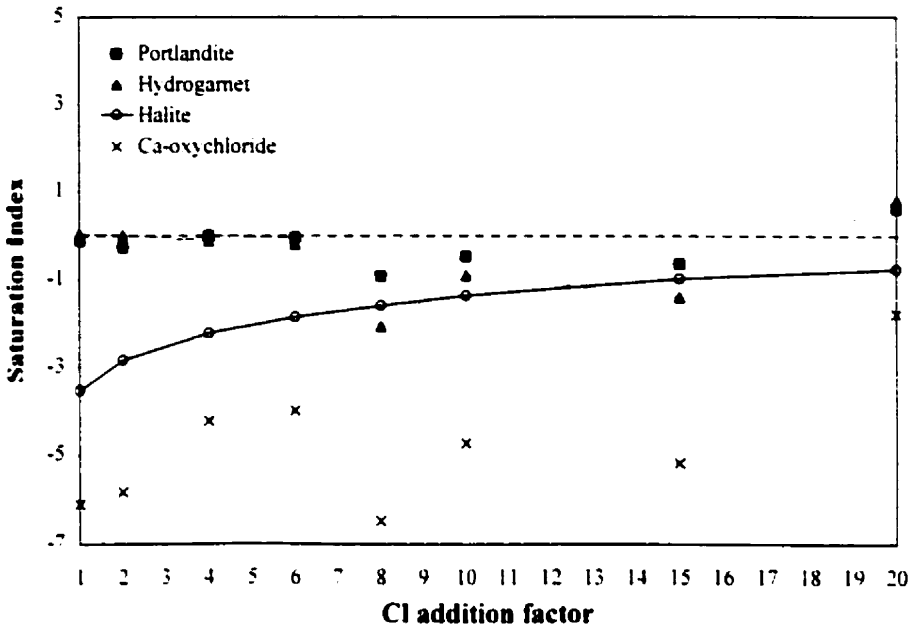


Figure 6.8: The calculated saturation indices for portlandite ($Ca(OH)_2$), hydrogarnet ($3CaO{\cdot}Al_2O_3{\cdot}6H_2O$), Ca-oxychloride ($3CaO{\cdot}CaCl_2{\cdot}15H_2O$), and halite (NaCl) are plotted versus the chloride addition factor (a factor of 2 is twice the amount of Cl^- theoretically required to exchange all of the OH^- ions in the OH end member).

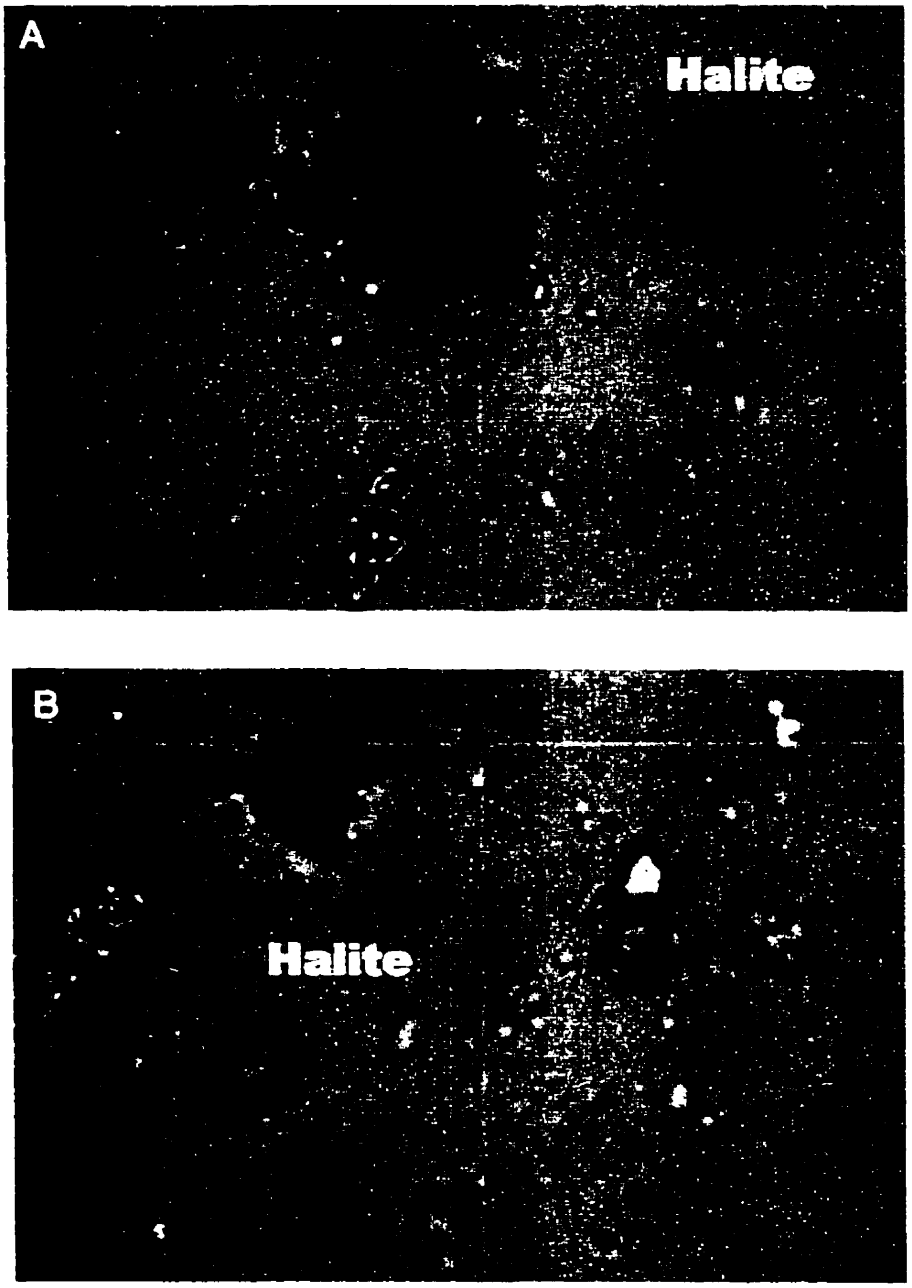


Figure 6.9: Photographs of solids where the factor of increase in the chloride added was 20. taken using an optical microscope (magnification 60x). The calcium aluminate hydrate phase forms small, platy hexagonal crystals, often occurring as aggregates. Large isometric halite crystals (9 - 20 μm) are easily distinguished by their high relief.

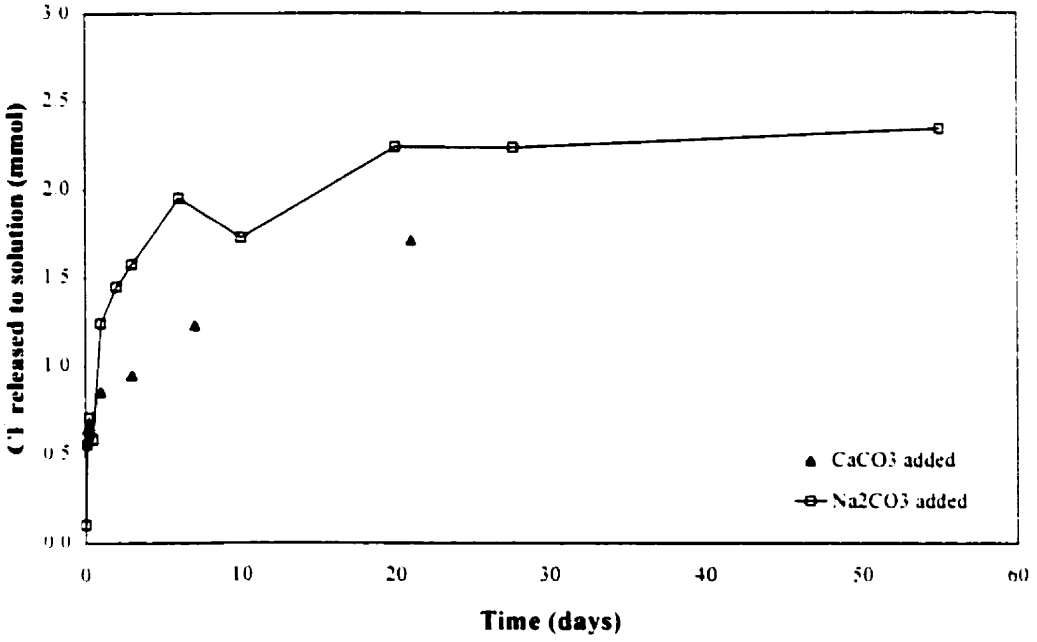


Figure 6.10: Quantity of chloride released from the Cl end member solid to solution as a function of reaction time. Carbonate was added as solid Na_2CO_3 or $CaCO_3$.

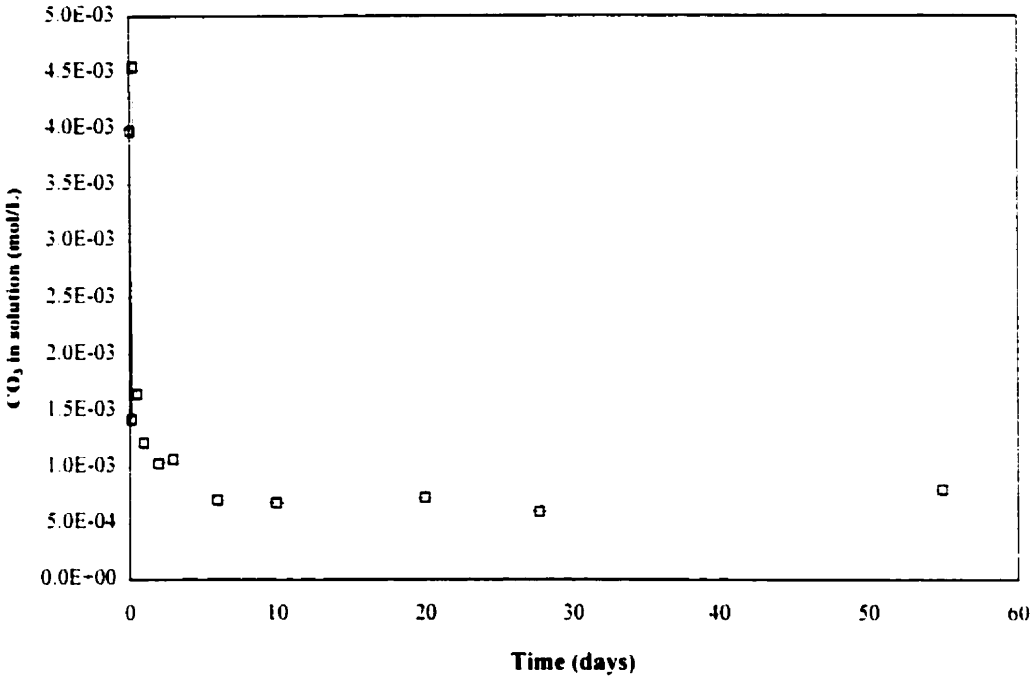


Figure 6.11: Carbonate concentration in solution as a function of the reaction time. In this experiment, the Cl end member formed for 35 days before it was spiked with Na_2CO_3.

The XRD patterns for selected solids from the Na_2CO_3 experiment are plotted in Figure 6.12. Both these solids consist predominantly of β-Friedel's salt, with approximately 20% calcite. Figure 6.13 shows the XRD patterns for solids from the $CaCO_3$ experiment after 1, 7 and 21 days of reaction. The solid consists predominantly of α-Friedel's salt, with some calcite (≈20%), as observed for solids in the experiment with Na_2CO_3 added. In solids after 7 and 21 days of reaction, there is a small split in the secondary peak. The two peaks are at $2\theta = 22.6°$ and $2\theta = 22.8°$, which correspond to d-spacings of 3.93 and 3.90 Å, respectively. This apparent splitting may be the result of poor resolution of the peaks for α-Friedel's salt at 3.94 and 3.86 Å.

6.4 Discussion

6.4.1 Exchange of OH by Cl

In general, the sorption or ion exchange of inorganic ions on mineral surfaces is a two-step process consisting of a short period of rapid uptake in which the ion(s) are sorbed or exchanged, followed by periods of progressively slower uptake. The rapid step is usually assumed to be a diffusion-controlled reaction that takes minutes to reach equilibrium when mass transport in the bulk solution is not limiting. Various processes such as surface precipitation, solid-solution formation, or structural re-arrangement of surface species may also be important at long reaction times (Davis and Kent, 1990), and these processes may take weeks or months to reach equilibrium. A period of rapid exchange is observed in experiment 1 (Figure 6.3), where sampling during the first few hours of reaction was intensive. In experiment 2, the fraction of Cl^- exchanged into the solid was already approximately 0.62 after 3 hours of reaction, and increased only slightly to 0.64 after 27 days. A mass balance of the quantity of Cl^- added to what will remain in solution at equilibrium (based on the results of the solubility experiments, Chapter 2) should give a final Cl^- fraction in the solid of approximately 0.91.

In solids where the mole fraction of Cl^- added was 1, the final Cl^- fraction in the solid may be 20% lower than expected, because the exchange reaction is not complete (i.e. it has not yet reached equilibrium). In this case, the OH^- ions remaining in the solid at the end of the experiment may be in sites near the middle of the crystals and therefore, require much longer times for exchange. The maximum fraction of Cl^- ion exchanged into the solid in the experiment as a function of concentration (0.7) was similar to that measured in both the timed OH-Cl exchange experiments (0.65). Further insight into the apparent discrepancy between the

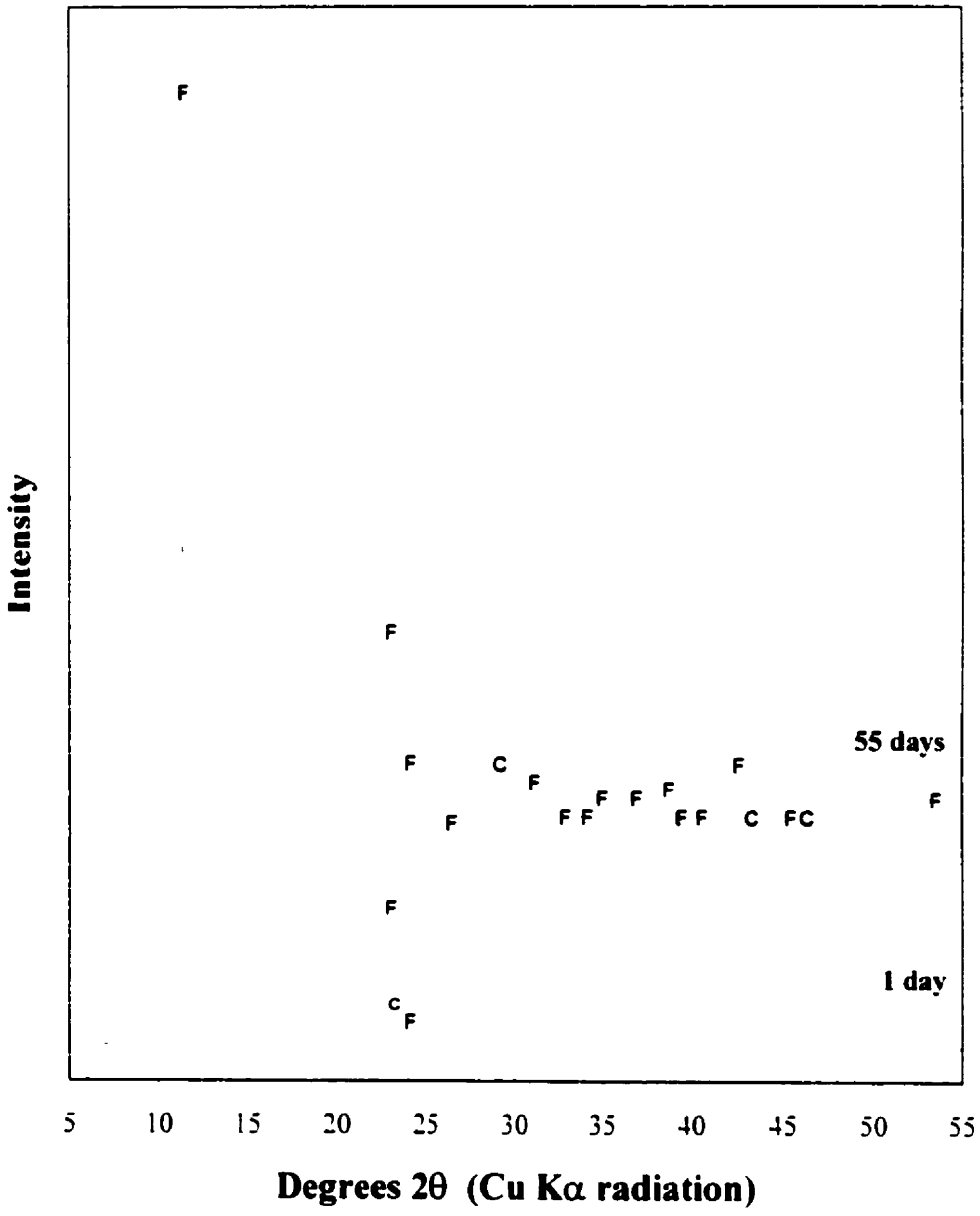


Figure 6.12: XRD patterns for solids from the chloride-carbonate ion exchange experiment 1 day and 55 days after spiking with Na_2CO_3. Labels: F = β-Friedel's salt ($3CaO{\cdot}Al_2O_3{\cdot}CaCl_2{\cdot}10H_2O$); C = calcite ($CaCO_3$).

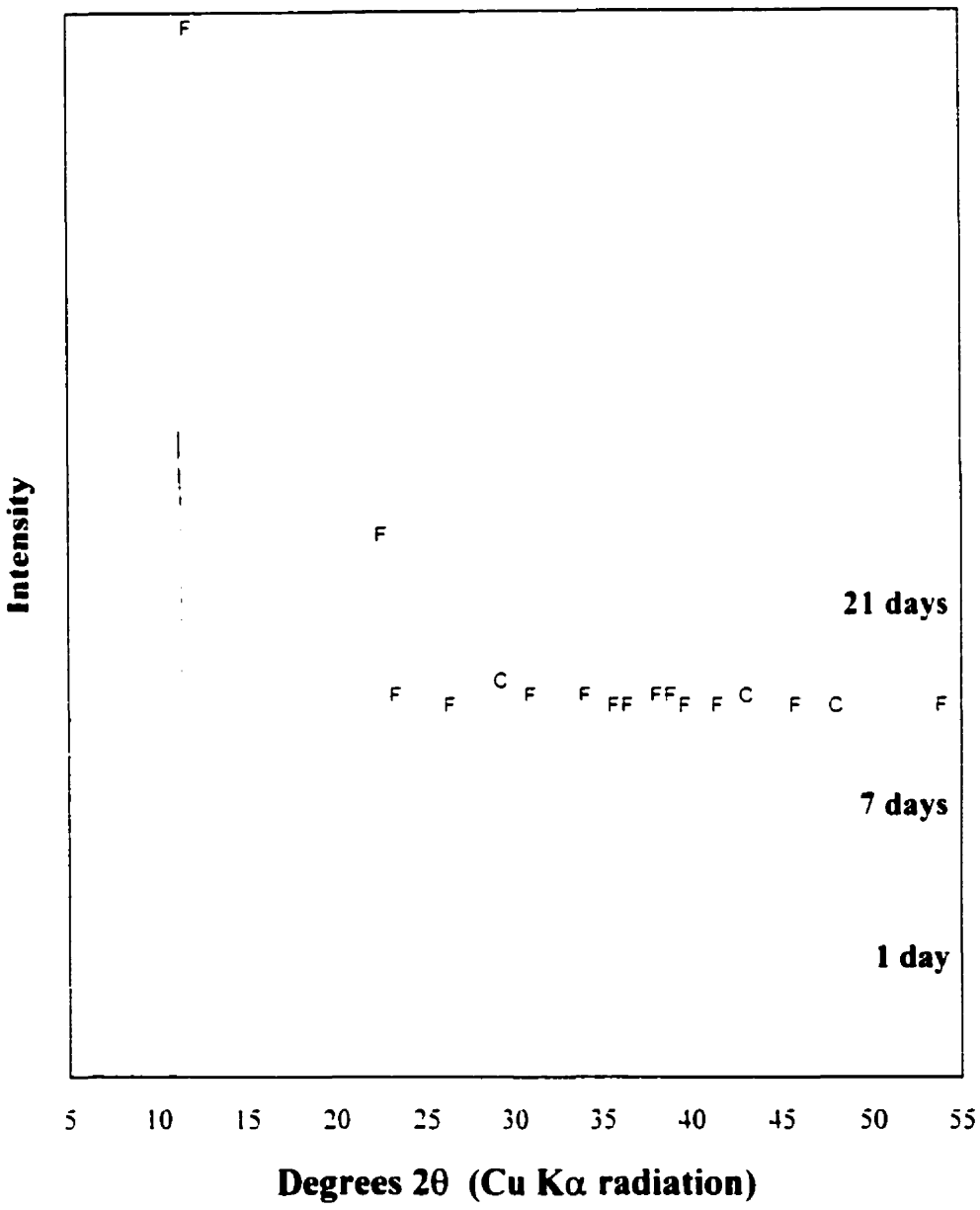


Figure 6.13: XRD patterns for solids from the chloride-carbonate ion exchange experiment 1, 7, and 21 days after spiking with $CaCO_3$. Labels: F = α-Friedel's salt ($3CaO{\cdot}Al_2O_3{\cdot}CaCl_2{\cdot}10H_2O$); C = calcite ($CaCO_3$).

expected and measured fractions of Cl^- in the solids is gained by comparing results of the ion exchange experiment as a function of Cl^- concentration (experiment 6), and the results of the long-term solubility experiments (Chapter 2). The results from the extended ion exchange experiment (#7) are not directly comparable to these results, because the presence of hydrogarnet and portlandite appear to have affected the amount of chloride exchanged (Section 6.3.2.2).

In Figure 6.14, the molar ratio of Cl^- relative to the total exchangeable ions in the solid ($Cl^- + OH^-$) is plotted versus the measured activity ratio of Cl^- to Cl^-+OH^- (or total exchangeable anions) in the solution phase. There is excellent agreement between the ion exchange and solubility studies. However, for a given total number of moles of Cl^-, the amount of Cl^- in the solid phase relative to $OH^- + Cl^-$ is different in these two studies. For example, the Cl end member sample in the solubility experiment from supersaturation was prepared to have a final Cl/(Cl+OH) ratio in the solid of 1.0. The final calculated ratio in the solid was 0.91, and the activity Cl/(Cl+OH) ratio in solution was 0.73. In the ion exchange experiment, the sample with sufficient Cl^- added to exchange 100% of the OH^- has the same total number of moles of Cl^- in the system as the Cl end member sample in the solubility experiment. However, the final ratio of Cl/(Cl + OH) in the solid was 0.65, and the activity ratio in the solution was 0.31. This can be explained by considering that in the solubility experiments, reagents are added in proportions that will result in a specific final ratio of Cl/(Cl+OH) in the precipitating solid. However, in the exchange experiments, the solid phase is initially the OH end member, and Cl^- is added afterwards as NaCl. As a result, this system is enriched in OH^- compared to a system with the same number of moles of Cl^- in the solubility experiments. Stated another way, the total Cl/(Cl+OH) ratio in the system is lower in the ion exchange experiment, and this results in a lower Cl/(Cl+OH) ratio in both the solid and solution phases.

These results strongly suggest that the Cl/(Cl+OH) ratio of 0.65 to 0.7 measured in the ion exchange experiment and at the end of both the timed experiments are equilibrium ratios, and are not due to kinetic controls on the exchange of OH^- and Cl^- ions. However, it should be emphasized that although the exchange reaction may have reached an apparent equilibrium (or metastable equilibrium), this does not necessarily represent thermodynamic equilibrium for the entire system.

Equilibrium partitioning of Cl^- and OH^- between the solid-solution and aqueous solutions could be predicted empirically by fitting the exchange and solubility data to a curve. The OH-Cl exchange data was fitted using the Langmuir adsorption isotherm using non-linear regression

analysis (Kinniburgh, 1986). The Langmuir isotherm is derived by assuming that the solid contains a fixed number of adsorption sites (S_T), which have identical adsorption characteristics, and act independently on the sorbate (Appello and Postma, 1994). At equilibrium with a given sorbate concentration in solution (C), a fraction of the sites are occupied (S/S_T) and the remainder are unoccupied ($1-S/S_T$). When the exchange reaction is at equilibrium, the opposing kinetic processes of adsorption and desorption must be equal. In the OH-Cl exchange experiments, the sorbate is Cl^-. Flux of chloride ions from the surface Q_d, is proportional to the fraction of sites containing Cl^-, with a rate constant K_d:

$$Q_d = K_d(S/S_T) \tag{6.2}$$

and the flux of Cl^- to the surface is proportional to the fraction of sites still occupied by OH^- and the concentration in solution with a rate constant K_a:

$$Q_a = K_aC(1-S/S_T) \tag{6.3}$$

At equilibrium, $Q_d=Q_a$, and setting $K_a/K_d = K$ results in the equation for the isotherm

$$S = S_TKC/(1 + KC) \tag{6.4}$$

The solid line in Figure 6.14 is the fitted Langmuir adsorption isotherm, where K = 7.65 and the maximum fraction of sorption sites $S_T = 0.976$ ($r^2 = 0.967$). However, it important to recognize that the fit of this experimental data to the Langmuir isotherm does not constitute evidence that adsorption is the mechanism involved. However, this model may be useful for semi-empirical predictions on the partitioning of OH^- and Cl^- between the calcium aluminate hydrates and aqueous solutions.

In experiment #3, the exchange of chloride ions in Friedel's salt by OH^- ions was investigated. The results of this experiment showed that after spiking the Cl end member with 1.5 times the OH initially in solution, the amount of Cl^- released to solution was less than 3%, and after extended reaction times of 60 to 127 days, the Cl^- concentration in solution appears to be decreasing. These results are not expected based on the partitioning relationship between Cl^- and OH^- observed in both the ion exchange experiments and solubility experiments. As the amount of OH^- in the system was increased, the quantity of OH^- partitioned to the solid would be expected to increase, and Cl^- would be released to solution. One possible explanation for the decreasing Cl^- concentrations is that the solid is re-crystallizing, and incorporating more Cl^- into

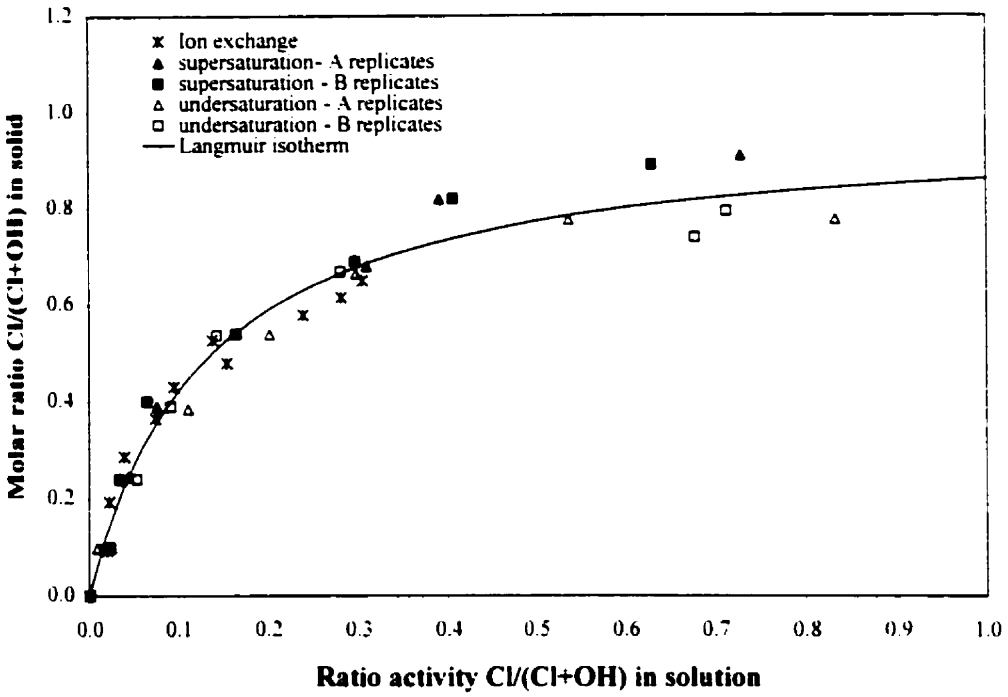


Figure 6.14: Molar ratio of Cl^- to Cl^- and OH^- ions in the solid versus the ratio of the activities of Cl^- to Cl^- and OH^- in the aqueous solution. Results are plotted for the ion exchange experiment and for two sets of replicate samples from solubility experiments in the Cl-OH system (one set was measured from supersaturated and the other from undersaturated conditions). The ion exchange measurements were made after 10 days of reaction, whereas reaction times in the solubility experiments were 6 months (from supersaturation) and over one and a half years (from undersaturation). The combined data set was fit to the Langmuir isotherm, where the constant K = 7.64 and the maximum fraction of sorption sites is S_T = 0.976, r_2 = 0.967.

its structure, as expected if the solid and aqueous phases are evolving towards equilibrium with respect to the Cl end member. This suggests that once formed, the Cl end member is more stable, and can not be easily converted back to an OH-rich phase.

6.4.2 Exchange of Cl by CO_3

The ion exchange process is characterized by an initial rapid step, during which time the concentration gradients are large, and exchange is confined to the outer surface of the crystals. This is followed by progressively slower rates as exchange proceeds. The rate of exchange decreases because the concentration gradients between the solution and the exchanger are reduced, and the remaining sites with exchangeable ions available are closer to the center of the crystals. In the chloride-carbonate exchange experiment with Na_2CO_3 added, it appears that an initially rapid period of exchange occurs between 1 and 20 days, after which time the rate of exchange decreases dramatically, with no apparent change in exchange after 55 days. Assuming that chloride ions released from the solid were replaced by carbonate ions, the maximum of 2.2 mmol of Cl^- released after 20 days in the experiment with sodium carbonate added corresponds to a maximum uptake of 1.1 mmol of carbonate ions (i.e. two Cl- ions are replaced by one CO_3^{2-} ion). In this case, the maximum measured exchange of chloride by carbonate is 22%.

In the experiment with calcite added, the quantity of Cl^- released from the solid after 21 days of reaction was 1.7 mmol, or 0.85 mmol of carbonate taken up into the solid. This is approximately 20% lower than the exchange measured in the sodium carbonate experiment after a similar reaction time (Figure 6.10). It is not possible to assess whether or not chloride release had reached a maximum at this point, because the experiment was terminated after 21 days.

The faster rate of carbonate exchange exhibited when sodium carbonate was used as a source of carbonate ions relative to when calcite was added, can be explained by considering the relative solubilities of these two compounds. When the solutions are initially spiked with sodium carbonate, it dissolves, releasing carbonate ions to solution. This is supported by the measured carbonate concentrations in solution, which reach a maximum after 6 hours of reaction (Figure 6.11). However, the carbonate concentration in solution quickly exceeds saturation with respect to calcite, and calcite precipitates from solution. This is supported by the identification of calcite in the XRD patterns of the solids from this experiment after 1 day of reaction (Figure 6.12). Once calcite has precipitated, the carbonate solution concentration will be controlled by the solubility of calcite, and will be substantially lower due to the low

solubility of calcite relative to sodium carbonate. In contrast, when solid $CaCO_3$ is added as the source of carbonate ions, the solubility of calcite maintains the carbonate ions at a lower concentration in solution from the beginning of the experiment.

The CO_3^{2-} ions are divalent and are expected to be preferentially exchanged into the Cl end member, due to their higher electroselectivity (Patterson, 1970). In addition, the results of the solubility experiments (Chapter 3) demonstrate that solid solutions with up to 85% (a carbonate mole fraction of 0.85) can exist in contact with aqueous solution. Therefore, the maximum extent of exchange (approximately 20%) after almost two months of reaction in the Na_2CO_3 is remarkable. When Fischer and Kuzel (1982) exposed crystals of the OH end member in solution to atmospheric CO_2, they observed the immediate formation of narrow, carbonated rim zones in the crystals. XRD patterns of single crystals showed the presence of both OH end member and hemicarboaluminate in the carbonated crystals. Fischer and Kuzel (1982) suggested that penetration of carbonate ions into the interlayer region of the OH end member is retarded by the formation of the carbonated rims, which acts as a diffusion barrier to the further exchange of carbonate for hydroxyl ions. It is possible that a similar diffusion barrier on the outer rims of the crystals was formed in the current study, during the carbonation of the Cl end member. The presence of one solid phase with a basal spacing similar to Friedel's salt in the final solid with approximately 20% carbonate is consistent with the formation of a limited solid solution between carbonate ratios of 0 and 0.85 in the series between the chloride and carbonate end members (Chapter 3).

Results of the chloride-carbonate exchange in the current study, and from the hydroxyl-carbonate experiments by Fischer and Kuzel (1982) emphasize that although the divalent carbonate ion is preferred in the structure of the calcium aluminate hydrates, only a small portion of the total OH^- or Cl^- ions are replaced. The current study shows that a maximum of approximately 20% of the Cl^- ions in Friedel's salt are readily exchanged by carbonate ions over a two month period. This has very important implications for the management of concrete materials containing radioactive chlorine-36, where the most probable mineralogical control on chloride in these materials is Friedel's salt. After disposal in the natural environment (e.g. in an underground storage facility), the portion of Cl^- in these phases that is readily replaced by carbonate ions in groundwater may be a relatively small fraction of the total chloride present in these materials, as long as conditions required for the stability of Friedel's salt are maintained (e.g. high pH).

6.5 Conclusions

The maximum fraction of Cl^- exchanged for OH^- ions in the OH end member was 0.65 and 0.7 in the experiments as a function of time and concentration, respectively. Comparison of the measured ratios of Cl/(Cl+OH) in the solid and the aqueous phases as function of concentration from both the ion exchange experiment and solubilities studies demonstrated that these final ratios are representative of exchange equilibrium. For samples containing a given number of moles of chloride in the solubility and ion exchange experiments, the lower measured fractions of Cl^- in the solid phase in the ion exchange experiments can be explained by the higher total number moles of OH^- in these systems. The lower Cl/(Cl+OH) ratios in these systems results in a lower quantity of Cl^- partitioned into the solid phase.

The Cl/(Cl+OH) ratios measured in the solid phase as a function of the activity ratio of Cl/(Cl+OH) for the combined data set (including data from both the solubility experiments, and from the ion exchange experiment) was fit to a Langmuir isotherm. The adsorption/desorption constant is K = 7.65, with a maximum fraction of sorption (or exchange) sites S_T = 0.976 (r^2 = 0.967). This isotherm may be used to predict the partitioning of Cl^- and OH^- between the solid and aqueous phases at exchange equilibrium. However, it must be emphasized that accordance of measured Cl/(Cl+OH) ratios with this curve does not mean that the system is at thermodynamic equilibrium, because the activities of the other ions in these phases (i.e. Ca^{2+}, $Al(OH)_4^-$ and H_2O) are not considered.

The faster exchange of Cl^- by carbonate ions when Na_2CO_3 is added as a source relative to $CaCO_3$ is explained by the higher initial concentrations of CO_3^{2-} resulting from the higher solubility of Na_2CO_3. Once calcite precipitates from solution, the concentrations of CO_3^{2-} in solution are controlled by this phase. This likely explains the lower rate of exchange observed when calcite is used as a source of carbonate ions. A maximum of 22% of the Cl- ions were exchanged by carbonate in the Na_2CO_3 experiment 20 days of reaction, and maintained as the reaction time increased to 55 days. These results are remarkable, given that the divalent carbonate ion is preferred in the structure of the calcium aluminate hydrates, and that solid solutions containing up to 85% carbonate can be formed, as demonstrated in the solubility experiments. The low exchange of carbonate may be due to the formation of a carbonated rim around the outside edges of the Friedel's salt crystals, forming a barrier which inhibits further diffusion of Cl^- out of the crystals, and/or the diffusion of CO_3^{2-} into the crystals.

6.6 Recommendations

Of particular interest is the surprisingly low quantity (approximately 20%) of chloride exchanged by carbonate. Given the possible solubility control on the concentrations of carbonate imposed by the presence of calcite, further experiments in which carbon dioxide is added to the system as a gas could be performed. In an experiment of this type, it would be necessary to add a base (e.g. NaOH or $Ca(OH)_2$) to maintain a constant solution pH.

6.7 References

Alkattan M., Oelkers E. H., Dandurand J.-L., and Schott J. (1997). Experimental studies of halite dissolution kinetics. 1. The effect of saturation state and the presence of trace metals. *Chemical Geology*, **137**, 201-219.

Apello C. A. J. and Postma D. (1994). Geochemistry, groundwater and pollution. A. A. Balkema Publishers, Brookfield, U.S.A.

Barker J. F. and Chatten S. (1982). A technique for determining low concentrations of total carbonate in geologic materials. *Chemical Geology*, **36**, 317-323.

Davis J. A. and Kent D. B. (1990). Surface complexation modeling in aqueous geochemistry. *In:* Reviews in Mineralogy, Volume 23 (eds. Hochella M. F. Jr. and White A. F.), pp. 177-260.

Glasser F.P., Kindness A., and Stronach S. A. (1999). Stability and solubility relationships in AFm phases Part I. Chloride, sulfate and hydroxide. *Cem. Concr. Res.*, **29**, 861-866.

Damidot D., Stronach S., Kindness A., Atkins M. and Glasser F.P. (1994). Thermodynamic investigation of the $CaO-Al_2O_3-CaCO_3-H_2O$ closed system at 25 °C and the influence of Na_2O. *Cem. Concr. Res.*, **24**, 563-572.

Fischer R. and Kuzel H.-J. (1982). Reinvestigation of the system $C_4A{\cdot}nH_2O-C_4A{\cdot}CO_2{\cdot}nH_2O$. *Cem. Concr. Res.*, **12**, 517-526.

Kinniburgh D. G. (1986). General purpose adsorption isotherms. *Environ. Sci. Tech.*, **20**, 895-904.

Mascolo G. and Marroccoli M. (1986). A study on the reactivity of $C_4A{\cdot}nH_2O$ with aqueous solutions. *Cem. Concr. Res.*, **16**, 679-684.

Patterson R. (1970). An introduction to ion exchange. Heyden & Son Ltd., Great Britain.

Reardon E.J. (1990). An ion interaction model for the determination of chemical equilibria in cement/water systems. *Cem. Concr. Res.*, **20**, 175-192.

Taylor H.F.W. (1997). Cement Chemistry (2nd edition). Academic Press 459p.

Chapter 7 Contributions

The purpose of this chapter is to highlight several observations which become apparent when the results from the solubility and ion exchange experiments are considered together, and to summarize the main contributions of the thesis to the scientific continuum.

7.1 The OH end member

It has not yet been proven conclusively that the α-form of the OH end member, with a d-spacing practically identical to hemicarboaluminate, does not exist. In the following sections, previous research on the OH end member is reviewed, and compared to the observations made in the current study.

7.1.1 Previous research

The reported primary d-spacings for the lower hydration state of the OH end member with 12 waters ($3CaO{\cdot}Al_2O_3{\cdot}Ca(OH)_2{\cdot}12H_2O$) range from 7.76 to 8.28 Å (Schwiete and Ludwig, 1969). Within this range, two different forms were originally identified: an α-form with a range of d-spacings from 8.18 to 8.28 Å, and a β-form with d-spacings ranging from 7.76-8.05 Å (Jones and Roberts, 1962; Buttler, Dent Glasser and Taylor, 1959; Roberts, 1957). Alégre (1962) determined that the two forms of this phase constituted different hydration states of the same phase. The alpha phase with a d-spacing of 8.18 Å contained 12 waters, and was converted to a solid with a d-spacing of 7.82 Å when dried over lithium chloride. Based on its water content, the phase with a d-spacing of 7.82 Å contains one less water molecule in its interlayer ($3CaO{\cdot}Al_2O_3{\cdot}Ca(OH)_2{\cdot}11H_2O$). When this phase was re-equilibrated over a saturated calcium sulphate solution, the d-spacing of the solid expanded to 8.18 Å, proving that the change in the d-spacing was reversible.

Despite the fact that strict precautions were taken in the studies by Alégre (1962) to exclude atmospheric CO_2, Roberts (1969) considered that there was still some doubt as to whether these precautions were successful. On this basis, Roberts (1969) reinterpreted the results of Alégre (1962), suggesting that the α-form of the OH end member (d-spacing of 8.2 Å) was actually hemicarboaluminate ($3CaO{\cdot}Al_2O_3{\cdot}0.5Ca(OH)_2{\cdot}0.5CaCO_3{\cdot}12H_2O$), and it dehydrated to a phase

containing 10 waters (d-spacing of 7.7 Å) when dried over LiCl. Upon re-equilibration over a calcium sulphate solution, the phase then re-hydrated to the 12-hydrate form. Roberts (1969) further suggested that the β-form ($3CaO{\cdot}Al_2O_3{\cdot}Ca(OH)_2{\cdot}12H_2O$) is the true ternary hydrate. This conclusion was based on a study in which the β-form of the OH end member was exposed to atmospheric CO_2, and treatment of suspensions of the highly hydrated form of the OH end member ($3CaO{\cdot}Al_2O_3{\cdot}Ca(OH)_2{\cdot}18H_2O$) in its mother-liquor with $CaCO_3$, $NaCO_3$, or CO_2. In all cases, a solid solution phase with a longest d-spacing of 8.2 Å was formed. The results of these experiments provide strong evidence that hemicarboaluminate has a major peak at 8.2 Å, and this conclusion is further supported by the results of Fisher and Kuzel (1982). However, these results do not preclude the existence of the α-form of the OH end member with the same d-spacing as hemicarboaluminate.

Roberts (1969) carried out experiments in which nitrogen at 11, 33 and 81% relative humidity was passed over samples of the highly hydrated form of the OH end member ($3CaO{\cdot}Al_2O_3{\cdot}Ca(OH)_2{\cdot}18H_2O$) in a humidity controlled cell. The solids were then examined using XRD analysis. In most samples, a phase with a primary d-spacing of 7.9Å was formed after dehydration. However, small peaks at 8.2 Å were observed in some samples subjected to successive dehydration and rehydration cycles, dried in a desiccator, or deliberately exposed to the atmosphere. Roberts (1969) assume that exposure to the atmosphere leads to carbonation of these phases by CO_2, generating the peak at 8.2 Å. However, whenever samples are inadvertently (i.e. leaking desiccator) or deliberately exposed to the atmosphere, control is lost over at least two variables: 1) exposure to atmospheric CO_2 and 2) relative humidity. If the OH end member was present in the β-form with 11 waters, but was then inadvertently exposed to the atmosphere with a higher relative humidity, it could hydrate further forming the "α-form", which would have a peak at 8.1 - 8.2 Å. In order to conclusively show that carbonation had occurred in Roberts experiments, the presence of carbon in the solid phase would have to be demonstrated.

7.1.2 OH end member solids as observed in the current study

In the solubility experiments (Chapters 2 and 4), three replicate samples of the OH end member were prepared. In two of the replicates from supersaturation, a small peak at 8.0-8.2 Å was identified, that could belong to hemicarboaluminate, if the sample has been contaminated by atmospheric CO_2. After an additional 16 months of reaction from undersaturation, the dominant peak for the solid solution phase was at 8.2 Å. This could indicated that the solid has completely

converted to hemicarboaluminate. An experiment was also conducted to determine the length of time required for the OH end member to form (Chapter 6). After reaction times of 8 hours to 7 days, the solids consisted primarily of the OH end member with a d-spacing of 7.9 Å. However, in the 1 and 7 day samples, the main peaks were split in two, with the second peak at 8.1 Å (Figure 6.1). Extensive precautions were taken to exclude atmospheric CO_2 during sample preparation and sampling in both sets of experiments, and the samples were dried at a relative humidity of 37% (over a saturated $CaCl_2$ solution) in a desiccator that was stored in a CO_2-free environment. However, the solids were exposed to atmospheric CO_2 during XRD analysis, and the relative humidity of the samples was not controlled during analysis.

An examination of the results of the solubility experiments appears to suggest a trend of increasing CO_2 contamination with increased reaction time (from 6 months to 16 months) in the experiments from super- and undersaturation, respectively. However, the results of the formation experiment for the OH end member demonstrate that the formation of a solid solution phase with a primary d-spacing of 8.1 Å is not dependent on reaction time. It is possible that contamination of the samples by atmospheric CO_2 occurred during the XRD analysis of the samples. If hemicarboaluminate was forming in the samples due to contamination by atmospheric CO_2, it seems probable that it would form more consistently, and not just in one or two samples, because all solids were exposed to the atmosphere during XRD analysis, for approximately the same length of time.

A comparison of two OH-Cl exchange experiments offers further collaborating evidence (Chapter 6, Section) that the OH end member may not be as susceptible to CO_2 contamination as currently believed. One experiment was carried out using the established procedures, with precautions taken to exclude atmospheric CO_2, and in the second, the samples were not protected from the atmosphere (i.e. filtration and sample handling was done in the laboratory environment). No XRD data are available from the samples exposed to the atmosphere, however, the similar Cl^- solution concentrations observed in these two experiments suggests that CO_2 contamination was minimal.

Apart from the different reaction times for the solids, other variables are the preparation method of the solid for XRD analysis, and the amount of time that the solids were dried at 37% relative humidity before analysis (Table 7.1).

Experiment	Type of sample	Drying time at 37% R. H.	Primary d-spacing (Å)
Supersaturation	glass slide	3 months	7.9
Undersaturation	solid packed into planchette	2 weeks	8.2
OH formation	glass slide	7 days	7.9, 8.1 in 2 solids

Table 7.1 Preparation methods for solids analyzed using XRD, and the length of time the samples were equilibrated before analysis. The d-spacing measured for the predominant solid solution phase is also given.

The re-evaluation of the literature discussed in the previous section suggests an alternate explanation for the peak at 8.1 to 8.2 Å. It is possible that these peaks are not hemicarboaluminate, but rather belong to the α-form of OH end member with 12 water molecules in its interlayer. In this interpretation, the peak at 7.9 Å corresponds to the β-form, with 11 water molecules. In the experiment from supersaturation, and in the OH formation experiment, solids for XRD analysis were prepared as thin slurries on glass slides. In the experiment from supersaturation, the primary d-spacing was 7.9 Å after the solids were equilibrated for 3 months at 37% relative humidity. This is consistent with the presence of the less hydrated β-form of the OH end member in these solids. In the experiment from undersaturation, the solids were placed in plastic vials, and equilibrated for 2 weeks before they were packed into aluminum planchettes for XRD analysis. It is probable that the solid had not completely equilibrated before analysis. In this case, the larger d-spacing of 8.2 Å could be indicative of the α-form of the OH end member with 12 water molecules in the interlayer. Solids from the OH formation experiment were prepared on glass slides, and equilibrated for 7 days before XRD analysis. In most of the solids, the predominant peak was at 7.9 Å. However, in two solids, two peaks were observed. This may suggest that both the α- and β-forms of the OH end member are present, perhaps as a result of uneven drying of the solids.

The XRD results from the current study are suggestive, but not conclusive. The implication of these results is that the importance of the drying conditions and determination of water content for the OH end member and its solid solutions may have been underestimated. Likewise, the importance of maintaining a CO_2 free environment may be over-emphasized. However, further experiments under carefully controlled conditions would be necessary to properly assess the importance of relative humidity, and exposure to atmospheric CO_2.

7.2 Preference for carbonate ions

It is well accepted in the literature that the CO_3^{2-} ion is preferred in the structure of the monocalcium aluminate hydrates (Glasser et al., 1999; Taylor, 1997). This preference is also reported for hydrotalcite-like minerals. Although Fischer and Kuzel (1982) demonstrated the formation of a reaction rim of hemicarboaluminate around crystals of the OH end member, to my knowledge, the ion exchange experiments performed in the current study are the first quantitative measurements on the exchange of any anion by carbonate in the interlayer of the monocalcium aluminate hydrates.

Remarkably, the ion exchange experiments revealed that only approximately 20% of the Cl^- ions present in the structure of Friedel's salt had been replaced by CO_3^{2-} after 2 months of reaction. In addition, calcite persisted in almost all samples after reaction times of between 6 and 16 months in the solubility experiments performed on Cl-CO_3 solid solutions (Chapter 3). Roberts (1969) also noted that during the formation of carbonate-bearing calcium aluminate hydrates, the reaction of $CaCO_3$ was often incomplete. If carbonate were easily exchanged into the interlayer, then we might expect that any carbonate in solution would be immediately incorporated into the structure, reducing the concentration of carbonate in solution, and thereby providing a driving mechanism for the dissolution of calcite.

The low measured exchange of carbonate ions has important implications to the management of concrete materials containing radioactive chlorine-36, where the most probable mineralogical control on chloride in these materials is Friedel's salt. After disposal of such materials in the natural environment (e.g. in an underground storage facility), the portion of Cl^- that is readily replaced by carbonate ions in groundwater may be a small fraction of the total chloride present in these materials, as long as conditions required for the stability of Friedel's salt are maintained (e.g. high pH).

7.3 Solubility and stability

7.3.1 Solubility

Published solubility data for the Cl, OH and CO_3 end members have been combined with the values measured in the current study and re-evaluated to determine average solubility products

for the end members, and the associated uncertainty in these values. The average solubility products calculated for Friedel's salt, monocarboaluminate, and the OH end member are -27.57 ± 0.86, -31.23 ± 0.80, and -25.80 ± 0.62, respectively (based on modeling using SIMUL). The uncertainty given for these values is one standard deviation from the mean. Using these average K_{sp} values, Gibbs free energies of formation ($\Delta G^{\circ}_{f,298}$) for Friedel's salt, monocarboaluminate and OH end member are -6822.51± 4.92, -7345.89 ± 1.09, and -8761.59 ± 3.54 kJ/mol, respectively. These values are consistent with those calculated based on the solubility products determined using PHREEQC (-6823.10± 4.69, -7347.86 ± 2.79, and -8761.13 ± 3.54 kJ/mol, respectively).

Solubility data for phases with compositions intermediate between the Cl-CO_3 end members, and OH-CO_3 end members, which were not previously available in the literature, have been presented in this thesis. The solubility measurements made as a function of solid solution composition were used to derive excess free-energy parameters for the OH-Cl and Cl-CO_3 systems. These values have been used to construct Lippmann diagrams, which can be used to make preliminary estimates on the partitioning of chloride between the aqueous and solid solution phases at thermodynamic equilibrium. It was not possible to determine excess free energy parameters for the OH-CO_3 system, primarily because there are two miscibility gaps in this system. A method for predictive modeling in this system is suggested, which involves dividing the system into two parts with the OH end member and hemicarboaluminate as end members in the first part, and hemicarboaluminate and monocarboaluminate in the second part. However, the amount of solubility data currently available on solid solution phases with compositions between the hydroxyl and carbonate end members was insufficient to test this approach. Alternatively, because the regions of solid solution are relatively restricted, it may be possible to adequately model this system by considering the OH-CO_3-calcium aluminate hydrate series as simple mixtures of one or two phases of the OH end member, hemicarboaluminate, and monocarboaluminate. In this case, OH end member-monocarboaluminate is an incompatible phase assemblage.

A comparison of the measured ratios of Cl/(Cl+OH) in the solid and the aqueous phases as function of concentration from both the ion exchange experiment and solubilities studies demonstrated that the final ratios are representative of at least a metastable equilibrium condition. The lower measured fractions of Cl^- in the solid phase in the ion exchange experiments can be explained by the higher total number moles of OH^- in these systems. The lower Cl/(Cl+OH) ratios in these systems results in a lower quantity of Cl^- partitioned into the solid phase. The Cl/(Cl+OH) ratios measured in the solid phase as a function of the activity ratio

of Cl/(Cl+OH) for the combined data set (including data from both the solubility experiments, and from the ion exchange experiment) was fit to a Langmuir isotherm, with an adsorption/desorption constant K = 7.65. This isotherm may be used for semi-empirical predictions of the partitioning of Cl^- and OH^- between the solid and aqueous phases.

Although the OH end member is ultimately unstable with respect to hydrogarnet and portlandite, it persists in a metastable state for reaction times up to two years. Consequently, determining the excess free energy parameters for systems between the OH end member and other end members is particularly challenging. It may take years to reach equilibrium with respect to hydrogarnet and portlandite, rendering solubility measurements at thermodynamic equilibrium unfeasible. An alternative approach in future studies may be to measure the solubility of the solid solution phases at stoichiometric saturation. Stoichiometric saturation refers to a metastable state between an aqueous solution and a solid solution "in situations where, owing to kinetic restrictions, the composition of the solid phase remains invariant, even though the solid phase may be part of a continuous compositional series" (Thorstenson and Plummer, 1977). Application of the stoichiometric saturation concept requires that single solid solution phases with various compositions are produced, including compositions within the miscibility gap. Using the ion exchange approach (Chapter 6), single solid solution phases were generated with compositions within the miscibility gap between the OH and Cl end members. This suggests that it may be possible to use this approach to prepare metastable solid solutions with compositions within the miscibility gap, which could then be used in an attempt to measure stoichiometric saturation solubilities.

7.3.2 Stability

A summary of the miscibility gaps observed between the OH-Cl, Cl-CO_3 and OH-CO_3 end members is presented on a triangular diagram in Figure 7.1. The existence of miscibility gaps between the OH and Cl end members and between the Cl and CO_3 end members has been confirmed. In the OH-Cl series, the results from the current study support the conclusion of Pöllmann and Kuzel (1988) that the miscibility gap begins at a Cl/(Cl+OH) ratio very close to 0.33, rather than above a ratio of 0.4 as suggested by Roberts (1969). The lower limit of the miscibility gap lies between ratios of 0.0 and 0.1, based on the XRD results of Birnin-Yauri (1993), Pöllmann and Kuzel (1988), Roberts (1969) and the current study.

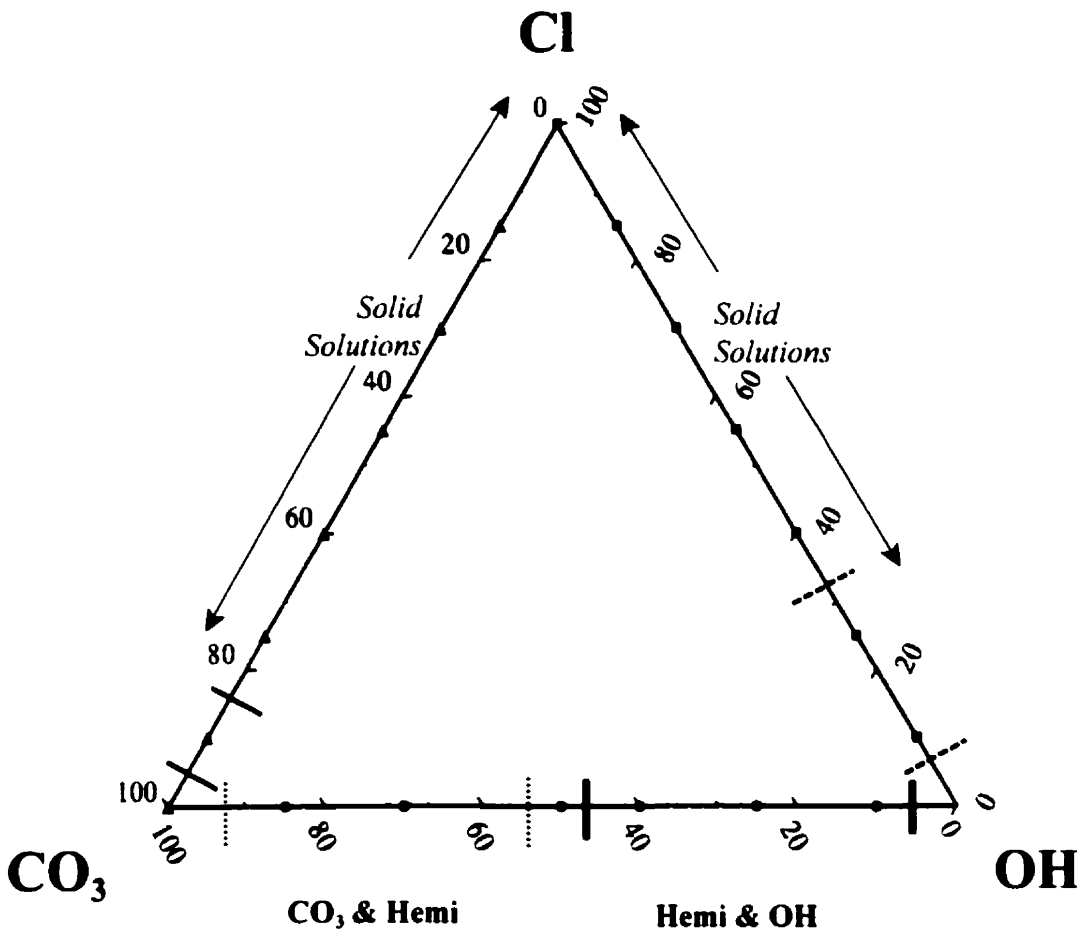


Figure 7.1: Summary diagram of phase relations in the system $Ca(OH)_2$-$CaCl_2$-$CaCO_3$-Al_2O_3-H_2O. The short lines indicate the approximate positions of the observed miscibility gaps in the system. Between the hydroxide and carbonate end member, two apparent miscibility gaps were observed: 1) between the CO_3 end member and hemicarboaluminate and 2) between hemicarboaluminate and the hydroxide end member (as shown). However, the results from the experiment from undersaturation indicate that hemicarboaluminate could be a metastable phase, which is converting to a mixture of the CO_3 end member and hydrogarnet with time.

Between the chloride and carbonate end members, a partial solid solution was observed to form in solids with carbonate ratios to 0.75. The lower limit of this miscibility gap occurs at a carbonate ratio of 0.83, as delineated by Pöllmann (1986). The results of the current study extend the upper limit of the miscibility gap to a carbonate ratio of at least 0.91, and may extend to the carbonate end member (1.0).

Between the hydroxyl and carbonate end members there are two miscibility gaps, one between the hydroxyl end member and hemicarboaluminate, and a second between hemicarboaluminate, and the carbonate end member (monocarboaluminate). The miscibility gap between the OH end member and hemicarboaluminate was previously observed between carbonate ratios of 0.05 to 0.40. In the current study, the miscibility gap was observed between carbonate ratios of 0.1 and 0.5 in the experiment from supersaturation, but over a much smaller range of 0.0 to 0.25 in the experiment from undersaturation. In the experiment from undersaturation, hemicarboaluminate may be converting to a mixture of monocarboaluminate and hydrogarnet with time according to a reaction similar to the following:

$$Ca_4Al_2O_6(OH)\cdot 0.5CO_3\cdot 12H_2O = 0.5Ca_4Al_2O_6\cdot CO_3\cdot 11H_2O + 0.5Ca_3Al_2O_6\cdot 6H_2O + 0.5Ca^{2+} + OH^- + 2.5H_2O$$

The second miscibility gap was identified in previous studies between carbonate ratios of 0.6 and 0.8. The results from supersaturation in the current study were consistent with this range, but in the experiment from undersaturation, these two phases were observed over a wider range of compositions, from 0.4 to 0.7, and hydrogarnet was also present. This may indicate that the stable phase assemblage is a mixture of monocarboaluminate and hydrogarnet.

Interestingly, in the solubility experiments from supersaturation, the β-form of Friedel's salt was identified, while the solid from undersaturation was identified as α-Friedel's salt. In the Cl-CO_3 ion exchange experiments, Friedel's salt occurred in the β-form in the experiment with sodium carbonate added, and in the α-form in the experiment when calcite was added. The occurrence of one or the other phase is not surprising, because the transition temperature from the α- to the β-forms is reported to be 28-30°C (Kuzel, 1969; Renaudin et al., 1999), which is close to ambient room temperature (25°C).

7.4 SSAS theory as applied to the monocalcium aluminate hydrates

Glynn and Reardon (1990) developed an expression for Lippmann's solutus curve for the general case of a non-ideal solution with the composition $B_{1-x}C_xA$. In this expression, the activities of the solid phase components are expressed in terms of activity coefficients and mole fractions. In this thesis, a similar approach has been used to solve for the solutus. However, because the stoichometric coefficients of the substituting ions in the solid phase are not equal to 1, it was recognized that a modification to the definition of the activity fractions of the substituting ions in solution was required. For example, in the hydroxide-chloride series of the calcium aluminate hydrates, two chloride ions substitute for two hydroxide ions. The dissolution reactions for the two end members are

$$3CaO{\cdot}Al_2O_3{\cdot}Ca(OH)_2{\cdot}18H_2O_{(s)} = 4Ca^{2+} + 2Al(OH)_4^- + 6OH^- + 12H_2O$$

$$3CaO{\cdot}Al_2O_3{\cdot}CaCl_2{\cdot}10H_2O_{(s)} = 4Ca^{2+} + 2Al(OH)_4^- + 2Cl^- + 4OH^- + 4H_2O$$

and the corresponding solubility product expressions:

$$K_{sp}\,OH = [Ca^{2+}]^4[Al(OH)_4^-]^2[OH^-]^6[H_2O]^{12}$$

$$K_{sp}\,Cl = [Ca^{2+}]^4[Al(OH)_4^-]^2[Cl^-]^2[OH^-]^4[H_2O]^4$$

Adding the solubility product expressions together and collecting like terms gives the expression for the total solubility product

$$\Sigma\,\Pi = [Ca^{2+}]^4[Al(OH)_4^-]^2\,[OH^-]^4[H2O]^4\,\{[Cl^-]^2 + [OH^-]^2[H_2O]^8\}$$

The corresponding expression for the solid solution $B_{1-x}C_xA$ is

$$\Sigma\,\Pi = [A^-]([B^-] + [C^-])$$

Comparing the two equations demonstrates that $[A^-]$ in the expression for the general solid solution is equal to $[Ca^{2+}]^4[Al(OH)_4^-]^2\,[OH^-]^4[H2O]^4$, $[B^-] = [Cl^-]^2$ and $[C^-] = [OH^-]^2[H_2O]^8$. In order to be able to substitute an expression for the aqueous activity fractions of $[Cl^-]^2$ and $[OH^-]^2[H_2O]^8$ in the expression for the total solubility product ($\Sigma\,\Pi$) and solve for the equilibrium value, the activity fractions in solution must be defined as:

$$X_{OH.\,aq} = \frac{[OH^-]^2[H_2O]^8}{[Cl^-]^2 + [OH^-]^2[H_2O]^8}$$

$$X_{Cl.\,aq} = \frac{[Cl^-]^2}{[Cl^-]^2 + [OH^-]^2[H_2O]^8}$$

These activity fractions can be considered to represent the difference between the mineral phases after substitution occurs (i.e. two hydroxide ions in the mineral structure are replaced by two chloride ions and 8 water molecules). This modification to the definition of the aqueous mole fractions of the substituting ions was applied in modeling both the OH-Cl (Chapter 2) and Cl-CO_3 (Chapter 3) solid solution series of the monocalcium aluminate hydrates.

No literature which specifically addressed this problem was found. However, Kersten (1996) applied SSAS modeling to the C-S-H-portlandite system. In the dissolution expression for the C-S-H phase, both calcium and silicate have stoichiometric coefficients of 2. Kersten's approach to this problem was to redefine the K_{sp} of the C-S-H phase as equal to $K_{sp}^{.5}$, and then take the square root of both sides of the dissolution equation. The solutus expression can then be solved according to the method outlined by Glynn and Reardon (1990). The Lippmann diagrams constructed using Kersten's approach and using the revised aqueous mole fractions described above were very similar, with the exception of the absolute values of the end member solubility products.

7.5 References

Alégre (1962). Investigations on hexagonal C_4AH_x. *Rev. Mater. Constr.*, **566**, 301-314.

Birnin-Yauri U. A. (1993). Chloride in cement: Study of the system $CaO-Al_2O_3-CaCl_2-H_2O$. Ph.D. Thesis. University of Aberdeen. Aberdeen. United Kingdom.

Buttler F. G., Dent Glasser L. S., and Taylor H. F. W. (1959). Studies on $4CaO{\cdot}Al_2O_3{\cdot}13H_2O$ and the related natural mineral hydrocalumite. *Jour. Amer. Cer. Soc.*, **42**, 121-126.

Fisher R. and Kuzel H. J. (1982). Reinvestigation of the system $C_4A{\cdot}nH_2O$ - $C_4ACO_3{\cdot}nH_2O$. *Cem. Concr. Res.*, **12**, 517-526.

Glasser F. P., Kindness A. and Stronach S.A. (1999). Stability and solubility relationships in AFm phases Part I. Chloride, sulfate and hydroxide. *Cem. Concr. Res.*, **29**, 861-866.

Glynn P. D. and Reardon E. J. (1990). Solid-solution aqueous-solution equilibria: Thermodyanmic theory and representation. *Am. Jour. Science*, **290**, 164-201.

Jones F. E. and Roberts M. H. (1962). The system $CaO-Al_2O_3-H_2O$ at 25 °C. *Building Research Current Papers*, Research series 1.

Kersten M. (1996). Aqueous solubility diagrams for cementitious waste stabilization systems. 1. The C-S-H solid solution system. *Environ. Sci. Tech.*, 30, 2286-2293.

Kuzel H.J. (1969). X-ray investigations of some complex calcium aluminate hydrates and related compounds. *Proc. 5th Int. Symp. Chem. Cem.*, Tokyo, **II**, 92-97.

Pöllmann H. (1986) Solid solution of complex calcium aluminate hydrates containing Cl^-, OH^- and CO_3^{2-} anions. *Proc. 8th Int. Symp. Chem. Cem.*, Rio de Janeiro, Supplementary paper, **Vol. III**, 300-306.

Pöllmann H. and Kuzel H. J. (1988). Synthesis and polymorphic transformations of solid solutions in the system $3CaO{\cdot}Al_2O_3{\cdot}CaCl_2{\cdot}nH_2O$- $3CaO{\cdot}Al_2O_3{\cdot}Ca(OH)_2{\cdot}nH_2O$-$H_2O$. *N. Jb. Miner. Mh.*, 193-202.

Renaudin G., Kubel F., Rivera J.-P. and Francois M. (1999). Structural phase transition and high temperature phase structure of Friedel's salt. $3CaO{\cdot}Al_2O_3{\cdot}CaCl_2{\cdot}10H_2O$. *Cem. Concr. Res.*, **29**, 1937-1942.

Roberts M. H. (1957). New calcium aluminate hydrates. *J. Appl. Chem.*, **7**, 543-546.

Roberts M. H. (1969). Supplementary paper II-29. Calcium aluminate hydrates and related basic salt solid solutions. *Proc. 5th. Int. Symp. Chem. Cem.*, Tokyo, **Vol. II**, 104-117.

Schwiete H. E. and Ludwig U. (1969). Crystal structures and properties of cement hydration products (hydrated calcium aluminates and ferrites). *Proc. 5th. Int. Symp. Chem. Cem.*, Tokyo, Principal paper, **Session II-2**, 37-67.

Taylor H.F.W. (1997). Cement Chemistry (2nd edition). Academic Press 459p.

Appendix A

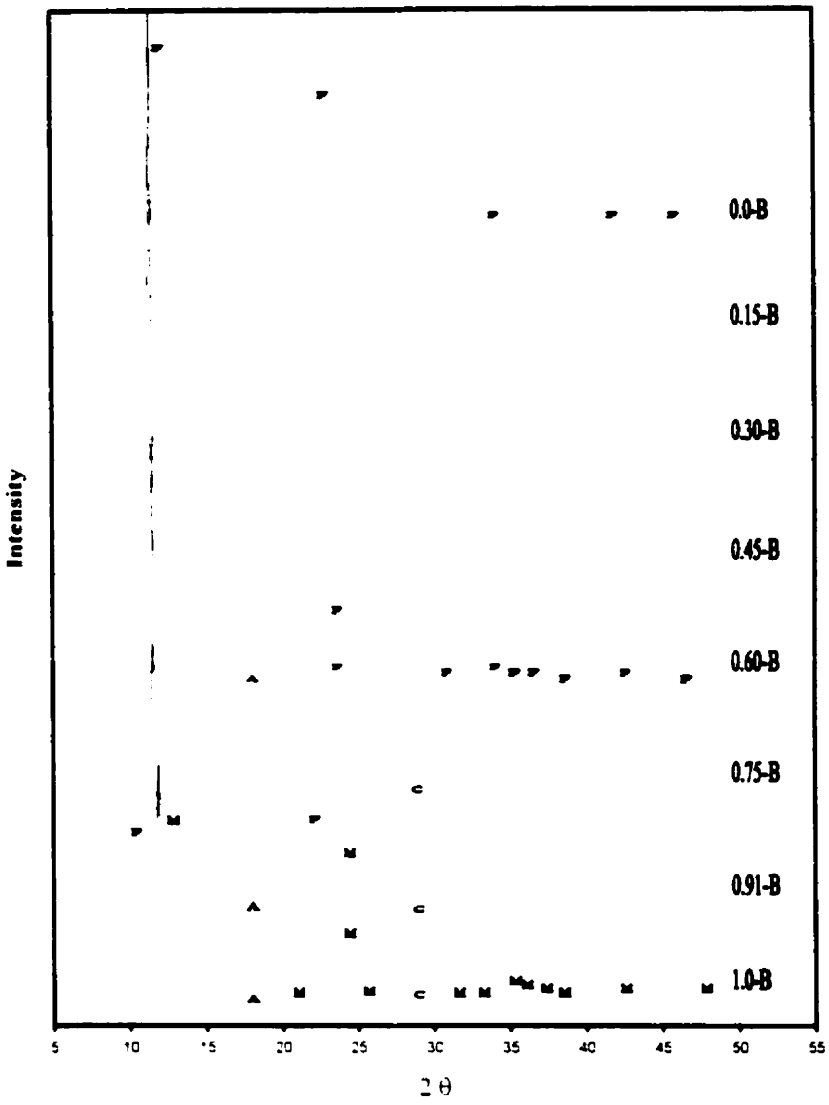


Figure A.1. XRD patterns from the supersaturation experiment for B-replicate samples in the series between the chloride (0.0) and carbonate (1.0) end members, where the label indicates the carbonate ratio in the solid. The occurrence of split peaks at $2\theta = 11^\circ$ and 23° in sample 0.91 indicates the presence of two solid solution phases. F = Cl end member ($3CaO{\cdot}Al_2O_3{\cdot}CaCl_2{\cdot}10H_2O$); M = CO_3 end member ($3CaO{\cdot}Al_2O_3{\cdot}CaCO_3{\cdot}11H_2O$); C = calcite ($CaCO_3$); A = gibbsite ($Al(OH)_3$).

Appendix B: Raw data from ion exchange experiments

Timed experiments (#1 through 5)

Experiment #1 Exchange of OH^- by Cl^- ions (Not protected from atm. CO_2).

Reaction time (hours)	pH	Cl^- concentration (mmol/L)
0.25	12.94	195.2
0.5	12.95	179.8
1.0	12.88	213.5
2.0	13.02	127.8
4.0	12.99	115.6
4.5	13.00	160.9
5.0	13.00	139.8
5.5	13.02	147.3
6.0	13.02	137.7
7.0	12.99	142.2
8.0	13.00	109.9
9.0	13.01	87.37
20	13.07	61.94
25	13.06	64.08
30	13.10	63.21
48	13.08	68.56
65	13.09	61.25
72	13.05	59.28
85	13.04	62.23
96	13.03	62.50
120	13.08	61.05
168	12.96	107.9
240	12.99	80.76
456	13.09	57.91

Experiment #2 Exchange of OH^- by Cl^- ions (protected from atm. CO_2).

Reaction time (hours)	pH	Cl (mmol/L)	Ca (mmol/L)	Al (mmol/L)	Na (mmol/L)
3	13.17	69.68	4.290	0.0957	190.7
6	13.23	71.93	4.331	0.0864	187.8
12	13.14	74.41	4.022	0.0401	190.4
24	13.16	70.79	4.095	0.0772	184.4
48	13.04	67.95	4.381	0.1066	184.7
72	13.03	69.62	4.114	0.0964	188.8
96	13.02	69.13	3 924	0.1410	192.9
144	13.00	66.78	3.997	0.1058	186.1
240	13.01	69.11	4.170	0.0926	186.3
648	13.20	65.92	4.014	0.0123	193.0

Experiment #3 Exchange of Cl^- ions in Friedel's salt by OH^- ions

Estimated Cl- concentration at t = 0: 65.94 mmol/L

Reaction Time (hours)	pH	Cl concentration (mmol/L)
1	13.39	63.40
6	13.01	66.00
12	13.06	67.40
24	13.01	66.62
48	13.06	65.38
96	12.96	61.00
192	12.97	67.55
288	13.04	59.53
384	13.18	64.01
768	13.29	65.81
1536	13.27	58.23
3048	13.07	55.17

Experiment #4 Exchange of Cl^- ions in Friedel's salt by CO_3^{2-} ions (Carbonate added as Na_2CO_3).

Initial Cl- concentration in solution at time zero: 63.45 mmol/L

Reaction time (hours)	Wt. Solution (g)	pH	Cl (mmol/L)	CO_3 (mmol/L)
1	55.19	12.85	65.07	0.2195
3	55.20	12.84	73.26	0.0784
6	55.04	12.79	76.27	0.2502
12	54.95	12.80	74.14	0.0904
24	55.03	12.78	85.98	0.0668
48	55.00	12.08	89.77	0.5666
72	55.13	12.86	91.89	0.0588
144	55.07	12.76	98.79	0.0389
240	55.15	12.86	94.62	0.0376
480	55.08	12.56	104.1	0.0399
648	55.03	12.83	104.1	0.0331
1320	55.05	12.52	105.9	0.0440

Experiment #5 Exchange of Cl^- ions in Friedel's salt by CO_3^{2-} ions (Carbonate added as $CaCO_3$).

Initial Cl- concentration in solution at time zero: 3.94 mmol/L

Reaction time (hours)	Wt. solution (g)	pH	Cl (mmol/L)	Ca (mmol/L)	Al (mmol/L)
3	55.04	11.58	15.60	11.2	0.4077
24	55.03	11.44	19.46	12.5	0.4744
72	55.09	11.31	21.12	14.0	0.9006
168	55.09	11.50	26.28	15.5	0.2231
504	54.99	11.53	35.07	17.0	0.3854

As a function of concentration:

Experiment #6 Exchange of OH^- ions in Friedel's salt by Cl^- ions

Fraction Cl added	pH	Cl (mmol/L)	Ca (mmol/L)	Al (mmol/L)	Na (mmol/L)
0	12.64	0.0031	19.84	0.0346	0.0614
0.1	12.67	0.9875	16.55	0.1798	19.90
0.2	12.72	1.227	11.31	0.1787	35.31
0.3	12.77	2.716	8.700	0.0931	54.95
0.4	12.92	6.345	6.962	0.1190	74.38
0.5	12.92	12.23	22.14	0.1704	94.11
0.6	12.99	21.33	15.09	0.1797	120.1
0.7	12.91	42.67	7.627	<0.0074	138.8
0.8	13.02	39.49	7.220	0.1756	165.3
0.9	13.01	51.18	8.530	0.2320	186.7
1.0	13.03	62.77	5.190	0.3731	198.6

Experiment #7 Extended experiment: Exchange of OH^- ions in Friedel's salt by Cl^- ions at high Cl^- concentrations

Cl addition factor	pH	Cl (mmol/L)	Ca (mmol/L)	Al (mmol/L)	Na (mmol/L)
1	12.98	100.4	4.34	0.0280	204
2	12.63	288.8	3.64	0.0452	393
4	12.80	672.4	5.81	<0.0180	796
6	12.79	1072	5.86	<0.0180	119
8	12.96	1492	3.64	<0.0180	154
10	12.72	1916	6.61	<0.0180	197
15	12.75	2841	3.62	<0.0180	290
20	12.77	3288	2.22	<0.0180	366

Glossary

Compounds and mineral phases

Name	Formula
Brucite	$Mg(OH)_2$
Calcium silicate hydrate (C-S-H)	a generic name for any amorphous or poorly crystalline calcium silicate hydrate formed by the hydration of dicalcium or tricalcium silicate. The dashes indicate that no particular composition is implied.
Chloride end member	Also known as Friedel's salt
Carbonate end member	Also known as monocarboaluminate
Dicalcium aluminate hydrate	$2CaO{\cdot}Al_2O_3{\cdot}8H_2O$
Dicalcium silicate	$2CaO{\cdot}SiO_2$. Also known as "belite" in the cement literature.
Ettringite	$Ca_6Al_2(OH)_{12}(SO_4)_3{\cdot}26H_2O$
Gibbsite	$Al(OH)_3$
Friedel's salt	$3CaO{\cdot}Al_2O_3{\cdot}CaCl_2{\cdot}10H_2O$. Another name for this phase is monochloroaluminate. Also referred to as the chloride end member of the monocalcium aluminate hydrates.
Hemicarboaluminate	$3CaO{\cdot}Al_2O_3{\cdot}0.5Ca(OH)_2{\cdot}0.5CaCO_3{\cdot}12H_2O$ is stable at 25 °C relative humidities between 53 and 81%. but may partially dehydrate to $3CaO{\cdot}Al_2O_3{\cdot}0.5Ca(OH)_2{\cdot}0.5CaCO_3{\cdot}10H_2O$ at lower relative humidities.
Hydrocalumite	Also used as a the name for the mineral phases belonging to the monocalcium aluminate hydrate group.
Hydrogarnet	$3CaO{\cdot}Al_2O_3{\cdot}6H_2O$

Hydrotalcite	$Mg_6Al_2(OH)_{16}CO_3 \cdot 4H_2O$
Monocalcium aluminate	$CaO \cdot Al_2O_3$
Monocalcium oxychloride	$CaO \cdot CaCl_2 \cdot 2H_2O$
Monocarboaluminate	$3CaO \cdot Al_2O_3 \cdot CaCO_3 \cdot 11H_2O$. Also referred to as the "carbonate end member" of the monocalcium aluminate hydrates.
Monochloride	Another name for Friedel's salt
Monochloroaluminate	Another name for Friedel's salt
Monochloroferrite	$3CaO \cdot Fe_2O_3 \cdot CaCl_2 \cdot 10H_2O$
OH end member	$3CaO \cdot Al_2O_3 \cdot Ca(OH)_2 \cdot 18H_2O$ in solution or at relative humidities above 88%, but dehydrates to $3CaO \cdot Al_2O_3 \cdot Ca(OH)_2 \cdot 12H_2O$ at lower relative humidities.
Portlandite	$Ca(OH)_2$
Tricalcium aluminate	$3CaO \cdot Al_2O_3$
Tricalcium chloroaluminate hydrate	$3CaO \cdot Al_2O_3 \cdot 3CaCl_2 \cdot 30H_2O$. Also know as Trichloroaluminate.
Tricalcium oxychloride	$3CaO \cdot CaCl_2 \cdot 15H_2O$
Tricalcium silicate	$3CaO \cdot SiO_2$. Also referred to as "alite " in the cement literature.
Trichloroaluminate	Another name for tricalcium chloroaluminate hydrate.
Trichloroferrite	$3CaO \cdot Fe_2O_3 \cdot 3CaCl_2 \cdot 30H_2O$
Tetracalcium aluminate hydrate	Another name for the OH end member of the monocalcium aluminate hydrates.
Tetracalcium aluminoferrite	$4CaO \cdot Al_2O_3 \cdot Fe_2O_3$